STUDIES ON DNA AS A BIORECOGNITION ELEMENT FOR THE DETECTION OF *PLASMODIUM* SPECIES LACTATE DEHYDROGENASE IN OPTICAL AND ELECTROCHEMICAL PLATFORMS

A Thesis

Submitted by

PRIYAMVADA JAIN

For the award of the degree

of

Doctor of Philosophy

DEPARTMENT OF BIOSCIENCES AND BIOENGINEERING
INDIAN INSTITUTE OF TECHNOLOGY GUWAHATI
GUWAHATI-781039, ASSAM, INDIA
FEBRUARY, 2017


Dedicated to all my fellow research scholars
Just Keep Swimming
(Finding Dory)

INDIAN INSTITUTE OF TECHNOLOGY GUWAHATI

Department of Biosciences and Bioengineering

Guwahati - 781039

STATEMENT

I do hereby declare that the matter embodied in this thesis is the result of investigations carried out by me in the Department of Biosciences and Bioengineering, Indian Institute of Technology Guwahati, Assam, India, under the guidance of Prof. Pranab Goswami, with co-supervision of Dr. Sanjukta Patra.

In keeping with the general practice of reporting scientific observations, due acknowledgements have been made wherever the work described is based on the findings of other investigators.

February, 2017
Priyamvada Jain

INDIAN INSTITUTE OF TECHNOLOGY GUWAHATI
Department of Biosciences and Bioengineering
Guwahati - 781039

CERTIFICATE

It is certified that the work described in this thesis, entitled "Studies on DNA as a biorecognition element for detection of *Plasmodium* species lactate dehydrogenase in optical and electrochemical platforms", done by Priyamvada Jain for the award of degree of Doctor of Philosophy is an authentic record of the results obtained from the research work carried out under my supervision, with co-supervision of Dr. Sanjukta Patra, in the Department of Biosciences and Bioengineering, Indian Institute of Technology Guwahati, India.

The results embodied in this thesis have not been submitted to any other University or Institute for the award of any degree.

Prof. Pranab Goswami, Ph.D. **Dr. Sanjukta Patra, Ph.D.**

(Supervisor) **(Co-supervisor)**

Acknowledgement

With the submission of this thesis, comes to an end an arduous journey, made beautiful with the efforts of all those who have constantly had my back through thick and thin. Amidst of the commotion of work, and merriment alike, I have often forgotten to express my gratitude towards these people, but here's my chance!

I extend my deepest gratitude towards my Ph.D. supervisor Prof. Pranab Goswami for teaching me to think like a researcher. His out-of-the-box ideas have greatly helped me to propel my work in a fruitful direction. I am fortunate to have the coolest, most optimistic supervisor, who made the difficult times of Ph.D. much more bearable. Thank you sir, for such a well equipped laboratory, and dedicated work culture, which were a constant source of inspiration for me. I am highly grateful to my Ph.D. co-supervisor, Dr. Sanjukta Patra, for her guidance, and support throughout my work. Her valuable suggestions helped me focus on the weaker areas of my research.

I fondly acknowledge the contributions of my Doctoral Committee consisting of Prof. V. K. Dubey, Prof. S. K. Khijwania, and Dr. V. Trivedi, for their appreciation, as well as critical assessment of my work. I thank all former, and present HODs, faculty members, and staff members of the Department of Biosciences and Bioengineering, IIT Guwahati, for well-maintained advanced infrastructure, and their valuable assistance. I appreciate the Central Instruments facility, IIT Guwahati, and the Center for Energy, IIT Guwahati, for providing relevant advanced facilities.

It is impossible to wind up this thesis without acknowledging the priceless help of my seniors in lab – Urmila, Seraj, Reddy, Madhuri, Mitun, Ankana, who never once balked from getting their own hands dirty to teach a fresh recruit like myself, how to correctly for instance, plate a petri dish, or load samples in the AUC. My good lab etiquettes are a result of their hard work! My special thanks to my fellow lab members Santhosh, Babina, Mrinal, Naveen, Phurpa, Smita, Vinay, Anil, Sharbani, Priyanki, Rupam, Abdul, for an invigorating environment in the lab. Thanks all of you, for your insights, lengthy discussions, and troubleshooting ideas. I extend my gratitude to Smita (M.Tech project fellow) for her tireless assistance in carrying out the work on graphene oxide-DNA aptasensor.

In times of distress my friends have always come to the rescue, and in the grueling course of Ph.D. they were much needed. I sincerely thank my dear friends – Babina, Ruchika, Tasneem, Archita, Sambhavi, Phurpa, Aruna, for all their zen-type life lessons, sharing my love for food, and making fun of my poor jokes. You guys were my very own stress-busters. I thank Babina, Phurpa, and Nama for helping me battle overweight, and driving me towards a fitter and healthier body. Thanks to my friends Asif, and Poulomi, for introducing me to Clash of Clans. It indeed was a refreshing filler to my leisure hours.

Lastly, I express my profound debt to my parents, and my husband for their unconditional love, and encouragement, their sacrifices, and faith in my capabilities, even when I failed. Your understanding, and patience, when I was being a crybaby, cannot be recollected in words. You both have always been the pillars of my strength. Thanks for surviving my Ph.D.

Priyamvada Jain

February, 2017

Table of Contents

Abstract

The current investigation focuses on the development of DNA based biorecognition elements for the detection of *Plasmodium falciparum* lactate dehydrogenase (PfLDH) or its corresponding native gene segment with an aim of developing novel malaria diagnostic systems endowed with stable and sensitive performance. Four independent approaches were embarked upon namely, (A) Development of aptamer based colorimetric detection for PfLDH, (B) Development of aptasensor for electrochemical detection of PfLDH, (C) DNA templated silver nanoclusters for fluorescence based detection of PfLDH and (D) High resolution melting of metallized DNA duplexes for species differentiation of *Plasmodium* parasite. Initially we concentrated on developing an aptamer as a biorecognition element to execute the approaches (A), and (B). A novel ssDNA aptamer (P38), with a 40 mer random region flanked by primer binding sites on both sides, targeting PfLDH was developed through systematic evolution of ligands by exponential enrichment (SELEX), incorporating counter SELEX against human lactate dehydrogenase A and B (hLDH A and B) to render the required specificity to the aptamer. The 2D structure of P38 discerned from the Mfold webserver showed that the aptamer possess three stem loops with a ΔG of -9.18 kcal.mole^{-1}. EMSA and ITC studies confirmed the specific interaction of P38 with PfLDH. From the EMSA studies the dissociation constant (K_d) for the interaction was discerned as 0.35 ± 0.02 µM.

(A) *Development of aptamer based colorimetric detection for PfLDH*

P38 was exploited for the quantitative detection of PfLDH using salt or cationic surfactant mediated aggregation of AuNPs (of size 16 $\pm$ 3.5 nm) as an optical probe. Briefly, the aptamer binds to PfLDH in a malaria positive sample leaving behind the colloidal AuNPs in the solution, which are then rapidly aggregated by the salt or cationic surfactant, changing the solution to a blue color. The change in color was linearly correlated with the concentration of PfLDH producing a dynamic range for quantitative detection of the biomarker in samples. Among the three different cationic surfactants, characterized by different hydrocarbon tail groups, benzalkonium chloride (BCK) was found to be the most efficient one, with a limit of detection of 281 $\pm$ 11 pM. This BCK-based approach with the novel highly selective aptamer provided simple and sensitive detection of PfLDH in the clinically relevant range.

(B) *Development of aptasensor for electrochemical detection of PfLDH*

In the second approach the P38 aptamer was immobilized over glassy carbon electrode (GCE) using graphene oxide (GO) as an immobilization matrix, and the modified electrode was investigated for detection of PfLDH. The GO was synthesized from powdered pencil graphite and characterized by XRD based on the increased interlayer distance between graphitic layers from 0.345 nm for graphite to 0.829 nm for GO. The immobilization of P38 on GO was confirmed by I_D/I_G intensity ratio in Raman spectra where, the ratio were 0.67, 0.915, and 1.35 for graphite, GO and P38-GO, respectively. The formation of the P38 layer over GO-GCE was evident from an increase in the surface height in AFM analysis of the electrode from ~3.5 nm for GO-GCE to ~27 nm for P38-GO-GCE. The developed

aptasensor when challenged with the target, a detection of as low as 0.5 fM of PfLDH was demonstrated. The specificity of the aptasensor was confirmed through a voltametric measurement at 0.65 V of the reduced cofactor generated from the PfLDH catalysis. Studies on interference from some common proteins, storage stability, repeatability and analysis of real samples demonstrated the practical application potential of the aptasensor.

(C) DNA templated silver nanoclusters for fluorescence based detection of PfLDH

The third approach for detection of PfLDH exploited a fluorescence platform where a set of 90 mer long ssDNA candidates, with different degrees of cytosine (C-levels) (% and clusters) was analyzed for their function as suitable silver nanocluster (AgNC) nucleation scaffolds. The sequence P4 with the highest C-level (42.2 %) emerged as the only candidate supporting the nucleation process as evident from its intense fluorescence peak at λ_{660} nm. Shorter DNA subsets derived from P4 with only stable hairpin structures could support the AgNC formation. The secondary hairpin structures were confirmed by PAGE, and CD studies. The number of base pairs in the stem region also contributed to the stability of the hairpins. A shorter 29 mer sequence (Sub 3) (ΔG = -1.3 kcal.mole^{-1}) with 3 bp in the stem of a 7 mer loop conferred highly stable AgNC. NAD^+ strongly quenched the fluorescence of Sub 3-AgNC in a concentration dependent manner, and the binding constant and number of binding sites for NAD^+ were 0.201 L.mole^{-1} and 3.6, respectively. Time resolved photoluminescence (TRPL) studies revealed that the quenching involves a combined static and dynamic interaction process. A dynamic NAD^+ detection range of 50-500 μM with a limit of detection (LOD) of 22.3 μM was discerned. The NAD^+ mediated quenching of AgNC was not interfered by NADH, $NADP^+$, monovalent and divalent ions, or serum

samples. The method was also used to follow alcohol dehydrogenase and lactate dehydrogenase catalyzed physiological reactions in a turn-on and turn-off assay, respectively. The turn-off assay was applied for detection of PfLDH, achieving a LOD of 1.32 $\pm$ 0.03 nM. The proposed method with ssDNA-AgNC could therefore be extended to monitor other NAD^+/NADH based enzyme catalyzed reactions in a turn-on / turn-off approach.

(D) HRM of metallized-DNA duplexes for species differentiation of Plasmodium parasite

In order to carry out differentiation among *Plasmodium* species the metal mediated structural change in DNA was exploited to amplify HRM signals leading to differentiation of target DNAs in an orthologous gene (*pldh*) corresponding to four *Plasmodium* species. Conserved 26 mer ssDNAs from the *ldh* gene of four *Plasmodium* species were employed as targets. A capture probe (CP) that is fully complementary to the *P. falciparum* target (FT) and has two base mismatches each, with the targets of *P. vivax* (VT), *P. malariae*, (MT), and *P. ovale* (OT) was considered. The DNA duplexes were treated with metal ions for structural perturbation and then analyzed by HRM. Distinct resolution of melting fluorescence signal in otherwise identical HRM profiles for each of the DNA duplexes was achieved by using Ca^{+2} or Mg^{+2} ions, where, Ca^{+2} conferred higher resolution. The increase in resolution for CP-FT vs. CP-OT, CP-FT vs. CP-VT, CP-FT vs. CP-MT, CP-VT vs. CP-OT, and CP-MT vs. CP-OT with Ca-DNA as compared to control were 67.3, 20.4, 22.0, 10.9, 8.3 fold, respectively. The signal resolution was highest at pH 8. The method could detect 0.25 pmoles.μl^{-1} of the target DNA. CD analysis confirmed that Ca^{+2} and Mg^{+2} ions perturb the structure of DNA. This perturbation helped to improve HRM signal resolution among DNA targets corresponding to the orthologous *pldh* gene of the four *Plasmodium* species. This

novel approach has great application potential not only for *Plasmodium* species specific diagnosis but also for differentiation of other DNAs with minor sequence variation.

List of Abbreviations

ACT	Artemisinin combination therapy
ADH	Alcohol dehydrogenase
AFM	Atomic force microscopy
AgNC	Silver nanocluster
ANG	Angipoietin
AO	Acridine orange
APAD	3-Acety pyridine adenine dinucleotide
APADH	3-Acety pyridine adenine dinucleotide hydrate
ATP	Adenosine triphosphate
AuNP	Gold nanoparticle
BCK	Benzalkonium chloride
BLASTP	Protein Basic local alignment search tool
BSA	Bovine serum albumin
CD	Circular dichroism
CDC	Centers for disease control and prevention
CM	Cerebral malaria
CP	Capture probe
CPE	Constant phase element
CSF	Cerebrospinal fluid
CTAB	Cetyl trimethyl ammonium bromide
CXCL	Chemokine interferon inducible protein
DAB	3,3'-Diaminobenzidine
DBT	Department of biotechnology
DDAB	Didodecyl dimethyl ammonium bromide
DMSO	Dimethyl sulfoxide
DNA	Deoxyribonucleic acid
DPV	Differential pulse voltammetry

EDTA	Ethylenediaminetetraacetic acid
EIS	Electrochemical impedance spectroscopy
ELISA	Enzyme linked immunosorbent assay
EMSA	Electrophoretic mobility shift assay
EPO	Erythropoietin
FAM	Carboxyfluorescein
FCM	Flow cytometry
FT	*P. falciparum* target
FTIR	Fourier transform infrared spectroscopy
G6PD	Glucose 6-phosphate dehydrogenase
GCE	Glassy carbon electrode
GNI	Gross national income
GO	Graphene oxide
GTS	Giemsa thick smear
GTTS	Giemsa thick and thin smear
HEPES	(4-(2-hydroxyethyl)-1-piperazineethanesulfonic acid)
hLDH	Human lactate dehydrogenase
hLDH A	Human lactate dehydrogenase A form
hLDH B	Human lactate dehydrogenase B form
HPLC	High performance liquid chromatography
HRM	High resolution melting
HRP II	Histidine rich protein II
HSA	Human serum albumin
ICAM	Intracellular adhesion molecule
ICMR	Indian council of medical research
IHEC	Institute human ethics committee
IL	Interleukin
IPTG	Isopropyl β-D-1-thiogalactopyranoside
iRBC	Infected red blood cell
ITC	Isothermal titration calorimetry

LAMP	Loop mediated isothermal amplification
LB	Luria Bertani
LDH	Lactate dehydrogenase
LDMS	Laser desorption mass spectrometry
LED	Light emitting diode
LOD	Limit of detection
mAb	Monoclonal antibody
MDR	Multi drug resistance
MM	Mild malaria
MOPS	3-morpholinopropane 1-sulfonic acid
MP	Microparticle
MQ	Milli-Q
MSP	Merozoite surface protein
MT	*P. malariae* target
MeT	Melting transition
MWCNT	Multiwalled carbon nanotube
NAD	Nicotinamide adenine dinucleotide
NADH	Nicotinamide adenine dinucleotide hydrate
NC	Nanocluster
NMR	Nuclear magnetic resonance
NTA	Nitrilotriacetic acid
NTB	Nitro tetrazolium blue
OD	Optical density
ORF	Open reading frame
OT	*P. ovale* target
PAGE	Polyacrylamide gel electrophoresis
PAH	Poly (diallyldimethylammonium chloride)
PBS	Phosphate buffered saline
PCR	Polymerase chain reaction
PDB	Protein data bank

PDDA	Poly (allylamine hydrochloride),
PfGDH	*Plasmodium falciparum* glutamate dehydrogenase
PfHsp	*Plasmodium falciparum* heat shock protein
PfLDH	*Plasmodium falciparum* lactate dehydrogenase
pGDH	Parasite glutamate dehydrogenase
pLDH	Parasite lactate dehydrogenase
PLIP	Protein-ligand interaction profiler
PmLDH	*Plasmodium malariae* lactate dehydrogenase
PoC	Point of care
PoLDH	*Plasmodium ovale* lactate dehydrogenase
PVDF	Polyvinylidene fluoride
PvLDH	*Plasmodium vivax* lactate dehydrogenase
QBC	Quantitative buffy coat
QD	Quantum dot
qPCR	Quantitative polymerase chain reaction
RBC	Red blood cell
RCF	Relative centrifugal force
RDT	Rapid diagnostic test
RMSD	Root mean square deviation
RNA	Ribonucleic acid
RSD	Relative standard deviation
RT	Room temperature
RT-PCR	Real time polymerase chain reaction
SAM	Self assembled monolayer
SD	Standard deviation
SDS	Sodium dodecyl sulfate
SELEX	Systematic evolution of ligands by exponential enrichment
SERS	Surface enhanced raman spectroscopy
SG	SYBR green I
SM	Severe malaria

SNP	Single nucleotide polymorphism
SPR	Surface plasmon resonance
ssDNA	Single stranded DNA
sTNF-R	Soluble tumour necrosis factor receptor
TAE	Tris acetate EDTA
TBE	Tris borate EDTA
TEM	Transmission electron microscopy
TRPL	Time resolved photoluminescence
TSS	Transformation and storage solution
USD	United States dollars
UV	Ultra violet
VT	*P. vivax* target
WB	Western blot
WHO	World health organization
XRD	X-ray diffraction spectroscopy

List of symbols

%	Percent
~	Approximately
<	Lesser than
=	Equal to
>	Greater than
≥	Greater than equal to
°C	Degree Celsius
µA	Microampere
µcal	Microcalorie
µg	Microgram
µl	Microliter
µM	Micromolar
µmole	Micromole
2D	Two dimensional
3D	Three dimensional
A	Ampere
Å	Angstrom
a.u.	Arbitrary units
bp	Basepair
c	Concentration
c(S)	Continuous distribution of sedimentation coefficient
cal	Calorie
cm	Centimeter
d	Interlayer spacing
Da	Dalton
ε	Extinction coefficient
F	Fluorescence in the presence of quencher

fM	Femtomolar
F_o	Fluorescence in the absence of quencher
g	Gram
h	Hour
Hz	Hertz
K_a	Association constant
kb	Kilobasepair
kcal	Kilocalorie
k_{cat}	Turnover number
K_d	Dissociation constant
K_D	Stern Volmer constant
kDa	Kilodalton
kHz	Kilohertz
k_q	Bimolecular quenching constant
kV	Kilovolt
L	Liter
M	Molarity
mA	Milliampere
mdeg	Millidegree
mg	Milligram
min	Minute
ml	Milliliter
mM	Millimolar
mm	Millimeter
mV	Millivolt
Mw	Molecular weight
MΩ	Mega ohm
N	Normality
n	No. of binding sites
ng	Nanogram

nM	Nanomolar
nm	Nanometer
nmole	Nanomole
ns	Nanosecond
pg	Picograms
pM	Picomolar
pmole	Picomole
Q	Quencher
R^2	Regression coefficient
Rct	Charge transfer resistance
rpm	Revolutions per minute
Rs	Solution resistance
S	Second
$S°_{20,w}$	Limiting sedimentation coefficient
$S_{20,w}$	Sedimentation coefficient at 20°C, in water
T	Temperature
τ	Fluorescence lifetime
T_m	Melting temperature
V	Volt
v/v	Volume/volume
w/v	Weight/volume
Wt	Weight
X	Times concentrated
x g	Centrifugation speed in RCF
Zw	Warburg impedance
ΔG	Change in free energy
ΔH	Change in enthalpy
ΔS	Change in entropy
Ω	Ohm

List of Figures

List of Tables

Introduction

Malaria is a life threatening disease occurring mainly in the tropical regions of developing and under developed countries. Most of these affected countries have a low gross national income (GNI) per capita and cannot adequately afford widespread application of malaria surveillance and control programs. In such countries, due to limited access to diagnostic centers, patients often resort to self-treatment of suspected malaria cases. Indiscriminate use of oral artemisinin based monotherapies has been identified as one of the factors that leads to drug resistance, which is a serious problem in malaria management. For example, a sulfadoxine-pyrimethamine combination, which is an effective treatment against multi drug resistant (MDR) malaria, has now been rendered useless in south-east Asia by its overuse and misuse (Choi *et al*., 2007). According to WHO, accurate and point of care (PoC) diagnosis of malaria are prerequisite in malaria management as these reduce evolution of multi drug resistant malaria caused by indiscriminate and overuse of drugs (Choi *et al.*, 2007), lessen mismanagement of non-malaria fevers (Chanda *et al*., 2009), offer improved care of parasite positive patients and raise public trust in the efficacy of artemisinin-based combination therapy (ACT).

Most symptomatic malaria infections are preceded and followed by a PCR positive phase which is submicroscopic. The length of this submicroscopic period varies with the age of the patients. The sexual gametocytes responsible for disease transmission can also exist at submicroscopic levels. The group of people with these submicroscopic infections in

endemic areas are contributors to the human infectious reservoir. In order to make malaria control and elimination programs more effective further effort needs to be made towards diagnosing these submicroscopic infections. Sensitive malaria detection techniques can not only reduce the presumptive treatment associated with antimalarial drug resistance but also facilitate the treatment of submicroscopic infections that have so far been widely ignored.

In order to develop an efficient test for diagnosis of malaria, a profound understanding on various malaria related biomarkers is prerequisite. Among the biomarkers identified till date, *Plasmodium* species lactate dehydrogenase (LDH) has emerged as a highly promising target. It is the last enzyme in the glycolytic cycle of the parasite and is involved in the reduction of pyruvate to lactate thus regenerating the NAD^+ cofactor. During the intra-erythrocytic stages, the parasite principally relies on anaerobic respiration for ATP generation from glucose, leading to an over expression of enzymes involved in the glycolytic pathway (Roth, 1990). Parasite LDH differs structurally and kinetically from its human counterparts. Structurally it has been shown to exhibit unique epitopes present on the surface of the enzyme (Hurdayal *et al.*, 2010). Kinetically it differs in the lack of substrate inhibition (Brown *et al.*, 2004) and higher affinity towards a cofactor analogue $APAD^+$ (3-Acetyl pyridine adenine dinucleotide) (Chaikuad *et al*., 2005). These differences make this parasite enzyme unique and easier to target using diagnostic methods.

At present, several analytical techniques exist for malaria diagnosis. However, these techniques are associated with certain limitations. Conventional malaria diagnosis techniques, like microscopy, ELISA and flow cytometry require skilled personnel and

expensive equipment facility, and thus these are difficult to use in PoC settings. The recent PoC malaria diagnostics largely belong to antibody based rapid diagnostic tests (RDTs). While these portable RDTs have greatly benefitted malaria control and surveillance programs, they are still plagued with issues related to high cost, poor stability in tropical climates, being non-quantitative and incapable of differentiating different *Plasmodium* species. These RDTs are susceptible to malfunction at high temperature and humidity due to the use of protein based antibody, which is a labile bio recognition element (Chiodini *et al*., 2007). Hence, the current interest in malaria diagnosis focuses on the development of robust recognition materials that are stable in hot and humid climate due to obvious reason of the malaria prevalence in these climatic conditions.

DNA based probes have received wide interest for different diagnostics applications due to various positive traits such as, thermal stability, easy chemical synthesis and modification, and fairly low costs of production. DNA possesses its own set of intelligent material properties that could be selectively garnered to design viable bio recognition elements for specific sensor applications. The properties of DNA like, hybridization specificity, self-assembly, conductivity, and ease of functionalization add edge to its said bio recognition capabilities to develop tailored applications. This study aims to exploit the inherent property of DNA, and the intrinsic properties of advance nanomaterials for developing stable, sensitive, and specific sensing systems for *Plasmodium* species detection and differentiation. The following objectives are thus defined for this study:

Objectives of the study

1. **Preparation of biomarker and control proteins:** cloning, expression, purification, and characterization of *Plasmodium falciparum*, and human lactate dehydrogenases
2. **Preparation of DNA based biorecognition elements:** development of sensitive and specific aptamer, and DNA based probes to target PfLDH
3. **Application of developed biorecognition elements to detect the biomarker on optical and electrochemical platforms**

This thesis has been subdivided into VII chapters as briefly described below. At the end of the chapters, a section describing the overall conclusion from the thesis and a critical evaluation on the work with the scope for future work has been included.

Chapter I: Literature review

The objective of this chapter is to report the recent progress and status of malaria detection methods, with special emphasis on *Plasmodium falciparum* lactate dehydrogenase (PfLDH) targeted detection. The chapter discusses in detail, the most reliable malaria biomarkers and advantages of using PfLDH as the biomarker of choice. The performance of conventional malaria detection methods is pointwise compared to the more recent detection platforms and effort has been made to identify the important gaps to be bridged for developing viable products in the future.

Chapter II: Cloning, expression, and purification of *Plasmodium falciparum* and human lactate dehydrogenases

This chapter outlines the work done towards cloning, and purification of recombinant proteins PfLDH, and its human counterparts hLDH A, and hLDH B. The cloned ORFs were confirmed by sequencing studies. Integrity of purified proteins was validated by western blot, and kinetic studies.

Chapter III: Development of aptamer specific for PfLDH and its characterization

In this chapter, development of specific DNA aptamers against PfLDH was accomplished by the process of SELEX, including counter-SELEX against hLDH A, and hLDH B. The primary and secondary structures of the evolved aptamer candidates were determined. The selected candidates were further investigated to explore their specificity using different tools and techniques such as, EMSA, ITC and docking studies.

Chapter IV: Development of aptamer based colorimetric detection of PfLDH

This chapter entails the development of a colorimetric assay using citrate stabilized gold nanoparticles modified with PfLDH specific DNA aptamer as the sensing element. Salt, and cationic surfactant based assay systems were individually developed and compared for their performance for the detection of PfLDH.

Chapter V: Development of aptasensor for electrochemical detection of PfLDH

The content in this chapter describes the fabrication of graphene oxide-DNA aptamer (GO-DNA) modified electrode and its application for the electrochemical detection of PfLDH.

Detailed chemical, morphological, and electrochemical characterizations of synthesized GO, GO-DNA, and GO-DNA modified electrode were accomplished by XRD, Raman spectroscopy, AFM, and voltammetry studies. The performance parameters for the modified electrode were estimated.

Chapter VI: DNA templated silver nanoclusters for fluorescence based detection of PfLDH

This chapter describes the optimization of fluorescent silver nanocluster preparation on a ssDNA template. Stability studies were conducted at various pH, temperature, in the presence of denaturants, with time, leading to the selection of a stable, highly fluorescent nanocluster. This was applied to the enzymatic detection of PfLDH using the NAD^+ mediated quenching of the nanocluster. Performance parameters of the assay were also estimated.

Chapter VII: High resolution melting of metallized-DNA duplexes for species differentiation of *Plasmodium* parasite

This chapter discusses the development of a high resolution melting assay for species differentiation of *Plasmodium* parasite, by exploiting a conserved 26 mer sequence in the LDH gene of the parasite. Improvement in resolution of otherwise identical HRM profiles across the four major *Plasmodium* species was achieved leading to species differentiation.

Conclusion and future directions of research

This section summarizes the work to reach a logical conclusion. Along with the concluding statements a critical evaluation on the works embodied in this thesis has been included in this section. Additionally, the scope of augmenting the work for translating the proposed proof of concept to technologically viable products has been discussed at the end.

Chapter I

Review of Literature

The World Health Organization (WHO) estimated ~ 214 million new cases and 438,000 malaria related deaths in the year 2015. Approximately, 80 % of these cases were concentrated in just 15 countries, especially in the African continent (World Malaria Report, 2015). Malaria in humans is transmitted by the bite of more than thirty species of female anopheles mosquitoes. The causative agent is a protozoan parasite of the genus *Plasmodium*. Five species, *P. falciparum, P. vivax, P. malariae, P. ovale*, and *P. knowlesi* are known to infect humans. Characteristic symptoms of the disease include episodes of high fever followed by chills and rigors which are repeated every 48 h in *falciparum*, *ovale* or *vivax*, every 72 h in *malariae*, and 24 h in *knowlesi* infections. *P. vivax* hypnozoites can lie dormant in the liver and may cause recurrence of the disease (Centers for disease control and prevention, 2016). The bite of an infected female anopheles mosquito injects parasite sporozoites into the blood stream. Sporozoites invade the liver hepatocytes and proliferate into merozoites. Sporozoites divide profusely, where one *P. falciparum* sporozoite develops into 40,000 merozoites per liver cell within a period of six days. Sporozoites may differentiate into hypnozoites in *vivax*, and *ovale* infections, which can lie dormant in the liver and later enter the life cycle as merozoites. Drugs targeting hypnozoites are fairly rare, with only one drug family capable of killing them namely 8-aminoquinolines. Unfortunately, the drugs from this family are toxic to populations with glucose-6-phosphate dehydrogenase

(G6PD) deficiency, which ironically also happens to be a common deficiency in malaria prone regions. As a result, there is a great need of new non-toxic therapeutic approaches that target this stage of the parasite life cycle, to eliminate the recurrence of *P. vivax* and *P. ovale* infections.

At the beginning of the intraerythrocytic state, merozoites invade erythrocytes. The remodeled red blood cells (RBCs) start expressing PfEMP1 (*Plasmodium falciparum* erythrocyte membrane protein 1) on the erythrocyte membrane within 12 h of invasion, thus preventing the clearance of infected RBCs (iRBCs) by the spleen. The sequestration of infected RBCs eventually injures endothelial cells (ECs) and disrupts blood flow, causing tissue hypoxia and lactic acidosis. These mechanisms contribute to organ-specific syndromes such as, cerebral malaria and placental malaria when sequestration occurs in the brain, and placenta, respectively. Malaria related anemia is a consequence of hemolysis of infected and uninfected RBCs, often accompanied by impaired erythropoiesis. iRBCs when lysed, release merozoites causing fever and rigors in the infected person. The released merozoites now have a divided fate; while most invade fresh RBCs and circulate as ring-stage parasites, some develop into male and female gametocytes and are taken up by mosquitoes during a blood meal (Miller *et al.*, 2013).

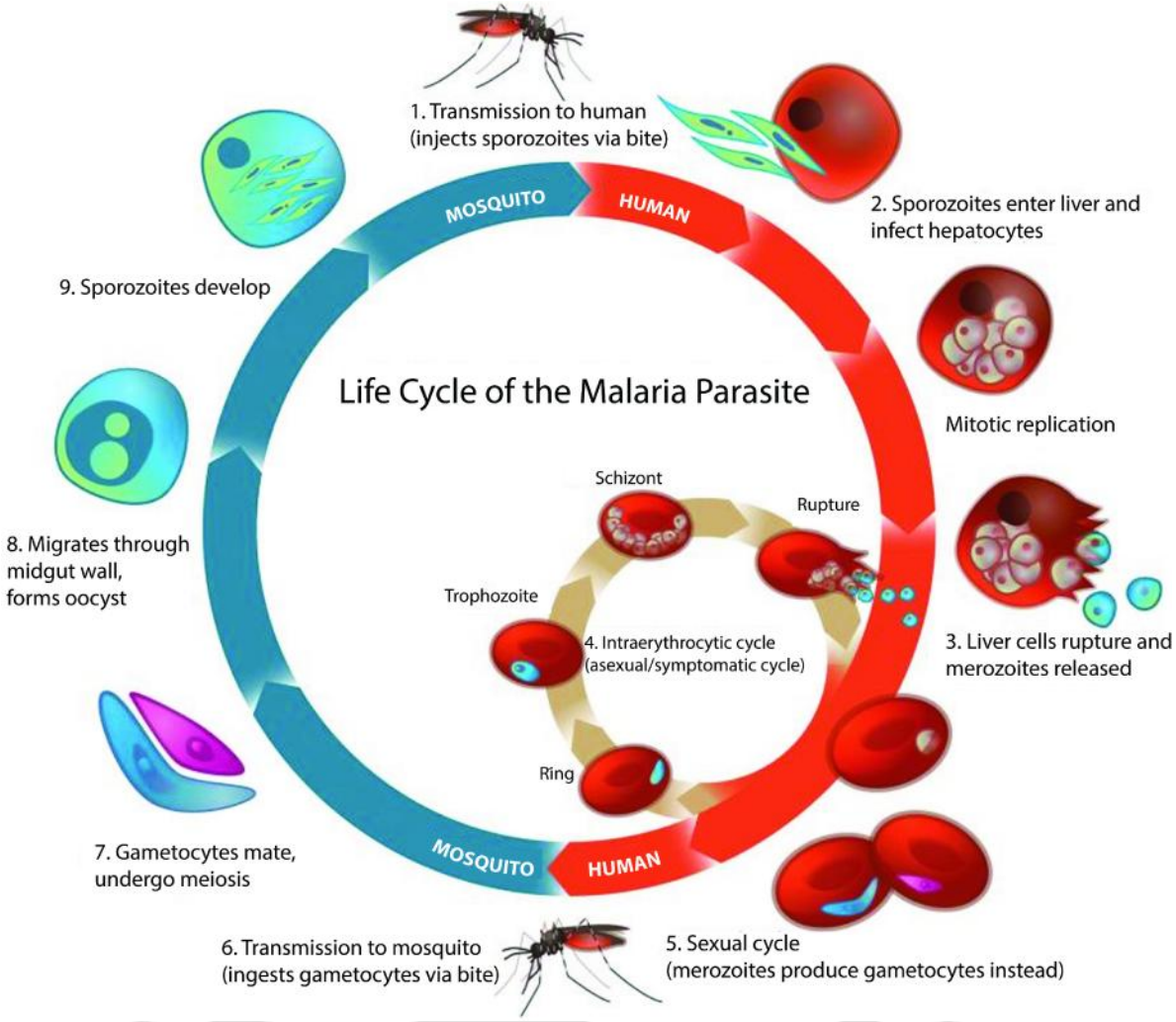

Figure 1.1: Life cycles of the malaria parasite (adapted with permission from Klein, 2013).

1.1 Biomarkers for malaria

Biomarkers are cellular, biochemical or molecular alterations measurable in biological samples which indicate any biological, pathogenic and therapeutic responses (Hulka, 1991). There has been no established classification system to categorize biomarkers till date. However, Frank and Hargreaves bring clarity to the subject by classifying them into three types; Type 0, Type 1 and Type 2 (Frank and Hargreaves, 2003). Type 0 biomarkers

are measures of the natural history of disease and correlate with clinical outcomes. Type 1 biomarkers usually determine the biological effect of a therapeutic intervention. Type 2 biomarkers are the equivalent of 'surrogacy' markers where a surrogate point has been defined as a biomarker intended to substitute for a clinical end point, the latter being a characteristic or variable that reflects how a patient feels, functions or survives. Biomarkers are useful for disease management, formulating strategies before the onset of disease, and for diagnosis in case of asymptomatic infections. For instance, in malaria endemic areas like Africa, where transmission is high, many *P. falciparum* infected individuals exhibit asymptomatic malaria (Dal-Bianco *et al.,* 2007). The prevalence of these asymptomatic infections can be as high as 52 %. Detection of such asymptomatic infections can be accomplished by targeting antigenic biomarkers. Potential antigenic biomarkers for malaria have been summarized in table 1.1, and discussed in brief here. The list of antigenic malaria biomarkers is populated by some unique parasitic proteins like lactate dehydrogenase, histidine rich protein II, glutamate dehydrogenase, aldolase, and also an insoluble crystalline iron compound, hemozoin.

Table 1.1: Brief description of potential antigenic malaria biomarkers.

Antigenic Biomarker	Chemical nature	Localization	Salient features	References
pLDH[1]	Homotetrame-ric protein with each monomer of 34 kDa	Inside infected RBCs	Presence of five amino acid residue insertion (DKEWN) in active site loop. Ability to actively utilize synthetic cofactor $APAD^+$. Reduced pyruvate substrate inhibition.	Brown *et al.*, 2004; Dunn *et al.*, 1996; Shoemark *et al.*, 2007
HRP II[2]	A 35 kDa protein	Secreted in serum of infected patient	Unique tandem repeats (Ala-His-His-Ala-Ala-Asp). 3_{10}-helix conformation when bound to heme. Secreted in abundance in serum, CSF[3] and urine of infected patients.	Wellems and Howard, 1986; Schneider and Marletta, 2005
Hemozoin	*β*-hematin	Inside digestive vacuole of parasite	Consists of Fe (III) PPIX centro-symmetric dimmers linked by hydrogen bonds. Accumulates in the digestive vacuole of parasite and appears as cluster as observed under electron microscope.	Pagola *et al.*, 2000; Solomonov *et al.*, 2007
Aldolase	Homo tetrameric protein with each subunit of 40 kDa	Inside infected RBCs	High sequence diversity from host and has potential as a drug target. Used for following response to therapy as it is detected only at high parasetemia	Döbeli *et al.*, 1990; Tjitra *et al.*, 1999; Eisen and Saul, 2000

Continued…

pGDH[4]	Homohexam -eric protein, with each monomer of 49.5 kDa	Inside infected RBCs	Plays a role in parasite's redox metabolism Not found in host RBC making it a potent biomarker	Wagner *et al.*, 1998; Roth, 1990

[1]Parasite lactate dehydrogenase, [2]Histidine rich protein II, [3]Cerebrospinal fluid, [4]Parasite glutamate dehydrogenase

1.1.1 Antigenic malaria biomarkers

P. falciparum synthesizes a unique set of soluble HRPs during the asexual erythrocytic development denoted as HRP I, II, and III in order of their discovery (Howard *et al.*, 1986). HRP II is exclusive to *P. falciparum* and is found in both Knob$^+$ as well as Knob$^-$ strains. This protein is reported to function in the detoxification of heme by forming hemozoin (Leech *et al.*, 1984; Lynn *et al.*, 1999). HRP II has also been projected as a model vaccine against malaria (Kilejian, 1978). HRP II is transported from the parasite, through the host cell cytoplasm, to the culture supernatant *in vitro* (Howard *et al.*, 1986) which also accounts for its presence in the serum of plasma, cerebrospinal fluid and urine of infected patients (Parra *et al.*, 1991; Valle *et al.*, 1991). It is also present in the food vacuole (Desakorn *et al.*, 2005), the digestive vacuole (Sullivan *et al.*, 1996) and the membrane surface of infected RBCs (Rock *et al.*, 1987). In short, HRP II is secreted in abundance in the fluids of malaria patients which is also a reason for its importance as an antigen biomarker of malaria.

Various antibody based immunosensors targeting HRP II were formulated and studied on electrochemical and piezoelectric platforms. Antibodies functionalized with

advanced nanomaterials like, multiwall carbon nanotubes (MWCNTs) and Au nanoparticles (Sharma *et al.*, 2008), magnetic micro and nanoparticles (de Souza Castilho *et al.*, 2011), self-assembled monolayers (SAMs) of thioctic acid and 1-dodecanethiol (Sharma *et al.*, 2011a) have been used and shown to perform comparably to commercial dipstick based tests. Although HRP II based tests are promising, they suffer from their own set of disadvantages like, false positive results due to persistent HRP II antigenemia (Mayxay *et al.*, 2001, Kyabayinze *et al.*, 2008) thus preventing follow up response to therapy, and false negative results due to excess antigen in case of high parasitemia (Jelinek *et al.*, 1999) or HRP II gene deletion (Palmer *et al.*, 1998; Iqbal *et al.*, 2004; Lee *et al.*, 2006a).

Hemozoin is an insoluble microcrystalline product formed from the digestion of blood by *Plasmodium* species and few other species of blood-feeding parasites (Oliveira *et al.*, 1999; Chen *et al.*, 2001; Pisciotta *et al.*, 2005). Hemozoin plays a role as visible marker in identifying malarial parasites and hence, it is popularly termed as malaria pigment. The parasites infect the RBCs and digest hemoglobin resulting in release of amino acids and toxic free heme (ferriprotoporphyrin IX) which is polymerized to hemozoin. The crystal structure of hemozoin consists of an unusual polymer of hemes linked between the central ferric ion of one heme and a carboxylate side-group oxygen of another heme (Slater *et al.*, 1991). Hemozoin has been used as a biomarker for detecting malaria microscopically. In fact, the characteristic morphology of the crystals can also be considered to distinguish different species of parasites (Noland *et al.*, 2003). With renewed interest in malaria diagnosis exploiting hemozoin, several novel methods have been added to the portfolio recently (Pirnstill and Cote, 2015; Garrett *et al.*, 2015; Lukianova-Hleb *et al.*, 2014; Rebelo *et al.*,

2013, Newman *et al.*, 2008; Newman *et al.*, 2010). Magneto-optical technology, and dark field microscopy are two commonly used techniques to detect the malaria pigment. Laboratory and field evaluations of these methods bring to light some limitations associated with malaria detection using hemozoin. One crucial limitation is that hemozoin in ring-stage parasites younger than six hours is often overlooked and hence hemozoin is a poor biomarker for field samples primarily composed of young ring-stage parasites because the crystal is not present in detectable quantities (Delahunt *et al.*, 2014). As a direct consequence of this limitation, hemozoin based tests often fair badly when compared to RDTs (rapid diagnostic tests) or PCR based malaria detection (Mens *et al.*, 2010)

Aldolase is a key enzyme in the glycolytic pathway of the parasite. It catalyzes the cleavage of fructose-1,6-bisphosphate into glyceraldehyde-3-phosphate and dihydroacetone phosphate (Srivastava *et al.*, 1990). The enzyme is a homotetrameric protein with each subunit of approximately 40 kDa (Döbeli *et al.*, 1990). Many reports have shown poor sensitivities of aldolase RDTs which encouraged studying more on its genetic diversity. Lee *et al.* studied the diversity in *P. falciparum* and *P. vivax* aldolase and showed that the aldolase gene was highly conserved, indicating that antigenic diversity is not a cause of variable RDT sensitivity (Lee *et al.*, 2006b), and the reason for the poor performance of aldolase based RDT tests thus remains to be investigated.

Glutamate dehydrogenases (GDHs) are ubiquitous enzymes that occupy an important branch point between carbon and nitrogen metabolism. They are generally involved in ammonium assimilation (NADP dependant GDHs) or glutamate catabolism

(NAD dependant GDHs). *P. falciparum* expresses three GDH isozymes. PfGDH1 is a NADP dependent glutamate dehydrogenase, which is a homo hexamer with a subunit of 49,500 Da (Wagner *et al.*, 1998). It has been postulated to play a role in the parasite's redox metabolism (Roth, 1990). GDHs possess a unique N terminal residue extension not found in the mature human enzyme and are present throughout the intraerythrocytic cycle of the parasite. Furthermore, GDHs are absent in the host RBC making them a potent biomarker (Wagner *et al.*, 1998). PfGDH1 was used to detect the presence of *P. falciparum* using western blotting (Rodríguez-Acosta *et al.*, 1998). Monoclonal antibodies in combination with colloidal gold were used in an immuno-chromatographic assay for diagnosis of *P. falciparum*. This assay showed a sensitivity and specificity of 86.6 % and 96.4 %, respectively (Li *et al.*, 2005). Although both aldolase, and GDH are promising antigenic targets, their efficacy to act as reliable malaria biomarkers needs to be further established.

1.1.2 Parasite lactate dehydrogenase

RBC is a non-proliferating cell with a modest requirement of glucose (~5 µmole glucose. 24 h^{-1} per 10^9 RBCs). However, *Plasmodium* is a voracious scavenger of blood glucose that increases the RBC glucose consumption up to 100 fold. In case of *P. falciparum*, about 60-70 % of the glucose is converted to lactic acid and excreted; however this percentage varies amongst different *Plasmodium* species and *in vitro* culture conditions (Jensen *et al.*, 1983). During the intra erythrocytic stages, the parasite principally relies on anaerobic respiration for ATP generation from glucose, and the NAD^+ is regenerated by conversion of pyruvate to lactate while the mitochondria contributes minimally to the ATP pool (Fry *et al.*, 1990). This reaction is catalysed by lactate dehydrogenase (LDH), the final

enzyme of the glycolytic pathway in *Plasmodium*. The absence of F_0 a and b subunits of the mitochondrial F_0-F_1 ATP synthase further implies the absence of the role of mitochondria for energy generation. However, since parts of the genome sequence are still not known, and the genome being A+T rich that causes difficulty in identifying enzymes, the lack of role of mitochondria for energy generation cannot be ascertained (Olszewski and Llinás, 2011). Nevertheless, due to the parasite's dependence on the glycolytic cycle for energy generation, enzymes involved in this pathway are over expressed (Roth, 1990). It has been found that *P. falciparum* LDH (PfLDH) RNA expression level gradually increases, with the peak expression being at 24 to 30 h in the intra erythrocytic cycle. This expression declines to zero in the schizont stage. A similar profile which slightly lags behind the RNA expression was observed for the enzyme activity as well (Pfaller *et al.*, 1982). With the help of microarray technology using *P. falciparum* transcription it was demonstrated that all glycolytic enzymes are up regulated at the early trophozoite stage during the asexual cycle, coinciding with the time of maximum metabolic activity by the parasite (Bozdech *et al.*, 2003).

The parasite LDH (pLDH) is a tetramer, where each monomer consists of two domains (figure 1.2). The larger domain comprises the Rossman fold that binds the cofactor NADH, while the catalytic residues (His 195, Asp 168, Arg 171) are located in the other (smaller) domain. These residues are conserved across all *Plasmodium* species except *P. knowlesi*, which lacks His 195. The active site of the enzyme is located between these two domains. Each monomer of the pLDH protein binds to one NADH molecule, and each of the four cofactors occupies identical positions in each monomer (Brown *et al.*, 2004).

Protozoal LDHs display some major structural and kinetic differences from their mammalian counterparts that may be exploited to develop selective drugs and detection systems for malaria. PvLDH (*Plasmodium vivax* LDH) and PfLDH share 26 % and 29 % sequence identity respectively, with human LDH A (hLDH A). Structurally the parasite enzymes differ in having a five residue insertion in their active site loop which closes down over the active site during catalysis (Brown *et al.*, 2004) and also causes a displacement of ~1 Å of the nicotinamide moiety of the NADH cofactor (Dunn *et al.*, 1996; Winter *et al.*, 2003). This insertion "DKEWN" (D-Aspartic acid, E-Glutamic acid, K-Lysine, W-Tryptophan and N-Aspargine) was used as a common diagnostic epitope by Hurdayal *et al.* to selectively detect pLDH from human LDH isoforms (Hurdayal *et al.*, 2010). The five amino acid insertion initially observed for *P. falciparum* was later discovered in all five *Plasmodium* species and in the LDH I and II of *T.gondii* (Yang and Parmley, 1995, 1997). However, this feature was absent in few other apicomplexan parasites like *Cryptosporidium parvum,* which causes cryptosporidiosis, a parasitic infection of the mammalian intestinal tract.

Kinetically, the parasite enzyme differs from its mammalian counterparts in lacking substrate inhibition in the presence of excess pyruvate (Sessions *et al.*, 1997). In hLDH enzymes, substrate inhibition occurs because of the slow release of the reduced cofactor from the active site due to the formation of a covalent adduct with pyruvate. Reduced substrate inhibition in pLDH is attributed to a single amino acid substitution in the enzyme (Ser163Leu). This single amino acid mutation has also been exploited as a general method to reduce substrate inhibition in other L-lactate dehydrogenase enzymes (Hewitt *et al.*,

1999). Ser 163 (in hLDH) interacts with the amine group of NADH via hydrogen bond. This residue is mutated to Leu 163 in all pLDH, which removes substrate inhibition. However, the mechanism for the lower substrate inhibition has also been stated to be the weaker binding of pyruvate to enzyme-cofactor complex rather than slower release of NAD^+ (Gomez et al., 1997, Brown et al., 2004).

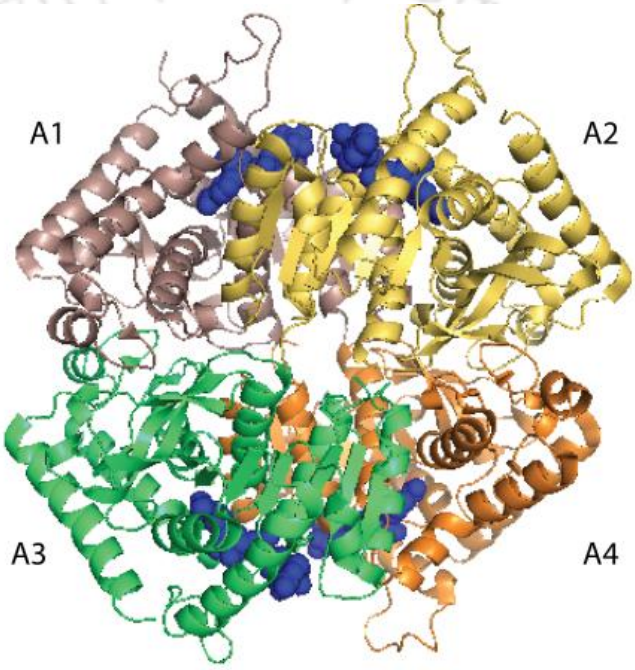

Figure 1.2: Crystal structure of *Plasmodium vivax* lactate dehydrogenase complexed to APADH, adapted from PDB file 2AA3, solved to a resolution of 2.05 Å. The structure shows the presence of four (A1-A4) identical monomer chains (coloured differently for clarity). One molecule of APADH (illustrated as blue spheres) binds to each monomer chain, in the Rossman fold (Chaikuad *et al.*, 2005).

Another kinetic difference is the ability of the pLDH to efficiently use the synthetic cofactor $APAD^+$ (3-Acetylpyridine adenine dinucleotide) (Dunn *et al.*, 1996, Chaikuad *et al.*, 2005). $APAD^+$ is a synthetic NAD^+ analogue which has a methyl group replacing the nicotinamide amide nitrogen (Figure 1.3 A). The structural basis of this preference may be the presence of a number of substitutions in the cofactor-binding groove of pLDHs that distinguish them from human LDHs. When the active site residues of PvLDH are overlaid with those of hLDH A, it becomes clear that the cofactor is displaced within the binding pocket, relative to its placement in human LDH enzymes (Figure 1.4). This displacement is observed in the nicotinamide moiety, which is shifted by about 1 Å relative to its position in the hLDH A structure. A similar displacement was also seen for the PfLDH enzyme. In PfLDH-APADH complexes, there is a displacement (0.45 Å) of both the acetyl-pyridine ring of APADH and of the imidazole ring of His 195 in the APADH structure when compared to the NADH structure. Similarly for PvLDH-APADH complexes, there is a displacement of 0.3 Å of both the acetyl-pyridine ring of APADH and the imidazole ring of His 195 when compared to the NADH structure (Figure 1.3 B, C). Kinetically, increase in entropy on $APAD^+$ binding leading to a change in the rate of active site movement, or a higher oxidation potential of $APAD^+$ than NAD^+ leading to faster hydride transfer to $APAD^+$, are ascribed as few of the reasons for this cofactor preference by pLDHs (Chaikuad *et al.*, 2005).

Another striking difference of pLDH from other dehydrogenases is its substrate specificity due to long substrate specificity loop. The enzyme efficiency decreases with the increase in number of methylene groups in the substrate, as seen when pyruvate is replaced

with α-ketobutyrate as a substrate. Also the enzyme does not show an activity with phenylpyruvate (Shoemark *et al.*, 2007), a behaviour that distinguishes the enzyme from the LDH of *T. gondii*. Although LDH from *P. falciparum* and *T. gondii* have very similar structures, the latter has an additional loop insertion of two residues and several changes in its active site that renders it this contrast property (Kavanagh *et al.*, 2004, Dando *et al.*, 2001). A characteristic feature of this family of enzymes is that the value of K_m for substrates is pH dependent, as the substrate pyruvate binds only when the active site histidine is in the protonated state (Baldwin, 2000).

pLDH is an attractive target for anti-malarial drug design because of its three important attributes: (1) It controls the production of ATP in the parasite, (2) It has unique amino acids at the active site compared to its counter parts from other species, (3) The protein data bank (PDB) contains many x-ray cryatallographic structures of pLDH complexed with various compounds which provide ideal targets for modelling of inhibitors. From the inhibition studies of various compounds including gossypol and its derivatives against the parasite enzyme pLDH (Royer *et al.*, 1986; Deck *et al.*, 1998; Cameron *et al.*, 2004; Conners *et al.*, 2005; Menting *et al.*, 1997; Read *et al.*, 1999) it has been revealed that these compounds specifically target pLDH and not hLDH. These findings underline the fact that there are vast structural and kinetic differences between the two enzymes that may be exploited for selective detection of pLDH for malaria diagnosis.

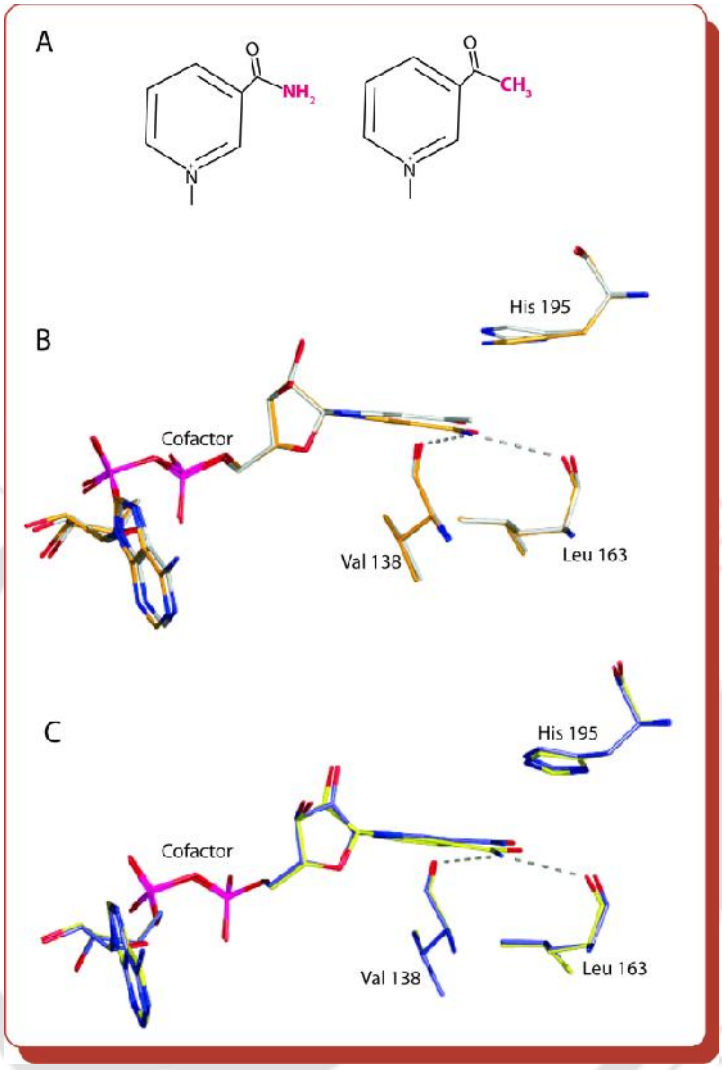

Figure 1.3: Placement of APADH and NADH in *Plasmodium* LDH enzymes. (A) Scheme of the chemical composition of the nicotinamide ring of NADH and the equivalent acetyl-pyridine ring in APADH. The nicotinamide amine group is replaced by an acetyl group in APADH. (B) Overlay of PfLDH-APADH (off-white) and PfLDH-NADH (orange) structures. (C) Overlay of PvLDH-APADH (blue) and PvLDH-NADH (yellow) structures (Chaikuad *et al.*, 2005).

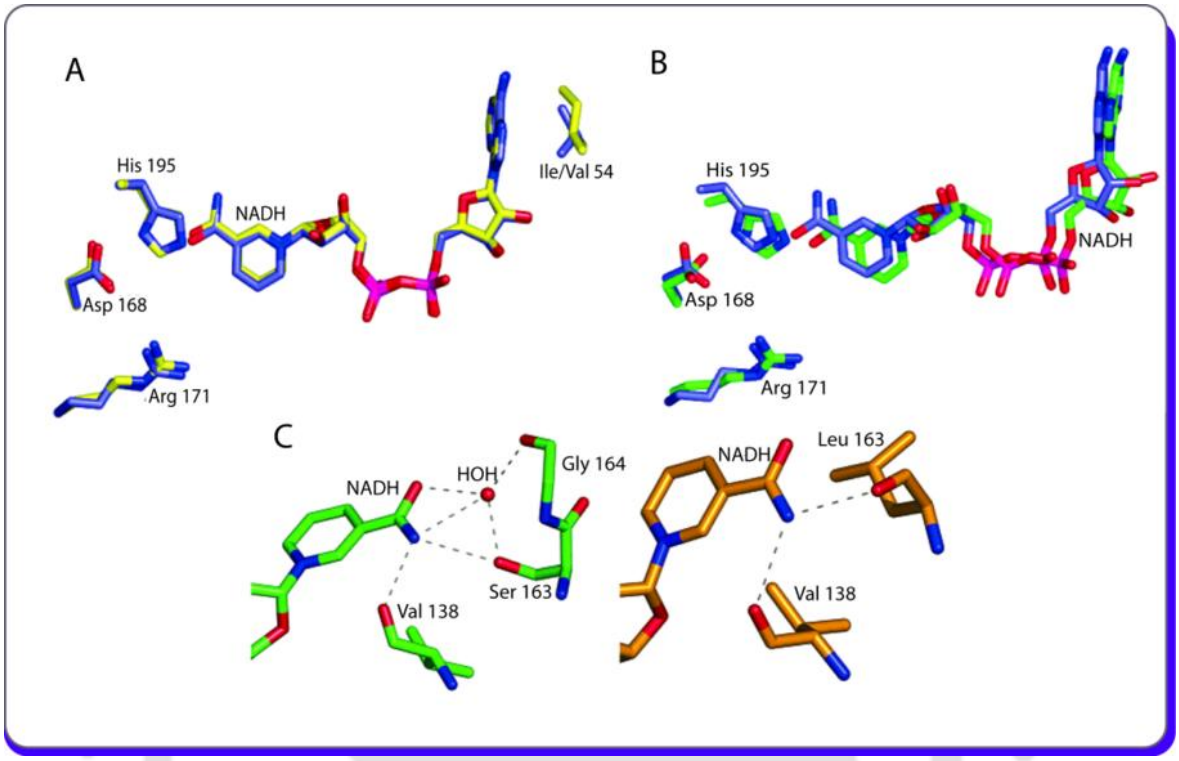

Figure 1.4: Cofactor placement in *Plasmodium* and human LDH enzymes. (A) Overlay of NADH from PvLDH-NADH (blue) and PfLDH-NADH (yellow) complexes with catalytic residues shown. Residue 54 is an isoleucine in PvLDH and a valine in PfLDH. (B) Overlay of NADH from PvLDH-NADH (blue) and hLDH A-NADH (green) complexes with catalytic residues shown. (C) Detail of binding interactions between the nicotinamide group, position 163, and surrounding residues. Left panel (green) shows the arrangement for human (and all non-apicomplexan) LDHs; right panel (gold) shows the same region from *Plasmodium* LDH structures. Hydrogen bonds are shown as dashed lines, and the conserved bound water molecule is shown as a red sphere (Chaikuad *et al.*, 2005).

1.1.3 Serological markers

Cerebral malaria (CM) is a life threatening complication of malaria and is defined as an unarousable coma with a *P. falciparum* infection in the absence of other causes of encephalopathy. If left untreated, it is fatal within 24-72 h (Lucchi *et al.*, 2011). The advantage of an early immunologically relevant serological biomarker for CM would be to stratify febrile patients into groups: those likely to develop CM and those likely to develop severe malaria (SM) or mild malaria (MM). Although no clear biomarkers have yet been identified for CM, several tentative biomarkes for CM have been investigated. Serum levels of chemokine interferon inducible protein (CXCL10 and CXCL4) (Armah *et al.*, 2007; Olszewski and Llinás, 2011), soluble tumor necrosis factor receptor (sTNF-R), soluble Fas ligand (sFas) (Armah *et al.*, 2007), interleukin-8 (IL-8), interleukin 1 receptor antagonist (IL-1ra), TNFα, (John *et al.*, 2008), endothelial regulators like angipoietin-I (ANG I), and ANG II (Lovegrove *et al.*, 2009; Conroy *et al.*, 2009), a neuroprotective factor, erythropoietin (EPO) (Casals-Pascual *et al.*, 2008), soluble adhesion molecules like intracellular adhesion molecule-I (ICAM-I), vascular cell adhesion molecule-I (VCAM-I) (Jakobsen *et al.*, 1994), Complement system components like C3 (Wenisch *et al.*, 1997) are also affected during CM. Microparticles (MPs) are fragments of plasma membrane shed by various cell types under physiological stress conditions and have also been linked with pathophysiology (Freyssinet, 2003). MPs have been reported in the serum of patients suffering from malaria and diabetes (Haest, 1982; Frasch, *et al.*, 2004), systemic lupus erythematosus (Bernal-Mizrachi *et al.*, 2003), acute coronary syndromes (Andree and Nemerson, 1995) and in conditions of severe trauma (Jacoby *et al.*, 2001). There is a

dramatic difference in the plasma levels of MP of endothelial origin among Malawian children suffering from CM, severe malarial anaemia and uncomplicated malaria caused by *P. falciparum* (Combes *et al.*, 2004).

The serological biomarkers however, are difficult to use reliably in diagnosing malaria. For instance CXCR3 and its ligands have been implicated in case of several neurological diseases like, west nile virus (Klein *et al.*, 2005; Zhang *et al.*, 2008), *Toxoplasma gondii* (Olszewski and Llinás, 2011) and HIV infections (Sui *et al.*, 2004). Serological biomarkers may be used to indicate CM only after the malaria diagnosis is confirmed using an antigenic biomarker. Antigenic markers detect malaria by a more direct and reliable approach. On thorough investigation of the available literature on antigenic markers, pLDH emerges as the most established malaria marker for accurate, and sensitive detection of the disease. Our efforts are hence aimed towards detection of this potential malaria marker.

1.2 Detection of malaria

1.2.1 Microscopy and conventional analytical techniques

Microscopy for malaria diagnosis has been used since the year 1904 when Gustav Giemsa introduced a mixture of methylene blue and eosin to stain the parasite (Fleischer, 2004). This method is however time consuming, labour intensive and requires expert skills. To enhance the sensitivity of microscopic detection, fluorescent microscopy using fluorophores such as, acridine orange and benzothiocarboxypurine have frequently been used in addition to quantiative buffy coat technique. Although microscopy was considered

as “gold standard” for malaria diagnosis, recent reports suggest otherwise. Bayesian latent class models were used to estimate sensitivities and specificities of various diagnostic tests and revealed that microscopy is a poor reference test (Goncalves *et al.*, 2012). Other limitations include the requirement of skilled personnel, low sensitivity (100 to 200 parasites.μl^{-1} of blood), poor species identification especially of *P. knowlesi* due to its similarities with *P. falciparum* in the early ring form stage and *P. malariae* in the later stages. Therefore, microscopy should be used in combination with other alternative methods (e.g. PCR, and RDTs) to improve the sensitivity of detection (Chua *et al.*, 2015).

Nucleic acid techniques such as PCR (Oddoux *et al.*, 2011; Lee *et al.*, 2002), nested PCR (Lee *et al.*, 2012a; Morassin *et al.*, 2002), and LAMP (loop mediated isothermal amplification) have also been used for malaria detection. LAMP can be conducted under isothermal conditions and does not need expensive thermocyclers (Lee *et al.*, 2012a). qRT-PCR assay using dsDNA intercalating dye are cheaper compared to using fluorescent probes. However, intercalating dyes usually also bind to non-specific dsDNA sequences leading to an increase in false positives. Also this method is not suitable to target DNA greater than 500 bp, as this causes a hindrance to strand displacement (Lau *et al.*, 2011). A relatively new analytical method known as High Resolution Melting (HRM) has been garnering increased interest, and is now often used in combination with qPCR to identify variations in nucleic acid sequences, and improve the accuracy of PCR based assays. This post-PCR method generates melting (dissociation) curves of DNA duplexes using improved dsDNA-binding dyes on a specialized instrument with extremely precise temperature ramp

control and advanced data capture capabilities. Using this methodology, minor differences in otherwise unresolvable DNA targets can be explored (Erali *et al.*, 2008).

Flow cytommetry (FCM) and automated blood cell counting techniques can be used to detect hemozoin or *Plasmodium* dsDNA in infected erythrocytes. However, the use of *Plasmodium* dsDNA as a marker in flow cytometry can result in false positives because pathological conditions are characterized by an efflux of normoblasts and erythroblasts in blood (Malleret *et al.*, 2011). LDMS (laser desorption mass spectrometry) detects small molecules (<1.5 kDa) like, phospholipids and porphyrins, hence it is ideally suited for heme detection. Hemozoin strongly absorbs UV light resulting in vaporization of individual heme molecules which can then be detected by LDMS. However, this detection is only semi quantitative and cannot differentiate between species (Feldman, 2006).

A unified sandwich ELISA (enzyme linked immunosorbent assay) targeting PfLDH and HRP II was reported that allowed concurrent measurement of the biomolecules (Martin *et al.*, 2009). ELISA is an efficient method to detect malaria in a short time frame. Despite the advantages such as, high sensitivity, the application of ELISA remains restricted to research settings and blood bank screening where large number of samples have to be screened every day (Noedl *et al.*, 2006). Conventional methods for malaria detection have been summarized in Table 1.2.

Table 1.2: Comparison on critical performance parameters among different conventional techniques (yellow and green), including lab based (yellow) and advanced techniques (blue) for malaria detection. Part of the table adapted with permission from Tangpukdee *et al.*, 2009.

Types of test	Principle of the method	Instrument used	Sensitivity and specificity	Detection limit *	Response time (min)
Peripheral blood smears (PBS)	Morphological changes in the stages of parasite by thick and thin blood smears	Optical microscope	Depends on the instrument quality and the skill of the handler	50-100	30-60
Quantitative buffy coat (QBC)	Blood staining by acridine orange (AO)	Epi-fluorescent microscope	Non specific: AO stains DNA from all cell types High variation in sensitivity at lower parasitemia	>5	<15
RDTs	Detection based on antigen- antibody interactions and enzyme assay	Disposable dipsticks	Moderate at higher parasitemia (>100 parasite.μl^{-1})	50-100	10-15
PCR	Specific amplification of malaria DNA	Thermocycler	High	≥1	45-360 depending on the methods
Serological tests	Detection of malaria antigen or anti-parasite antibodies in blood	Microplate reader (for ELISA)	Relatively high	Not mentioned	30-60
LAMP	Detection of turbidity after amplifying DNA sequences	Turbidity meter	High	>5	<60

Continued…

Microarrays	Hybrization of DNA and quantification by fluorescent based detection	DNA chip	High	Not mentioned	<60
Flow cytometry	Detection of hemozoin	Flow cytometer	Variable sensitivity, high specificity	Poor correlation with parasitema	<1
Automated blood cell counters	Detection of hemozoin in activated monocyte	Hematology analyzers	Variable sensitivity and specificity	5-20	<1
Mass spectrometry	Identification of heme	Laser desorption mass spectrometry	Undetermined	100 for whole blood	<1
Electrochemical aptasensor (Lee *et al.*, 2012b)	Aptamer specific to PvLDH immobilized on gold electrode	Electrochemical impedance spectroscopy	High sensitivity	108.5 fM for PvLDH and 120.1 fM for PfLDH	Not mentioned
Colorimetric aptasensor (Cheung *et al.*, 2013)	AuNP[1]-Aptamer-Salt	Spectrophotometer	High	57 pg.μL^{-1} for PfLDH	~10
(Jeon *et al.*, 2013)	AuNP-Aptamer-Cationic polymer	Spectrophotometer	High	For PvLDH: 8.7 pM and 8.3 pM using polymers PDDA[2], PAH[3] respectively	~10
(Lee *et al.*, 2014)	AuNP-Aptamer-Cationic surfactant	Spectrophotometer	High	1.25 pM for PvLDH	~10
Fluorescence aptasensor (Geldert *et al.*, 2016)	FAM[4]-aptamer-MoS_2 nanosheets	Spectrofluorometer	High	550 pM for PfLDH	10

*Unit in parasite.μl^{-1}, unless otherwise mentioned. [1]Gold nanoparticle, [2]Poly (diallyldimethylammonium chloride), [3]Poly (allylamine hydrochloride), [4]Carboxyfluorescein

1.2.2 Rapid diagnostic test (RDT)

RDTs are quick and portable immuno-chromatographic dipsticks whose sensitivity generally reaches >95 % at *P. falciparum* density of 1000-2000 parasites.μl^{-1} (Bjorkman and Martensson, 2010). They rely on capture of parasite antigen from peripheral blood using monoclonal antibodies conjugated to either a liposome containing selenium dye or gold particles. A second monoclonal antibody applied to a strip of nitrocellulose acts as the immobile phase. The antigen-antibody complex in the mobile phase, migrates along the strip and is captured by the monoclonal antibody of the immobile phase, thus producing a visible coloured line (Moody, 2002).

Dipsticks can be divided into two classes based on their target antigenic biomarkers namely: HRP II (only for *P. falciparum*) and pLDH. Most commercial RDTs that detect *P. falciparum* target HRP II and few others target pLDH. To enhance the efficiency of malaria detection, RDTs targeting many biomarkers at the same time were prepared. The combined immuno-chromatographic malaria dipstick targets HRP II and aldolase for the diagnosis of *P. falciparum* and *P. vivax* (Tjitra *et al.*, 1999; Eisen and Saul, 2000). The authors suggest using aldolase based RDT for monitoring response to therapy as it is sensitive only at higher parasitemia in sample. Another combined dipstick CareStart™ (Access Bio, Princeton, USA) Malaria HRP II /pLDH Combo Test performed well for detection of *P. falciparum* (based on HRP II) and pan LDH for non-*falciparum* infections, but sensitivities for *P. ovale* and *P. malariae* were poor (Maltha *et al.*, 2010).

Dipstick operation is varied and may include dipping a nitrocellulose test strip into a blood specimen, placing a blood drop directly on the test strip, or onto a sample pad

impregnated with labelled monoclonal antibody (mAb). Results are usually obtained in 5-15 min (Chansuda, 2001). In many ways dipsticks appear ideal: they are rapid (<30 min) and can be easily used by healthcare workers or semi-skilled volunteers.

Variations in RDT performance have been seen with season, year, age of patient, presence or absence of fever during consultation (Abeku *et al.*, 2008). The most common cause of poor performance of RDTs on the tropics is exposure to high temperature/humidity (Jorgensen *et al.*, 2006). The loss in activity is attributed to damage to monoclonal antibodies or the nitrocellulose membrane. This was further confirmed in another report (Chiodini *et al.*, 2007) where five RDTs from the same lot were stored at different temperatures of 35 °C, 45 °C and 60 °C. Although dipsticks are widely used they have certain limitations such as, poor species and stage differentiation and quantification, false positives results due to persistent HRP II antigenemia (Mayxay *et al.*, 2001, Kyabayinze *et al.*, 2008) and rheumatoid factors in some patients (Laferi *et al.*, 1997; Iqbal *et al.*, 2000), false negative results due to excess antigen in case of high parasitemia (Jelinek *et al.*, 1999) or HRP II gene deletion (Palmer *et al.*, 1998; Iqbal *et al.*, 2004; Lee *et al.*, 2006a). The sensitivity of Parascreen™ (Zephyr Biomedical Systems) was found low for *P. falciparum* infections. This RDT was not acceptable for malaria diagnosis under the field conditions in the Peruvian Amazon due to HRP II and HRP III gene deletions in the malaria parasite genome (Gamboa *et al.*, 2010; Maltha *et al.*, 2012; Bendezu *et al.*, 2010). Since HRP II persists after parasite clearance, the presence or absence of pLDH appears to be a more reliable diagnostic target, as it is produced by live parasites (Palmer *et al.*, 1998; Makler *et al.*, 1998; Piper *et al.*, 1999). HRP II antigenemia is suspected to be a result of gametocytemia (Tjitra *et al.*, 2001).

Genetic polymorphism may lead to false negative results as was observed when a country wise assessment of polymorphism was carried out for HRP II, pLDH and aldolase genes in Madagascar. Higher levels of polymorphism was observed for HRP II and HRP III genes predicting that about 9 % of Malagasy isolates could not be detected at parasite densities < 250 parasites.μl^{-1} (Mariette *et al.*, 2008). This genetic variation was seen both within and among different countries. Logistic regression analysis predicted that due to this variation only 84 % of the *P. falciaprum* infections in the Asia-Pacific region are likely to be detected at densities < 250 parasites.μl^{-1}. HRP III is also suspected to play a role in the performance of HRP II based tests (Baker *et al.*, 2005). However, a study on the assessment of plasma concentration, and hence the disease severity has indicated that sequence polymorphism is not a significant cause of variation in HRP II concentration in plasma samples from African children (Ramutton *et al.*, 2012). In African children it is a major challenge to distinguish severe *falciparum* malaria from other severe febrile illnesses with *P. falciparum* infection. Plasma HRP II has prognostic significance and provides a tool to assess the risk of ‘‘true’’ severe malaria as compared to other severe illnesses in parasitemic African children (Hendriksen *et al.*, 2012). This justifies the development of plasma HRP II concentration as a method for assessing severe *falciparum* malaria of African children.

Several reviews outline various RDTs (Murray and Bennett, 2008) and their evaluation reports (Chansuda, 2001). In spite of over 100 such reports their comparative assessment is, however difficult due to difference in population sizes, their clinical and epidemiological characteristics, different trial guidelines etc. (Wongsrichanalai *et al.*, 2007). A comparison of sensitivity and specificity of few prominent field evaluations has however

been attempted and is shown in table 1.3. It can be observed from the table that the sensitivity and selectivity of RDTs significantly vary over different studies and thus there is a need of more sensitive, selective and reliable method for rapid detection of malaria. One such effort was made by Peng *et al.* by developing the Wondfo rapid diagnostic test which is a nano-gold based immuno-chromatography assay that uses monoclonal antibodies. It is a more rapid and sensitive parasite detection method and results showed very good concordance with microscopy examination with a sensitivity and specificity of 95.49 % and 99.53 %, respectively (Peng *et al.*, 2012).

Table 1.3: Comparison on the performance factors of different dipstick RDTs as evaluated in some prominent reports.

Dipstick	Standard	Population	Sensitivity (%)	Specificity (%)	Reference
Carestart AccessBio, (Princeton, NJ, USA)	GTTS*	Southwestern Uganda	95.6	91.5	Fogg *et al.*, 2008
Vistapan Mitra, (New Delhi, India)			91.9	89.6	
Parabank Orchid/Zephyr, (Goa, India)			84.7	94.3	
Paracheck pf, Orchid/Zephyr, (Goa, India)			94	87.3	
Optimal-IT, DiaMed, (Cressier, Switzerland)	GTS**	Gabon	94	97	Mawili-Mboumba *et al.*, 2010
Acon, Acon Labs, (San Diego, CA)		Children under 11 years	94	90	
PALUTOP+4 ALL.DIAG, (Strasbourg, France)	GTTS* and PCR	Madagascar	95.4	97.1	Rakotonirina *et al.*, 2008
Optimal-IT, DiaMed, (Cressier, Switzerland)			75.8	99.0	
ParaHIT *f* Test, Span Diagnostic Ltd., (Surat, India)	GTTS* and PCR	Tanzania	69.2	100	Nicastri *et al.*, 2009
Malaria Pf™, ICT Diagnostics, (South Africa)	GTTS*	Uganda	98	72	Kyabayinze *et al.*, 2008

Continued…

Paracheck Pf, Orchid Biomedical Systems, (Goa, India)	GTTS*	Kenya	91.7	96.7	de Oliveira *et al.*, 2009
Malar-Check_*Pf* test, Cumberland Diagnostics, (USA)	GTS**	Brazil	97.4	88.5	Avila *et al.*, 2002
Makromed Dipstick Assay, Makro medical, (South Africa)	PCR	Cananda	97.0	96.0	Richardson *et al.*, 2002
ParaSight®-F, Becton Dickinson, (USA)	Thin blood smears and QBC malaria test	France	94	99	Uguen *et al.*, 1995
ParaSight®-F, Becton Dickinson, (USA)	Microscopy	Iquitos, Peru, and Maesod, Thailand	95	86	Forney *et al.*, 2001
Paracheck Pf, Orchid Biomedical Systems, (Goa, India)	Microscopy	India	93	84	Singh *et al.*, 2005
ParaHIT-f, Span Diagnostics, (Surat, India)	GTS**	Tanzania	90.7	73.5	McMorrow *et al.*, 2010
ParaHIT-f , Span Diagnostics, (Surat, India)	Microscopy	India	87.5	97	Singh *et al.*, 2005

* Giemsa thick smear
** Giemsa thick and thin smear

1.2.3 Advanced techniques: pLDH based biosensors

A biosensor is a self-contained integrated device that is capable of providing specific quantitative or semi-quantitative analytical information using a biological recognition element that is retained in direct spatial contact with a transduction element (Schmidt and

Schaechter, 2011). The bio recognition elements commonly reported for developing biosensors are enzyme, antibody, aptamer, DNA, and cells. The transduction principles widely used to develop biosensors are electrochemistry, piezoelectricity, and optical spectroscopy. Biosensor research holds promise for developing stable portable devices for rapid, sensitive, selective, reproducible and economical detection of many analytes of clinical importance. It has the advantage of being used by semi-skilled operators in point of care (PoC) testing and by patients themselves. However, research on biosensors for detecting malaria is in nascent stage as evident from the limited number of publications on the area. The bio recognition systems reported so far for developing malaria biosensors are mostly confined to aptamer and antibody.

Nucleic acid aptamers are single stranded DNA, RNA, modified RNA or DNA that can uniquely bind to a ligand with high affinity and specificity. Unique aptamer candidates are generally picked up from 10^{12}-10^{15} combinatorial oligonucleotide libraries over multiple rounds of *in vitro* selection, the process commonly known as SELEX (Cho *et al.*, 2009). Aptamers offer several advantages over the conventional antibodies. For instance, SELEX allows greater control over aptamer binding conditions, robustness of phosphodiester backbone renders them more stability as compared to protein based antibody, they can be easily amplified using PCR and are highly specific (McKeague and DeRosa, 2012). Due to these advantages, aptamers have gradually replaced antibodies as the bio recognition element. The biomarkers against which aptamer or antibody have been raised to develop malaria biosensors are mostly limited to pLDH and HRP II. The promising malaria

biosensors targeting the antigenic biomarker pLDH, reported so far are briefly described below.

An immunocapture spectrophotometric diagnostic assay based on PfLDH, which showed a detection limit of 50 parasites.μl^{-1} and sensitivity of 88 % was developed by Piper *et al.* (Piper *et al.*, 1999). This assay could be further re-created to develop an advanced biosensor with enhanced selectivity. Since it incorporates the functional activity of PfLDH in a secondary enzymatic reaction for generating the signal, this assay considerably reduces the number of false positive signal, which may occur on non-specific binding of serum proteins to antibodies. pLDH specific aptamer-gold nanoparticle based detection of the target using cationic polymer/salt/cationic surfactant mediated aggregation and concentration dependent reporting of pLDH was achieved by two separate groups (Lee *et al.*, 2014; Jeon *et al.*, 2013; Cheung *et al.*, 2013). These colorimetric advanced assay platforms are summarized in table 1.2. Besides colorimetric platforms, a fluorescent PfLDH sensor using FAM labelled aptamer on MoS_2 nanosheets has also been developed achieving a detection limit of 550 pM (Geldert *et al.*, 2016).

An electrochemical aptasensor targeting pLDH with a detection limit of 108.5 fM and 120.1 fM for PvLDH, and PfLDH, respectively has been reported (Lee *et al.*, 2012b). Electrochemical impedance spectroscopy is a desirable detection platform because of its sensitivity (Ohnoa *et al.*, 2013) and label-free attributes (Min *et al.*, 2008).

Recently, there has been a great push towards development of PoC sensors for malaria diagnosis with emphasis on pLDH. A colorimetric pLDH enzyme assay, coupled with aptamer based capture of enzyme and colour development using nitrotetrazolium dye

was further developed into a paper based syringe test and a magnetic bead based well test. Both the tests could detect PfLDH at a lowest concentration of $ng.ml^{-1}$ (Dirkzwager *et al.*, 2016; Dirkzwager *et al.*, 2015). In another innovative report, twelve aptamers that recognize PfLDH were integrated into a rectangular DNA origami. The captured PfLDH was shown to retain enzymatic activity and protein-aptamer binding was observed dynamically using high-speed AFM (Godonoga *et al.*, 2016).

The malarial biosensor research, as evident from the above references is more inclined towards colorimetric sensors. The reason may be attributed to some advantages of this biosensing platform such as, better scope of converting them to portable devices, cheaper infrastructure requirements, and small sample volume needed for the analysis. From the sensitivity point of view, few nanomaterial based sensors for pLDH showed lowest detection limits in the picomolar range, which is a significant improvement over the conventional malaria detection methods (Table 1.2). Notably, a higher sensitivity is an important requirement especially for diagnosis of asymptomatic submicroscopic infections. Additionally, the selectivity to clearly differentiate different *Plasmodium* species is also a highly desirable performance factor for the malarial diagnostics. While, PoC based sensors are cheaper and portable, the sensitivity and selectivity functions so far served by them are not adequate for detection of submicroscopic infections and differentiation of *Plasmodium* species.

1.2.4 Potential advanced materials for developing malaria diagnostics

Nanoscience has emerged as a dominating subject with great application potential in the bioanalytical fields. Different nanomaterials like, nanoparticles, nanoclusters, and quantum dots, with diverse physical, chemical, and electronic properties have been well described in the current literature. Over the years, various strategies for surface functionalization of nanomaterials are evolved for subsequent formulation of biomolecule-nanomaterial hybrid systems with potential bioanalytical applications. These hybrid systems acquire selectivity function and desirable physical or chemical properties from the corresponding biorecognition element and nanomaterials (Guo and Dong 2009). An elegant example on this strategy is the coupling of antibody with magnetic micro or nanoparticle to enhance the performance of antibody based ELISA system. The magnetic micro particles enable pre concentration and separation of the targets and improve the signal to noise ratios (Markwalter, 2016b). Nanoscale materials like, carbon and zinc oxide nanofibers with good electrochemical properties have been used to functionalize antibodies for developing highly sensitive electrochemical malaria sensors (Paul *et al.*, 2016; Gikunoo *et al.*, 2014). Apart from the nanoparticles, few chemical fluorophores have also been used to enhance the signal in ELISA based platforms for detection of malaria (Yeo *et al.*, 2014; Guirgis *et al.*, 2012). Advanced materials that have successfully been applied for developing antibody based malaria detection platforms are summarized in table 1.4.

Table 1.4: Advanced materials for malaria detection using antibody as the biorecognition element.

Advanced material	Biomarker	Signal	Detection Limit	Reference
Coumarin derived dendrimer	PfLDH	Fluorescence	0.01ng.ml^{-1}	Yeo *et al.*, 2014.
AuNP conjugated antibody and Cy3 labelled recombinant antigen	PfHsp70[1]	Fluorescence	2.4 µg.ml^{-1}	Guirgis *et al.*, 2012
Magnetic beads and coloured dye based enzyme assay	PfLDH	Spectrophotometric	21.1 parasites.ml^{-1}	Markwalter *et al.*, 2016a
Magnetic microparticle and enzyme assay based reporter system	pLDH and HRPII	Spectrophotometric	2 parasites.ml^{-1}	Markwalter *et al.*, 2016b
Magnetic micro and nanoparticles	HRP II	Electrochemical	0.36 ng.ml^{-1}	de Souza Castilho *et al.*, 2011
SAM of thioctic acid and 1-dodecanethiol	HRP II	Piezoelectric	12 ng.ml^{-1}	Sharma *et al.*, 2011a
4-mercaptobenzoicacid(4-MBA) modified gold SPR chip	HRP II	SPR[2]	5.6 pg	Sikarwar *et al.*, 2014
Copper doped zinc oxide nanofibers	HRP II	Electrochemical	6 attogram.ml^{-1}	Paul *et al.*, 2016
Coumarin derived dendrimer	PvLDH	Fluorescence	0.1 ng	Song *et al.*, 2012
Carbon nanofiber	HRP II	Spectrophotometric and electrochemical	0.025 ng.ml^{-1}	Gikunoo *et al.*, 2014

[1]*Plasmodium falciparum* heat shock protein 70, [2]Surface plasmon resonance

Since malaria is a tropical disease, availability of stable detection platforms that can withstand humidity and high temperatures, with no significant loss of functionality, is imperative. Due to this reason, the research on malaria detection systems is growingly shifting focus towards development platforms that use DNA or other chemical recognition elements (Chakma *et al.*, 2016). Intelligent material properties of DNA render this

biomolecule immense potential as a biorecognition element. Besides its capability of evolution to detect a target with high specificity as seen with aptamers, DNA also exhibits several other interesting properties which can be exploited for construction of advanced sensors. DNA hybridization is specific between complementary sequences and has been exploited for detection of SNPs in the human genome (Guo *et al.*, 2002). Indirectly this property has been applied for the construction of molecular beacons and DNAzymes which find application in clinical diagnosis and therapeutics (Tyagi and Kramer 2012; Fokina *et al.*, 2015). DNA origami is another interesting property of DNA where the oligonucleotides are assembled into a nanoscale shape triggered by certain external stimuli. This property of DNA has been exploited to develop low cost miniaturized detection devices (Hernández-Ainsa and Keyser, 2014; Keyser, 2016; Kuzuya *et al.*, 2014; Rothemund, 2006). DNA also acts as a molecular wire when coupled with suitable redox mediators, and thus finds use in the development of nanoscale electronic devices (Wohlgamuth *et al.*, 2013). Finally, DNA can be functionalized with novel nanomaterials with ease, which transform it into a hybrid sensing elements that exhibits a change in response (optical, fluorescence or electrochemical) in the presence of target.

Table 1.5: Advanced materials for malaria detection using DNA (aptamer or probe) as biorecognition element.

Advanced material	Biomarker	Signal	Detection Limit	Reference
Cationic polymers PDDA and PAH with AuNP	pLDH	Spectrophotometric	80 parasites.µl^{-1} for PDDA and 74 parasites.µl^{-1} for PAH	Jeon *et al.*, 2013
Cationic surfactant CTAB[1] with AuNP	pLDH	Spectrophotometric	1.25 pM for PvLDH and 2.94 pM for PfLDH	Lee *et al.*, 2014
Magnetic bead with SERS[2] core shell nanorattle	*P. falciparum* gene Art-R	SERS	100 attomole	Ngo *et al.*,2016
Silver nanoshell coated QD[3]	18 s rRNA	Fluorometric	-	Chen *et al.*, 2013
NTB[4] dye	PfLDH	Spectrophotometric	4.9 ng.ml^{-1}	Dirkzwager *et al.*, 2015
AuNP	MSP[5] 10	Spectrophotometric	12 parasites.µl^{-1}	Alnasser *et al.*, 2016
AuNP	18s rRNA	Spectrophotometric	-	Veigas *et al.*, 2015
FAM-aptamer, MoS_2 nanosheets	PfLDH	Fluorometric	500 pM	Geldert *et al.*, 2016

[1]Cetyl trimethyl ammonium bromide, [2]Surface enhanced raman spectroscopy, [3]Quantum dot, [4]Nitro tetrazolium blue, [5]Merozoite surface protein

Table 1.5 lists the advanced materials that have been used to functionalize DNA (aptamers and probes) for development of malaria sensors. Among these, the most prominent material is AuNP. The conductivity, colorimetric attributes, and amenable functionalization of AuNP with biomolecules, hold great promise for biological and clinical applications (Xiao *et al.*, 2003). AuNPs functionalized with oligonucleotides find application in diagnosis, therapy (Stoeva *et al.*, 2006) and materials design (Lee *et al.*, 2007). Colorimetric sensors using AuNPs offer high specificity and sensitivity, especially when coupled to

recognition elements like DNA probes, and aptamers. Their easy preparation, simple operation, and detection of colorimetric signal with the naked eye are also highly desirable attributes for developing portable PoC devices (Zhao *et al.*, 2008). The colour and absorbance properties on a AuNP suspension is greatly affected by their size and inter particle distance (Wang *et al.*, 2006). While dispersed, AuNPs are red in colour and are transformed to their purple-blue form when they are aggregated. The AuNP based colorimetric sensors are devised to introduce this change in colour when a target of interest in presented. The stability of unmodified AuNPs is improved by the physically adsorbed oligonucleotides at high salt conditions, while their aggregation is triggered by desorption of the adsorbed oligonucleotide, in the presence of a suitable target.

Recently, MoS_2 nanosheets were used as FAM-aptamer matrix for developing fluorescence based sensor for PfLDH. These are two-dimensional atomically thin nanomaterials with high surface area, unprecedented physicochemical properties, ease of large-scale production and dispersion in aqueous solutions. Similar to MoS_2 sheets is graphene, a one-atom thick layer of sp^2 bonded carbon atoms that has elicited remarkable attention due its excellent physical characteristics like, superior chemical stability, large surface-to-volume ratio, and good electronic, mechanical, and thermal stabilities (Zhang *et al.*, 2016). The large surface area helps to interface with high density of analyte molecules and its high electrical conductivity enables the evolution of direct electron transfer based sensing strategies that forgo the use of mediators (Tiwari *et al.*, 2015). Surface conditions greatly influence the conduction of electrons and holes in the single atom thick layer of graphene. Thus, changes in the surface conditions due to interactions with proteins or DNA

hybridization can be electrically detected (Wu *et al.,* 2011). These unique and desirable properties of graphene based materials have been exploited in the fabrication of LEDs, sensors, flexible screens, and energy storage devices like supercapacitors (Jiang *et al.*, 2016). Graphene oxide, a water soluble derivative of graphene, is known for its dispersibility and facile surface chemistry (Peng *et al.*, 2015). Amenable to functionalization, GO/reduced-GO have been used to develop a variety of nanocomposites which find application in diverse sensing platforms (Lin *et al.*, 2011; Wang *et al.*, 2014a).

Au–Ag core–shell structures forming SERS nanorattles, and silver shell coated QDs for detection of *P. falciparum* have been reported (Ngo *et al.*, 2016; Chen *et al.*, 2013). Both these methods were shown to have remarkable sensitivity. Silver based nanomaterials like silver nanoclusters (AgNCs) can easily be grown on DNA templates, forming hybrid sensing materials that form a link between small molecules (e.g., organometallic compounds) and bulk crystals (diameter typically >2 nm) owing to their unique size-dependent optical, electronic, magnetic, and catalytic properties (Yang *et al.*, 2013). Photoluminescence properties of AgNPs result from the interaction of light through electronic transition between discrete energy levels which are a direct consequence of the small size of these nanomaterials. DNA stabilized AgNCs exhibit remarkable spectral and photophysical properties, complementarily offering the opportunity of tunability through modification of DNA base sequence or length (Han and Wang, 2011). As compared to semiconductor quantum dots or dye molecule, the nanoclusters show low toxicity, good biocompatibility, and are hence more environment friendly (Lesniak *et al.*, 2005; Richards *et al.*, 2008). Although DNA stabilized AgNCs have not yet been used for malaria detection platforms,

silver nanorods, and silver nanoparticles have found application in the detection of iRBCs, and hemozoin crystals (Chen *et al.*, 2016a, 2016b).

Table 1.6: Advanced materials for malaria detection without a specific biorecognition element.

Advanced material	Biomarker	Signal	Detection Limit	Reference
Peg 4-Ni-NTA AuNP	HRP II	Colorimetric	7.4 nM	Gulka *et al.*,2015
–	Hemozoin	Micromagnetic resonance relaxometry	10 parasites.μl^{-1}	Peng *et al.*, 2014
Murexide dye and Ni(II) ions	HRP II	Spectrophotometric	30 nM	Chakma *et al.*, 2016
Ni-NTA gold plated polystyrene particles	HRP II	Spectrophotometric	10 pM	Gulka *et al.*, 2014
Silver nanorod array	iRBC	SERS	1.5×10^7.ml^{-1} iRBC	Chen *et al.*, 2016a
Transdermal excitation of hemozoin forming vapor nanobubbles	Hemozoin	Acoustic detection	-	Lukianova-Hleb *et al.*, 2014
Ni-NTA[1] Ag and AuNPs	HRP II	Spectrophotometric	32.6 nM with AuNPs and 27.4 nM with AgNPs	Swartz *et al.*, 2011
Silver nanoparticle	Hemozoin	SERS	2.5 parasites.μl^{-1}	Chen *et al.*, 2016b
Gold coated butterfly wings	Hemozoin	SERS	0.0005% iRBC	Garrett *et al.*, 2015
Silver-Iron oxide core shell magnetic particles	Hemozoin	SERS	30 parasites.μl^{-1}	Yuen and Liu, 2012

[1]Nitrilotriacetic acid

Table 1.6 summarizes various malaria detection methods where the advanced material itself has been tailored to act as a biorecognition material by exploiting the unique properties of the biomarkers.

Chapter II

Cloning, Expression, and Purification of *Plasmodium falciparum* and Human Lactate Dehydrogenases

2.1 Overview

Plasmodium falciparum lactate dehydrogenase (PfLDH) is the last enzyme of the glycolytic pathway of the parasite. The enzyme in the native state catalyzes the reduction of pyruvate to lactate with concomitant oxidation of its cofactor NADH to NAD^+. It is a tetrameric protein with a molecular weight of 136 kDa (Brown *et al.*, 2004). PfLDH has been established as a promising malaria biomarker due to its several distinct properties from the human counterpart. Firstly, this glycolytic enzyme is over expressed in the parasite cellular system during the anaerobic intra erythrocytic stages of the organism for generating ATP. Secondly, it possesses noticeable structural differences from its human counterparts. The most prominent difference is the presence of an additional sequence of five amino acids "DKEWN" in its active site loop (Brown *et al.*, 2004). Thirdly, it exhibits kinetic differences from the human LDH enzymes in not undergoing substrate inhibition (Sessions *et al.*, 1997), and exhibiting higher affinity towards a synthetic cofactor $APAD^+$, than the natural cofactor NAD^+ (Dunn *et al.*, 1996, Chaikuad *et al.*, 2005).

As a part of the work, this thesis aims to develop nucleic acid aptamer against the target PfLDH for which a recombinant His-tagged PfLDH was considered. To render high specificity to the evolved aptamer during its enrichment through the SELEX process,

recombinant His-tagged hLDH A and B proteins were introduced in the counter-SELEX cycles as negative controls.

The LDH enzyme in humans exists in five electrophoretically distinct isozymic forms, numbered as 1-5 depending on their tissue specificity (Handa, 1967). The localization of these enzymes is: LDH 1 and 2 in cardiac muscles, erythrocytes, and kidney; LDH 3 in lung, and pancreas; LDH 4, and LDH 5 in liver, skeletal muscle, skin. Each of these LDH is a tetramer, composed of varying proportions of A and B subunits, where LDH 1 consists of four B subunits (B4), LDH 5 consists of four A subunits (A4), while the others are heterotetramers (Vesell, 1965). In this study, His-tagged hLDH A (i.e. LDH 5), and His tagged-hLDH B (i.e. LDH 1) were used as control proteins. Henceforth, we will be referring to His-tagged-PfLDH, His-tagged hLDH A, and His-tagged hLDH B, as PfLDH, hLDH A, and hLDH B, respectively for brevity of expression. In this chapter we discuss the cloning, purification, and characterization of the target protein PfLDH, and the control proteins hLDH A, and hLDH B.

2.2 Experimental approaches

2.2.1 Materials

Dried blood spots on filter paper, carrying the *P. falciparum* strain 3D7, were kindly provided by Dr. P. K. Mohapatra, from the Regional medical research center, ICMR, Dibrugarh, India. Recombinant vectors pMCSG7_*hldh A*, and pDNR dual_*hldh B*, carrying the *hldh A*, and *hldh B* gene respectively, were obtained from DNASU plasmid repository (USA). Primers were synthesized by IDT (USA). BioMix^{TM} Red PCR kit was purchased

from Bioline (UK). Quick ligation™ kit was procured from New England Biolabs (NEB) (UK). Gel extraction kit was obtained from Sigma Aldrich (USA). All other chemicals were of analytical or molecular biology grade and their sources have been cited in the methodology, wherever necessary.

2.2.2 Bacterial cell culture

E.coli strains were cultivated in Luria Bertani broth (Himedia, India) with the addition of suitable antibiotics when required, at 37 °C, overnight, in a shaker incubator at 180 rpm. The *E.coli* strains and composition of the culture media used in this work have been mentioned in table A1, and A2, respectively in the appendix. Glycerol stocks of *E.coli* cultures were maintained at -80 °C for further use.

2.2.3 Quantification of DNA

The concentration and purity of DNA samples were estimated spectrophotometrically. Samples were diluted in nuclease free water at a ratio of DNA: water of 1:1000 and the ratio of optical density (O.D) at $\lambda_{260\ nm}$ to $\lambda_{280\ nm}$ were calculated. A value of this ratio ranging from 1.8 to 2.0 indicates pure DNA. An O.D value of 1 at $\lambda_{260\ nm}$ was considered to represent a concentration of 50 $\mu g.ml^{-1}$ or 33 $\mu g.ml^{-1}$, respectively for double stranded DNA and single stranded DNA (Barbas III *et al.*, 2001). The DNA concentration was calculated using the equation:

DNA concentration ($\mu g.ml^{-1}$) = $O.D_{260}$ X dilution factor X 50 or 33

2.2.4 Quantification of protein

Spectrophotometric determination of protein concentration was carried out using the method of Bradford (Bradford, 1976) at $\lambda_{595\ nm}$ using Coomassie Brilliant Blue (CBB) G-250 as a colorimetric dye, and BSA as a standard.

2.2.5 Isolation of genomic DNA

P. falciparum genomic DNA was isolated from dried blood spots on filter paper, following the protocol of Bereczky *et al*. (2005). In brief, 4–5 blood spot punches were taken together in a 1.5-ml Eppendorf tube and soaked in 10 mM Tris, 0.1 mM EDTA, pH 8 buffer for 5–10 min. The tubes were then incubated at 50 °C for 15 min, and the spot punches were gently crushed using a sterile micro tip. The tubes were further heated at 90 °C for 15 min. Following a brief spin, the supernatant containing the eluted DNA was collected and stored at 4 °C for further use.

2.2.6 Isolation of plasmid DNA

Plasmid DNA was isolated following the alkaline lysis method (Green and Sambrook, 2012). Table A3 in the appendix section, lists the composition of the solutions used in this process. A recombinant *E.coli* colony was grown in 5 ml LB broth supplemented with appropriate antibiotic, overnight at 37 °C, with a stirring speed of 180 rpm. The grown culture was pelleted at 12,000 x g for 1 min at 4 °C and the culture pellet was resuspended in 100 µl of ice-cold solution I. The lysis of cell suspension was carried out by adding 200 µl of freshly prepared solution II and gently inverting the tube 4-5 times. The tube was then incubated on ice for 3-5 min. Differential precipitation of bacterial genomic DNA and

bacterial cell debris was performed by adding 150 µl of ice cold solution III and incubation on ice for 5 min followed by centrifugation at 12,000 x g for 10 min at 4 °C. The supernatant was transferred to a fresh tube and an equal volume of Tris saturated (pH 8.0) phenol: chloroform: iso-amyl alcohol (25:24:1 v/v), Sigma Aldrich, USA, was added. The organic and aqueous phases were separated by centrifugation at 12,000 x g for 10 min at 4 °C. The aqueous phase was aspirated out to a fresh tube and 2 volumes 100 % ethanol was added to precipitate the plasmid DNA by incubating at -20 °C overnight. After incubation the nucleic acid was precipitated by centrifugation at 12,000 x g for 10 min at 4 °C. The supernatant was removed gently and the DNA pellet was washed with 70 % ethanol. The precipitated plasmid DNA was incubated at room temperature (RT) for 10 min, and then pelleted by centrifugation at 12,000 x g for 15 min, at 4 °C. The supernatant was gently aspirated, and the tube was allowed to dry in an inverted position on a paper towel. After a second wash with 70 % ethanol, the plasmid DNA pellet was air dried and dissolved in suitable volume of nuclease free water.

2.2.7 Agarose gel electrophoresis

Agarose gel (0.8-2 % w/v) preparation was carried out in suitable volume of 1X TAE buffer (appendix table A3) with the addition of 0.5 µg.ml^{-1} of ethidium bromide. To prepare DNA samples, 0.20 volume of 6X gel loading buffer was added to them. Electrophoresis was carried out in 1X TAE at 75 V until the desired resolution was achieved. A wide range DNA marker (DirectLoad^{TM}) was run along with DNA samples, wherever necessary. The DNA fragments were visualized on a UV-Trans-illuminator and then imaged using a gel documentation system (ChemiDoc XRS+ Imaging System, BIO RAD)

2.2.8 Gel elution of DNA

PCR amplified products, digested plasmids and inserts were eluted out of agarose gels using GenElute^{TM} Gel Extraction kit (Sigma Aldrich, USA) following the manufacturer's protocol. Agarose gel carrying the DNA band of interest was excised using a sterile scalpel. The gel was completely dissolved by adding 300 µl of gel solubilization solution for every 100 mg of gel, at 50-60 °C for 10 min, with intermittent vortexing. A binding column was prepared by placing in a 2 ml collection tube and washing with 500 µl of column preparation solution followed by centrifugation at 12,000 x g, for 1 min. The solubilized gel was mixed with equal volume of 100 % isopropanol. The solution was then loaded on to the prepared binding column and subjected to 12,000 x g, for 1 min. The flow through was discarded. The column was washed with 700 µl of wash solution, and again subjected to 12,000 x g, for 1 min. Another centrifugation step was performed to remove the residual ethanol. Elution of DNA was carried out in suitable volume of pre heated (65 °C) nuclease free water, by incubation at RT for 2 min followed by centrifugation at 12,000 x g, for 1 min, in a fresh sterile collection tube.

2.2.9 Polymerase chain reaction

PCR was carried out using BioMix^{TM} Red PCR kit. The composition of the reaction mixture was as follows:

Component of reaction mixture	Amount added
2 x BioMix Red	12.5 µl
Forward primer	1 µl
Reverse primer	1 µl
DNA template	25-30 ng
Nuclease free water	To achieve a final volume of 25 µl

A typical thermal cycling involved the following protocol:

Step I: initial denaturation 95 °C, for 5 min, **Step II:** 30 cycles of 94 °C, for 1 min, 64 °C or 64.4 °C, for 45 sec, 72 °C, for 1 min, **Step III:** final extension at 72 °C, for 10 min. The sequence of primers used are listed in table A5 in the appendix.

2.2.10 Digestion of DNA by restriction enzyme

Plasmids or PCR amplified DNA fragments were subjected to double digestion using restriction endonucleases obtained from NEB, UK. The typical composition of a digestion mixture was as follows:

Components of digestion mixture	**Amount**
10 x Buffer 4 or 10 x Buffer 3	5 µl
Restriction endonuclease (20 units.µl^{-1})	1 µl
Restriction endonuclease (20 units.µl^{-1})	1 µl
DNA template	~1 µg
Nuclease free water	To make final volume to 50 µl

Restriction endonuclease sets used varied with the gene being cloned. Double digestion using BamHI/XhoI in buffer 4 was carried out for *pfldh*, BglII/XhoI in buffer 3 was carried out for *hldh A*, and EcoRI/XhoI in buffer 4 was used for *hldh B*. Digestion was carried out for 6 h, according to the manufacturer's instructions. Digested products were resolved on 0.8 % agarose gel for analysis.

2.2.11 Ligation of digested DNA fragments

After restriction digestion of vector and insert, their digested products were gel eluted using the GenElute Gel Extraction kit. Ligation of eluted products was achieved by using T4 DNA ligase. The ligation reaction was carried at RT (25 °C) for 5 min, incubated on ice and then used for transformation of competent *E.coli* cells. The composition of the reaction mixture is as follows:

Component of ligation reaction	Amount
Insert DNA (~1 kb)	37.5 ng (0.06 pmole)
Linearized Plasmid DNA, 5.4 kb (pET 28a, Novagen)	70.2 ng (0.02 pmole)
2 x Quick ligation buffer	12.5 µl
T4 DNA ligase	1 µl
Nuclease free water	To make final volume to 25 µl

2.2.12 Preparation of competent cells

Preparation of competent *E.coli* DH5α/BL21 (DE3) cells was carried out as described by Chung *et al*. (1989). A colony of *E.coli* was cultured in 5 ml of LB media overnight at 37 °C under constant stirring at 180 rpm. 1 % of this primary culture was inoculated in 25 ml of LB broth and grown until an optical density (O.D) value of 0.4-0.5 was achieved at $\lambda_{660\ nm}$. The culture was then pelleted at 3000 x g for 10 min at 4 °C. The media supernatant was discarded and the bacterial pellet was resuspended in 2.5 ml of sterile ice-cold transformation and storage solution (TSS solution) (Table A3, appendix). Aliquots of thus prepared competent cells were frozen and stored at -80 °C until further use.

2.2.13 Transformation of competent *E. coli* cells

For transformation of competent *E. coli* cells, 10 µl of ligation mixture was added to a 100 µl volume of competent cells, and gently mixed by a pipette, followed by incubation

of the mixture on ice for 30 min. The mixture was then subjected to a heat shock of 90 s by incubating it in a water bath maintained at 42 °C, followed by incubation on ice. 800 µl of pre-warmed LB broth was added to the mixture, and it was incubated at 37 °C, for 1 h, in a shaker incubator maintained at 180 rpm. The cells were pelleted by centrifugation at 3000 x g for 10 min at 4 °C and the pellet was resuspended in 100 µl of fresh LB broth. Resuspended cells were plated on LB agar plates containing the appropriate concentration of antibiotic corresponding to the antibiotic resistance gene present in the recombinant plasmid. Transformed colonies were selected following an overnight incubation at 37 °C, and further screened by restriction digestion.

2.2.14 Sequencing of cloned inserts

Sequencing was performed at a DBT-supported DNA sequencing facility at Delhi University, south campus, India, using 96 capillary high throughput sequencer, ABI 3730 XL following Sanger sequencing protocol.

2.2.15 Cloning of *pfldh, hldh A*, and *hldh B*

The *pfldh* ORF was PCR amplified from *P. falciparum* genomic DNA, isolated as described elsewhere. The amplified ORF was ligated to BamHI/XhoI digested pET28a vector. The ORF for *hldhB* (clone ID HCD00000408) was PCR amplified and sub-cloned into EcoRI/XhoI digested pET28a vector. Recombinant vector pET 28a carrying ORFs for *pfldh* or *hldhB*, and recombinant pMCSG7 carrying *hldhA* were used to transform competent *E. coli* DH5α cells. Transformed cells were selected on antibiotic containing LB agar plate, after 16 h of incubation at 37 °C. The recombinant clones were further screened by restriction

digestion of their respective recombinant plasmids. The positive clones were stored at -80 °C as glycerol stocks. One of the selected clones for each gene was confirmed through sequencing and the recombinant plasmids were further transformed to *E.coli* BL21 (DE3) for protein expression.

2.2.16 Expression of His-tagged PfLDH, hLDH A, and hLDH B in *E. coli* BL21 (DE3) cells

A colony of *E.coli* BL21 (DE3) carrying the recombinant vector pET 28a_*pfldh*, or pET 28a_*hldh B*, or pMCSG7_*hldh A*, was grown in 5 ml of sterile LB broth containing appropriate antibiotic (50 $mg.L^{-1}$ or 100 $mg.L^{-1}$) at 37 °C overnight, in a shaking incubator at 180 rpm. The primary culture was sub cultured in 300 ml of LB broth with the same concentration of antibiotic till the O.D. at $\lambda_{660\ nm}$ reached 0.5-0.6. Protein expression was induced with isopropyl *β*-D thiogalactopyranoside (IPTG) added at a concentration of 0.5 mM IPTG, at 28 °C in case of hLDH B, and PfLDH and 0.25 mM at 20 °C in case of hLDH A, for 12 h in a shaker incubator maintained at 180 rpm. Cells were pelleted at 8000 x g and resuspended in 20 mM PBS, pH 8. The cells were then subjected to sonication using an ultrasonic processor (Hielscher) at 25 % amplitude with 0.5 cycle at 4 °C till the lysate appeared clearer. The sonicated sample was subjected to 12,000 x g for 25 min at 4 °C. The supernatant was collected and stored at 4 °C for further use.

2.2.17 Purification of His tagged PfLDH, hLDH A, and hLDH B

The proteins were purified using Ni affinity chromatography. For this, Ni NTA HisTrap™ column (GE Healthcare) was equilibrated with 10 column volumes of

equilibration buffer (20 mM PBS, pH 8). The supernatant after sonication of recombinant clones was passed through the pre-equilibrated column at a rate of 0.5 $ml.min^{-1}$. The column was then washed with 20 column volumes of washing buffer (20 mM PBS, pH 8) using a step gradient of 30, 50 and 60 mM imidazole to remove unbound proteins. The target protein was then eluted using 350 mM imidazole at a rate of 2 $ml.min^{-1}$. The residual imidazole was removed from the purified protein by dialysis against an appropriate buffer as required. The purified proteins were quantified using the Bradford assay. The composition of solutions used for protein purification have been listed in table A3, appendix.

2.2.18 Sodium dodecyl sulfate polyacrylamide gel electrophoresis (SDS PAGE) of proteins

The proteins purified through Ni affinity chromatography were analyzed on SDS PAGE following the protocol of Laemmli, (1970). Appropriate amount of purified recombinant proteins or unpurified crude cell lysate was mixed with 4 x SDS-PAGE gel loading buffer with reducing agent (2-mercaptoethanol) and heated in a boiling water bath for 5 min to denature the proteins. Pre stained protein marker for SDS PAGE were obtained from New England Biolabs (USA) and processed according to manufacturer's instruction. Electrophoresis was carried out on a discontinuous buffer system with a 5 % stacking on top of a 12 % separating gel, with a thickness of 0.75 mm at a constant voltage of 120 V in a MiniVE vertical electrophoresis unit (GE Healthcare). Visualization of resolved protein bands on the gel was carried out using "Blue silver staining" protocol of Candiano *et al.*, (2004), where colloidal Coomassie G-250 (Sigma Aldrich, USA) (Table A3, appendix) was the staining dye.

2.2.19 Western blotting

The recombinant protein expression in the bacterial system was confirmed by western blot analysis. Following SDS PAGE of the protein, the bands were transferred to a PVDF membrane at a fixed voltage of 25 V, 300 mA for 3-4 h at 4 °C in Blot module (GE Healthcare). Successful protein transfer was confirmed by Ponceau S staining (Sigma Aldrich, USA), which was later removed by rinsing in a washing buffer (PBS, pH 7.4 with 0.1 % Tween 20 (PBS-T)) for 10 min. To prevent non-specific adsorption of primary antibody to membrane, blocking of membrane was performed in a blocking buffer supplemented with 5 % BSA, overnight. A washing protocol consisting of three cycles of washing, 10 min each, in excess PBS-T followed the blocking step. The membrane thus prepared was incubated with monoclonal anti-His antibody as the primary antibody (Sigma Aldrich, USA) using an optimized concentration in PBS containing 1 % BSA for 2 h at RT (Table A4, appendix). The membrane was then washed three times for 10 min each in PBS-T, and incubated in an optimized concentration of anti-mouse IgG (Fab specific)-peroxidase antibody (Sigma Aldrich, USA) as the secondary antibody appropriately diluted in PBS (1 % BSA) for 1 h at RT (Table A4, appendix). This was followed by washing the membrane thrice in excess PBS-T, 10 min each. The membrane was then developed with peroxidase substrate 3, 3'-Diaminobenzidine (DAB) tetrahydrochloridehydrate (Amresco, USA) at a concentration of 0.4 $mg.ml^{-1}$ in 10 ml of PBS with the addition of 10 µl 30 % hydrogen peroxide (Sigma Aldrich, USA) followed by imaging with a gel documentation system (ChemiDoc XRS+ Imaging System, BIO RAD). Details of the solutions/buffers used are given in table A3, appendix.

2.2.20 Circular dichroism study

Circular dichroism (CD) spectra were recorded using a spectropolarimeter (J-815, Jasco, Japan.) after calibrating the instrument with (±)-10-camphorsulfonic acid for optical rotation. The spectra were recorded from $\lambda_{190\ nm}$ to $\lambda_{240\ nm}$, using a 1 mm path length suprasil quartz cuvette at a scan rate of 50 nm.min^{-1}, interval of 0.5 nm, time constant of 1 s, and taking an accumulation of 4 scans. The spectrum was corrected for baseline and smoothed by Savitsky–Golay filter using Jasco spectral analysis software.

2.2.21 Sedimentation velocity study

Sedimentation velocity experiments were carried out on an analytical ultracentrifuge (Beckman XL-A/XL-I) instrument, using an An-50 Ti rotor, and 12-mm double sector charcoal epon centre piece with quartz windows. In a typical experiment, 120 absorbance profiles were recorded at 1,42,2499 x g and 20 °C. The scan profiles were analyzed using the program SEDFIT (Schuck, 2000). The partial specific volume of PfLDH and the buffer density and viscosity were calculated using Sednterp (Laue *et al.*, 1992).

2.2.22 Enzyme kinetic studies

The enzyme activity of recombinant proteins was assayed using a continuous spectrophotometric rate determination method involving the measurement of cofactor generation (NADH or APADH) accompanying the oxidation of lactate as the substrate. The reaction mixture consisted of 20 nM recombinant enzyme, lactate 50 mM, NAD^+ 0.1-10 mM, or $APAD^+$ 0.01-1 mM, in a final volume of 1 ml 100 mM Tris-Cl pH 9.2. For analysis, all the components except lactate were added to a quartz cuvette. After addition of lactate initial rate measurements in a range of concentrations of the cofactors NAD^+or $APAD^+$ were

monitored, by following change in absorbance at $\lambda_{340\ nm}$ (extinction coefficient, $\varepsilon = 6.2\ mM^{-1}.cm^{-1}$) for NAD^+, or at $\lambda_{363\ nm}$ ($\varepsilon = 8.2\ mM^{-1}.cm^{-1}$) for $APAD^+$. Initial rate of reaction was studied using a double beam spectrophotometer (CARY 100 bio, Varian USA). The Michaelis-menten constant, K_m and turnover number, k_{cat} value for the enzyme catalysis were discerned from Lineweaver–Burk plots.

2.2.23 Zeta potential studies

Zeta potential of purified PfLDH was determined in appropriate 20 mM buffer solutions ranging in pH from 4 to10 on the Zetasizer Nano series (Malvern Instruments Limited, UK) using the capillary cell with gold plated beryllium/copper electrode (Malvern Instruments Limited, UK). A plot of zeta potential versus pH gradient was then constructed. The pH value corresponding to zero zeta potential was identified as the isoelectric point (pI) of the protein.

2.3 Results and discussion

2.3.1 Cloning and purification of PfLDH, hLDH A, and hLDH B

P. falciparum genomic DNA isolated from parasite infected blood spots dried on filter paper served as the source for the *pfldh* ORF, while the clones for *hldh A*, and *hLDH B* were obtained from DNASU plasmid repository. Our cloning strategy is depicted in (Figure 2.1). Genomic DNA template (10 µl) of *P. falciparum* isolated from blood spots, in a 25 µl PCR reaction resulted in an amplification at ~951 bp, the size of *pfldh* gene (Figure 2.2). The PCR amplification of *hldh B* using pDNR dual_*hldh B* as a template was similarly done successfully, obtaining an amplified band at ~1005 bp, the size of the *hldh B* gene

(Figure 2.2). In order to confirm the presence of *hldh A* ORF in the recombinant expression vector pMCSG7_*hldh A*, a restriction digestion using Bgl II/Xho I was performed, which resulted in the release of an insert at ~999 bp, the size corresponding to *hldh A* gene (Figure 2.2). Following the PCR amplification (for *pfldh* and *hldh B*) and confirmation (for *hldh A*) of ORFs of the target genes, they were cloned into suitable expression vectors and the recombinant vectors thus generated were used to transform competent *E.coli* DH5α cells. Confirmation of the positive clones was done by restriction digestion of recombinant plasmids isolated from single colonies (Figure 2.3). Subsequently, DNA sequencing of the insert in the selected clone was performed and the translated sequence result was compared with the respective Uniprot entries of the three proteins (Q76NM3, P00338 and P07195) yielding a similarity of 99–100 %. The recombinant plasmids carrying these confirmed inserts were then transformed into competent BL21 (DE3) cells, and proceeded with protein expression. The protein expression profiles for the three proteins were studied in the soluble supernatant fractions of the lysed recombinant BL21 cells (Figure 2.4). The His-tagged PfLDH and hLDH B proteins were purified from the soluble fractions of the induced cell lysates using nickel affinity chromatography. The hLDHA was expressed predominantly as an insoluble protein; however, decreasing the cell growth temperature and inducing the cells at a lower IPTG concentration of 0.25 mM yielded a small fraction of the protein in the soluble cell lysate. In each case, the crude cell lysate and the purified eluate were analyzed using SDS PAGE (Figure 2.5). A typical purification experiment using 100 ml bacterial culture led to approximately 1.4, 0.4 and 2.9 mg of PfLDH, hLDH A and hLDH B, respectively, as estimated from the Bradford assay. The purified proteins were further

successfully confirmed by western blotting using anti-His monoclonal antibody and anti-mouse IgG (Fab specific)-peroxidase antibody as the primary and secondary antibodies respectively (Figure 2.5).

2.3.2 Characterization of PfLDH

The PfLDH protein was cloned as a monomer, which assembled into a homotetramer in solution. To check the integrity of the tetrameric enzyme, sedimentation velocity studies were carried out. The sample (0.6 $mg.ml^{-1}$ PfLDH) was found to be primarily homogeneous with the major fraction corresponding to the homotetramer (136 kDa) (Figure 2.6). The minor heterogeneity resulted from fractions that roughly correspond to the monomeric (34 kDa), dimeric (68 kDa) and octameric (272 kDa) forms of the enzyme. The concentration dependence of the sedimentation coefficient of PfLDH (Figure 2.7) is expressed in terms of k, which is defined by the relation $S_{20,w} = S°_{20,w} - kc$, where c is the concentration in $mg.ml^{-1}$, and $S°_{20,w}$ is the limiting sedimentation concentration obtained upon extrapolation to zero. The value of k discerned from the relation was 2.02. The concentration dependence of the sedimentation coefficient arises from the increased viscosity of the solution at higher concentrations, and from the fact that sedimenting solute particles must displace solvent backwards as they sediment (Tanford, 1961). This concentration dependence for LDH enzymes has also been reported from other vertebrates (Pesce *et al.*, 1967; Sabato and Kaplan 1964); however, in the present case of PfLDH, the dependence was more pronounced. Structural integrity of PfLDH was also validated by CD studies (Figure 2.8). Zeta potential studies of PfLDH at various pH revealed a pI of ~ 5.5 (Figure 2.8). The result

distantly corroborated with the pI value of 6.5 reported for PfLDH from *P. falciparum* D6 strain (Brown *et al.*, 2004).

2.3.3 Determination of kinetic parameters of PfLDH, hLDH A, and hLDH B

Functional integrity of the three proteins were validated by determining their kinetic parameters. Activity studies were carried out with a fixed concentration of lactate and varying concentrations of the cofactors NAD^+, or $APAD^+$. The kinetic parameters estimated for the three enzymes are listed in table 2.1. The result shows that PfLDH had much higher affinity for the synthetic cofactor $APAD^+$ than NAD^+. This is a hallmark of the native PfLDH enzyme (Chaikuad *et al.*, 2005). Hence, the recombinant PfLDH cloned by us was active and structurally well folded.

Table 2.1: Kinetic parameters of PfLDH, hLDH A, and hLDH B, for cofactors NAD^+, and $APAD^+$.

List of cofactors	Enzyme	K_m(µM)	k_{cat} (min^{-1})	k_{cat}/K_m($min^{-1}.M^{-1}$)
NAD^+	PfLDH	800	$9.3x10^6$	$1.16x10^{10}$
	hLDH A	696	$1.5x10^6$	$2.18x10^9$
	hLDH B	1000	$5x10^7$	$5x10^{10}$
$APAD^+$	PfLDH	333	$1.55x10^7$	$4.6x10^{10}$
	hLDH A	63.5	$1.3x10^5$	$2.08x10^9$
	hLDH B	66.67	3.3×10^6	$5x10^{10}$

2.4 Conclusion

As a starting step towards the objective of developing specific aptamers against the malarial biomarker PfLDH, the target protein along with all the control proteins were prepared in pure form following molecular techniques. Briefly, *P. falciparum* genomic DNA was isolated from dried blood spots followed by amplification of *pfldh* ORF. Recombinant clones of *hldh A* and *hldh B* were obtained from DNASU plasmid repository. *pfldh, hldh A,* and *hldh B,* in suitable expression vectors were used to transform competent BL21 (DE3) cells, and the successful transformants were selected by restriction enzyme digestion. Expression of recombinant proteins in soluble form was achieved by IPTG induction. The His-tagged recombinant proteins were purified using Ni affinity chromatography and further confirmed by western blotting. PfLDH cloned directly from *P. falciparum* genomic DNA was characterized using CD, analytical ultracentrifugation, and zeta potential studies. The population of purified PfLDH was primarily homogeneous with the major fraction corresponding to the tetrameric form of the protein. Kinetic studies on PfLDH, hLDH A, and hLDH B proved the functional integrity of the three enzymes. PfLDH was shown to have higher affinity for the synthetic cofactor $APAD^+$ than NAD^+, a feature also known to be shared by the native PfLDH.

Figures

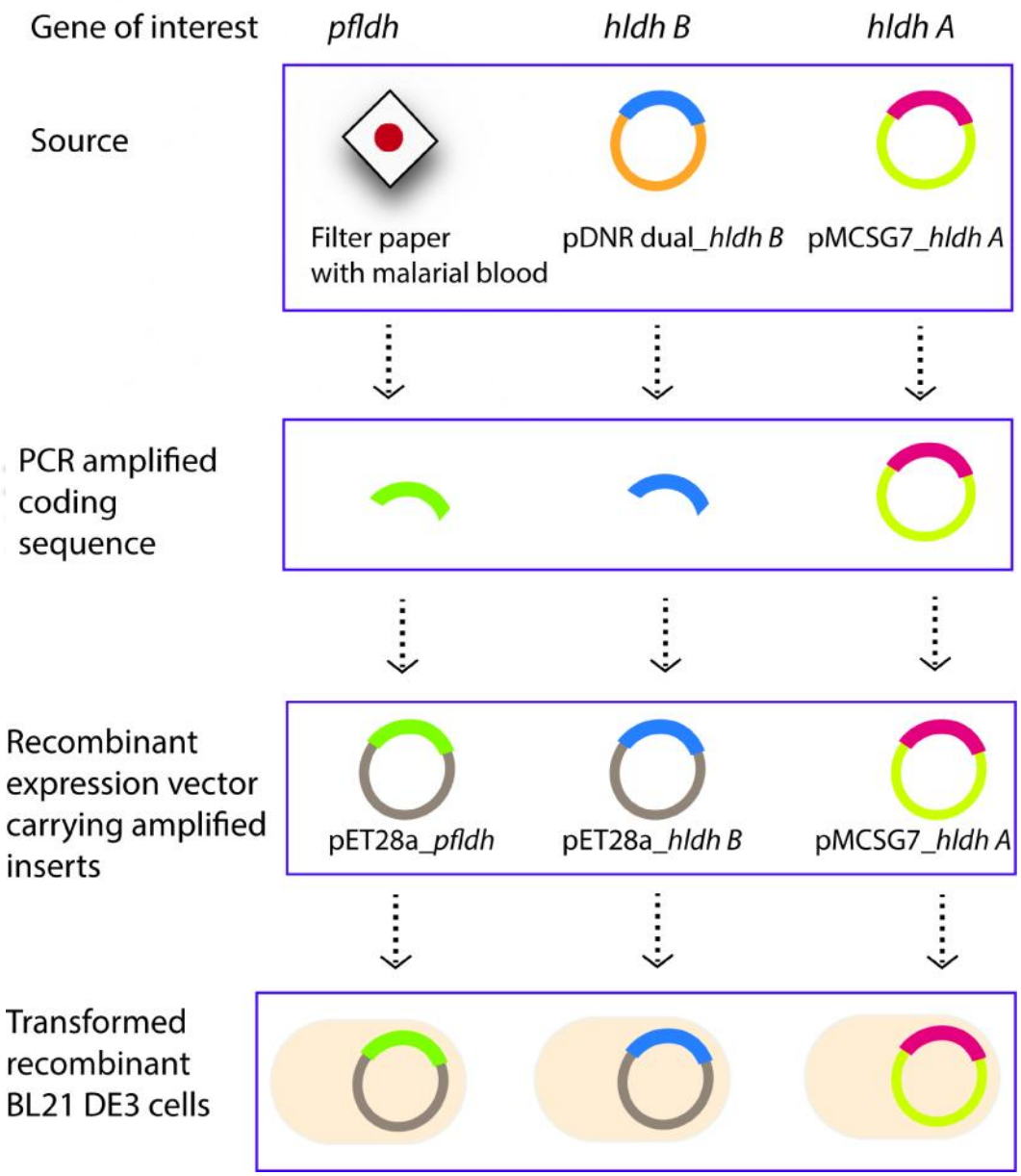

Figure 2.1: Scheme of cloning strategy followed for *pfldh*, *hldh A*, and *hldh B.*

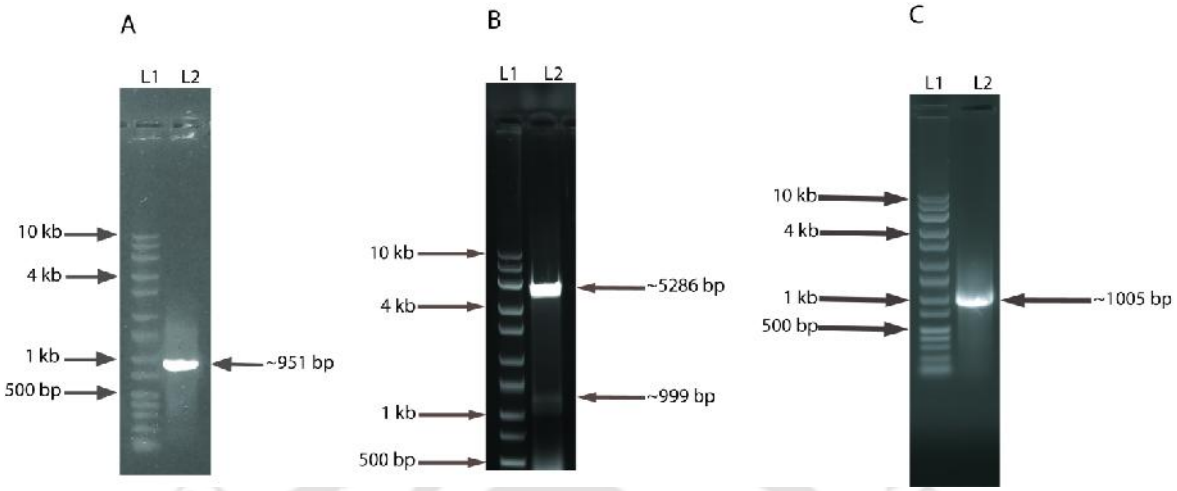

Figure 2.2: PCR amplification of (A) *pfldh* (C) *hldh B* observed in 0.8 % agarose gel. L1: Wide range DNA marker, L2: amplified product. (B) Restriction digestion of pMCSG7_hLDH-A with BglII and XhoI. L1: Wide range DNA marker, L2: Restriction digestion product release of insert.

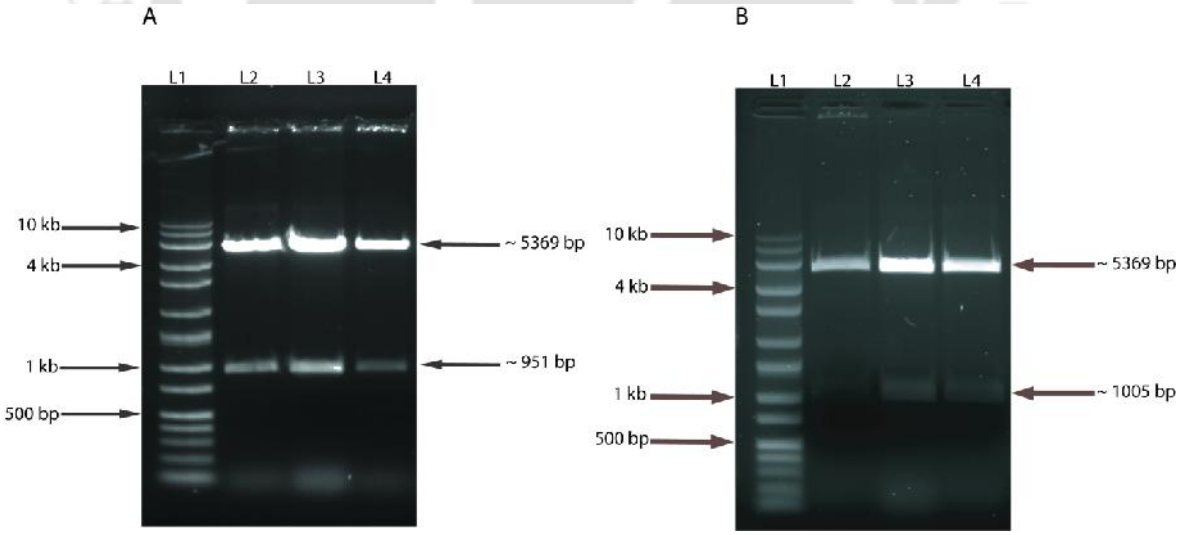

Figure 2.3: Restriction enzyme digestion of recombinant vector pET 28a carrying the gene inserts (A) *pfldh*, and (B) *hldh B*. Lane L1: DNA marker, L2-L4: released insert and linearized plasmid for three positive clones.

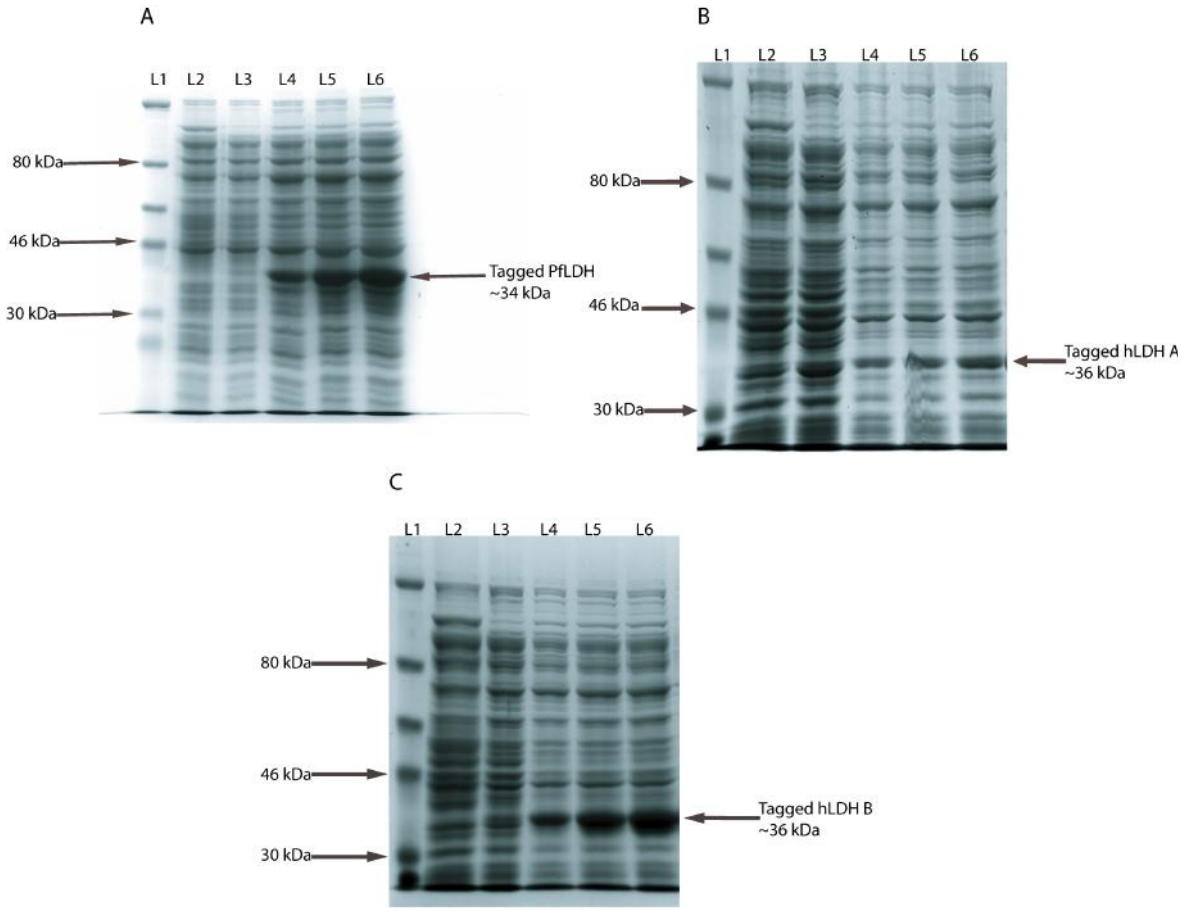

Figure 2.4: SDS PAGE (12 % gel) analysis on the expression profile of (A) PfLDH, (B) hLDH A, and (C) hLDH B. (A) and (C) were induced at 28 °C, 500 µM IPTG concentration for 4, 8 and 12 h, (B) was induced at 20 °C, 100 µM IPTG concentration for 4, 8 and 12 h. In each case Lane L1: protein molecular weight marker, L2: BL21 (DE3) induced, L3: clone uninduced, L4: clone induced for 4 h, L5: clone induced for 8 h, L6: clone induced for 12 h.

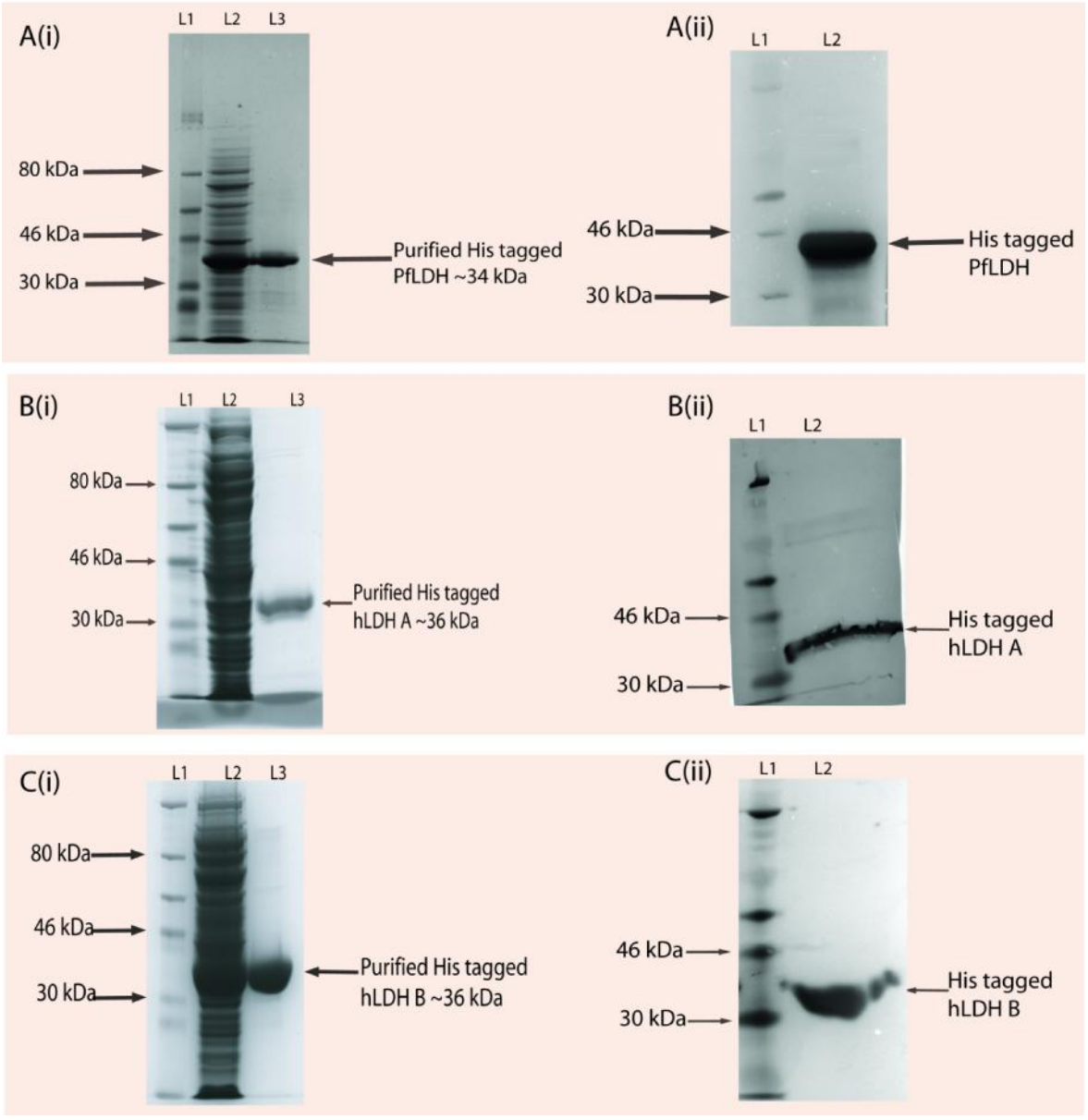

Figure 2.5: (i) SDS PAGE of purified recombinant proteins (A) PfLDH, (B) hLDH A, (C) hLDH B. L1: molecular weight marker, L2: crude cell lysate, L3, purified protein; (ii) Western blot of purified protein (A) PfLDH, (B) hLDH A, (C) hLDH B, L1: Molecular weight marker, L2: blot of purified protein.

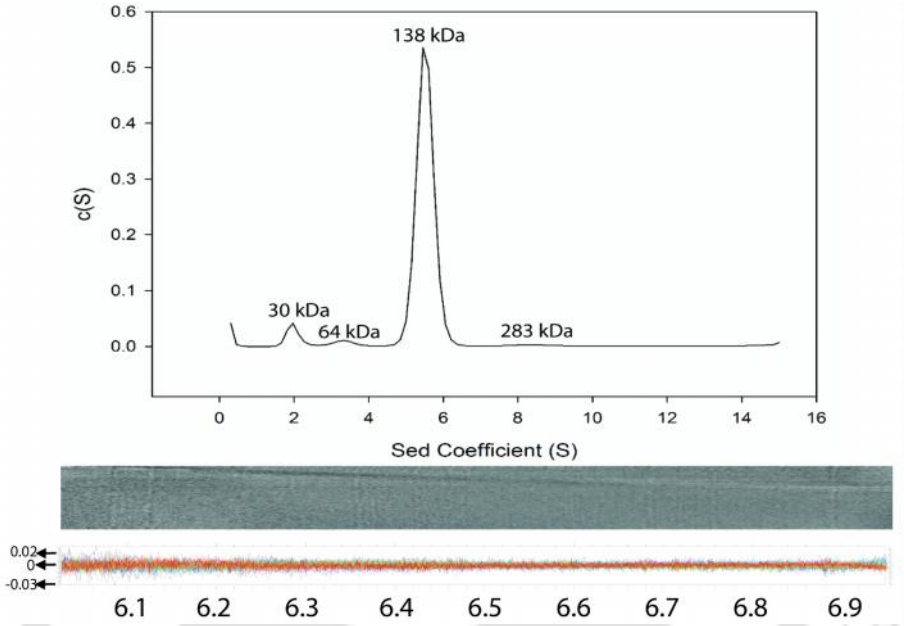

Figure 2.6: Distribution plot of PfLDH (0.6 mg.ml^{-1}) in 100 mM PBS, pH 7.5, 20 °C with residual bitmap images and residuals. The time-invariant noise (Ti) and radially invariant noise (Ri) of the fit were eliminated using SEDFIT for obtaining the best RMSD value.

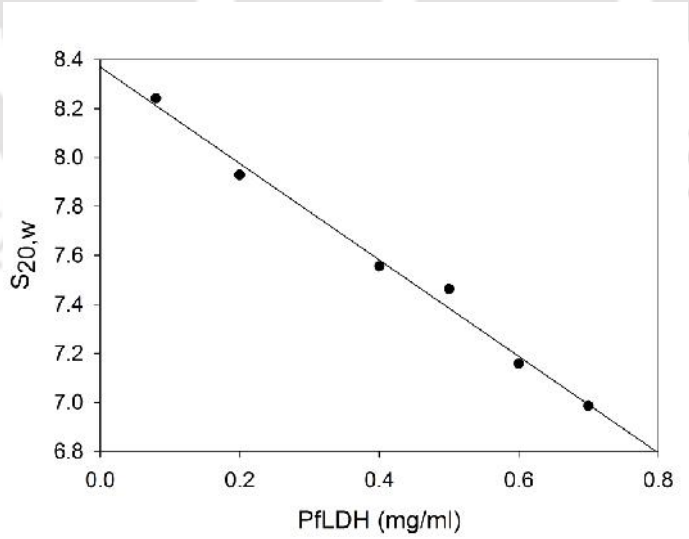

Figure 2.7: $S_{20,w}$ values as a function of PfLDH concentration.

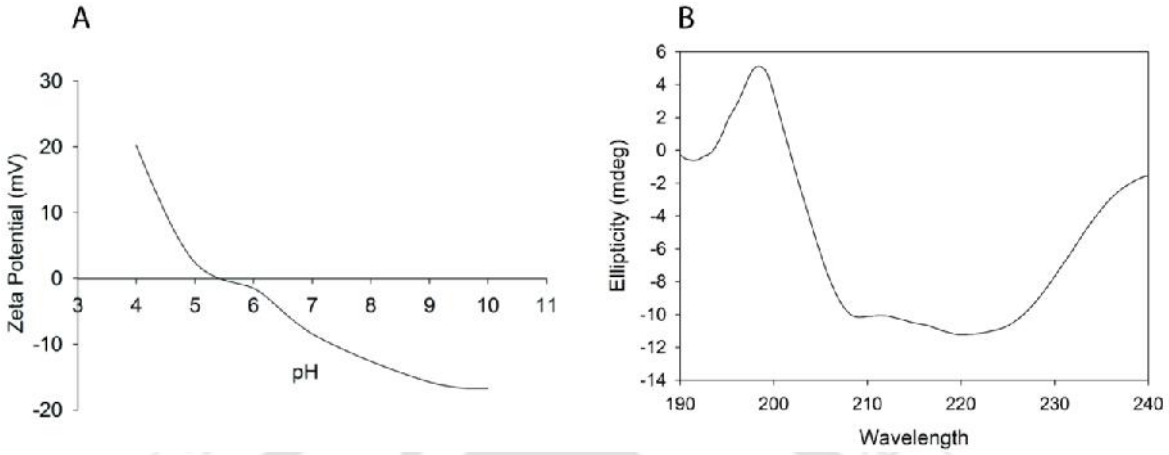

Figure 2.8: (A) Zeta potential of PfLDH at varying pH; (B) CD spectra of PfLDH.

Chapter III

Development of Aptamer Specific for PfLDH and its Characterization

3.1 Overview

The word “aptamer” was derived from the Latin words “aptus” meaning “to fit”, and Greek “meros” meaning “region”. Aptamers were first developed independently by Ellington and Szostak, Tuerk and Gold, and Robertson and Joyce, in the year 1990, and have been the subject of much diagnostic, and therapeutic research interest since then. Nucleic acid aptamers are short single stranded oligonucleotides (DNA, RNA, or modified RNA, DNA) which bind to a target with great specificity and affinity often surpassing that of antibodies. They are screened from a random library of 10^{12}–10^{15} sequences through an *in vitro* selection process known as systematic evolution of ligands by exponential enrichment (SELEX) (Cho *et al.*, 2009). The thus developed aptamers possess the ability to fold in to three dimensional shapes and bind to their targets via a combination of hydrogen bonding, π-π system stacking, van der Waals forces, and electrostatic interactions (Kakoti and Goswami, 2016). Aptamers boast of several advantages over antibodies as biorecognition elements - high thermal stability, low cost of production, non-immunogenicity, nontoxicity, lower batch to batch variability, and rapid large scale synthesis to name a few. Aptamers have thus evolved as an attractive tool in the fabrication of diagnostic devices.

In the past, detection of PfLDH was mainly attempted by antibody based immunoassay (Piper *et al.,* 1999) and western blot (Hurdayal *et al.,* 2010). To circumvent the disadvantages of antibodies such as high cost, thermal instability, and batch to batch variations, aptamers against PfLDH were developed independently by two groups (Lee *et al.,* 2012b; Cheung *et al.,* 2013). However, the specificity of the aptamer candidate developed by Lee *et al.* needs to be properly validated as it was selected without rational design omitting counter-SELEX against human LDH enzymes. Besides, *in vitro* selection in both the cases was attempted by using expensive Ni-NTA magnetic beads as the matrix for immobilization of the target.

This chapter describes the selection of ssDNA aptamers against PfLDH following the SELEX process. The PfLDH protein purified in Chapter I was used as the target for SELEX whereas hLDH A, and hLDH B served as control proteins for counter-SELEX. We used PVDF membrane as an immobilization matrix for the target and control proteins. Following the process we isolated one candidate which was then characterized for its specificity, and affinity of binding to the target. A detailed account of the work is included in this chapter.

3.2 Experimental approaches

3.2.1 Materials

DNA oligonucleotides (primers, ssDNA library) were synthesized from IDT, USA. The aptamers generated through the work were synthesized by Bioserve Biotechnologies, India Pvt. Ltd. PVDF membrane (Hybond P) was obtained from Amersham, UK. SYBR

Gold (10,000 X) nucleic acid stain was obtained from Invitrogen (USA), Restriction endonucleases, and streptavidin coated magnetic beads were procured from New England Biolabs (USA), pGEM-T easy TA cloning kit was obtained from Promega (USA). All other chemicals were of analytical grade.

3.2.2 Construction of the ssDNA library

The construction of the ssDNA library was such that a stretch of 40 randomized nucleotides was flanked by constant primer binding sites on both sides.

5′-CACCTAATACGACTCACTATAGCGGATCCGA-N_{40}-CTGGCTCGAACAAGCTTGC-3′

The primer sequences used for PCR amplification of the library are listed in table A5, appendix.

3.2.3 *In vitro* selection of ssDNA aptamers

PVDF membrane was cut to 0.5 cm x 0.5 cm and taken in a 2 ml Eppendorf tube. The membrane was immersed in methanol for 10 min followed by equilibration in binding buffer for 20 min. A total of 1 ml (1 $mg.ml^{-1}$) target protein (PfLDH) in binding buffer was added to the tube followed by gentle agitation on a rocking platform for 1 h. The membrane was then washed twice and stored in binding buffer at 4 °C. The amount of protein immobilized on the membrane was quantified using Bradford assay, by subtracting the amount of protein in the eluate from the original protein solution. The change in morphology of the PVDF membrane with subsequent protein immobilization was studied using atomic force microscopy (AFM) on an ambient air scanning probe microscope (Agilent Technologies 5500, USA) and a silicon nitride probe. Images were recorded with non-contact mode using Picoscan 5 software.

Before use, the library was denatured at 90 °C for 3 min, followed by incubation at 4 °C for 5 min. The ssDNA library (2.5 nmol) was suspended in 1 ml of the binding buffer, and then incubated with PfLDH immobilized onto PVDF membrane at RT for 1 h, on a rocking platform. The tube was spun down and the supernatant was stored as unbound library. Elution of bound candidates was performed in 200 µl PCR grade water by heating the membrane at 90 °C for 5 min and crushing with a sterile microtip. Bound ssDNAs were amplified using BioMix Red DNA polymerase (Bioline) following the amplification protocol - initial denaturation at 95 °C for 10 min, followed by 18 cycles of 95 °C, for 15 s, 68 °C, for 15 s, 72 °C, for 3 s; and final extension at 72 °C for 3 s. To separate ssDNA from amplified dsDNA, the PCR product was incubated with 30 µl of streptavidin-coated magnetic beads in a coupling buffer at RT for 1 h. The beads were then washed with coupling buffer, and ssDNA strands were separated from biotinylated strands using 100 µl of 100 mM NaOH. The separated ssDNA strands were used for the next round of SELEX after neutralizing their pH with sodium dihydrogen phosphate (NaH_2PO_4).

The counter SELEX against hLDH A and hLDH B was carried out after cycle 4 and 8, respectively. The counter proteins were immobilized on PVDF in a manner similar to that for PfLDH and allowed to interact with the aptamer population. Counter SELEX against bare PVDF membrane was carried out twice, once at the very beginning and the second one after cycle 6. After every counter SELEX cycle, the unbound aptamer population was collected for the next cycle of operation. Details of buffers/solutions used have been listed in table A3, appendix.

3.2.4 Cloning of enriched aptamer population

At the end of the 10th positive SELEX cycle, the PCR product was cloned into pGEMT easy vector and transformed into competent *E. coli* DH5α cells. The positive clones carrying aptamer inserts were selected on the basis of Blue/White screening, and PCR. The recombinant plasmids from positive clones were sequences, and the aptamer sequences were aligned using Clustal X2, for comparison.

3.2.5 Electrophoretic mobility shift assay (EMSA)

10 % polyacrylamide gel with a cross linker ratio of 75:1 was prepared and pre-run in TBE buffer for 45 min at 120 V. PfLDH at various concentrations (0.2–12 µM) was mixed with 25 nM of selected aptamer candidate in 20 µl binding buffer and incubated for 1 h at RT. The mixture was loaded onto the pre-run gel, and separation was carried out for 2 h, at RT and 120 V. The gel was stained using SYBR gold dye. EMSA gel bands were quantified using ImageJ software, and the data were fit to the equation of rectangular hyperbola in SigmaPlot 13.0 to estimate the dissociation constant (K_d). The 2D structure of selected aptamer was determined using Mfold web server (Zuker, 2003).

3.2.6 Isothermal titration calorimetry

The ITC experiments were performed on a GE Healthcare UK, MICROCAL iTC 200 microcalorimeter. 20 µM of aptamer and 2 µM of PfLDH protein solutions in 50 mM HEPES buffer, pH 7.4, were prepared to be used as ligand, and macromolecule, respectively. The protein, and aptamer solution were degassed for 10 min before their use in the ITC experiment. Following the first injection of 0.4 µl aptamer solution, subsequent injections of 1.2 µl each were administered by the ITC syringe to the reaction cell in 20 titrations, at

150 s intervals, at 25 °C, and a stirring speed of 450 rpm. Control experiment without aptamer was performed to correct for heat of dilution. Analysis of ITC data was performed by Origin v 7.0 (OriginLab, USA).

3.2.7 Prediction of aptamer-protein interactions

The 3D structure of the aptamer was predicted using the RNA Composer web server (http://rnacomposer.cs.put.poznan.pl/) (Popenda *et al*., 2012), for which the Mfold dot-bracket notation was provided as an input. The sequence of the ssDNA aptamer was first converted to its corresponding RNA sequence. Docking studies involving PfLDH (PDB ID 4B7U) and aptamer were carried out on the PatchDock web server. (http://bioinfo3d.cs.tau.ac.il/PatchDock/) (Duhovny *et al.,* 2002; Schneidman-Duhovny *et al.,* 2005) and analyzed using PyMOL. Chemical interactions at the protein-aptamer interface were studied using the PLIP (protein-ligand interaction profiler) web server (https://projects.biotec.tu-dresden.de/plip-web/plip/index) (Salentin *et al*., 2015).

3.3 Results and discussion

3.3.1 Selection of aptamers

To select DNA aptamers specific for PfLDH, a single stranded DNA library which theoretically contained 10^{12}– 10^{15} different sequences with a 40-nucleotide random region, flanked by constant primer binding regions for amplification, was used as a starting pool. The SELEX methodology followed for developing the aptamer is schematically represented in figure 3.1 A. PVDF membrane served as the protein immobilization support during the course of SELEX. The protein molecules bind to the PVDF membrane via a combination of

hydrophobic and dipole interactions (Matsudaira, 1987) and are oriented in a non-uniform fashion on the membrane surface. This exposes a more stochastic and wider array of ‘‘aptatopes’’ in each cycle compared to the scenario of using a linker for the binding of protein to the membrane surface. The change in membrane morphology was investigated by AFM and revealed that the bare PVDF membrane, a comparatively smooth surface, was transformed into a rougher and non-uniform one after protein binding. The thickness of the membrane was increased from ~250 nm for the bare membrane to ~350-400 nm for the protein immobilized one, and finally the thickness reached to ~750-800 nm upon aptamer immobilization (Figure 3.2). Counter selection steps against uncoated PVDF membrane, and membrane coated with hLDH A, and hLDH B were included to eliminate non-specific aptamer candidates against PfLDH.

The evolved pool of aptamers generated at the end of each positive cycle when analyzed by gel electrophoresis, a gradual enrichment of aptamer candidates occurring at each subsequent cycle was revealed (Figure 3.3). A total of 52 positive clones selected from the blue white screening were then further screened by using PCR (Figure 3.4) to a final total of 23 recombinant clones carrying the enriched aptamer inserts. The plasmids from overnight cultures of these clones were then isolated, and the corresponding aptamer amplicons were sequenced. Analysis of the sequenced candidates by Clustal X2 revealed that 9 sequences were enriched at levels more than the others. The sequences of these candidates are listed in table 3.1. Analysis of alignment results did not display any strong conserved regions across these sequences (Figure 3.5).

Table 3.1: Sequence profile of the enriched aptamer candidates.

Serial No.	Sequence (5′-3′)	Assigned Aptamer name
1	CACCTAATACGACTCACTATAGCGGATCCGACCACGCCCAACTCCC CTCCGCATCCGTGTCATCCACCATCCTGGCTCGAACAAGCTTGC	P4
2	CACCTAATACGACTCACTATAGCGGATCCGAAAAGTGAAGGGGGAC TGACGGCGGGGGGGCGACGACGGGCCTGGCTCGAACAAGCTTGC	P6
3	CACCTAATACGACTCACTATAGCGGATCCGAACAAGCGAAGGGGCC GGACGCGGGCGGGGCGTCGACCGTCCTGGCTCGAACAAGCTTGC	P8
4	CACCTAATACGACTCACTATAGCGGATCCGATTACCCACCCGACTC CCCTAGCATTCTCCATCCAACCGGCCTGGCTCGAACAAGCTTGC	P9
5	CACCTAATACGACTCACTATAGCGGATCCGACTGACACTGGTAATT GAAGACGGCTGACATGAATACATGGCTGGCTCGAACAAGCTTGC	P29
6	CACCTAATACGACTCACTATAGCGGATCCGAATCCATTCTTCGTAG TTATAGACAACGGCAAGCACGGTACCTGGCTCGAACAAGCTTGC	P34
7	CACCTAATACGACTCACTATAGCGGATCCGACAATAATACACTTTG CTCCCCTGTGGCTTTTCGCACTCGCCTGGCTCGAACAAGCTTGC	P38
8	CACCTAATACGACTCACTATAGCGGATCCGACAGTCCTCTCACCAT TCTTCTACATGTACTTTTCGGCCTCCTGGCTCGAACAAGCTTGC	P44
9	CACCTAATACGACTCACTATAGCGGATCCGACAGTCCTCTCACCAT TCTTCTACATGTAATCTTCCGCGTCCTGGCTCGAACAAGCTTGC	P45

3.3.2 Affinity and specificity of aptamer-protein interactions

To study aptamer-protein interactions for the 9 enriched aptamer candidates, EMSA was conducted with complexes of a fixed concentration of the aptamer with increasing concentrations of PfLDH as target protein. From the EMSA gel the fluorescent signal in each DNA band was estimated using ImageJ, and a plot of protein concentration vs. fraction of (bound aptamer/total aptamer) was generated. From the plot, the dissociation constant

(K_d) was approximated by fitting the data to the model of rectangular hyperbola in SigmaPlot 11.0 (Heffler *et al.*, 2012). The K_d values thus obtained for each of the studied aptamers have been listed in table 3.2

Table 3.2: Dissociation constant of the tested aptamers derived from the band intensity in EMSA gel.

Aptamer Candidate	**K_d (µM)**
P38	0.35 ± 0.02
P9	0.73 ± 0.05
P45	0.89 ± 0.14
P8, P6, P29, P34, P44, P4	N.E.*

[a]Not estimated

Based on these observations, three candidates with higher affinity for PfLDH namely P38 (0.35 ± 0.02 µM), P9 (0.73 ± 0.05 µM), and P45 (0.89 ± 0.14 µM) with K_d values in the parentheses, were identified. While for the rest of the studied candidates, the signal of bound aptamer-PfLDH failed to achieve saturation, and was not suitable for determination of K_d. The probable reason for this has been attributed to weaker binding force of these candidates to the target, which was disrupted by the applied electrical force during the course of electrophoresis. Figure 3.6 A, B, and C, shows the EMSA profile of two high affinity binders P38 and P9, and a low affinity binder P8 to PfLDH. From visual comparison it was evident that P38 had higher affinity than P9, for PfLDH, while P8 had significantly lower affinity for PfLDH, in comparison to P38, and P9.

The specificity of three potential aptamers P38, P9, and P45 was again examined in EMSA using hLDH B as the control protein. All the studied candidates did not bind to hLDH B (Figure 3.6 D). Notably, the hLDH B protein is the major human LDH in host erythrocytes, which house the *Plasmodium* parasite (Vesell, 1965), and hence the negative response of the aptamers to hLDH B is a positive trait for the study. Since P38 showed the lowest K_d it was considered for further studies. The 2D structure of P38 (Figure 3.1 B) had a ΔG of -9.18 kcal.mole^{-1} and contained three major stem loop regions that arise from a central bigger loop. Alignment of P38 sequence with previously selected aptamers for *Plasmodium* species lactate dehydrogenase (Cheung *et al.,* 2013, Lee *et al.,* 2012b) yielded no significant similarity.

3.3.3 Interaction of P38 with PfLDH

Calorimetric titration of P38 to PfLDH resulted in a rectangular hyperbola that yielded a dissociation constant of 0.243 $\pm$ 0.3 µM (Figure 3.7). This value is in close agreement with the K_d determined by EMSA study. The contribution towards free energy from enthalpy (ΔH) was -3.39 x 10^7 cal.mole^{-1}, while that from entropy (TΔS) was -2.85 x 10^6 cal.mole^{-1}, therefore the reaction was spontaneous and enthalpically driven.

The binding site of P38 to PfLDH as predicted by the PatchDock web server is represented in figure 3.8. Here, we observe that the aptamer primarily interacts with two chains of the tetrameric protein. Interacting residues at the aptamer protein interface were also predicted by the PLIP server. Results of this prediction are shown in table 3.3. The PLIP output points to only two chains i.e. C, and D being involved in hydrophobic interaction, and

salt bridges with the aptamer. Besides this several hydrogen bonds with residues in C, and D chains were also predicted.

Table 3.3: Prediction of interacting residues at the aptamer-protein interface.

Type of Interaction	Interacting amino acid (position/chain/name of amino acid)	Interacting base of the aptamer (base type and position)
Hydrophobic interactions	197C(Asn)	A12
	236D (Ala)	C15
Salt bridges	60C (His)	T44
	195D (His)	C15
	198D (Lys)	A34
	198D (Lys)	A33
	314D (Lys)	C32
	314D (Lys)	A33

3.4 Conclusion

A specific ssDNA aptamer P38 against PfLDH was developed following the SELEX process. Counter SELEX against bare PVDF membrane, and the human proteins hLDH A, and hLDH B were carried out to exclude the candidates that bind non-specifically to these controls. Notably, incorporation of the counter screening in the SELEX process against potential interfering agents may be considered as an important step towards rational design of developing selective aptamers. The affinity of the aptamer towards PfLDH was confirmed by EMSA and ITC studies. The binding constants were determined independently following these studies (EMSA, ITC) and found agreeable value. The aptamer P38 developed by us against PfLDH is significantly different from the other reports with no common discernible motifs. The present methodology employed PVDF membrane as an immobilization support. This further simplified the SELEX process and also contributed towards the economy of the method.

Figures

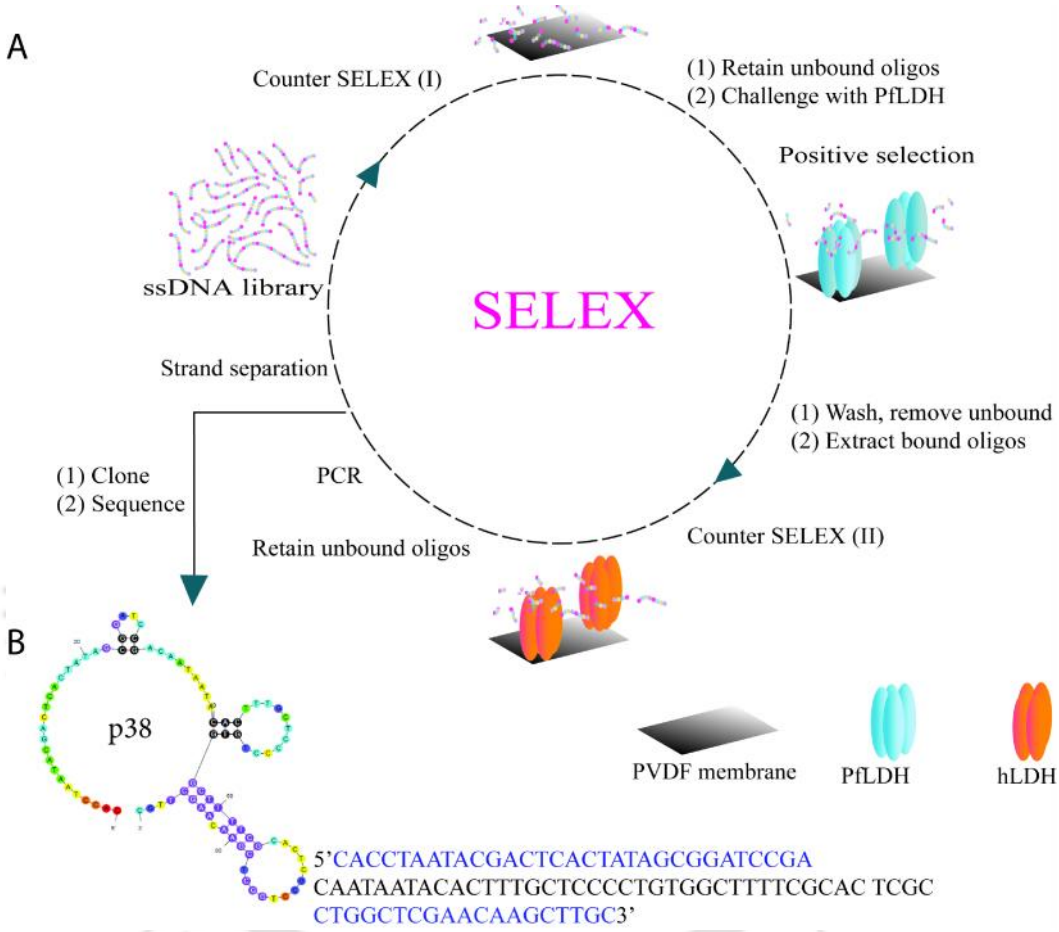

Figure 3.1: (A) Schematic of the SELEX process; (B) 2D structure of P38 derived from Mfold and its sequence are shown as the final output of the selection process. The sequence of P38 shows a central 40-nucleotide variable region (black), flanked by constant primer-binding regions (blue).

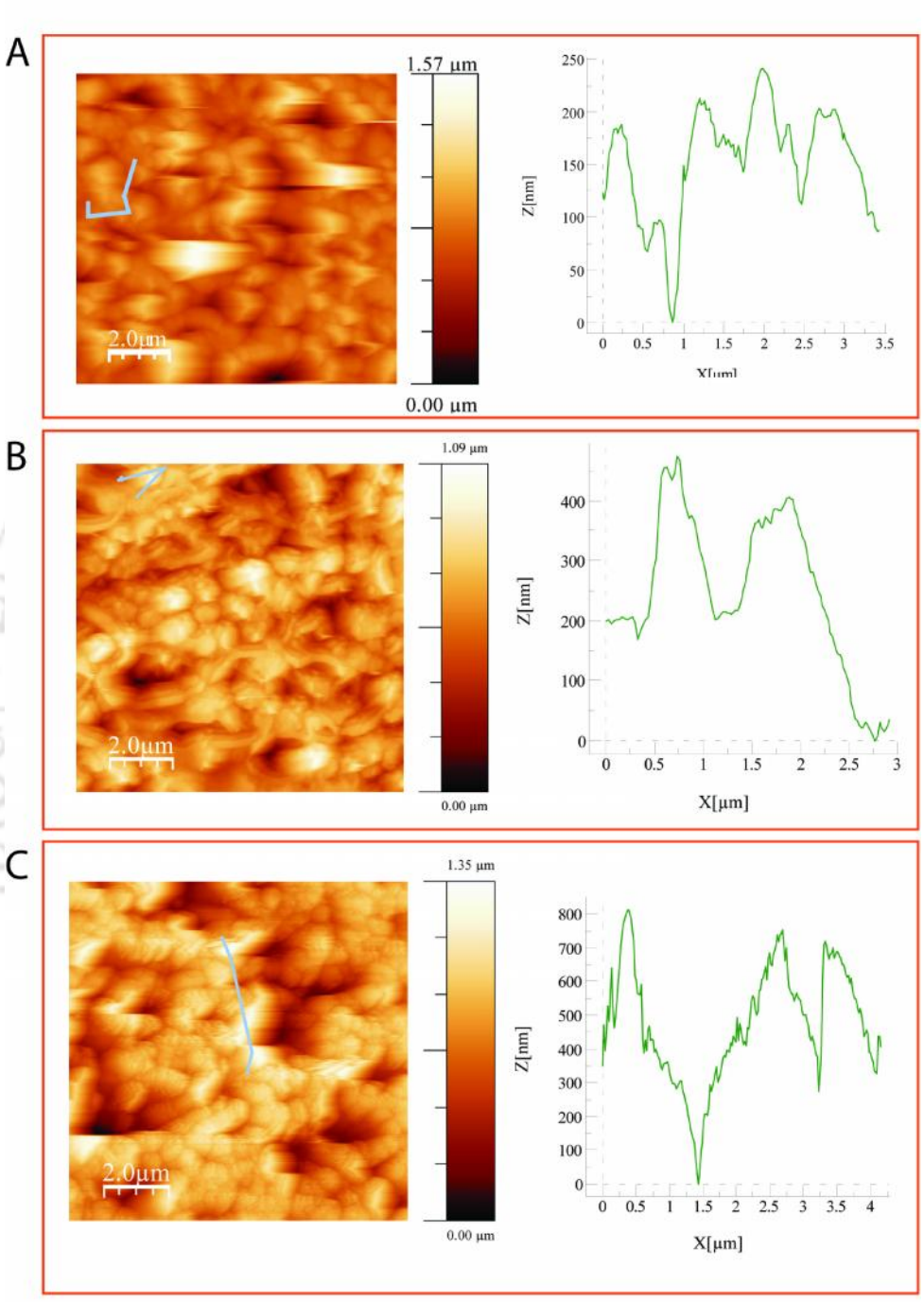

Figure 3.2: AFM topography and height profile of (A) bare PVDF membrane; (B) PfLDH immobilized on PVDF membrane; (C) after interaction of aptamer library with (B).

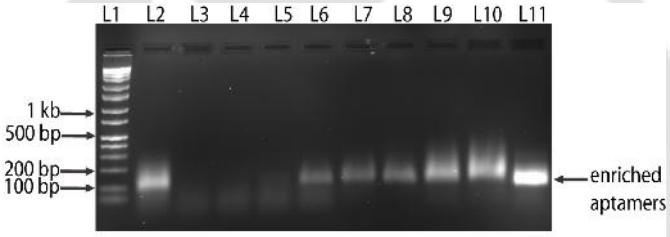

Figure 3.3: PCR amplification of enriched aptamer population at the end of each positive cycle. L1: DNA marker, L2-L11: Amplified population after cycles 1-10 respectively, observed on a 2 % agarose gel.

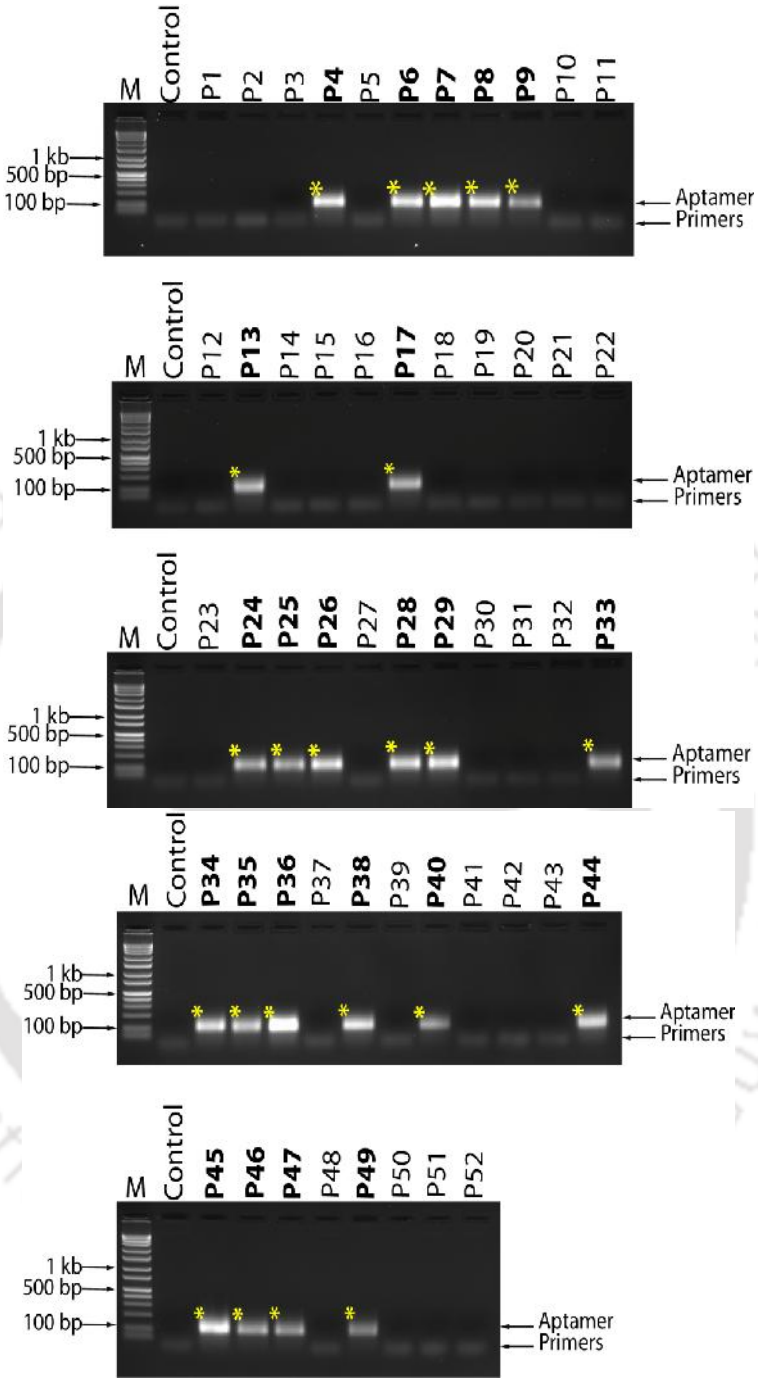

Figure 3.4: Screening of 52 white colonies by PCR. M: DNA marker; Control: negative control, representing the amplification product from a blue colony. Other lanes are labelled as name of the colony screened, with positive colonies written in bold.

```
                *         20          *         40          *
P34 : -------------ATCCATTCTTCGTAGTTATAGACAACGGCAAGCACGGTAC : 40
P38 : --------CAATAATACACTTTGCTCCCCTGTGGCTTTTCGCACTCGC----- : 40
P4  : --------CCACGCCCAACTCCCCTC-CGCATCCGTGTCATCCACCATC---- : 40
p44 : ----CAGTCCTCTCACCATTCTTCTA-CATGTACTTTTCGGCCTC-------- : 40
P45 : ----CAGTCCTCTCACCATTCTTCTA-CATGTAATCTTCCGCGTC-------- : 40
P9  : ------TTACCCACCCGACTCCCCTAGCATTCTCCATCCAACCGGC------- : 40
P6  : ------AAAGTGAAGGGGGACTGACGGCGGGGGGGGCGACGACGGGC------- : 40
P8  : -----ACAAGCGAAGGGGC-CGGACGCGGGCGGGGCGTCGACCGTC------- : 40
29  : CTGACACTGGTAATTGAAGACGGCTGACATGAATACATGG------------- : 40
                      a  c  c  c          c  c
```

Figure 3.5: Multiple sequence alignment of the random regions of P4, P6, P8, P9, P29, P34, P38, P44, and P45. Green and yellow coloured regions represent 80 % and 60 % sequence similarity, respectively.

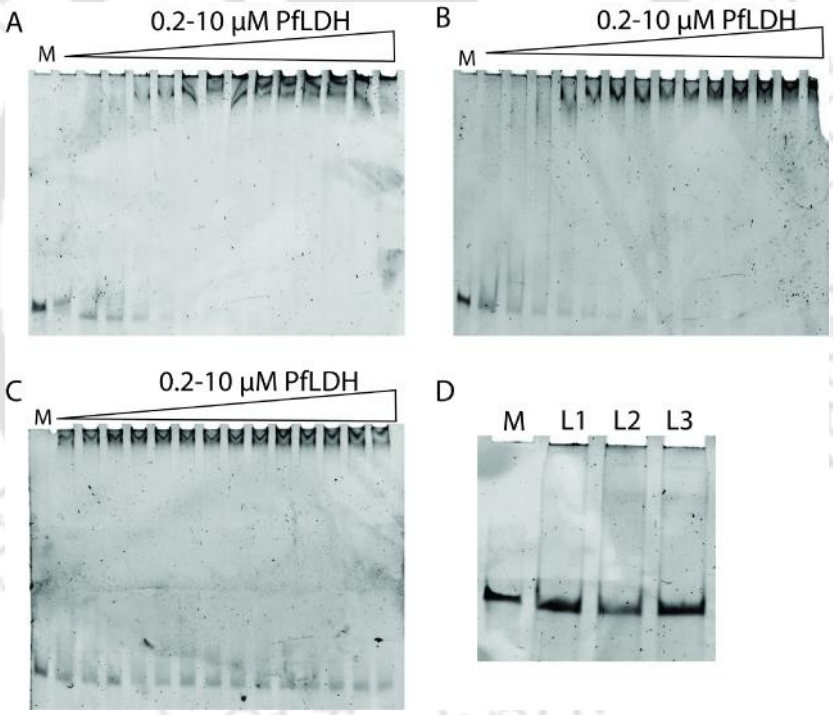

Figure 3.6: EMSA gels used for estimating K_d for (A) P38, (B) P9, and (C) P8. PfLDH concentration ranged as 0.2 µM, 0.35 µM, 0.7 µM, 1.4 µM, 2 µM, 2.5 µM, 3 µM, 3.5 µM, 4 µM, 4.5 µM, 5 µM, 6 µM, 8 µM, 10 µMM: the free aptamer (90 mer) was used in each gel as the molecular weight marker. (D) EMSA of control protein hLDH B with P9 (L1), P38 (L2), and P45 (L3). The concentration of hLDH B was 3 µM in each case.

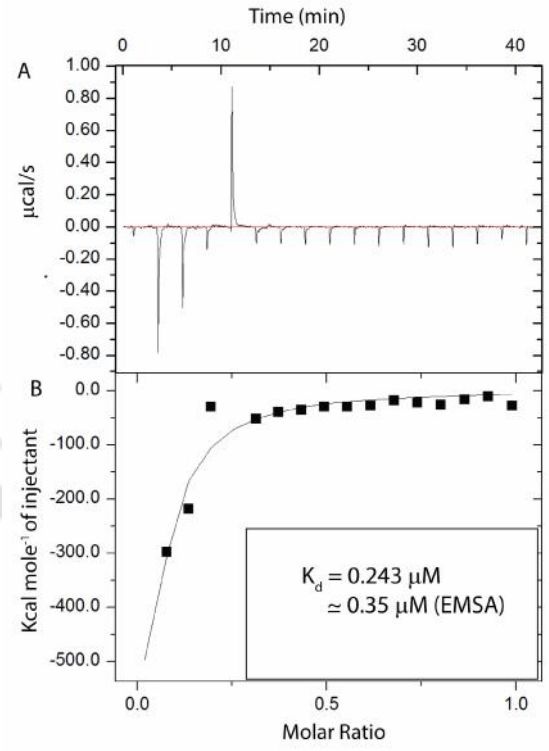

Figure 3.7: Isothermal titration calorimetry analysis for binding of P38 aptamer to PfLDH protein. (A) Raw heat of binding obtained on titration of P38 to PfLDH. (B) Fitted binding isotherm of P38 binding to PfLDH. The titration revealed a dissociation constant of 0.243 µM which was similar to that obtained by EMSA (0.35 µM).

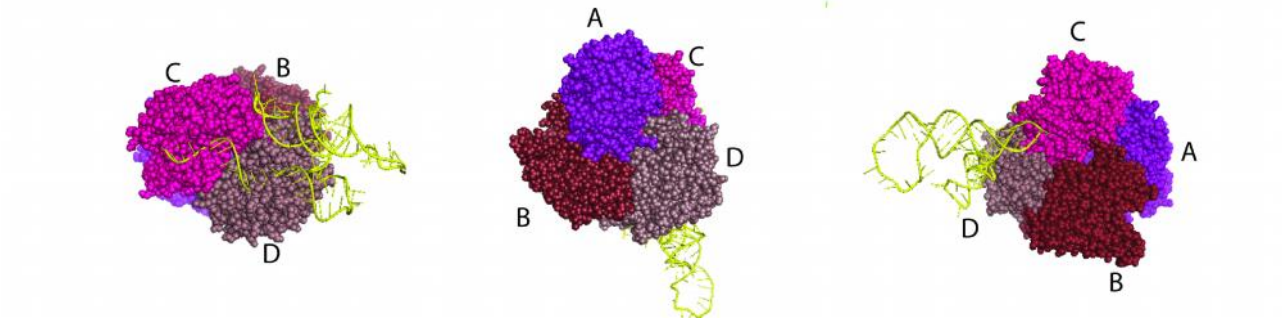

Figure 3.8: Docking results of P38 with PfLDH as predicted by PatchDock server. P38 is represented in yellow, while the four chains of PfLDH are numbered A, B, C, and D, and represented in shades of purple.

Chapter IV

Development of Aptamer Based Colorimetric Detection of PfLDH

4.1 Overview

Precise diagnosis of malaria in a PoC setup is a prerequisite in malaria management as it helps to prevent evolution of multidrug-resistant malaria caused by indiscriminate and overuse of drugs (Choi *et al.,* 2007) and lessens mismanagement of non-malaria fevers (Chanda *et al.,* 2009). Malaria is commonly diagnosed using conventional techniques like microscopy, ELISA, PCR, and lateral flow based rapid diagnostic tests (RDTs). The conventional techniques require skilled personnel and are difficult to incorporate into point of care systems. Whereas, the RDTs though have the advantage of being portable, they often suffer from poor performance due to denaturation of the antibodies, which are used as biorecognition element, under high temperature and humid climate as discussed previously (Chiodini *et al.,* 2007). As an alternative to antibody, aptamers have emerged as robust and reliable biorecognition elements for various analytical applications. We propose here to explore the aptamer that has been developed by us through the SELEX process as a biorecognition element against PfLDH, a malarial biomarker, in an optical platform. In order to generate profuse optical signal for sensitive detection of the biomarker in serum sample we focused our attention on gold nanoparticles (AuNPs) as optical probe to work in conjunction with the aptamer. Notably, AuNPs exhibit size and aggregation dependent

colour change due to their plasmonic electronic behaviors. This optical property of the AuNPs can be exploited in hybrid elements by conjugating them with various biorecognition elements to develop optical sensing systems. The colorimetric assays using AuNPs conjugated aptamers have been reported for many targets, including PfLDH (Cheung *et al.*, 2013). In these assays, the AuNPs are stabilized by the adsorbed aptamers primarily at high salt concentration. When sample containing the targets are added to the solution of high salt concentration the AuNPs get aggregated leading to a colour change in the solution, the intensity of which can thus be correlated with the concentration of the target in the samples. However, the high assembly time of the above assay coupled with relatively poor detection limits obtained by using salts prompted the use of alternative aggregating agents like, polyelectrolytes (Xia *et al.*, 2010), cationic surfactants (Wu *et al.*, 2012a), and cationic polymers (Wu *et al.*, 2012b) for developing AuNP based optical detection assays.

This chapter describes our work towards the development of an AuNP based aggregation assay for the detection of PfLDH. The PfLDH specific P38 aptamer developed by us was used for the surface modification of citrate stabilized AuNPs. This hybrid probe was tested initially with NaCl solution followed by some cationic surfactant solutions to evaluate the assay performance of these ionic compounds. Previous studies on AuNP based detection of PfLDH utilized covalent attachment of aptamer to AuNPs (Cheung *et al.*, 2013). We proposed to revise the conjugation procedure, where instead of using the covalent conjugation a physical interaction between P38 and AuNPs was exploited for the stabilization. Thus, this revised protocol also curtailed additional chemical steps on preparing the conjugate probe. A detailed account on the performance of the P38-AuNP

based detection of PfLDH following the aforesaid revised approaches has been presented in this chapter.

4.2 Experimental approaches

The current study was approved and ethically cleared by the Institute Human Ethics Committee (IHEC) of the Indian Institute of Technology Guwahati, India.

4.2.1 Materials

P38 ssDNA aptamer developed by us was synthesized by Bioserve Biotechnologies India, pvt ltd. Gold (III) chloride solution (~30 wt % in dilute HCl), was obtained from Sigma Aldrich (USA). All other chemicals were of analytical grade.

4.2.2 Synthesis and characterization of AuNPs

AuNPs were synthesized by the citrate reduction of $HAuCl_4$ via the Turkevich method (Turkevich *et al.*, 1951). The concentration of the AuNPs was estimated using UV/Vis spectrophotometer (Cary 100 Bio, Varian) taking extinction coefficient 2.43 9 10^8 $M.cm^{-1}$ at $\lambda_{520\ nm}$ (Kim *et al.*, 2010). The size of the AuNPs was determined using Transmission electron microscopy (TEM) at an accelerating voltage of 200 kV (JEOL JEM, 2100).

4.2.3 AuNP aggregation based colorimetric assay

For salt based aggregation assay, 1.6 µl P38 from a stock of 25 µM was mixed with 80 µl AuNPs from a stock of 5 nM, and the volume was made up to175 µl using 20 mM HEPES buffer, pH 7.4. This mixture was incubated at RT for 45 min. 10 µl of PfLDH at various dilutions in 20 mM HEPES buffer, pH 7.4, was added to the mixture and allowed to

incubate for 1 h, followed by the addition of 20 µl of NaCl (1 M). The colour change was monitored using UV/Vis spectrophotometer (Cary 100 Bio, Varian) taking absorbance at $\lambda_{650\ nm}$ and $\lambda_{520\ nm}$.

For cationic surfactant based aggregation studies, 6 or 10 µl P38 (from stock of 1 µM) was mixed with 10 µl PfLDH at various dilutions and allowed to incubate for 1 h at RT in a final volume of 90 µl. 30 µl of cationic surfactant benzalkonium chloride (BCK) (20 µM), cetyltrimethylammonium bromide (CTAB) (30 µM) or didodecyl dimethyl ammonium bromide (DDAB) (10 µM) was then added, and incubated for 20 min at RT, followed by the addition of 80 µl of AuNPs (5 nM). The colour change was monitored at $\lambda_{650\ nm}$ and $\lambda_{520\ nm}$.

4.2.4 Real sample analysis

To check the assay performance in real samples, blood was drawn from a healthy donor. 50 µl of blood (containing approximately 225 x 10^6 RBCs) was subjected to 600 x g for 10 min to precipitate RBCs. The supernatant was discarded, and the pellet was resuspended in 50 µl of 5X RBC lysis buffer (155 mM NH_4Cl, 12 mM $NaHCO_3$, 0.1 mM EDTA) and incubated for 15 min. The lysed RBC sample was subjected to 840 x g for 5 min, and the supernatant was collected. This extract was diluted with 20 mM HEPES pH 7.4, and spiked with recombinant PfLDH protein to mimic real sample, while unspiked RBC lysate served as negative control.

Real sample from two malaria positive patients (denoted as A, and B for ease) was graciously provided by Dr. Archana Jain, Toshi Pathology, Allahabad, India. The presence of *Plasmodium vivax* parasitemia in the two patients was confirmed by microscopy. 10-fold and 20-fold dilutions of each of the patient samples were tested using the developed assay,

while blood sample obtained from a healthy volunteer served as a negative control. For analysis of real samples in a commercial RDT, 5 µl of patient whole blood spotted in the sample zone was allowed to flow over by 100 µl of buffer supplied along with the RDT to the test zone. The color developed in the test zone was monitored visually.

4.3 Results and discussion

4.3.1 Salt-mediated detection of PfLDH

For linking oligonucleotide probes to the AuNP surface, a single-step adsorption is advantageous over covalent attachment. Covalent attachment of probes to AuNPs requires additional probe modification steps and may affect the biorecognition ability of the probe. Unlike dsDNA which has a rigid double helix structure, ssDNA is flexible, and is able to partially uncoil and allow its bases to interact with the AuNPs via van der Waals forces. The adsorption of DNA on the surface of AuNPs stabilizes them, preventing their aggregation in the presence of salt (Li and Rothberg, 2004). The displacement of ssDNA aptamer from the surface of AuNP in the presence of target molecule leading to AuNP aggregation in the presence of salt, can be implemented in developing a colorimetric assay (Kim *et al.*, 2010). In this study, the affinity of 90 mer long P38 aptamer for PfLDH was exploited to develop a colorimetric assay based on the above principle (Figure 4.1 A). Citrate-stabilized AuNP solution when incubated with single-stranded aptamer, the aptamer was adsorbed on the surface of the nanoparticles via van der Waals forces. When the target PfLDH is presented, aptamer-protein complex is formed, leaving the AuNPs free to aggregate in the presence of salt. In the absence of the target, P38 remained adsorbed on AuNPs, not allowing NaCl to

screen the repulsion between nanoparticles. Scouting for the NaCl concentration (from 25 to 200 mM) that causes aggregation of AuNPs (2 nM), showed that the aggregation gradually increased with the increasing amount of salt and reached a saturation around 100 mM NaCl (Figure 4.2 A). To prevent the AuNP aggregation in the presence of aptamer, 200 nM of P38 was incubated with 2 nM AuNPs followed by addition of NaCl (75 or 100 mM) (Figure 4.2 A inset). In both cases, aggregation was prevented to a certain degree. Therefore, 100 mM NaCl, and 200 nM P38 were chosen as the optimal salt and aptamer concentrations for further experiments.

PfLDH at various concentrations was allowed to incubate with P38-coated AuNPs, followed by addition of NaCl. The aggregation of AuNPs increased with the increasing concentration of PfLDH as evident from the colour change from red to blue. However at PfLDH concentrations higher than 1 nM, the AuNPs were disaggregated as evident from the colour gradually reverting back to red. Therefore, the graph (Figure 4.2 B) could be divided into two zones: (i) the ascending curve, starting from 0 pM to 1 nM of PfLDH. Here, the aggregation of AuNPs increased with increasing the target concentration. (ii) the descending curve which starts as PfLDH concentrations become higher than 1 nM. The linear part of the curve yielded a detection limit (LOD) of 402 $\pm$ 40 pM, calculated using the formula LOD = (3.3 x S.D. of Blank)/Slope of the linear part. The disaggregation of AuNPs at higher protein concentrations is puzzling, and could be attributed to the increased repulsive force between high negative charges on the PfLDH target protein (zeta potential ~ -12 mV) at pH 7.4 and citrate-capped AuNPs (zeta potential ~ -25 mV) that stabilize the AuNPs in solution.

However, crowding effect of the protein at high concentration cannot be ruled out for such disaggregation effect.

4.3.2 Cationic surfactant-mediated detection of PfLDH

Disaggregation of AuNPs at high protein concentration resulting in a narrow linear range in the salt-based assay prompted us to explore cationic surfactant-mediated AuNP aggregation for PfLDH detection. A surfactant is a bulky molecule, typical Mw ranges from 300 to 400, which consists of two moieties: (i) one or more hydrophobic alkyl chains and (ii) an ionic or highly polar hydrophilic group. The positively charged group of cationic surfactants usually contains a quaternary ammonium, although analogues containing sulphur, phosphorus or arsenic exist as well (Cross and Singer, 1994). Due to the versatility of quaternary ammonium surfactants ‘‘quats’’ to retain their positive charge at any pH, they have been used for the synthesis and control of nanomaterials (Smith and Korgel, 2008; Moon *et al.*, 2009). CTAB has been shown to interact with single and double stranded DNA to form cubic and hexagonal nanostructures, respectively (Liu and Abbott, 2010). CTAB has also been used to develop an AuNP based colorimetric assay for small molecules (He *et al*., 2013), ions (Wu *et al.*, 2012a) and proteins (Lee *et al.*, 2014). For the present work, we studied three different surfactants: (i) alkyl dimethylbenzyl ammonium chloride, commonly known as benzalkonium chloride (BCK) which contained an aromatic group and a long (C12) alkyl chain; (ii) hexadecyl(cetyl) trimethyl ammonium bromide (CTAB), which contained a single long (C16) alkyl chain; and (iii) didodecyl dimethyl ammonium bromide (DDAB) which contained two long (C12) alkyl chains. We compared their aggregation efficiency for naked AuNPs and their detection efficacies using PfLDH as the target and

aptamer P38 as the biorecognition molecule. To our knowledge, the aggregation potentials of BCK and DDAB have not been investigated before, using a protein as target molecule. Figure 4.1 B, D shows the principle for cationic surfactant based detection assay for PfLDH using the aptamer P38, and the chemical structure of the three surfactants used in the study. In the presence of PfLDH, P38 forms a complex with it, and the aptamer is hence unavailable for binding when a cationic surfactant is present. With addition of AuNPs, the free cationic surfactant causes their aggregation, leading to a blue colour. In the absence of a target, the aptamer is free to assemble with cationic surfactant, and the AuNPs remain unaggregated due to unavailability of free positive charge in the system. Multiple, long alkyl chains on the quaternary ammonium of the surfactant enables better aggregation of AuNPs.

Among the three surfactants studied, DDAB with two long alkyl chains caused complete aggregation of the free AuNPs at a much lower concentration of 1.5 µM, followed by BCK and CTAB at 3 µM, and 4.5 µM, respectively (Figure 4.3 A). Although BCK has an alkyl chain with four carbons fewer than CTAB, the presence of an aromatic ring probably gives it a significant advantage in aggregating AuNPs. In order to obtain appropriate signal respective to the surfactant concentration used in each assay, the P38 concentration was optimized. 30 nM P38 was sufficient to achieve minimum background in the absence of PfLDH, when BCK (3 µM) or CTAB (4.5 µM) was used. However, 50 nM P38 was used to mitigate the aggregation caused by 1.5 µM DDAB (Figure 4.3 B). Hence, DDAB has been identified as a stronger and more potent aggregating agent than BCK and CTAB.

The abilities of BCK, CTAB and DDAB to detect various concentrations of PfLDH in the assay format were investigated. The disaggregation of AuNPs using any of these three

surfactants at high concentration of PfLDH was not as pronounced as the case when NaCl was used. However, the lesser disaggregation is likely to generate a wider dynamic detection range, and is thus considered a suitable property for analytical perspective. For NaCl, BCK, CTAB and DDAB, the minimum concentrations of PfLDH beyond which disaggregation starts were 1, 5, 5, 10 nM, respectively. Although DDAB has a better aggregation efficacy for AuNPs and tolerates higher concentration of PfLDH without allowing disaggregation, BCK showed better sensitivity with an LOD of 281 $\pm$ 11 pM which is far higher than the corresponding CTAB and DDAB based detections (Figure 4.4). Thus, from the above results, the order of detection sensitivity was BCK>NaCl followed by CTAB and DDAB, both of which did not produce any significant response for PfLDH concentrations up to 1 nM (Figure 4.4). It is expected that BCK will also maintain its higher sensitivity with other DNA aptamers with similar chain length as well, since the charge of such aptamers may not significantly vary. In a previous study, CTAB has been reported to have a better sensitivity than NaCl for an arsenic aptamer (Wu *et al.*, 2012a). Thus, the sensitivity of an assay may be dependent on the type of target analyte.

The detection limits obtained by us (38 pg.μl^{-1} with BCK and 55 pg.μl^{-1} with NaCl) with P38 are superior to a similar assay developed by Cheung *et al.* (2013) for PfLDH. A number of variations have been included in the present detection protocol. Unlike covalently conjugating the PfLDH aptamer with AuNPs, P38 was physically adsorbed on the nanoparticles, and thereby, we omitted additional steps of preparing the detection probe. Additionally, insight obtained from comparison of salt and cationic surfactants based aggregation methods led to significant improvements in the detection limit and range.

Conversely, the sensitivity reported previously (Lee *et al.*, 2014) using different aptamers was found to be better than the one obtained by us. However, the sensitivity reported by us is in the clinically relevant picomolar range (Martin et al, 2009) for the reliable detection of malaria.

4.3.3 Interference studies

Specificity of the assay for PfLDH was investigated by measuring the assay response to competitive and relevant non-specific targets like HSA, a predominant protein in blood and another malarial biomarker, histidine-rich protein II (HRP II). The results showed very good selectivity to PfLDH as compared to the non-specific targets (Figure 4.5 A). The marginal interference from HSA protein could be nullified by subtracting the background noise data equivalent for a healthy individual.

4.3.4 Practicability of the assay

To demonstrate applicability of the method, the assay performance was validated in real samples using (i) PfLDH spiked RBS lysate, and (ii) real patient sample from two malaria patients. Lysis of RBCs in 50 µl blood was optimized in 2X and 5X RBC lysis buffer. Thorough RBC lysis was observed in 5X buffer, yielding a clear red supernatant. While contrary to previous reports (Lee *et al.*, 2012b), lysis observed in case of 2X buffer was incomplete (Figure 4.6). Hence supernatant from RBC lysis using 5X buffer was spiked with 400 pM PfLDH to mimic the real sample, and the assay response was recorded for different background RBC concentrations (Figure 4.5 B). In each case, a control with the same volume of extract without PfLDH was added. A higher response in the presence of PfLDH spiked sample indicated the potency of the assay for real samples. Response of the

assay to 10-fold and 20-fold diluted blood samples from *P. vivax* infected patients revealed that the assay was able to positively detect malaria in both patients A, and B, compared to the negative control (Figure 4.5 C). Although the aptamer P38 was selected using PfLDH as a target, its positive response to PvLDH (present in patient blood) can be easily explained. A BLASTP search reveals a 99 % percent sequence similarity between PfLDH and PvLDH. Considering this high similarity percentage the cross reactivity of the aptamer to other *Plasmodium* species LDH is expected. In the past, similar observations were made by Lee *et al.* (2012b), where a PvLDH specific aptamer, gave excellent response to PfLDH.

The same samples were then tested with a commercial antibody based LDH pan malaria RDT. To validate the proper functioning of the RDT, the appearance of the positive control line in the RDT kit was checked. The RDT was not successful in detecting the parasitemia in both the infected samples. However, the RDT could detect the parasitemia in the sample of patient B when the dilution of the sample was restricted to 10 folds. Result implies that the developed assay could surpass the performance of the commercial malaria RDT in case of lower parasitemia samples.

The storage stability of the components of the assay was monitored over a period of one week, where the unmodified AuNPs, and P38 adsorbed AuNPs were stored at RT, in dark, and their efficiency in the assay was tested intermittently over a period of time. While unmodified AuNPs showed a drastic reduction in assay response after one day due to possible aggregation of AuNPs, the storage stability of P38 modified AuNP was relatively better (Figure 4.5 D).

4.4 Conclusion

An aptamer (P38) based colorimetric method using surfactant mediated aggregation of citrate stabilized AuNPs to detect the target was developed. The aromatic cationic surfactant BCK, was identified as the most efficient agent for highly sensitive detection of PfLDH. BCK gave better sensitivity than the well-known salt based or cationic surfactant CTAB based aggregation method. This is the first report on the use of BCK in an AuNP colorimetric assay. The sensitivity reported by us is in the clinically relevant range, and thus, the reported method using benzalkonium chloride as aggregating agent has potential to be developed as a sensitive and selective method for detecting malaria in clinical sample.

Figures

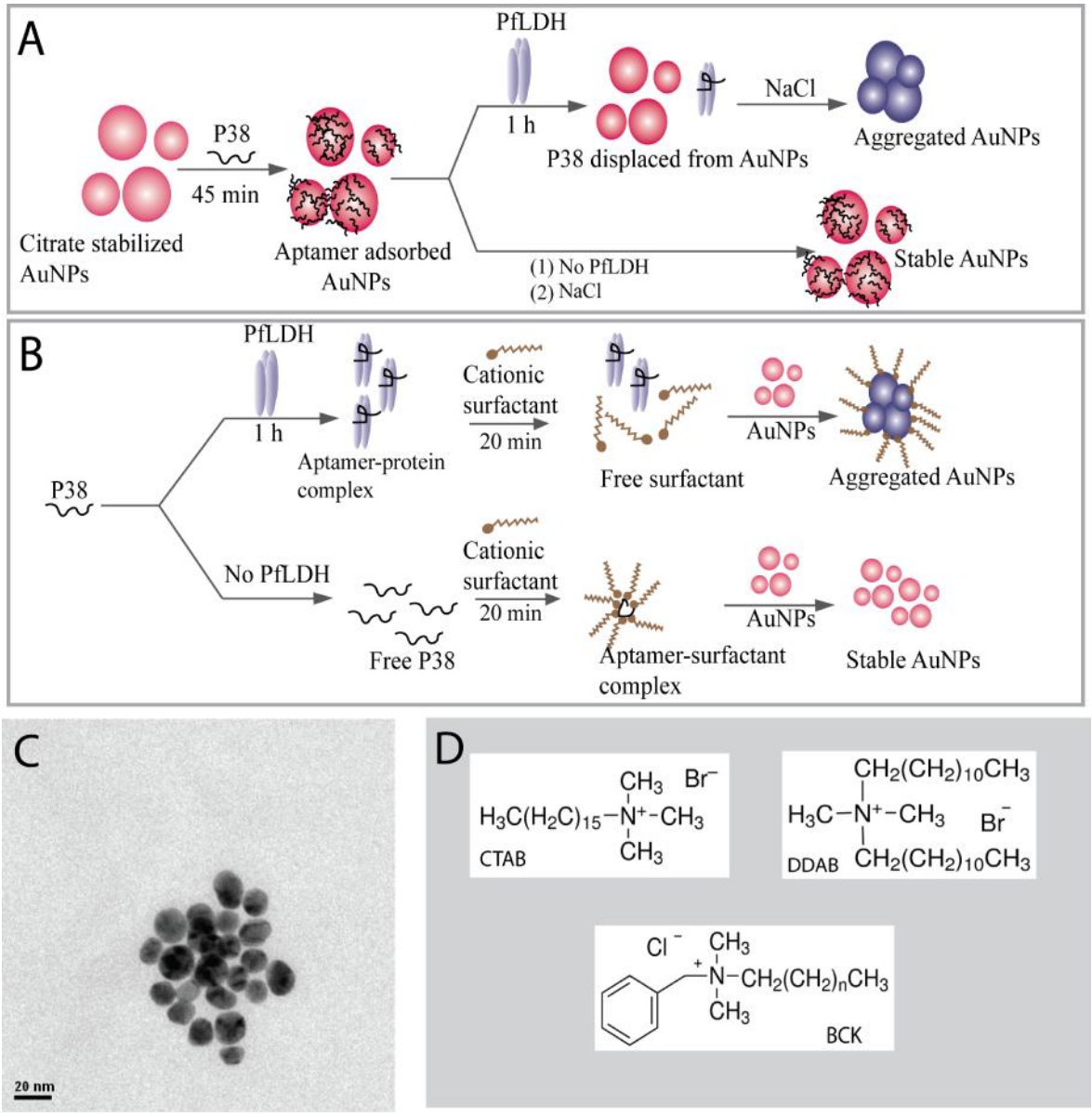

Figure 4.1: Simplified representation of the assay based on (A) NaCl and (B) cationic surfactant assisted aggregation of AuNPs for detection of PfLDH, (C) TEM image of citrate stabilized AuNPs revealed an average diameter of 16 $\pm$ 3.5 nm, (D) chemical structure of cationic surfactants used in the study.

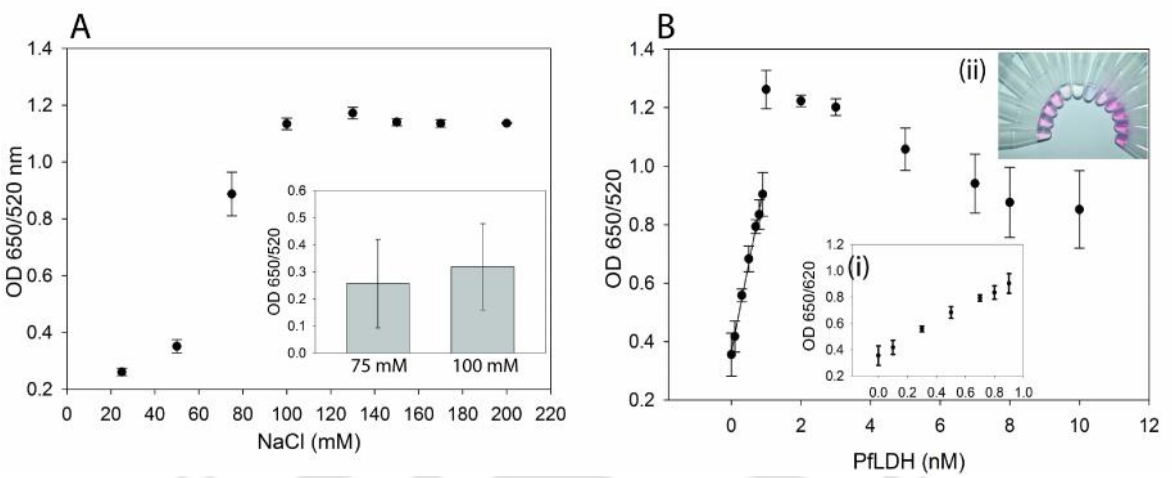

Figure 4.2: (A) Effect of NaCl concentration on the aggregation of free AuNPs. Inset: aggregation of P38 modified AuNPs with 75 mM, and 100 mM NaCl. After adsorption of P38 on nanoparticles, their aggregation by NaCl was comparably reduced. (B) NaCl assisted AuNP aggregation assay response to the increasing concentration of PfLDH. The linear segment of the response is shown in inset (i). Inset (ii) Image of the change in colour of the assay with 0, 1 pM, 10 pM, 100 pM, 900 pM, 1 nM, 10 nM, 100 nM, 1 µM, 3 µM, 5 µM, and 7 µM of PfLDH.

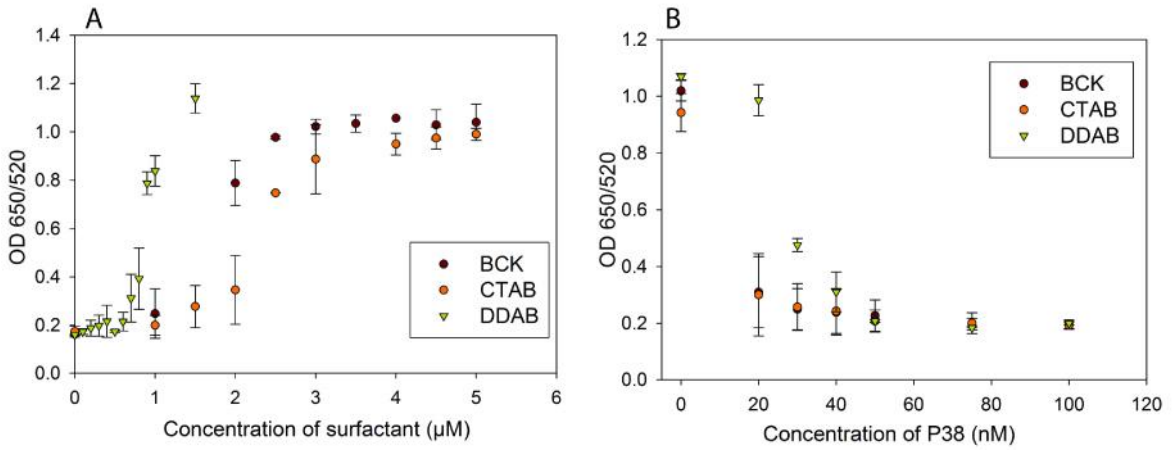

Figure 4.3: (A) Effect of BCK, CTAB and DDAB on the aggregation of 2 nM citrate stabilized AuNPs. (B) Optimization of P38 aptamer concentration to obtain minimum background AuNP aggregation for 3 µM BCK, 4.5 µM CTAB, and 1.5 µM DDAB.

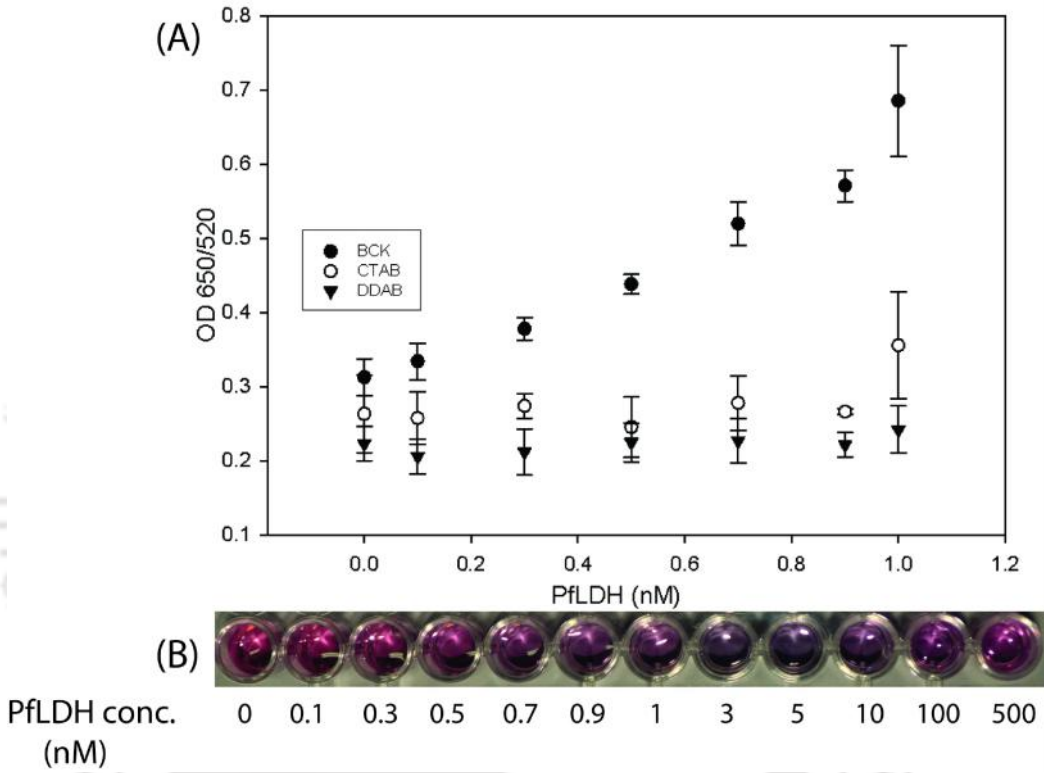

Figure 4.4: (A) Response of BCK, CTAB, DDAB assisted AuNP aggregation, for detection of PfLDH using P38 aptamer as detection probe. (B) Image shows the change in colour of the assay mixture, using BCK as the aggregating agent.

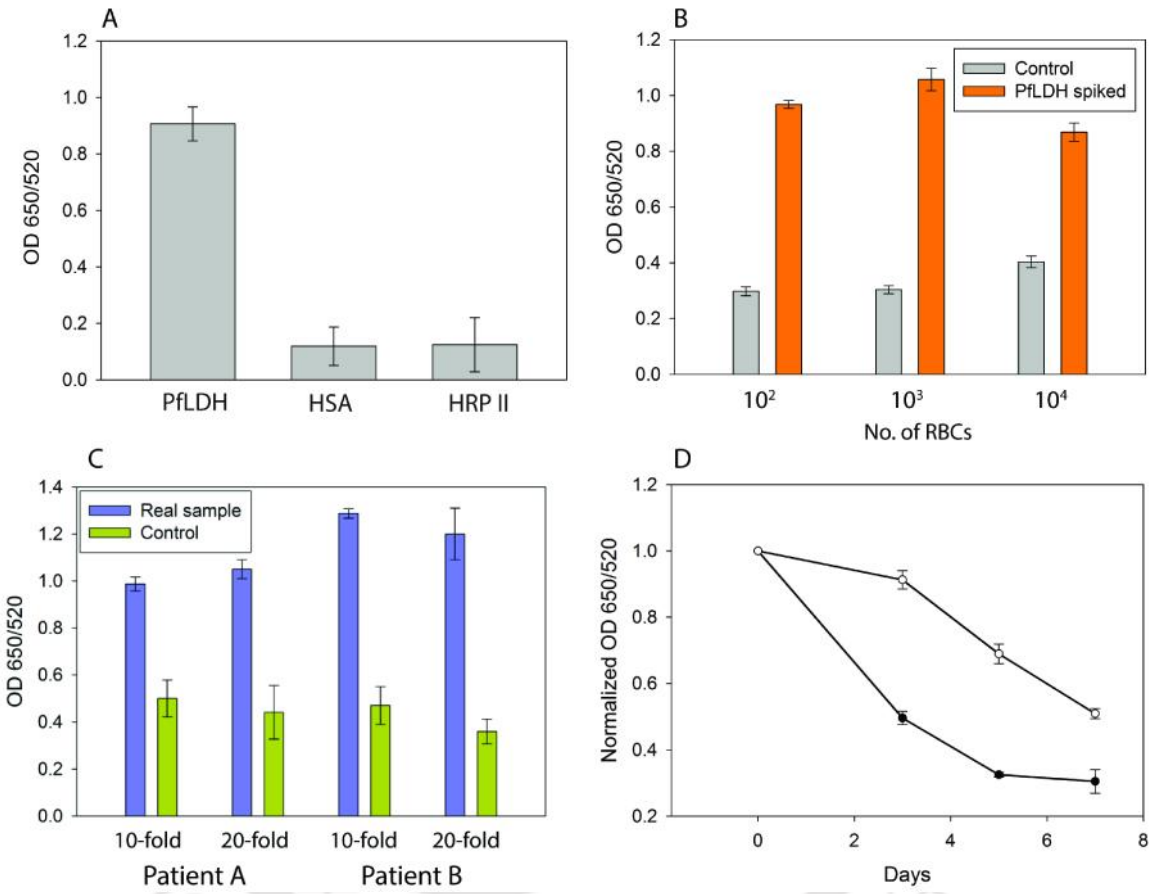

Figure 4.5: (A) Response of the AuNP based optical assay for 1 nM each of, PfLDH, HSA, and HRP II. Background values have been subtracted for ease of comparison, (B) Real sample analysis using extract from 10^2, 10^3 and 10^4 RBCs spiked with 400 pM PfLDH, (C) Analysis of real samples from patient A, and B, at two different dilution for each, (D) Stability of unmodified AuNP, and P38-AuNP, over a period of one week.

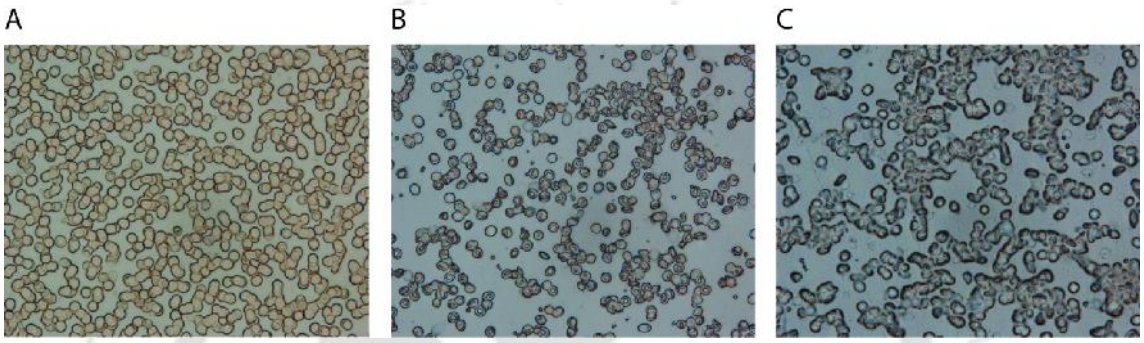

Figure 4.6: Microscope image of (A) Untreated RBCs, (B) RBCs treated with 2X lysis buffer, (C) RBCs treated with 5X lysis buffer.

Chapter V

Development of Aptasensor for Electrochemical Detection of PfLDH

5.1 Overview

Speedy diagnosis of suspected cases is considered as one of the key activities in malaria management that warrants a highly sensitive, rapid, portable, stable and low cost malaria detection system to use in malaria endemic resource limited locations. Such a system will be useful to detect low parasitemia in asymptomatic individuals, who are vast contributors to the human infectious reservoir (Hopkins *et al.,* 2013). Conventional techniques like microscopy, and the more recent, RDTs, cannot detect such widely reported low-density *Plasmodium* infections of submicroscopic levels (Okell *et al.,* 2009; Bousema *et al.,* 2014). This chapter describes a DNA aptamer based highly sensitive detection test for malaria using PfLDH as a target biomarker in an electrochemical transducer based dual detection platform. The aptamers against PfLDH which have been developed so far are mostly explored to detect malaria in optical transduction platforms (Jeon *et al.,* 2013; Lee *et al.,* 2014; Cheung *et al.,* 2013; Dirkzwager *et al.,* 2015). We propose to utilize an electrochemical platform to enhance the signal of interaction between the aptamer developed by us and PfLDH, for sensitive detection of malaria. Notably, the electrochemical transducer based platforms offer label free detection, and are widely known for their very high sensitivity, selectivity, scope for miniaturization, and low cost (Ohnoa *et al.,* 2013; Min *et*

al., 2008), which thus, have potential to address the current need of malaria management including monitoring submicroscopic infections.

To develop the electrochemical transducer platform, we proposed to fabricate an aptamer-electrode by immobilizing the aptamer physically on graphene oxide (GO). Unlike chemical immobilization, this physical mode of contact between the aptamer and GO is an inexpensive, simple and gentle process supporting the structural and functional integrity of the native DNA aptamer. In this physical process of immobilization the oligonucleotide aptamers are known to adsorb on the graphene derived nanomaterials by a combination of π−π stacking, hydrophobic interaction, hydrogen bonding, and van der Waals forces (Liu *et al.*, 2013a). GO, which is a hydrophilic derivative of graphene, is known for its dispersibility in aqueous medium, and facile surface chemistry (Peng *et al.*, 2015; Chen *et al.*, 2012). Amenable to functionalization, the GO/DNA conjugate based sensors have gained vast popularity due to their ease of design, admirable signal to noise ratio and high sensitivity (Lin *et al.*, 2011; Wang *et al.*, 2014a).

The aptamer based detection of PfLDH on the electrode surface was then probed impedimetrically, using a redox probe and voltammetrically by monitoring the accumulation of the reduced cofactor generated from the PfLDH catalysed reactions. This double detection approach adapted here helped to confirm the existence of the biomarker. While the impedimetric measurement detected the PfLDH to a femtomolar level, the complementary enzyme activity linked voltammetric detection ascertained the specificity of the developed aptasensor.

5.2 Experimental approaches

5.2.1 Apparatus and reagents

Electrochemical measurements were performed on an Autolab PGSTAT 1212 (Eco Chemie, Netherlands). A three-electrode system with platinum rod as counter electrode, Ag/AgCl (saturated KCl) as reference electrode, and GCE or modified GCE as the working electrode, was used in all the measurements. Electrochemical responses were measured in 50 mM PBS, pH 8, 0.1 M KCl (Buffer E) as the electrolyte. Differential pulse voltammetry (DPV) measurements were carried out at potentials ranging from 0.0 V to 0.4 V (during electrode characterization) and 0.5 to 0.8 V (for enzyme assay), with a step potential 0.05 V, modulation amplitude 0.025 V, equilibration time 5 s, modulation time 0.05 s and interval time 0.5 s. Electrochemical impedance spectroscopy (EIS) experiments were performed in a background of 2.5 mM $[Fe(CN)_6]^{-3}$ over the frequency range of 0.05 Hz to 10 kHz. All the measurements were carried out at RT. Atomic force microscopy (AFM) was performed on an ambient air scanning probe microscope (Agilent Technologies 5500, USA). Images were recorded with tapping mode using Picoscan 5 software. X-ray diffraction (XRD) patterns were recorded on a Bruker D2 Phaser diffractometer (USA) using Cu Kα irradiation operated at 30 kV and 10 mA. Raman spectra were recorded on a Horiba Jobin Vyon, LabRam HR (Japan). All chemicals used were of analytical grade and were used without further purification. Ultrapure water (18.2 MΩ) from a MiliQ filtration (USA) was used throughout this work.

5.2.2 Preparation of graphene oxide (GO)

Graphite from pencil lead grounded in to a fine powder was used to synthesize GO by modified Hummers method (Cote *et al.,* 2009). Briefly, 23 ml of H_2SO_4 from a stock of 12.1 M was added to a mixture of 0.5 g of powered graphite and 0.5 g of $NaNO_3$ and the mixture was stirred in an ice bath for 15 min. 3 g of $KMnO_4$ was slowly added and continued stirring for 15 min. The mixture was then transferred to a water bath (35 $\pm$ 5 °C) and stirred for 1 h. 40 ml H_2O was then added to the reaction and stirred for 30 min at 90 °C. Finally, 100 ml of H_2O was added followed by slow addition of 3 ml H_2O_2 (30 %), which changed the solution color from light brown to yellow. The solution was filtered and washed with 100 ml H_2O, to obtain a filtered cake. The cake further underwent 3-5 cycles of washing and centrifugation. The final solution was exfoliated in a bath sonicator to obtain the desired GO.

5.2.3 Fabrication of P38-GO-GCE electrode

Strategy followed for stepwise fabrication of the electrode is shown in Figure 5.1 A. Briefly, a glassy carbon electrode (GCE) of diameter 0.5 cm, was cleaned by polishing it with 0.3 µm alumina slurry and washing it ultrasonically in ethanol and water separately for 10 min each. 20 µl of GO solution (2 $mg.ml^{-1}$) was spotted on the cleaned GCE, dried in vacuum and incubated for 2 h. The modified electrode (GO-GCE) was carefully washed to remove any unbound GO. The PfLDH specific aptamer (P38) was used as a biorecognition element for electrode fabrication. Before use, the aptamer was denatured at 90 °C for 3 min, followed by incubation at 4 °C for 5 min. The GO-GCE electrode was then incubated in 50 µM P38 (2 µl) in 50 mM PBS, containing 7 mM (5.8 µl) $MgCl_2$ for 6 h. The aptamer spotting

was then repeated once again, followed by drying in vacuum for 16 h to make the aptamer-electrode (P38-GO-GCE) ready for use.

5.2.4 Real sample analysis

All experiments on blood samples were approved and ethically cleared by the Institute Human Ethics Committee of Indian Institute of Technology Guwahati, India. To prepare a sample that mimics real sample, 50 µl of blood (~225 X 10^6 RBCs) was subjected to 600 x g for 10 min. The pelleted RBC was suspended in 50 µl of 5X RBC lysis buffer (155 mM NH_4Cl, 12 mM $NaHCO_3$, 0.1 mM EDTA) and incubated for 15 min. The lysed RBC sample was subjected to 840 x g for 5 min. A suitable volume of the lysed RBC extract was diluted with Buffer E, to obtain a final background of 10^5 RBCs. The extract was then spiked with PfLDH to a final concentration of 5 fM. To test the efficiency of the aptasensor to probe the biomarker directly in the real sample, 0.5 µl whole blood isolated from malaria infected patient was diluted with 9.5 µl of Buffer E. The diluted sample was spotted on P38-GO-GCE electrode, incubated for 10 min, and then subjected to EIS measurement.

5.3 Results and discussion

5.3.1 Fabrication and characterization of aptamer-electrode (P38-GO-GCE)

GO was synthesized by oxidative exfoliation of low cost pencil graphite powder. The oxidative reaction yielded GO as evident from the formation of an intense peak at 10.7° and disappearance of the diffraction peak of the pure graphite powder at 26.5° in the XRD spectra

(Figure 5.2 A). A small portion of graphite oxide was also formed during the reaction as manifested by a broad peak at 21°. GO is an electronically hybrid material, composed of conducting π states from sp^2 bonded carbons and a carrier transport gap between the σ-states of its sp^3 bonded carbons. The ratio of sp^2 and sp^3 fractions can be tailored and the conductivity of GO can thus be controlled to transform it from a semi-conductor to a graphene like semi-metal (Loh *et al.*, 2010). The interlayer spacing (d) between the graphitic layers can be calculated using the Bragg's law: $\lambda = 2d \sin\theta$, where, λ is the wavelength of the X-ray beam used (0.154 nm) and θ is the diffraction angle. The interlayer distance increased from 0.345 nm for graphite to 0.829 nm for GO. The increase in interlayer distance suggests inclusion of oxygen containing functional groups in the oxidation process (Krishnamoorthy *et al.*, 2013; Abdolhosseinzadeh *et al.*, 2015).

For graphite and derived materials, typically three bands can be seen in the Raman spectra: the G band, which originates from a conventional first order Raman scattering, and the D and 2D bands that originate from a second-order double resonant process between non-equivalent K points in the Brillouin zone of graphene (Frank *et al.*, 2011). While the Raman G and 2D bands vary as a function of doping, the D band usually suggests the presence of defects such as bond-angle or length disorder, vacancies, etc. (Liu *et al.*, 2013b). The Raman spectrum of graphite powder (Figure 5.2 B) shows in-phase vibration of the graphite lattice (Hassan *et al.*, 2009) with the appearance of a high intensity band at 1571.13 cm^{-1} (G band) and two low intensity bands at 1324.6 cm^{-1} (D band) and 2671.4 cm^{-1} (2D band). On oxidation of graphite to GO, the intensity of the D band increases and the G band is blue shifted to 1599.7 cm^{-1}. This blue shift has been attributed to the increase in the sp^3

content due to the formation of covalent bonds during the oxidation of graphite (Ferrari and Robertson, 2000).

We used GO to physically capture P38 on the electrode surface. On binding to P38, the D and G bands appear at 1358.8 cm^{-1} and 1599.2 cm^{-1}, respectively and a small 2D band appears at 2703 cm^{-1}. The increase in D band frequency and appearance of a small 2D band is due to the p-doping of graphene sheets by DNA (Liu *et al.*, 2013b). The I_D/I_G intensity ratio is a measure of disorder in graphene and was estimated to be 0.67, 0.915, and 1.35 for graphite, GO and P38-GO, respectively. The high I_D/I_G on oxidative exfoliation of graphite powder to GO suggests that the prepared GO had defects, which is typical for such a process (Liu *et al.*, 2011). On P38 adsorption to GO, the disorder further increased leading to an increase in I_D/I_G. This demonstrated the successful adsorption of P38 on GO sheets. Single stranded DNA has been shown to bind to GO via hydrophobic interactions and π- π stacking. The aromatic and hydrophobic rings of ssDNA can bind to GO once the negative charges between the two molecules are screened by electrolytes (Wu *et al.*, 2011). In our study we used an ionic buffer with divalent Mg^{+2} ions to screen the repulsive forces between the polyanionic DNA and negative functional groups on GO.

For electrochemical characterization of P38-GO-GCE, DPV was carried out in 50 mM PBS, pH 8, 0.1 M KCl with 2.5 mM $[Fe(CN)_6]^{-3}$ to investigate the changes in electrochemical behavior during stepwise fabrication of the electrode. A defined $[Fe(CN)_6]^{-3}$ redox peak at 0.2 V was observed for the bare GCE (Figure 5.3 A). On immobilization of GO on the electrode, there was a dramatic decrease in the peak current at 0.2 V as compared to the bare GCE. This is attributed to the slow electron transfer kinetics due to the negative

charge imparted by the GO to the electrode surface that prevents easy access of $[Fe(CN)_6]^{-3}$ to the electrode. The immobilization of P38 decreases the current value at 0.2 V further due to obvious reason of incremental negative charges caused by the DNA-aptamer on the electrode surface. A new peak at ~0.3 V appears, due to possible interaction of P38 with GO, which however, needs further investigation to clearly elucidate its formation.

The interfacial properties of the electrode at each step of electrode assembly were also studied by EIS (Figure 5.3 B). The obtained spectra were represented in the form of Nyquist plots, where the arc radius of the semicircle part corresponds to the magnitude of the charge transfer resistance (Rct) while the straight tail corresponds to the magnitude of the Warburg impedance. The bare GCE showed a very low Rct. An increase in Rct was observed on treatment of the electrode surface with GO. This suggests that the negatively charged GO repels the $[Fe(CN)_6]^{-3}$ ions and limits the charge transfer at the electrode surface. When P38 was immobilized on GO-GCE, a significant increase in Rct occurred, which confirmed the successful immobilization of the aptamer. The DNA phosphate backbone being highly negatively charged, further prevented the communication of $[Fe(CN)_6]^{-3}$ ions with the electrode leading to a notable increase in the Rct.

Topography studies of GO, and P38-GO were carried out using AFM. Drop coated GO showed bright colored stacks of GO islands that appear to have a sheet like morphology in the image (Figure 5.4 A). Height profiling ascertains a uniform thickness of 3-3.5 nm across the GO islands. This height profile corresponds to the presence of few layered GO, which results from self-assembly and aggregation of GO monolayers during the spotting and drying process (Krishnamoorthy *et al.*, 2013). P38 application on GO in a layer-by-layer

fashion leads to significant increase in the thickness of the GO islands to ~ 25 nm suggesting the attachment of DNA to GO (Figure 5.4 B).

5.3.2 Response characteristics of P38-GO-GCE towards PfLDH

A dual electrochemical detection approach was adopted for detection of PfLDH using the modified electrode. This has been schematically depicted in Figure 5.1 B. The increase in Rct with increasing PfLDH concentration implies (Figure 5.5 A) that PfLDH was effectively captured on the aptamer electrode surface. The obtained Nyquist plots have been fitted to Randles–Ershler type equivalent circuit, (Figure 5.5 A inset), where Rs is the solution resistance, Zw is the Warburg impedance and CPE is the constant phase element. The results of the fitting when plotted generated response data (Figure 5.5 B) a non-linear trend was observed, from which the PfLDH concentration as low as 0.5 fM was discerned. Increase in PfLDH concentration in the sample leads to increase the magnitude of Rct as a consequence of decrease in the redox peak current for the reporter $[Fe(CN)_6]^{-3}$, thus impelling the detection towards a "switch off" approach.

To ensure the specificity of the constructed aptamer-electrode, DPV measurement for the reduced cofactor (NADH) generated from the PfLDH catalysed reaction was included concurrently with the above impedimetry based detection. The NAD/NADH redox couple is an attractive probe to monitor the LDH activity. To achieve this, NADH oxidation peak was characterized at the modified electrode surface (Figure 5.5 C). The activity of PfLDH at the aptamer-electrode surface was electrochemically monitored with increasing lactate concentrations in Buffer E and 10 mM NAD^+. NADH generated from the PfLDH catalyzed

oxidation of lactate, was oxidized at 0.65 V, producing a current response with increasing lactate concentration (Figure 5.5 D). For most electrochemical sensors, the oxidation of NADH is usually achieved at a high over potential (~ 0.75 V) leading to a loss of the sensor's functionality. However, the electrode modification with GO reduced this over potential to a suitable measurable range. The role of reduced-GO to decrease the oxidation potential of NADH on GCE has been reported (Tang *et al.,* 2009). Using this strategy, the presence of PfLDH on P38-GO-GCE electrode surface could be probed through a "switch on" approach.

The high specificity of P38 towards PfLDH has been previously confirmed by electrophoretic mobility shift assay (EMSA). In the present work, the aptasensor was challenged with HSA, which is the major protein present in blood serum, and two other common proteins, BSA and lysozyme. As expected, no current response in DPV was observed with all these proteins (Figure 5.6 A).

5.3.3 Practicability of the sensor

Initially, the applicability of the aptasensor to detect recombinant PfLDH in mimicked real sample was explored. The extract from lysed RBCs was spiked with 5 fM recombinant PfLDH to mimic real sample. The sensor could detect PfLDH in a background of 10^5 RBCs as demonstrated by EIS spectra (Figure 5.6 B). This concentration of the biomarker is known to fall within the clinically relevant range for malaria detection (Martin *et al.*, 2009). The aptasensor was also tested directly in the 10-fold, and 20-fold diluted whole blood samples collected from two *P. vivax* infected persons (patient A and B) and from a

healthy volunteer as a negative control. In all the three cases the aptasensor had conferred appropriate results. (Fig 5.6 C).

The aptasensor retained 62 % of its functionality even after storing it for a month at RT (25 °C -30 °C) with a relative humidity in the range of 70-90 % (Figure 5.6 D). The stability of the aptasensor could be attributed to the robustness of the DNA-based bio-recognition element, the aptamer. The reproducibility of the fabricated electrode was studied by exposing five different electrodes prepared in the same way to 0.5 fM PfLDH under similar conditions. The results revealed a high reproducibility of the fabrication procedure with a relative standard deviation (RSD) of 8.4 %. The non-covalent bonding involved in the immobilization maintains the native conformation of the aptamer and prevents any loss of functionality.

5.4 Conclusion

We report here a DNA aptasensor for unprecedented highly sensitive detection of malaria using PfLDH as the target biomarker in an electrochemical transducer based dual detection platform using impedimmetry and voltammetry techniques. Low cost GO prepared from powdered pencil graphite was effectively used as a conductive support to physically immobilize PfLDH specific aptamer, P38. With the help of a redox probe the presence of PfLDH in human serum sample was impedimetrically detected down to a femtomolar level. The specificity of the biorecognition system on the electrode was confirmed voltametrically by measuring the NADH formed as a result of enzymatic activity of PfLDH captured by the GO immobilized P38 aptamer. Interference studies with the relevant control proteins

demonstrated specificity of the sensor towards PfLDH. The developed aptasensor could also detect the biomarker in the real samples obtained for two *P. vivax* infected patients. This highly sensitive aptamer based electrochemical sensor thus has the potential to be developed as a viable product for detecting low parasitemia samples in yes/no format.

Figures

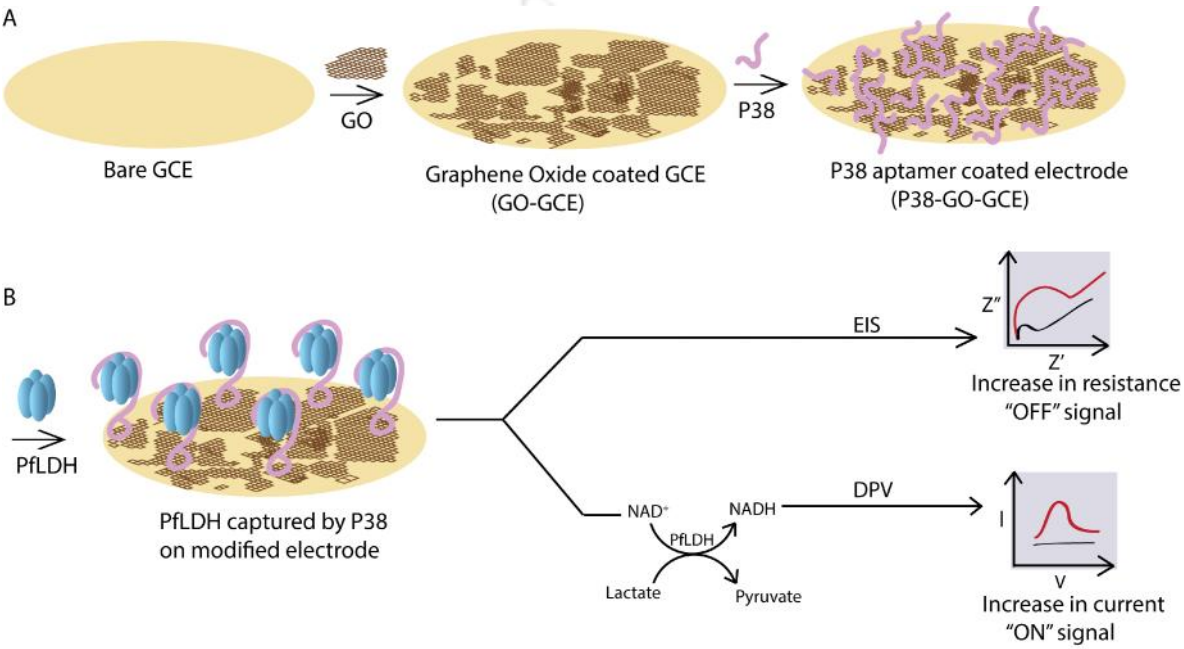

Figure 5.1: (A) Scheme for stepwise electrode fabrication of P38-GO-GCE. (B) Scheme for dual electrochemical detection of PfLDH using modified electrode P38-GO-GCE.

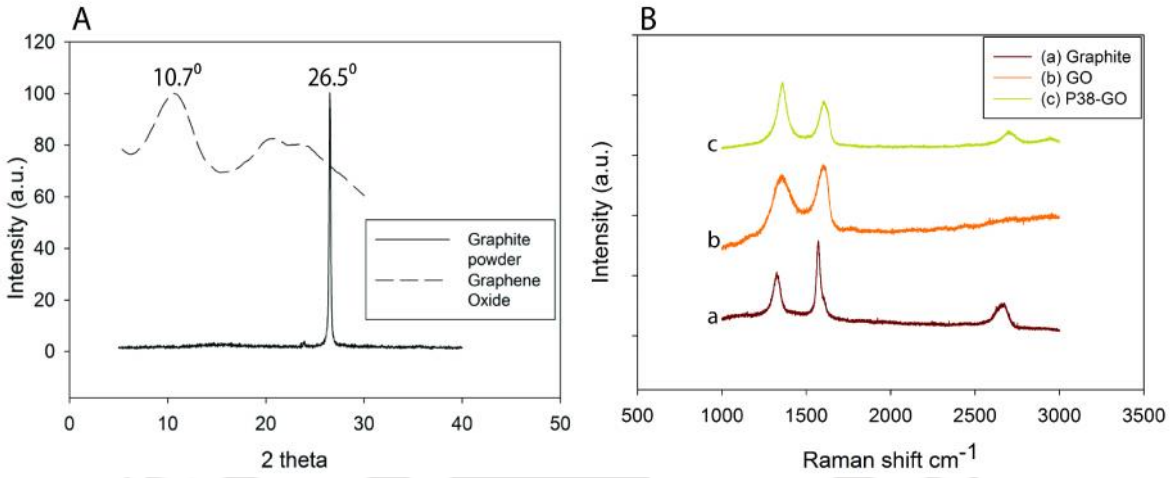

Figure 5.2: (A) XRD of powdered graphite and graphene oxide. (B) Raman spectra of graphite, GO and P38-GO.

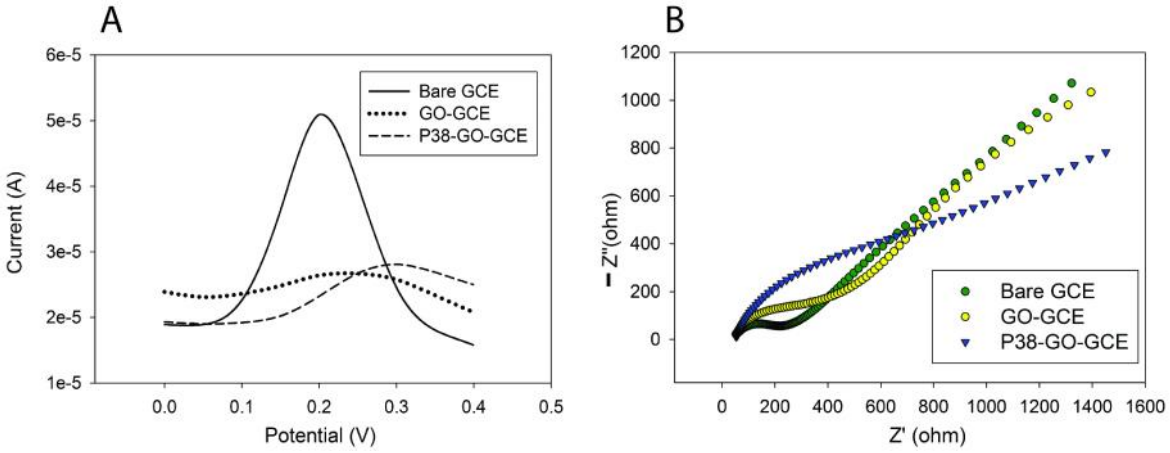

Figure 5.3: Electrochemical characterization of stepwise electrode fabrication using (A) DPV and (B) EIS.

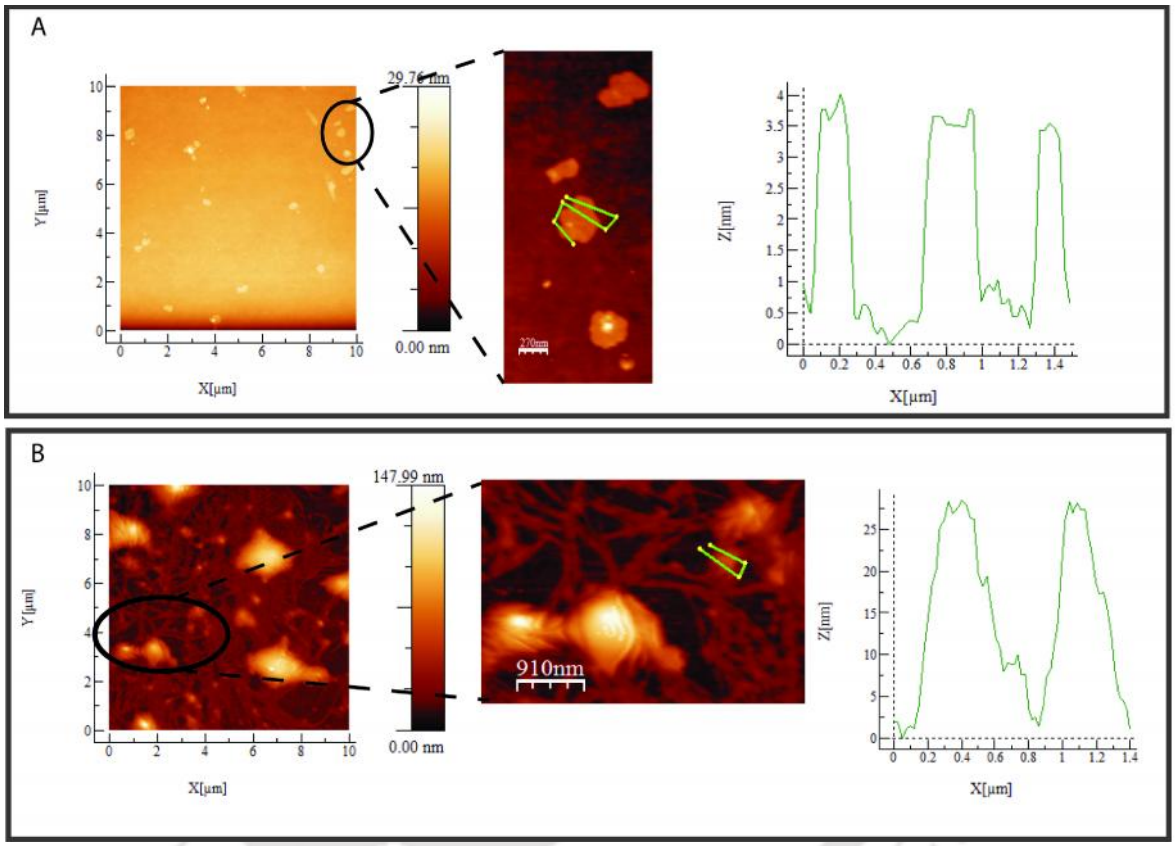

Figure 5.4: Topography including height profiles studies of GO-GCE (A) and P38-GO-GCE (B) using AFM.

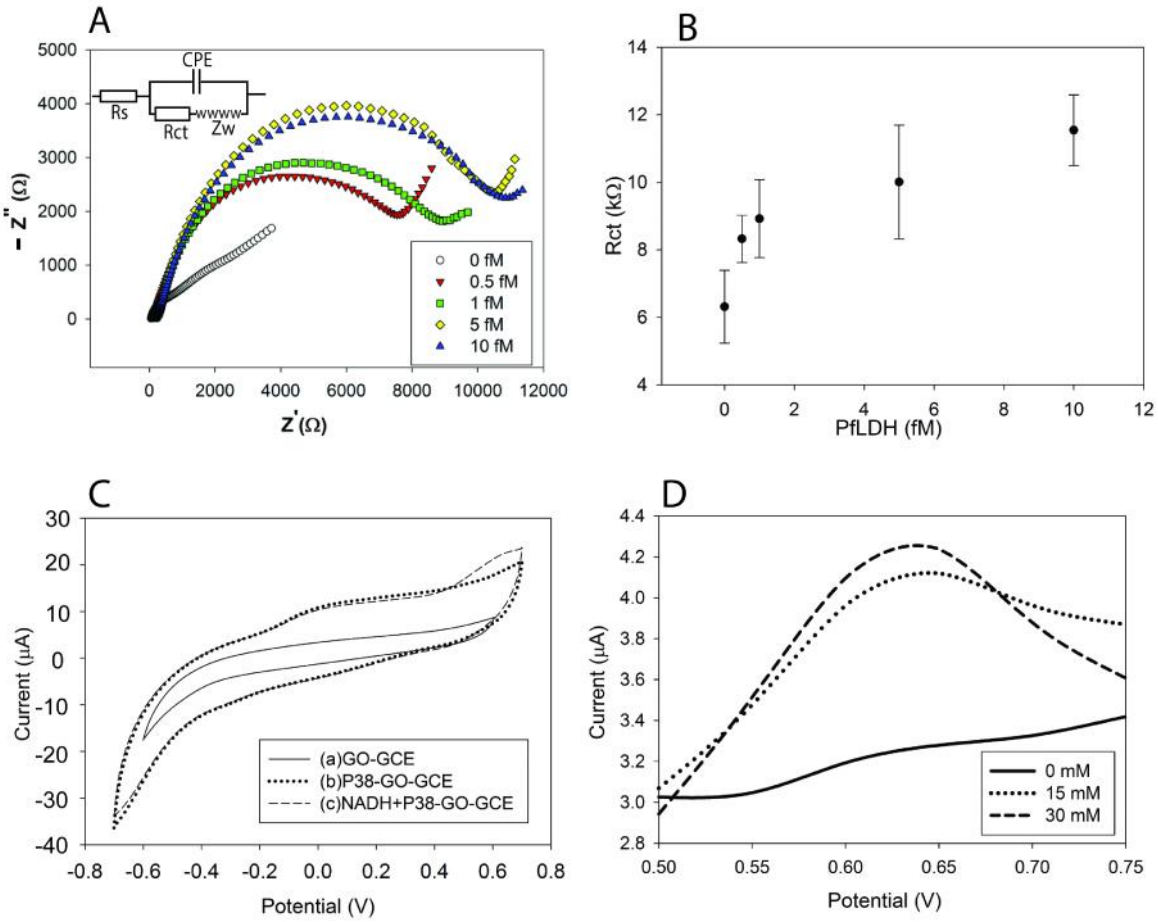

Figure 5.5: (A) Nyquist plots on the response of P38-GO-GCE towards increasing PfLDH concentration from 0.1 fM, to 10 fM. (B) Response curve of Rct vs increasing PfLDH concentration. Each data point is an average of at least three individual experiments. Error bars indicate the SD. (C) Oxidation of NADH on P38-GO-GCE, in the absence and presence of lactate. (a) GO-GCE in buffer E, (b) P38-GO-GCE in buffer E, (c) P38-GO-GCE response in presence of 0.4 mM NADH in buffer E. (D) DPV current response of PfLDH-P38-GO-GCE against various concentrations of lactate at 10 mM NAD^+.

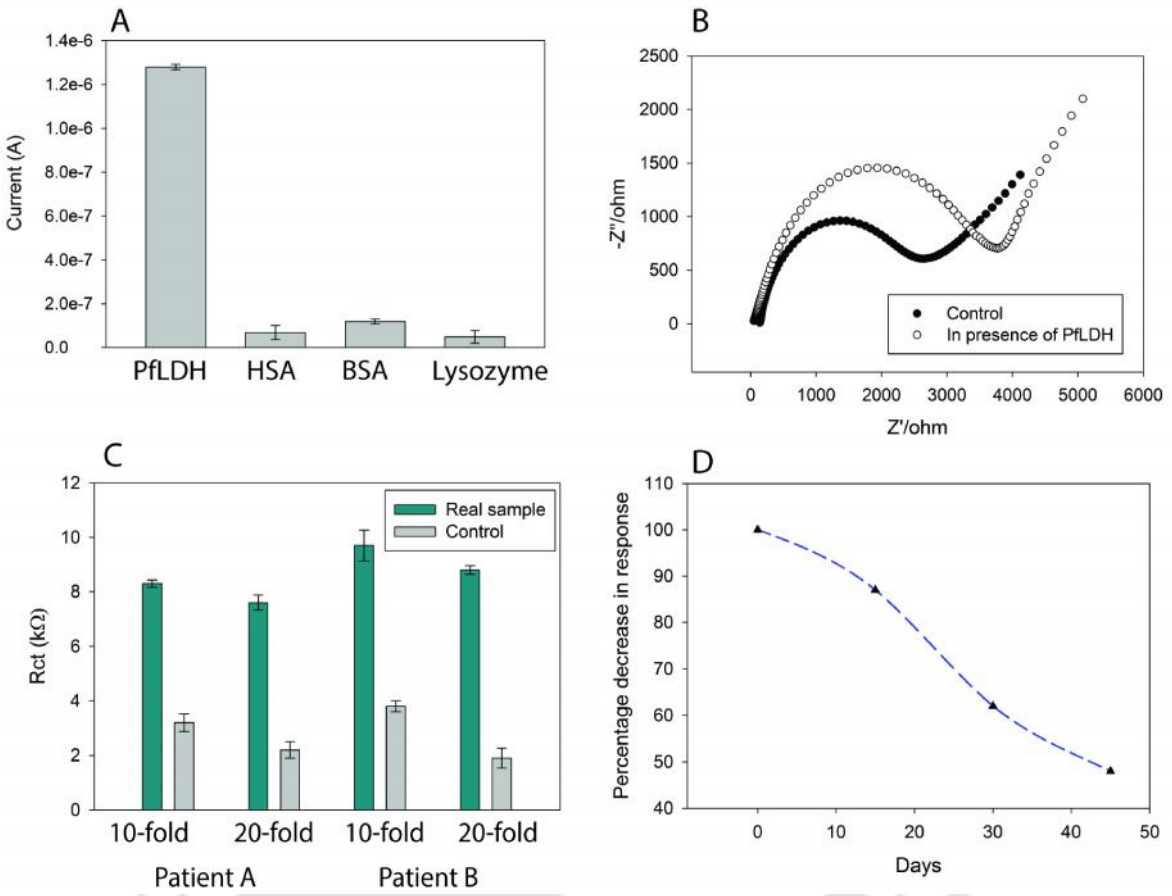

Figure 5.6: (A) DPV current response of the aptasensor at 0.65 V to different control proteins each at 100 nM. (B) EIS responses of the aptasensor to the extract of lysed RBC (10^5 cells) (•) and lysed RBC (10^5 cells) containing 5 fM PfLDH (o). (C) The performance of the developed aptasensor when challenged with *P. vivax* infected samples from two patients and an uninfected sample from a healthy volunteer (as negative control), at two dilutions for both patients. (D) Storage stability of the developed electrode as a function of time. Data points represent an average of two independent experiments.

Chapter VI

DNA Templated Silver Nanoclusters for Fluorescence Based Detection of PfLDH

6.1 Overview

Silver nanocluster (AgNC) is a novel class of fluorophore widely recognized for its remarkable photophysical properties, biocompatibility, and application potential for detection of a variety of targets including metal ions (Adhikari and Banerjee, 2010), proteins (Sharma *et al.,* 2011b), DNA (Petty *et al.,* 2012) etc. A suitable scaffold is essential for the stability of AgNC in solution, which prompted the use of polymers, dendrimers, and biologically relevant supports like peptides, nucleic acids, and so on, to template AgNC (Li *et al.,* 2013). DNA templated AgNC offers the advantage of tunability, due to the strong dependence of optical properties on DNA sequence. ^{1}H NMR studies show that Ag^{+} ions have significantly more affinity for cytosine through C-Ag-C coordination, in comparison to other bases (Petty *et al.,* 2004). Few other bases have also been found to modulate the properties of AgNC (Yeh *et al.,* 2010, 2012). Despite the ability of regulative optical properties based on sequence changes in the DNA template, an understanding on the structural basis for NC formation is incomplete. Studies on pH dependence of fluorescence and structural studies from size exclusion chromatography on two short cytosine-rich sequences revealed that multidentate coordination within DNA structures determines the favorability for the formation of fluorescent silver clusters (Sengupta *et al.,* 2009).

Intensive knowledge on the DNA dependent structural basis for AgNC nucleation and growth is fundamental for controllable synthesis of AgNC with desired photophysical properties. To focus beyond the primary base sequence-nanocluster interactions, we aim to explore the template structural dependence on the formation of AgNC. DNA hairpins, capable of assembling in complex patterns of resolution below 10 nm, have been proven to act as good AgNC scaffolds (Gwinn *et al.*, 2008). Hairpins with poly C loops, a special class of DNA secondary structures, were recently used to spatially arrange AgNCs on DNA nanotubes (O'Neill *et al.*, 2012). So far AgNC DNA templates have been restricted to shorter length nucleotides, with most reports concentrating on 12-30 mer sequences (Yuan *et al.*, 2014) and adequate information on the feature of ssDNA hairpin structures conducive for AgNC formation is unavailable.

In this chapter, a set of long ssDNA (90 mer) candidates with varying cytosine levels was examined as AgNC nucleation scaffolds. Four subsets of a positive candidate (P4) were selected by a combinatorial arrangement of tandem C repeats, and tested again as AgNC nucleation scaffolds. Results provide some critical insights on the size of the hairpin loop and the nature of the stem length on the formation and stabilization of the NCs. A smaller sequence, Sub 3, was finally identified as scaffold for strong fluorescent AgNC with much higher photo stability. The highly stable Sub 3-AgNC was applied to detect NAD^+ concentration in solution. The NAD^+ dependent quenching of Sub 3-AgNC was then exploited for development of a turn-off fluorescence assay for PfLDH. So far, a fluorescence based platform for detection of PfLDH has not been developed. Besides the inherent advantages of AgNCs in improving the performance of the sensor, the exploitation of

enzyme activity in the sensing mechanism provided a specificity screen to the detection system. A detailed account on the findings is included here.

6.2 Experimental approaches

6.2.1 Chemicals

DNA probes were commercially synthesized by Bioserve, India and obtained in a desalted lyophilized condition. DNA probes longer than 30 mer were HPLC purified. All DNA probes were reconstituted in autoclaved MQ water (18.2 MΩ). Before using in experiments, all DNA probes were heated at 90 °C for 5 min, followed by cooling in ice for 2-3 min. $AgNO_3$ (99.9 %) and 3-morpholinopropane 1-sulfonic acid (MOPS) were purchased from SRL, India. $NaBH_4$ (98 %), boric acid, HEPES, NaH_2PO_4, Na_2HPO_4, NaCl, acetic acid, sodium acetate, NADH, NAD^+ and Tris were purchased from Himedia, India. Alcohol dehydrogenase (ADH) (cat no A7011) was obtained from Sigma. All reagents used were of analytical grade.

6.2.2 Preparation of AgNC

A total 6 µl of $AgNO_3$ (1.5 mM) was added to 15 µl of DNA probe (100 µM) and the volume was made up to 100 µl with Milli-Q (MQ) water. The mixture was stored in dark for 15 min after which 6 µl of $NaBH_4$ (1.5 mM) was added to it. The AgNCs were formed after 1.5-2 h at RT, in dark. The morphological characterization of AgNC was performed by Transmission Electron Microscopy (TEM) at an accelerating voltage of 200 kV (JEOL JEM, 2100).

6.2.3 Fluorescence, UV-visible, and circular dichroism (CD) spectroscopy

Fluorescence measurements were performed on a Tecan infinite M200 PRO, using black, flat, clear bottom fluorescence microplates (Thermo Fisher scientific) by diluting 5 µl of AgNC, in 95 µl of MQ water. Absorbance was measured on a UV/Vis spectrophotometer (Cary 100 Bio, Varian) between $\lambda_{300\ nm}$ to $\lambda_{800\ nm}$ using a quartz cuvette. For the measurements, 100 µl of AgNC were diluted with 900 µl of MQ water. The CD spectra were recorded on a Jasco J-815 spectropolarimeter calibrated with (+)-10- camphorsulfonic acid for optical rotation. The spectra were measured from $\lambda_{350\ nm}$ to $\lambda_{190\ nm}$, using a 1 mm path length suprasil quartz cuvette at a scan rate of 50 $nm.min^{-1}$, interval of 0.5 nm, time constant of 1 s, and taking an accumulation of 3 scans. For CD studies 10 µl of (100 µM) DNA probe was mixed with 2.7 M urea and the volume was made up to 200 µl using MQ water, obtaining a DNA: urea molar ration of 1.9. The mixture was stored for 20 min at RT before carrying out the CD experiment. For each probe analysis, a control experiment, with no added urea was also performed.

6.2.4 DNA PAGE

Native and denaturing gel electrophoresis were performed on 20 % polyacrylamide gels in a miniVE vertical electrophoresis system (Amersham) using TBE buffer (54 g of Tris base 27.5 g of boric acid, 20 ml of 0.5 M EDTA (pH 8.0)). For denaturing conditions the gel was run in the presence of 7 M urea, at RT. Native gel was run in a cold cabinet maintained at 4 °C. Both gels were run at 120 V, for 4 h, at RT. The gels were stained with SYBR gold dye (Invitrogen).

6.2.5 Effect of pH, temperature, denaturants, and time

The formation of the NCs was studied in buffers ranging in pH from 4 to 10. AgNC formation was carried out in 15 mM buffer solution for 2 h, at RT in the dark, followed by fluorescence measurement. To study the effect of temperature on AgNC formation, DNA probes were mixed with $AgNO_3$ and $NaBH_4$ at the required concentrations and the mixture was incubated at RT, 70 °C, and 90 °C water bath for 2 h, in the dark, followed by fluorescence measurements.

The interference in AgNC formation in the presence of DNA denaturants was studied. For this, AgNC nucleation was carried out in the presence of various denaturants followed by fluorescence measurement.

6.2.6 Interaction studies between AgNC and NAD^+

In order to study the interaction of Sub 3-AgNC with NAD^+ a series of solutions containing a fixed volume of AgNC (5 µl) with increasing concentrations of NAD^+ (0-800 µM) was prepared. The binding process is described by the following equilibrium:

$$AgNC + n\,(NAD^+) \rightarrow [AgNC\text{-}(NAD^+)_n] \qquad (1)$$

According to this equation, the AgNC binds with n equivalents of NAD^+ to form an AgNC-NAD^+ complex. The fluorescence intensity at $\lambda_{660\ nm}$ was used to calculate the binding constants (K_a) and number of binding sites (n) by using the Scatchard equation (Liang *et al.*, 2008; Min *et al.*, 2004).

$$\log [(F_0\text{-}F)/ F] = \log K_a + n \log NAD^+ \qquad (2)$$

In this equation, F_0 is the initial fluorescence intensity prior to addition of NAD^+, and F is the fluorescence intensity at a specific NAD^+ concentration. By titration of NAD^+ and plotting log $(F_0 - F)/F$ against log $[NAD^+]$, a linear curve was obtained with a slope of n. The y-intercept is equal to log K_a and provides the value of K_a (Kang *et al.*, 2004; Min *et al.*, 2004).

Both static and dynamic quenching processes are described by the Stern-Volmer equation:

$$F_0/F = 1 + k_q\tau_0 [Q] = 1 + K_D [Q] \quad (3)$$

Where F_0 and F are the fluorescence intensities of the fluorophore in the absence and presence of quencher, [Q] is the concentration of the quencher, K_D is the Stern-Volmer constant, k_q is the bimolecular rate constant, and τ_0 is the lifetime of the fluorophore in the absence of quencher

Time resolved photoluminescence (TRPL) studies of the fluorescent AgNC and their complex with NAD^+ were carried out on a picosecond time-resolved cum steady state luminescence spectrometer (Edinburgh Instruments, UK, Model FSP920) using an LED source, at an excitation of $\lambda_{599\ nm}$ and emission of $\lambda_{650\ nm}$.

6.2.7 Interference studies

Specificity of AgNC for NAD^+ was assessed by monitoring the quenching of Sub 3-AgNC by various homologues of NAD^+, namely $NADP^+$, NADH and a synthetic cofactor $APAD^+$. For this, 5 µl of Sub 3-AgNC was incubated with 5 µl of a particular cofactor of 100 mM stock concentration, in a final volume of 100 µl, followed by fluorescence measurement. Interference to NAD^+ detection by Sub 3-AgNC was assessed by carrying out

the experiments in a background of monovalent or divalent salts. The effect of salts on plain Sub 3-AgNC was monitored by mixing 5 µl of Sub 3-AgNC with 8 µl of (100 mM) monovalent salts, or 10 µl of (10 mM) divalent salts, in a final volume of 100 µl. To validate the efficiency of NAD^+ mediated quenching of AgNC in the presence of salts, 1 µl of (100 mM) NAD^+ was mixed with 5 µl of AgNC in the presence of 8 mM monovalent salt or 1 mM divalent salt, followed by fluorescence measurement. The applicability of the AgNC to measure NAD^+ in serum samples was also investigated. Fresh human blood was collected from healthy human volunteer and centrifuged at 900 x g for 10 min to precipitate the RBCs. 100 µl of supernatant (serum) was collected, mixed with MQ to a final volume of 1 ml and stored at 4 °C for further use. To carry out the assay, we mixed 5 µl of AgNC, with 5 µl of serum and varying NAD^+ concentrations, in a final volume of 100 µl, followed by monitoring the fluorescence emission.

6.2.8 Turn-on, and turn-off fluorescence assay

For the AgNC-NAD^+ interaction based turn-on assay using ADH, 5 µl (1 $mg.ml^{-1}$) ADH was mixed with 5 µl (100 mM) NAD^+, 5 µl (100 %) ethanol, 5 µl (20 mM Tris-Cl, pH 8.8), 75 µl of MQ water, and allowed the enzyme catalysis for 5 min, followed by addition of 5 µl of AgNC. To carry out the turn-off fluorescence assay using PfLDH, 3.2 µl of (31 µM) PfLDH was mixed with 5 µl (20 mM, pH 6) HEPES buffer, 10 µl (100 mM) NADH, 30 µl (100 mM) sodium pyruvate, and 46.8 µl MQ water, and allowed the enzyme catalysis for 5 min, followed by addition of 5 µl of AgNC. In each case a control experiment with no enzyme was also performed.

6.3 Results and discussion

6.3.1 Studies on the formation of AgNC in ssDNA scaffolds

Nine different ssDNA candidates with a common template consisting of a 40 mer random region flanked by two constant regions of 31 mer and 19 mer were considered (Figure 6.1). The candidates were selected based on different distribution of the nitrogenous base C in terms of % and different cluster numbers (Figure 6.2 A) with C-poor constant regions and C-rich random regions. The constant flanking regions were included so that a suitable scaffold could be later amplified by PCR. The sequences were tested and found that P4 was the only sequence capable of producing AgNC. Excitation of P4 templated AgNC at $\lambda_{580\ nm}$ yielded an intense fluorescence emission, peaked around $\lambda_{660\ nm}$ (Figure 6.2 B). Since only one out of nine oligonucleotide candidates assisted in AgNC formation, the contribution of constant C-poor regions in AgNC formation may be considered minor or void. P9 was though almost as C rich as P4 with only one C and two CC clusters less than P4 (Figure 6.2 A), it did not produce any detectable fluorescence. The free energy values of folding for P4, and P9, obtained from the Mfold web server (Zuker, 2003) were -7.93 kcal.mole^{-1} and -4.33 kcal.mole^{-1}, respectively indicating higher stability of the secondary structure of P4 than P9. The Mfold secondary structures of unsuccessful scaffolds are shown in figure 6.3.

To understand the structural aspect of AgNC formation, four subset sequences (Sub1-Sub4) from P4 were strategically selected to include various combinations of tandem C repeats and maintain a stem loop structure in each except in Sub 1 (Figure 6.4). All clustered C repeats except one in P4 were present in the four subsets. The Sub 1 (11 mer), which is in the form $C_3X_4C_4$ and smallest, had no predicted secondary structure. Sub 2 (12 mer), Sub 3

(29 mer) and Sub 4 (45 mer) all had stem loop structures with free energy of folding -0.89 kcal.mole^{-1}, -1.3 kcal.mole^{-1}, -2.29 kcal.mole^{-1}, respectively.

In order to assess the predicted secondary structure, Sub 2, Sub 3 and Sub 4 were analyzed under gel electrophoresis. As DNA assumes a more compact secondary structure, its mobility in gel electrophoresis is increased (Fan *et al.*, 2006). On native polyacrylamide gel electrophoresis, a marked presence of secondary structural components in Sub 3 and Sub 4 populations became evident from the formation of multiple bands of faster mobility in addition to the primary DNA band (Figure 6.5 A). In the case of Sub 2, which is a comparatively smaller DNA fragment with only two base pairs in the stem region of the predicted hairpin, a minor forward band albeit less clear, appeared along with the main band. To confirm that the observed bands were indeed a result of DNA folding into secondary structure and not impurities, we analyzed the same DNA fragments in denaturing gel electrophoresis (Figure 6.5 B). The disappearance of faster moving bands other than the primary bands indicated that Sub 2, 3 and 4 populations contained secondary structures. The subsets were used as templates for AgNC preparation and examined under UV trans-illuminator. As expected, Sub 1 and Sub 2 did not yield any fluorescence, probably due to lack of, or presence of very weak secondary structures as mentioned above. Conversely, Sub 3 and Sub 4 produced bright red fluorescence. UV-Vis spectra of the AgNC templated on P4, Sub 3 and Sub 4 candidates (Figure 6.6 A) generated a broad peak centered on $\lambda_{565\text{-}585\ nm}$ with corresponding peaks at $\lambda_{583\ nm}$, λ_{573nm}, and $\lambda_{567nm,}$ respectively. The order of peak intensity was Sub 3> P4> Sub 4. A second broad peak was observed around $\lambda_{430\text{-}440\ nm}$ where corresponding peaks for P4, Sub 1, Sub 2, Sub 3 and Sub 4 were at λ_{435nm}, $\lambda_{441\ nm}$, $\lambda_{435\ nm}$,

$\lambda_{433\ nm}$, and $\lambda_{435\ nm}$. The order of peak intensity for the peak centered on $\lambda_{430\text{-}440\ nm}$ was Sub 2>Sub 4> Sub 1>P4> Sub 3. Excitation at $\lambda_{440\ nm}$, did not yield fluorescent signal from any of the studied subsets, while excitation at $\lambda_{580\ nm}$ yielded high and moderate intensity fluorescent peaks for Sub 3 and Sub 4, respectively. We thus conclude that the peak around $\lambda_{430\text{-}440\ nm}$ and $\lambda_{565\text{-}585nm}$ belonged to silver nanoparticles and nanoclusters, respectively. Interestingly, in the case of Sub 3 and P4, where the most fluorescent NCs were formed, a low absorbance exhibited at $\lambda_{440\ nm}$ indicating the formation of fewer amounts of nanoparticles. On the contrary, Sub 1 and Sub 2, which did not form fluorescent NCs, gave high absorbance at $\lambda_{440\ nm}$, and hence assisted in forming maximum nanoparticles. The formation of nanoparticles and nanoclusters may thus be mutually exclusive to one another to a greater extent.

The changes in fluorescence were examined continuously for P4, Sub 3 and Sub 4 templated NCs over a period of 20 h (Figure 6.6 B). We observed from the intensity that P4 and Sub 3 resulted in highly fluorescent NCs, while Sub 4-AgNCs were the least fluorescent out of the three. A steady rise in fluorescence intensity was observed in all the three cases in the first three hours, after which a gradual fall in the intensity occurred. The fluorescence of P4-AgNC and Sub 4-AgNC consistently decreased with time at the rate of 1395 $a.u.h^{-1}$ and 574 $a.u.h^{-1}$, respectively, while the decrease in Sub 3-AgNC was more gradual (279.6 $a.u.h^{-1}$) for the first five hours of waning stage and eventually Sub 3-AgNC was maintained at a higher fluorescence intensity than P4-AgNC. Sub-4 eventually lost almost its entire fluorescence intensity after 14 h of incubation. Thus, Sub 3 formed higher and more stable fluorescent NCs than Sub 4, even though the latter was more C rich. This challenges our

belief that C rich templates are the only important factor in seeding AgNC. Sub 3-AgNC was also more stable than P4-AgNC. It is likely that most of the structural scaffolds in P4 that host the seeding of NCs failed to stabilize them.

Each of the DNA denaturants, namely urea (8 M), formamide (50 %), and DMSO (50 %) was added independently to the reaction mixture while preparing AgNC (Figure 6.7 A). Both P4-AgNC and Sub 4-AgNC were less affected by urea, compared to Sub 3-AgNC, which was drastically affected by urea, retaining only 23 % of the original fluorescence. Formamide and DMSO were also effective in disruption of AgNC preparation, with effect seen across all the three studied sequences. While P4-AgNC and Sub 3-AgNC both retained 60-70 % of their fluorescence in the presence of either formamide or DMSO, Sub 4-AgNC showed a significant decrease in fluorescence in both cases (fluorescence decreased to 24 % and 38 % with formamide and DMSO). In conclusion, all the three DNA denaturants tested, had disrupted the seeding of AgNC to various degrees. Perturbations in AgNC preparation in the presence of denaturants arise due to the breakage of DNA secondary structure by the denaturants (Wang *et al.*, 2014b; Japrung *et al.*, 2010).

The effect of urea on the secondary structure of the evolved candidates was studied using CD spectroscopy. P4, Sub 3 and Sub 4, all gave a positive CD peak at $\lambda_{280\ nm}$. The peaks shifted to lower wavelengths by 2-5 nm on adding urea (Figure 6.8). We observed that with increase in structural complexity of the ssDNA candidates, the shift was more prominent. This was further confirmed by studying Sub 1 and Sub 2 in the absence and presence of urea. Both these candidates showed negligible shift (< 1.5 nm) in CD peak at

$\lambda_{280\ nm}$. Thus the fluorescence and CD studies together indicated that P4, Sub 3 and Sub 4, exhibit strong secondary structure offering scaffold for the formation of AgNC.

P4, Sub 3, and Sub 4 were analyzed using the oligoanalyzer tool in IDT (Integrated DNA technologies) and the highest melting temperature of their predicted hairpins were found to be 43.8 °C, 34.8 °C, 38.3 °C, respectively. To further emphasize the importance of structure, we carried out AgNC preparation at temperatures of 70 °C, and 90 °C. The temperatures of 70 °C, and 90 °C were chosen because these were high enough to disrupt all hairpins and self-dimers that might be present in solutions of P4, Sub 3, and Sub 4. All the studied sequences failed to form AgNC at both 70 °C, and 90 °C.

The effect of a range of buffers on the preparation of Sub-3-AgNC was also examined (Figure 6.7 B). Sodium phosphate buffer and MOPS were found to be conducive for AgNC formation. A fractional fluorescence of 1.3, 1.1 and 0.98 corresponding pH values of 6, 7 and 7.5 was observed. A loss of more than 50 % fluorescence intensity was observed as the pH value decreased to more acidic (< 5) or increased to more basic (> 8) values. The destruction of hairpin secondary structure at such extreme pH values is the likely reason for the reduction of fluorescence intensity.

The overall findings of the above investigation prompted us to conclude that C-rich ssDNA candidates though support the NC formation, the hairpin structure in the candidate is also equally important for this effect. Additionally, the stability and size of the hairpin are also important parameters to confer a stable NC. The number of base pairs in the stem region correlates to the stability of the hairpin structures. Sub3 with a hairpin constituting of a 7 mer ring and a 3 bp stem supported the most stable NCs, whereas, Sub 4 with a ring size

bigger than 7 mer did not yield stable NCs even though it had a stable 3 bp stem and was more C rich than Sub 3. The loop in Sub 2, though built with 6 mers, was less stable to host NCs as the stem was constituted of only 2 bp. The analogy is applicable to explain the poor performance of P9 as compared to P4. P9 (40 % C) has both 6 and 7 mer rings but with 2 bp stems hence was not suitable to yield NCs. P4 has a large number of loops comprising a smaller loop of 7-mer with 3-bp stem and produced highly fluorescent NCs which however rapidly declined probably, due to transformation of the NCs formed in the other hairpins of bigger sizes to nanoparticles as evident from its high intensity peak for nanoparticles at $\lambda_{430\text{-}440\ nm}$ (Figure 6.6 A).

6.3.2 Detection of NAD^+ using AgNC formed in ssDNA scaffold

As Sub 3 produced the most stable NCs it was chosen for further studies. The TEM image of Sub 3-AgNCs reveals a size ~3.5-4 nm (Figure 6.9). Fluorescence emission response of Sub 3-AgNC in the presence of different concentrations of NAD^+ was studied by exciting the AgNC at $\lambda_{580\ nm}$ and monitoring the fluorescence emission from $\lambda_{600\ nm}$ to $\lambda_{800\ nm}$. The fluorescence emission of AgNC decreased gradually with increasing concentration of NAD^+ (Figure 6.10 A). On the assumption that the fluorescence quenching was mainly static, we calculated the binding sites n and the binding constant K_a using equation (2). The plot of log $(F_0 - F)/F$ against log $[NAD^+]$ yields a linear curve with n as the slope and log K_a as the y-intercept (Figure 6.10 B). From the plot, K_a and n were calculated as 0.201 $L.mole^{-1}$, and 3.6, respectively.

The fluorescence quenching of Sub 3-AgNC when incubated with NAD^+ could be used to follow the change in concentration of NAD^+. Figure 6.11 A shows the Stern-Volmer

plot for NAD^+ mediated quenching of Sub 3-AgNC. The linear plot of F_0/F as a function of $[NAD^+]$ according to the equation (3) is given in the inset of figure 6.11 A. The plot exhibited a dynamic range of 50-500 µM (R^2 =0.977) for NAD^+. A Stern-Volmer constant K_D of 1.207 x 10^5 M^{-1} was obtained from the linear regression of the plot. A detection limit (LOD) of 22.3 µM was obtained using the relation: LOD = 3*Sy/b, where Sy is the SD of y-intercept, and b is the slope of the linear curve. However, at higher concentrations of NAD^+, we found that the curve bends upward, instead of following a linear relationship. A possible reason for such a deviation from the Stern-Volmer equation is that the quenching progresses with a combination of static and dynamic processes (Wei *et al.,* 2015). Therefore, we used an exponential equation $F_0/F = Ae^{(B.[NAD])} + C$, where A, B and C are constants, for fitting the data. The data could be fitted to the equation F_0/F = 23.12 exp (0.0025[NAD]) - 24.17 perfectly obtaining a correlation coefficient of R^2=0.987. The value of Stern-Volmer constant from the exponential fitting could be obtained by the product of the constants A and B (Liu *et al.,* 2010) and was calculated to be 0.578 x 10^5.M^{-1}. To gain further insight into the quenching mechanism TRPL studies were carried out. Figure 6.11 B shows the TRPL profile of Sub 3-AgNC in the absence and in the presence of 15 µM and 100 µM NAD^+. The fluorescence lifetime of AgNC gradually decreased as the concentration of NAD^+ was increased indicating a dynamic quenching process.

To test the specificity of this method, we monitored the fluorescence intensity of Sub 3-AgNC in the presence of other cofactors like $NADP^+$, NADH and the synthetic cofactor $APAD^+$ (Figure 6.12 A). Both $NADP^+$ and NADH were ineffective in quenching the fluorescence of AgNC, while $APAD^+$ was effective in quenching the fluorescence of

AgNC. Notably, $APAD^+$ is a specific cofactor for PfLDH and has been used to detect PfLDH in malaria diagnostic assay (Markwalter *et al.*, 2016a). The $APAD^+$ led quenching of AgNC thus has promising implications for developing malarial diagnosis. Not only Sub 3-AgNC, but also P4-AgNC, and Sub 4-AgNC showed the same profile of quenching with all the tested cofactors (data not shown).

Real samples often contain several ions that may bind to free AgNC or interfere with NAD^+ interaction with AgNC. To validate the applicability of our detection method for real samples, we monitored the fluorescence emission of AgNC in the presence of various monovalent and divalent salts. None of the tested salts showed affinity for the AgNC. Moreover, the AgNC also responded to NAD^+ mediated quenching in a background of monovalent or divalent salts, which confirms that none of the studied salts interfered with the interaction of NAD^+ with AgNC (Figure 6.12 C). The AgNC was then used to detect NAD^+ in human serum samples. A suitable volume of human serum was spiked with various concentrations of NAD^+ and the decrease in the fluorescence emission was monitored. A plot of the relative fluorescence F_0/F vs $[NAD^+]$ in the presence of diluted human serum was linear in the $[NAD^+]$ range of 0.5-500 mM ($R^2 = 0.9914$), and yielded a detection limit of 0.36 mM NAD^+ (Figure 6.12 B). These results show that the AgNC has great potential for NAD^+ detection in real samples.

6.3.3 Monitoring NAD^+ dependent enzyme assays

Finally, the AgNC-NAD^+ interaction was exploited to monitor the enzyme catalysis of two different dehydrogenase models, ADH and PfLDH, where NAD^+ is consumed and

formed, respectively in their physiological enzymatic reactions the scheme of which are shown below:

$$\text{Ethanol} + NAD^+ \rightarrow \text{Acetaldehyde} + NADH + H^+ \quad (4)$$

$$\text{Pyruvate} + NADH + H^+ \rightarrow \text{Lactate} + NAD^+ \quad (5)$$

The fluorescence signals for the reactions (Figure 6.13) responded reciprocally. For the ADH catalyzed reaction where NAD^+ is consumed the signal is eminent, and thus, "ON" due to lack of NAD^+ triggered quenching in the process (Figure 6.13A). Whereas, for PfLDH, the catalysis of which produces NAD^+, the signal is diminished, and thus "OFF" due to NAD^+ triggered quenching in the process (Figure 6.13 B). Notably, ADH and PfLDH are widely used enzymes for alcohol (Lee and Tsai, 2009) and malaria detection (Jain *et al.*, 2014), respectively. The proposed method with ssDNA scaffolded AgNC could therefore be used for quantitative detection of NAD^+/NADH based enzyme catalyzed reactions in a turn-on / turn-off assay approach as demonstrated here for ADH and PfLDH catalyzed systems.

Response of the assay to increasing concentrations of PfLDH was also studied. Figure 6.14 shows the Stern-Volmer plot for NAD^+ mediated AgNC fluorescence quenching with increasing PfLDH concentrations. From the linear part of the curve a LOD of 1.32 $\pm$ 0.03 nM could be estimated.

6.3.4 Practicability of the assay

The developed assay was applied to detect real samples from two *P. vivax* infected patients, A, and B, at two dilutions i.e. 10-fold, and 20-fold. Sample obtained from a healthy volunteer was used as negative control. The assay could not significantly differentiate

between the control and real sample for patient A, at both the studied dilutions, while it could positively differentiate between control and real sample in case of patient B at the lower (10-fold) dilution only. This might be due to (i) lower sensitivity of the assay in the nanomolar range for PfLDH detection, (ii) interference from a variety of proteins and small molecules in the blood. The efficiency of Sub 3-AgNCs to detect PfLDH was also investigated with time. With decreasing stability of AgNCs over time, their efficiency for PfLDH detection also suffered, decreasing by 50 % by the first 10 h of formation.

6.4 Conclusion

This investigation has demonstrated that in addition to the well acclaimed requirement of C-rich regions in the DNA sequence, the presence of suitable hairpin structure is essential to confer stable fluorescent AgNC. The study also signifies the tentative size of the ring and length of the stem on the formation and stabilization of AgNC in the ssDNA scaffolds and hence, it may be considered as a guideline in selecting ssDNA candidates for developing AgNC. Further, the developed AgNC in one of the suitable ssDNA scaffolds has been exploited to detect NAD^+ quantitatively in solution with high sensitivity and specificity and the practical applicability of the method was demonstrated in human serum. The detection limit reported here can satisfy the NAD^+ detection requirements of clinical samples. This fluorescence quenching based method was applied to monitoring NAD^+/NADH based enzyme catalyzed reactions in a turn-on / turn-off assay approach as demonstrated here for ADH and PfLDH catalyzed systems. PfLDH was quantitatively detected using this approach.

Figures

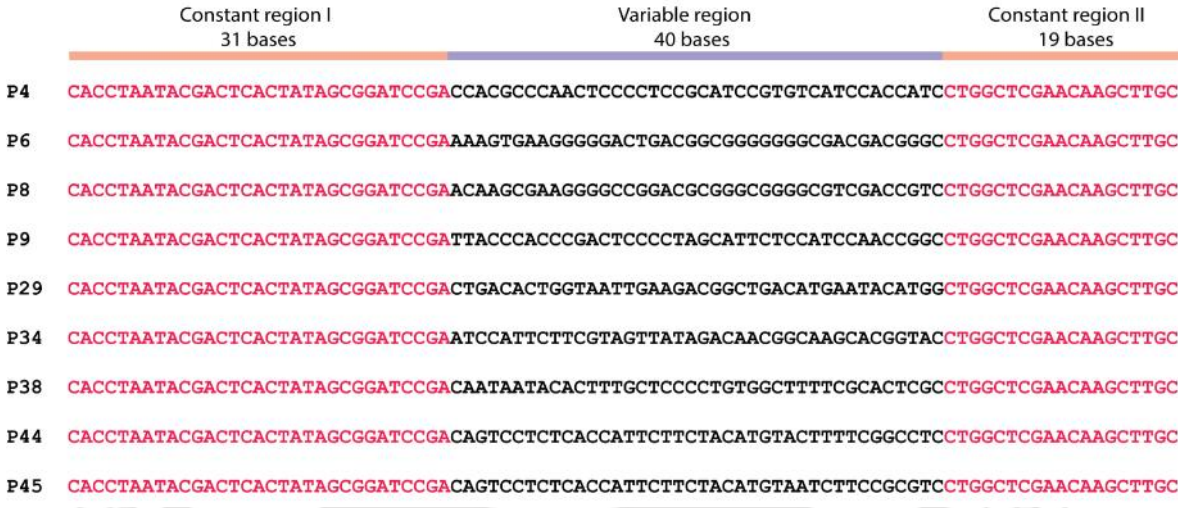

Figure 6.1: Sequence of nine ssDNA used for templating AgNCs. All sequences are flanked by two constant regions (31 mer and 19 mer) with a random region (40 mer) between them.

A

Sequence	Number C	CC	CCC	CCCC	Total C %
P4	15	8	1	1	42.2
P6	17	3	0	0	25.6
P8	18	5	0	0	31.1
P9	14	6	2	1	40
P29	19	2	0	0	25.6
P34	18	4	0	0	28.9
P38	20	3	0	1	33.3
P44	19	6	0	0	34.4
P45	19	6	0	0	34.4

B

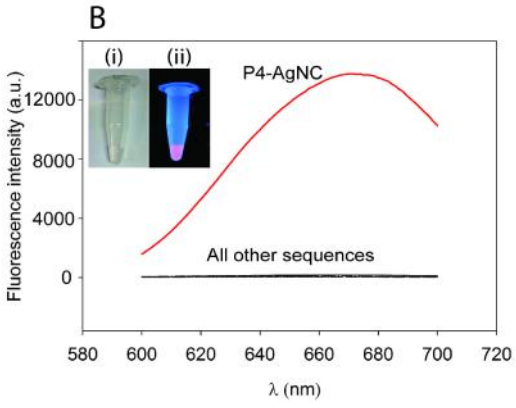

Figure 6.2: (A) Number of C residues in ssDNA sequences considered for the study. (B) Emission spectra of P4-AgNC when the nanoclusters were excited at $\lambda_{580\ nm}$. Inset shows an image of P4-AgNCs under (i) white light, and (ii) UV trans-illuminator.

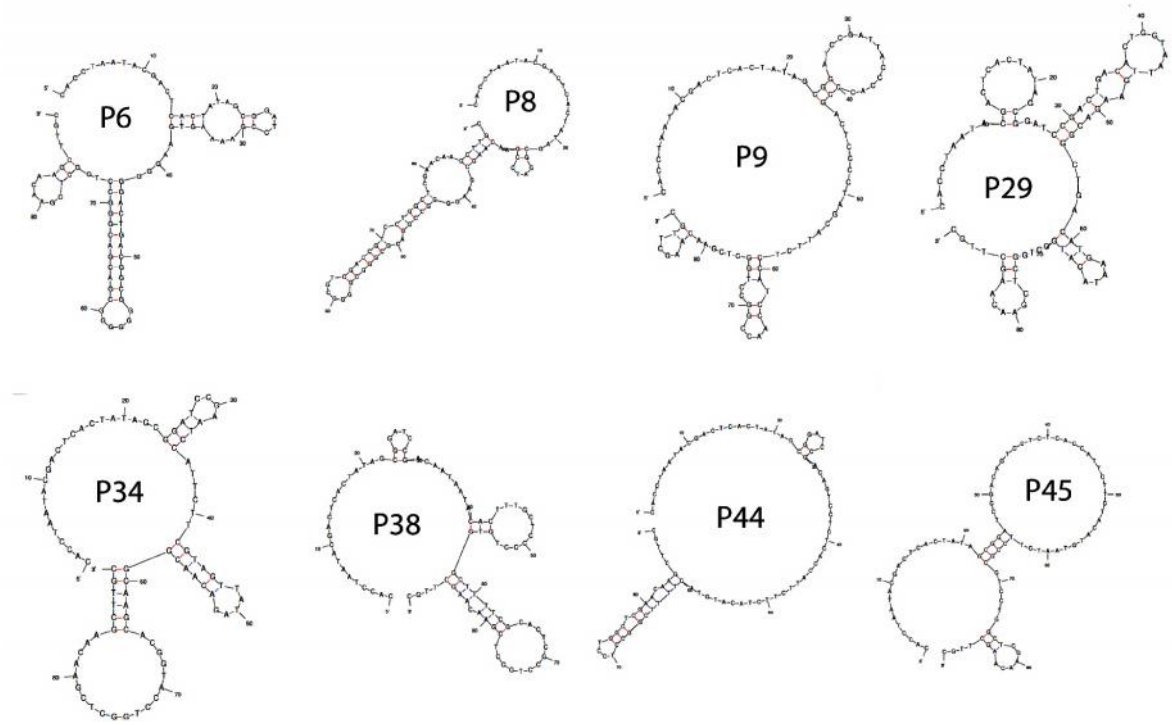

Figure 6.3: Secondary structures of all unsuccessful scaffolds used for templating NCs.

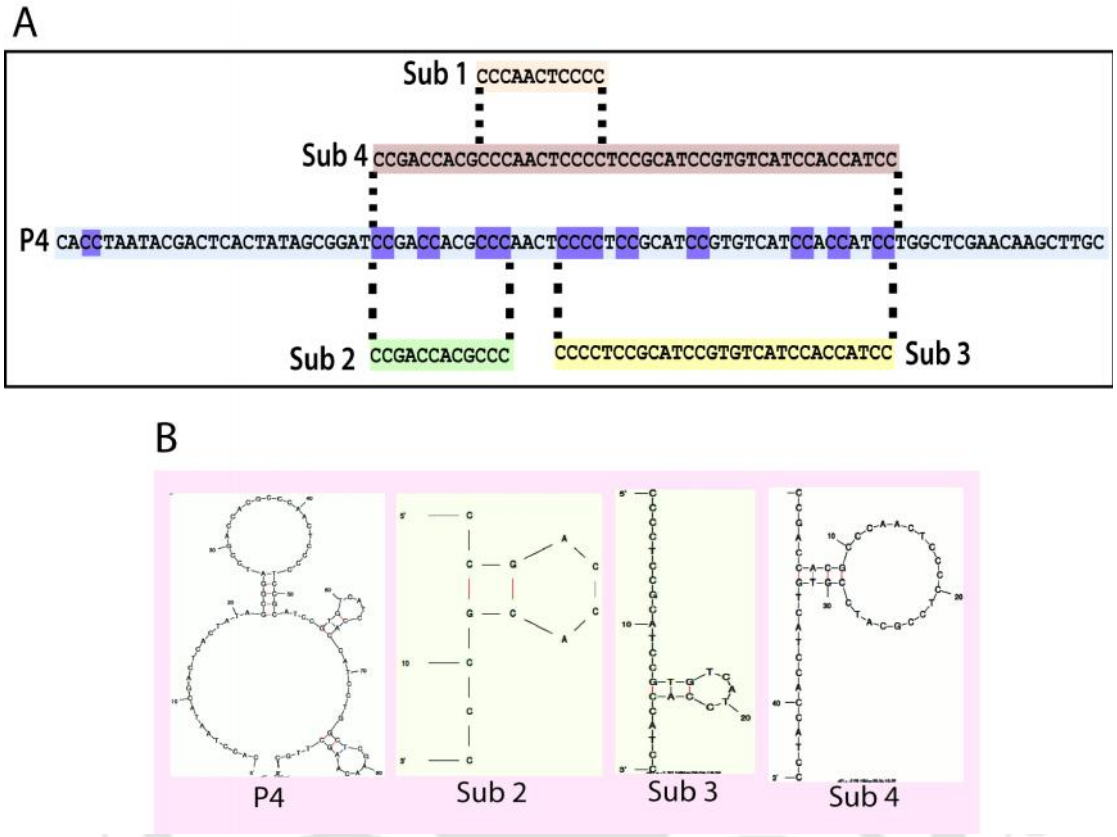

Figure 6.4: (A) Sequences of subsets of P4 used to study their ability to template AgNC. Tandem C repeats in P4, have been highlighted in purple. (B) Secondary structures of P4 and its subsets.

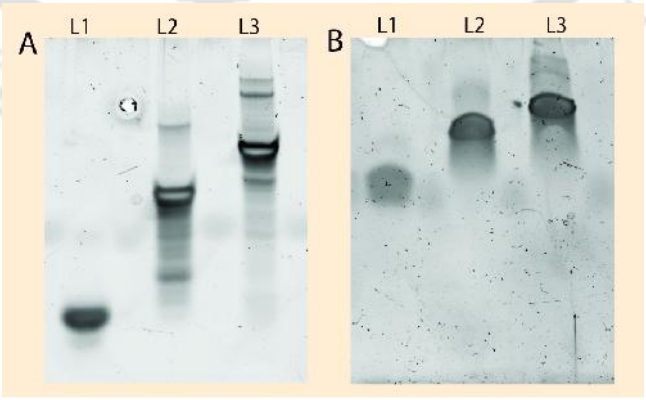

Figure 6.5: (A) Native PAGE of L1: Sub 2, L2: Sub 3, and L3: Sub 4. (B) Denaturing PAGE of L1: Sub 2, L2: Sub 3, L3: Sub 4.

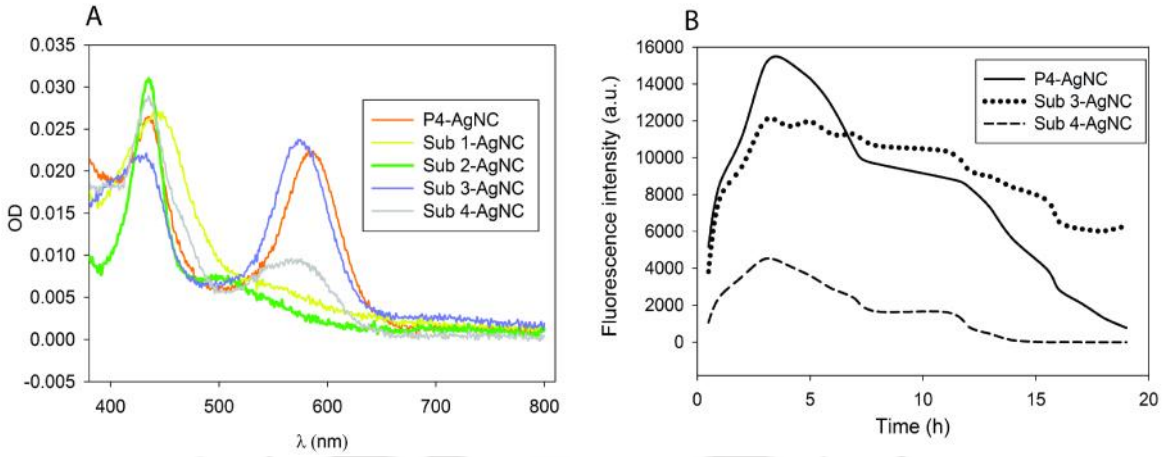

Figure 6.6: (A) UV-Vis spectra for AgNC templated on P4, Sub 1-Sub 4. (B) Changes in the fluorescence emission spectra of P4-AgNC, Sub 3-AgNC, and Sub 4-AgNC with time.

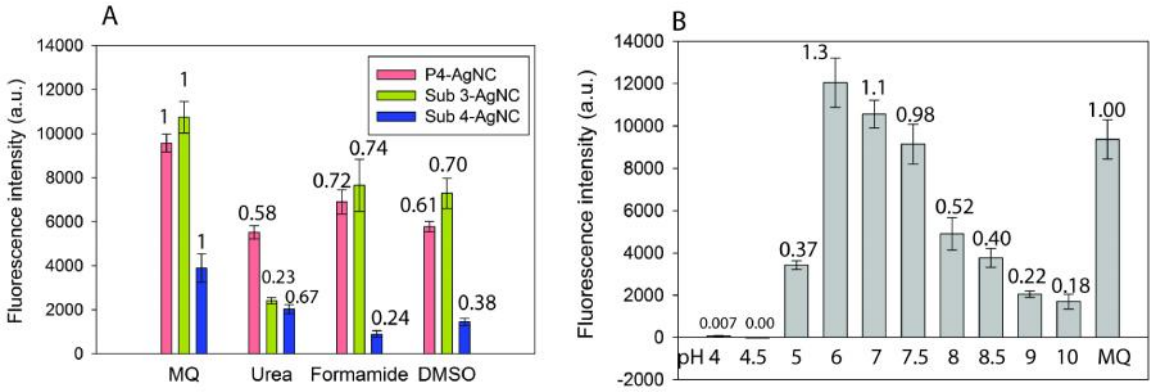

Figure 6.7: (A) Preparation of P4, Sub 3, and Sub 4 templated AgNC in MQ water in the presence of DNA denaturants. (B) Effect of various buffers (15 mM) on the fluorescence of Sub 3-AgNC. Bars from left to right represent AgNC prepared in buffers: HEPES (pH 4, pH 5); Sodium phosphate buffer (pH 6, pH 7, pH 8); Tris (pH 9, pH 10); MOPS (pH 7.5); Acetate (pH 4.5); Borate (pH 8.5). For both (A), and (B) the numbers on the top of the bars indicate the fractional residual fluorescence w.r.t AgNC prepared in MQ.

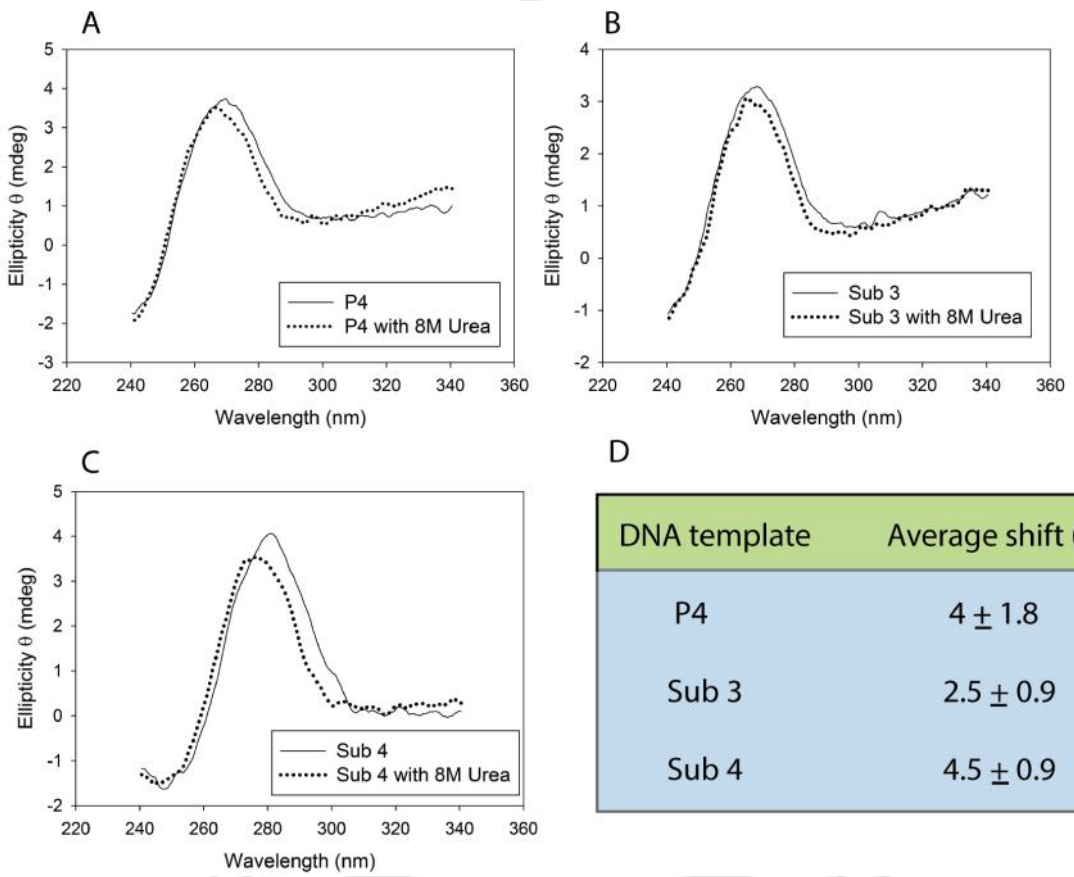

DNA template	Average shift (nm)
P4	4 ± 1.8
Sub 3	2.5 ± 0.9
Sub 4	4.5 ± 0.9

Figure 6.8: CD profile of ssDNA nucleotides P4 (A), Sub 3 (B), and Sub 4 (C) in the presence of 8 M urea. (D) Table shows the average shift in peak position at $\lambda_{280\ nm}$, on adding 8 M urea.

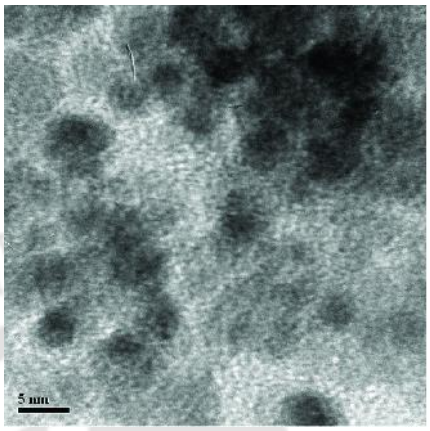

Figure 6.9: TEM image for Sub 3-AgNC.

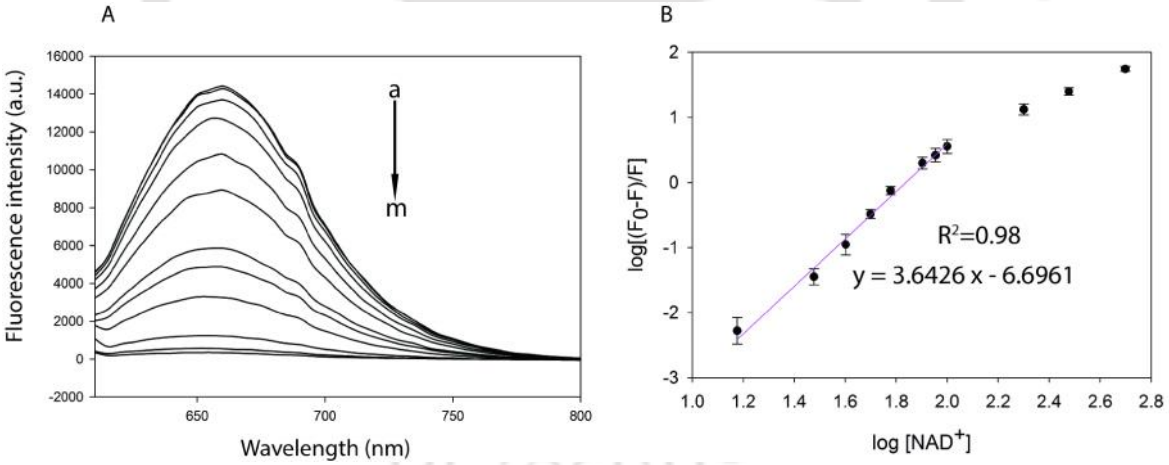

Figure 6.10: (A) Fluorescence emission spectra of Sub 3-AgNC in the presence of different concentrations of NAD^+ in µM (a) 0, (b) 15 (c) 30 (d) 40 (e) 50, (f) 60, (g) 80, (h) 90, (i) 100, (j) 200, (k) 300 (l) 500, (m) 800. (B) Plot of log $(F_0 - F)/F$ against log $[NAD^+]$. Each point is an average of at least three independent experiments, error bars represent the SD.

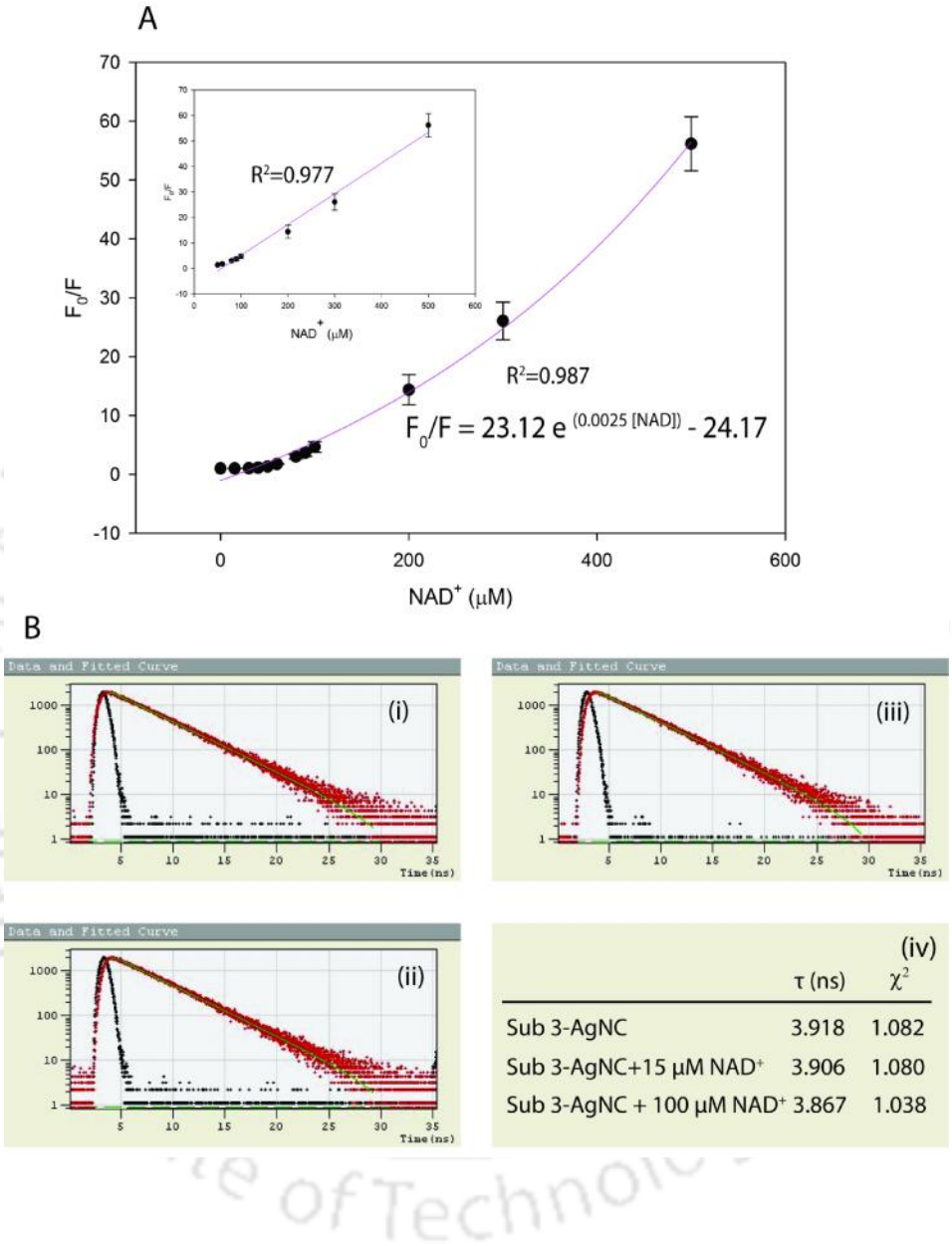

Figure 6.11: (A) Stern-Volmer plot of Sub 3-AgNC. Inset shows the linear plot with corresponding R^2 value. Each point is an average of at least three repeat experiments. Error bars indicate the SD. (B) TRPL profile of Sub 3-AgNC in the (i) absence, and presence of (ii) 15 μM (iii) 100 μM NAD^+, (iv) fluorescence lifetimes (τ) and χ^2 value of fitting for (i), (ii), and (ii) have been listed.

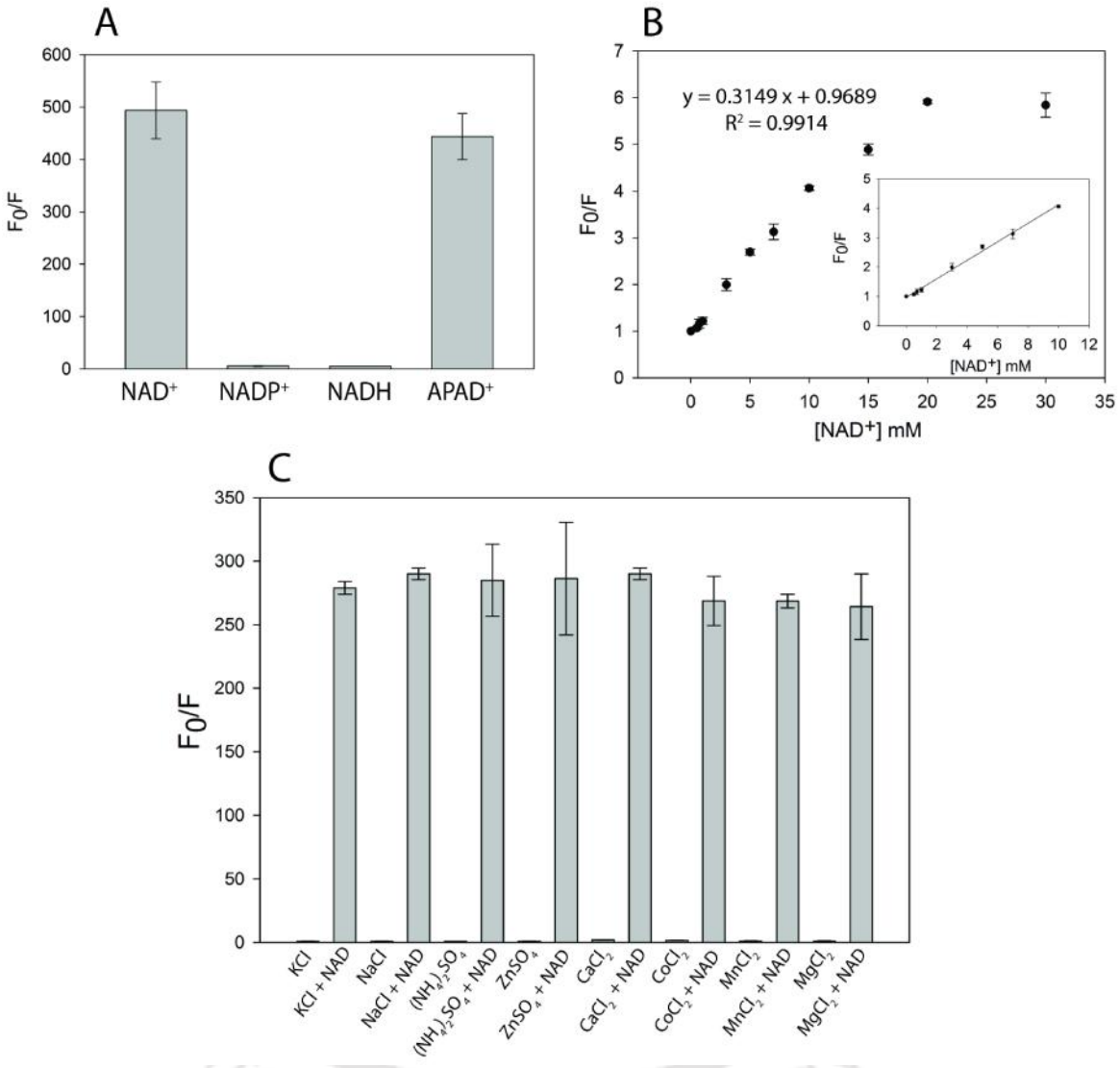

Figure 6.12: Relative fluorescence (F_0/F) of Sub 3-AgNC in the presence of (A) 5 mM of various cofactors, (B) Stern-Volmer plot of F_0/F vs [NAD^+], in the presence of human serum. (C) 8 mM of various monovalent salts, or 1 mM of various divalent salts, both in the presence or absence of 1 mM NAD^+. In all cases, data points are average of at least three repeat experiments, error bars reflect the SD.

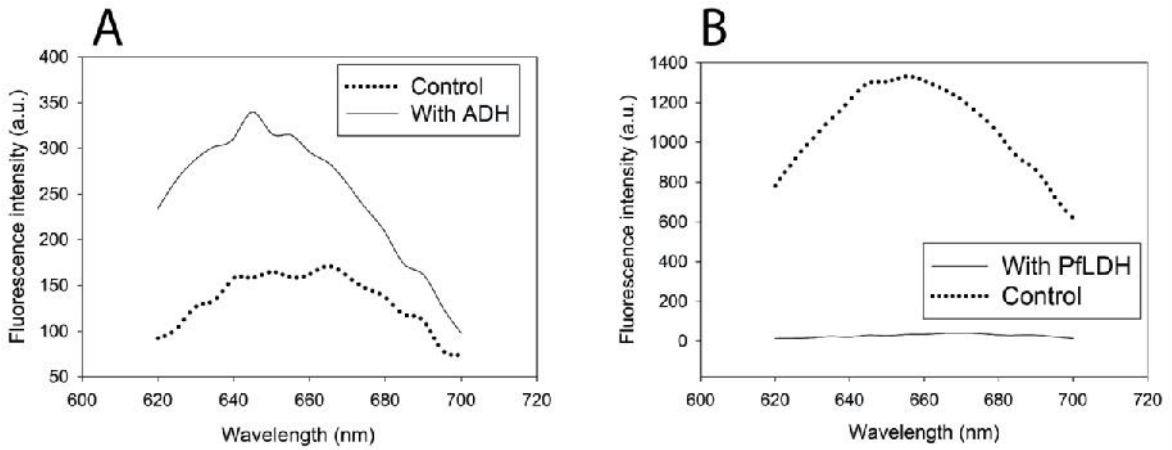

Figure 6.13: AgNC-NAD interaction based (A) turn-on assay using ADH, and (B) turn-off fluorescence assay using PfLDH.

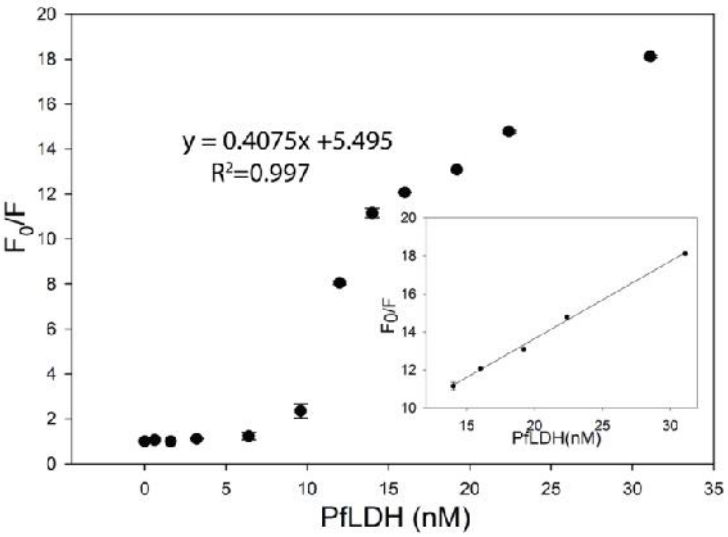

Figure 6.14: Response curve for PfLDH detection by NAD^+ mediated quenching of Sub 3-AgNC.

Chapter VII

High Resolution Melting Studies on Metallized DNA Duplexes for Species Differentiation of *Plasmodium* Parasite

7.1 Overview

Simple and accurate detection of single nucleotide polymorphisms (SNPs) has enormous application potential in developing diagnostics (Frazer *et al.*, 2009; Kim *et al.*, 2014). The application of routine PCR and sequencing strategies conventionally used for SNP detection are often restricted by their complexity, high cost, and infrastructure requirements (Maurer, 2011). The major hurdle for other direct hybridization based detection of SNPs is the insignificant effect of single nucleotide change on perturbing the overall stability of the double stranded DNA. Besides, several experimental parameters, such as, temperature, ionic strength, oligonucleotide concentration, also have impact on the hybridization process and thus these parameters need to be stringently controlled for achieving limited variability and reproducible efficiency in the results (Knez *et al.*, 2014). DNA melting studies advance the SNP detection problem in a more holistic way, and are considered as a better alternative than the direct hybridization or protein mediated detection platforms (Knez *et al.*, 2014). Recently, the high resolution melting (HRM) technique has been acclaimed as an attractive approach in laboratory practice. The application potential of the technique in resource limiting environment is revealed from the progress like,

incorporation of microfluidics to HRM and development of a PoC HRM device where the application of expensive thermocyclers has been circumvented (Crews *et al.,* 2009). However, an adequate success through HRM technique is yet to be achieved in cases where resolution among multiple similar DNAs with varying SNP positions is warranted. To create discrimination among this homogeneous pool of DNAs with meager differences, introduction of additional effectors to the HRM analysis may be suggested that in conjunction with the temperature effect are likely to amplify the discrimination signals among the DNA candidates leading to improved resolution.

The *Plasmodium* parasite LDH enzyme (pLDH) has been identified as a promising malaria biomarker with the potential for sensitive detection of the disease (Jain *et al.*, 2014). The parasite enzyme differs from its human counterparts in several structural and kinetic aspects making it a viable biomarker. One such difference is the presence of a conserved five amino acid residue insertion 'DKEWN' immediately in front of the catalytic residue R109 (Figure 7.1 A) (Brown *et al.*, 2004). However, this amino acid stretch is conserved across all the species of *Plasmodium* parasite and hence, is not suitable to utilize directly in analytical platforms to distinguish different species of the parasite. This pan-LDH epitope along with another species specific LDH epitope has been used to generate anti-peptide antibodies for malaria diagnosis (Hyrdayal *et al.*, 2010). However, the current interest in malaria diagnosis focuses on the development of methods which are free from labile bio recognition elements such as, antibody and enzyme. Notably, there has been a drive to explore robust biorecognition elements for malaria detection that are stable in hot and humid

climate due to obvious reason of the malaria prevalence in these climatic conditions (Chakma *et al.,* 2016). Although the amino acid stretch of pLDH described above is conserved, there are minor differences in the nucleotide sequence corresponding to this region in the native genes across the four major malaria species. This chapter describes our work to incorporate differences in the otherwise identical HRM profiles of the four DNA candidates in hybridized forms with a common complementary capture probe, by using metal ions as resolution probes. Notably, many metal ions are known to interact with DNA through the base ring nitrogen atoms, the negatively charged phosphate groups, ribose hydroxyls, and the exocyclic base keto groups. There are also reports on the effect of metal ions on the structural properties of DNA (Aich *et al.,* 1999; Anastassopoulou 2003). Recently, specific DNA structures have been engineered by introducing metal ion mediated structural changes in the DNA helix (Ono *et al.,* 2011; Bin and Kraatz, 2009). However, metal mediated structural changes in DNA duplexes have not been exploited yet in DNA melting based analytical investigations. Our results obtained with alkaline earth metals (Ca^{+2} and Mg^{+2}) demonstrated remarkable improvement in resolution among the HRM profiles of the DNA sequences corresponding to this highly conserved region from the LDH genes of the four *Plasmodium* species, and thereby offer the possibility of species specific differentiation of the parasite.

7.2 Experimental approaches

7.2.1 Chemicals and reagents

Magnesium chloride anhydrous ($MgCl_2$), mercury (II) chloride ($HgCl_2$), nickel (II) chloride hexahydrate ($NiCl_2.6H_2O$), cobalt chloride hexahydrate ($CoCl_2.6H_2O$), Tris (tris-(hydroxymethyl)-aminomethane), di-sodium hydrogen phosphate (Na_2HPO_4), sodium di-hydrogen phosphate (NaH_2PO_4), were obtained from Himedia, India. Calcium chloride ($CaCl_2$) was obtained from Merck, Germany. Manganese chloride ($MnCl_2$) was obtained from SRL, India. SYBR green I (10,000X) was from Invitrogen (U.S.A). All chemicals were of analytical grade and were used as received without further purification. HPLC purified, desalted lyophilized DNA probes were obtained from Bioserve Biotechnologies India Pvt. Ltd. and reconstituted to obtain a stock concentration of 100 µM. Prior to their use, the probes were heated at 90 °C for 5 min, followed by cooling in ice for 2-3 min. The sequences of all the probes along with their notations are illustrated in Figure 7.1 B. Deionized water (18.2 MΩ) from Milli-Q water system, Millipore, was used throughout the experiments.

7.2.2 Assay design

A scheme showing the strategy used for the work is depicted in Figure 7.2. Briefly, 5 µl (1 µM stock) of CP was mixed with 5 µl (1 µM stock) of complementary DNA probe (FT/VT/MT/OT/NC), 6 µl Tris-Cl (50 mM, pH 8.8), and 2 µl water. Since M-DNA has been previously used to denote transition metal ion-DNA complexes (Aich *et al.*, 1999), and we explore here both transition metal as well as alkaline earth metal DNA interactions, the

generic notation “metallized DNA” has been used throughout the chapter, to denote DNA-metal ion complex, irrespective of the group of metal ions being used. To prepare metallized DNA, 5 µl (1 µM stock) of CP was mixed with 5 µl (1 µM stock) of complementary DNA probe (FT/VT/MT/OT/NC), 6 µl Tris-Cl (50 mM, pH 8.8) and 2 µl (4 mM stock) metal salt solution ($MgCl_2$/ $HgCl_2$/ $NiCl_2.6H_2O$/ $CoCl_2.6H_2O$/ $CaCl_2$/ $MnCl_2$). In each case, the mixture was heated at 90 °C for 5 min, and cooled on ice for 2-3 min, followed by incubation for 20 h at room temperature (RT). Before carrying out HRM analysis, 2 µl of (10X) SYBR green I was added to the mixture, making the final volume to 20 µl.

To study the effect of pH on the formation of metallized DNA, we performed the hybridization and metallization step in a range of pH buffers. Here Tris-Cl, pH 8.8 was replaced by various buffers namely, 50 mM PBS pH 7, 50 mM Tris-Cl pH 8, 8.5, and 10. All other conditions were maintained similar to the previous experiment.

7.2.3 High resolution melting (HRM)

HRM experiments were performed on a Rotor Gene Q instrument (Qiagen, Germany). The assay mixture was melted by increasing the temperature from 25 °C to 80 °C, with an increment of 0.1 °C, a delay of 2 s per increment, and 90 s of pre-melt conditioning before initiating the first step. Data were recorded using the HRM channel. Data analysis to obtain normalized melt curve and derivative melt curve [(dF/dT) vs T] was performed using the commercial Rotor Gene Q series software after defining the range of the target melt region. For each analysis at least three or more samples were run and the standard deviation of T_m was discerned to indicate the reproducibility of the assay.

7.2.4 Circular dichroism (CD) spectroscopy

The CD spectra were recorded on a Jasco J-815 spectropolarimeter calibrated with (+)–10- camphorsulfonic acid for optical rotation. The spectra were measured from $\lambda_{360\ nm}$ to $\lambda_{190\ nm}$, using a 1 mm path length suprasil quartz cuvette at a scan rate of 100 $nm.min^{-1}$, interval of 0.5 nm, time constant of 1 s, and taking an accumulation of 3 scans. For CD studies 7.5 µl (100 µM) of CP was mixed with 7.5 µl (100 µM) of complementary DNA probe (FT/VT/MT/OT/NC) in 45 µl of Tris, 50 mM, pH 8.8, and the volume was made up to 150 µl using Milli-Q water. For studying the effect of metal ions on DNA, 20 µl of metal salt solution (60 mM) was added to the above mixture, maintaining identical DNA : metal ion molar ratio as used in HRM studies. In each case, the mixture was heated at 90 °C for 5 min, and cooled on ice for 2-3 min, followed by incubation for 20 h at RT before carrying out the CD experiment. For each analysis, a baseline experiment, without addition of DNA was also performed.

7.3 Results

7.3.1 Design of DNA probes

A conserved sequence of eight amino acid residues (PGKSDKEW) in pLDH which is absent in the human LDH (hLDH) was identified to consider the corresponding native DNA sequences as targets for the study. A capture DNA probe (CP) was synthesized which is fully complementary to the *Plasmodium falciparum* target (FT) and had two base

mismatches each, with the target DNAs of *P. vivax* (VT), *P. malariae*, (MT), and *P. ovale* (OT) (Figure 7.1B). The polymorphisms across the species compared to *P. falciparum* were (T→C and A→G), (C→T, A→G), and (A→T, G→A), in VT, MT, and OT, respectively. A non-complementary probe (NC) that voids base pairing with CP was also included as a negative control.

7.3.2 HRM analysis of un-metallized DNA

The HRM profiles for the four DNA duplexes (CP-FT, CP-VT, CP-MT, CP-OT) are shown in figure 7.3 Ai. Since the intrinsic fluorescence intensity slightly varied from sample to sample, the results were plotted as normalized melt curves barring the melting profile of CP-NC that did not exhibit significant fluorescence intensity due to lack of stable duplex structure (Figure 7.4). Two melting transition ranges extending from 30 °C to 50 °C (MeT1) and 50 °C to 75 °C (MeT2) were observed for all the four duplexes. CP-FT could be easily distinguished from the rest of the duplexes based on the unique shape of its curve in the MeT2 region. However, the melt profiles of the remaining three duplexes were overlapped, and could not be differentiated from each other on casual observation of the curves. For a thorough examination of the results, derivative curves (dF/dT vs T) from the normalized melt data were generated for the MeT1 and MeT2 transitions (Figure 7.3 Bi, Ci). MeT1 was characterized by a more prominent peak along with a subdued shoulder peak, in all duplexes. The T_m (melting temperature) was identified from the temperature maxima of the principal peak in MeT and will referred to as, T_{m1} and T_{m2} for the corresponding MeT1 and MeT2 regions. This assignment of T_m is considered as per the general convention being followed

in HRM based analysis. The T_{m1} values of the four duplexes were fairly close (Table 7.1) (Figure 7.3 Bi). As compared to T_{m1} values, there was a minor improvement in the resolution among the T_{m2} peaks (Figure 7.3 Ci) which however, was not enough to distinguish the individual species (Table 7.2, Figure 7.5 A). Nevertheless, if uniqueness of any region of the derivative melt curves is considered, then CP-FT could be differentiated from other duplexes by the appearance of a secondary peak in the region of MeT2 transition.

Table 7.1: T_m values for un-metallized, Mg-metallized, Ca-metallized, Ni-metallized (each at pH 8.8), and Ca-metallized (at pH 7, 8, 8.5, 10) DNA in the melting transitions MeT1 (35-50) °C and MeT2 (50-80) °C, for the dsDNA complexes, CP-FT/VT/MT/OT. The melting temperature values showing S.D. >1 were considered unreliable and have been written in red.

			T_m (°C)			
Metallization state	**pH**	**Temperature range**	**CP-FT**	**CP-VT**	**CP-MT**	**CP-OT**
Un-metallized	8.8	MeT1	37.2 ± 0.36	37.4 ± 0.14	37.13 ± 0.38	37.4 ± 0.14
		MeT2	51.85 ± 0.21	52.25 ± 0.40	52.25 ± 0.31	52.01 ± 0.18
Mg-metallized	8.8	MeT1	37.28 ± 0.25	37.2 ± 0.38	37.03 ± 0.43	37.2 ± 0.29
		MeT2	65.82 ± 0.16	56.96 ± 0.26	57.04 ± 0.16	55.36 ± 0.37
Ca-metallized	8.8	MeT1	40.61 ± 0.58	41.40 ± 0.36	40.34 ± 0.12	40.34 ± 0.24
		MeT2	64.14 ± 0.18	55.99 ± 0.90	55.36 ± 0.26	53.37 ± 0.16
	7	MeT2	51.61 + 0.16	51.85 + 0.20	**53.89 ± 1.88**	51.98 + 0.17
	8	MeT2	65.56 + 0.30	57.86 + 0.91	56.90 + 0.37	52.23 + 0.16
	8.5	MeT2	64.49 + 0.23	55.68 + 0.21	55.68 + 0.45	52.49 + 0.23
	10	MeT2	63.61 + 0.27	54.99 + 0.34	55.34 + 0.54	53.73 + 0.81
Ni-metallized	8.8	MeT1	**43.93 ± 5.16**	47.56 ± 0.34	**43.90 ± 5.1**	47.25 ± 0.30
		MeT2	**57.72 ± 1.51**	51.40 ± 0.14	**52.18 ± 1.48**	51.65 ± 0.37

Table 7.2: Resolution in T_{m2} between HRM profiles of duplex pairs at un-metallized and various ion metallized DNA and three different alkaline pH values.

	T_{m2} difference (°C)					
Difference between HRM profile	**Un-metallized pH 8.8**	**Mg-metallized pH 8.8**	**Ca-metallized pH 8.8**	**pH 8**	**pH 8.5**	**pH 10**
(CP-FT)-(CP-OT)	0.16 ± 0.28	10.46 ± 0.40	10.77 ± 0.24	13.33 ± 0.34	12 ± 0.33	9.88 ± 0.85
(CP-FT)-(CP-VT)	0.4 ± 0.45	8.86 ± 0.31	8.15 ± 0.92	7.7 ± 0.96	8.81 ± 0.31	8.62 ± 0.43
(CP-FT)-(CP-MT)	0.4 ± 0.37	8.78 ± 0.23	8.78 ± 0.32	8.66 ± 0.48	8.81 ± 0.51	8.27 ± 0.60
(CP-VT)-(CP-MT)	N.A.*	0.08 ± 0.31	0.63 ± 0.94	0.96 ± 0.98	N.A.*	0.35 ± 0.64
(CP-VT)-(CP-OT)	0.24 ± 0.44	1.6 ± 0.45	2.62 ± 0.91	5.63 ± 0.92	3.19 ± 0.31	1.26 ± 0.88
(CP-MT)-(CP-OT)	0.24 ± 0.36	1.68 ± 0.40	1.99 ± 0.31	4.67 ± 0.40	3.19 ± 0.39	1.61 ± 0.97

* Difference was zero

7.3.3 HRM analysis of metallized DNA

The HRM resolution abilities of a range of divalent metals, comprising of alkaline earth and transition metals namely, Ca^{+2}, Mg^{+2}, Hg^{+2}, Ni^{+2}, Co^{+2}, and Mn^{+2}, were assessed. All the transition metal ions except Ni^{+2}, were found to be unsuitable as all the DNA duplexes gave no absolute fluorescence at the start of the melting experiment, generating no melting curve. The resolution ability of Ni^{+2} though detected (Figure 7.3 Aiv-Civ), its performance however, was poor as compared to Ca^{+2} and Mg^{+2}. Besides, the HRM profiles of Ni-metallized duplexes severely lacked in reproducibility, especially for the melting profiles of CP-FT, and CP-MT. T_{m1} and T_{m2} peak values for Ni-duplexes were derived from the curves (Table 7.1). T_{m1} values for CP-FT and CP-MT were highly variable, with the primary and shoulder peaks constantly exchanging positions across all the repeated experiments; whereas, T_{m2} values though gave better separation between the species as compared to un-metalized DNA, had high standard deviations.

The HRM normalized curves of DNA duplexes for all the *Plasmodium* species for Ca and Mg-metallized DNA are illustrated in Figure 7.3 Aii and 7.3 Aiii, respectively. Similar to un-metallized duplexes, two melting transitions, MeT1 and MeT2, were observed with greater resolution achieved between curves in the MeT2 region. Among all the tested metal ions, both these alkaline earth metals conferred better resolution amongst the curves as compared to un-metalized DNA. For a quantitative assessment of the resolution, the derivative melt curves were further analyzed. In the MeT1 region, both Ca-metallized (Figure 7.3 Bii) and Mg-metallized (Figure 7.3 Biii) duplexes produced primary peaks, along

with a shoulder peak of lower intensity, similar in profile to un-metallized DNA. The T_{m1} peak values were fairly close to each other (Table 7.1), and thus could not be used for distinction between the duplexes. In the MeT2 region of the Ca-metallized DNA (Figure 7.3 Cii) a single peak was observed in each case of CP-VT, CP-MT, and CP-OT, while a primary peak along with a shoulder peak was observed in case of CP-FT. For the Mg-metallized profiles in MeT2 (Figure 7.3 Ciii), all the species produced a primary and a shoulder peak. In case of both the alkaline earth metals, the primary peak of CP-FT not only increased in intensity but also shifted its position from ~51 °C to ~65 °C achieving a higher resolution (Table 7.2). Thus, a greater HRM resolution among the species duplexes was observed by using the alkaline earth metals (Table 7.2, Table 7.3, Figure 7.5 A). An impressive increase in resolution between *vivax-ovale*, and *malariae-ovale* species of 10.9 and 8.3 fold respectively, was obtained for the Ca-metallized duplexes. From figure 7.5 A, Tables 7.3, and 7.2 it is evident that resolution between Ca-metallized duplexes was marginally better than the Mg-metallized duplexes, especially for differentiating *vivax-ovale*, and *malariae-ovale*.

Table 7.3: Increase in resolution between HRM profiles of various duplexes for Ca, and Mg-metallized DNA from the un-metalized DNAs.

Compared duplex pairs	**Fold increase in resolution**	
	Ca-metallized	**Mg-metallized**
(CP-FT) vs.(CP-OT)	67.3	65.4
(CP-FT) vs. (CP-VT)	20.4	22.2
(CP-FT) vs. (CP-MT)	22.0	22.0
(CP-VT) vs. (CP-OT)	10.9	6.7
(CP-MT) vs. (CP-OT)	8.3	7.0

7.3.4 Effect of pH on the resolution of melting temperatures

Since nucleic acid-metal ion interactions are often charge based, the effect of pH on the resolution of the melt curves using Ca-metallized DNA (Figure 7.6 Ai-Aiv) was studied. The derivative curves from the MeT1 and MeT2 transitions were analyzed for various pH values, and observed no distinction in MeT1 range. The T_{m2} peak values for all the duplexes were clustered together at pH 7 (Fig 7.5 B, and Figure 7.6 Bi). The resolutions among T_{m2} peak values for all the duplexes except between CP-VT and CP-MT, were increased with the increasing pH (Figure 7.5 B) and gradually declined beyond pH 8.5 (Table 7.2).

Therefore, we conclude that pH 8-8.5 is the best range for better resolution among the duplexes.

7.3.5 Interaction of metal ions with DNA duplexes: structural studies

All the DNA duplexes exhibited positive long wavelength band between $\lambda_{260\text{-}280\ nm}$, and a negative band at around $\lambda_{245\ nm}$ in CD spectra (Figure 7.7) which are the characteristic of the B-form of DNA (Chang *et al.,* 2012). The CD spectra of the DNA duplexes also exhibited additional positive peaks at $\sim\lambda_{200\ nm}$ and $\sim\lambda_{220\ nm}$ due to high (A+T) content of ≥ 50 % in all the target probes (Table 7.4). These characteristic CD peaks for (A+T) rich nucleotides have been previously reported from a study on synthetic nucleotides poly[d(A).polyd(T)] and poly[d(AT)] (Kypr *et al.,* 2009). The (A+T) rich nucleotides are also known to exhibit an increase in amplitude and cause red shift of the positive CD band at $\sim\lambda_{260\ nm}$ with increase in temperature (Kypr *et al.,* 2009). In the present case, on interaction of the DNA duplexes with the alkaline earth metals (Ca^{+2} or Mg^{+2}), a decrease in peak intensity at $\sim\lambda_{260\ nm}$ was observed (Figure 7.7). This signifies the influence of these metals ions on the secondary structure of the DNA. Contrary to the above findings, a featureless CD profile was obtained when Co^{+2} was used with the duplexes indicating significant loss of the secondary structure due to destabilization effects of transition metal ions on the DNA duplex (Anastassopoulou, 2003; Oliveira and Oliveira-Brett, 2010; Duguid *et al.,* 1993). With the addition of Ca^{+2} ions, an increase in peak intensity at $\lambda_{200\ nm}$ was observed. The % increase in intensity was lowest in case of CP-FT (26.3 %) (Figure 7.7 A), while it was quite high for CP-VT, CP-MT, CP-OT where the corresponding % increase in intensity were

109.3, 118.2, and 73.2 (Figure 7.7 B, C, D). The metal ions thus, interact differently with the fully hybridized DNA, and DNA with mismatches, leading to enhanced resolution of the melting curves.

Table 7.4: Percent (A+T) content in ssDNA probes used in the study.

ssDNA probe	% (A+T)*	Poly (dA)	Poly (dT)
FT	(15/26) 58	3A X 2	-
VT	(13/26) 50	3A	-
MT	(15/26) 58	3A	-
OT	(16/26) 62	5A and 3A	-
NC	(14/26) 54	-	4T

* Ratio of (A+T) to (A+T) + (G+C) are shown in parentheses

7.4 Discussion

Mainly, two types of interactions exist between DNA and metal ions (1) ligand mediated interactions via, H-bond, π–π interactions, and other weak interactions, (2) direct metal bonding between the filled orbital of a nucleobase and an empty orbital of the metal ion (Shamsi and Kraatz, 2013). Metal ions, particularly alkaline earth metals, stabilize the DNA helix primarily by neutralizing the repulsive forces between the negatively charged phosphate groups (Anastassopoulou, 2003; Oliveira and Oliveira-Brett, 2010). Divalent metal ions are effective at much lower concentrations than monovalent metal ions. However, transition metal cations have been found to disorder the B-DNA backbone as these may

interact with N7 of purines or the N3 of pyrimidines, decreasing the duplex stability with a reduction in base pairing and base stacking (Duguid *et al.,* 1993). Overall, the question of DNA-metal complex stability is answered by the relative affinity of metal ions for phosphate groups over nucleobases. The preference of metal ions for the phosphate backbone over nucleobases decreases in the order of $Mg^{+2} > Co^{+2} = Ni^{+2} > Mn^{+2} > Zn^{+2} > Cd^{+2} > Cu^{+2}$ (Eichhorn and Shin, 1968). In the present case, the metal-DNA interaction has been explored in HRM analysis where SYBR Green I (SG) has been used as reporter molecule. SG contains phenyl-quinilinium and benzo-thiazole aromatic ring systems, along with dimethyl amino propyl and propyl elongated chains. The aromatic rings of SG intercalate between bases in a confined manner via van der Waals interactions. Additionally, the positively charged thiazole groups of SG are involved in electrostatic interaction with the negatively charged phosphate backbone of DNA. Owing to this electrostatic interaction, the stability of the SG-DNA complex is strongly influenced by the ionic strength / pH of the solution (Dragan *et al.*, 2012). It has been reported that both Na^{+} and Mg^{+2} ions acted as quenchers to SG fluorescence, where the effect of Mg^{+2} was more pronounced than Na^{+} (Zipper *et al.*, 2004). Essentially, this quenching is a result of neutralization of DNA negative charges by positive metal ions, thus affecting the electrostatic attraction of SG to DNA. In our experiments, three forces are expected to interplay (1) metal ion-phosphate interaction, (2) metal ion-nucleobase interaction, (3) metal ion quenching of SG-DNA complex fluorescence. A culmination of these three forces results in the resolution of T_m between the duplexes. While (1) is a stabilizing force and results in an increase in T_m, (2) and (3) result in a decrease in T_m (Table 7.1). All the three metal ions increased both the T_{m1} and T_{m2} peak values in the

order of $Mg^{+2} = Ca^{+2} > Ni^{+2}$. The destabilization effect of Ni^{+2} is due to its high preference towards nucleobase interactions, whereas, the lack of fluorescence with Hg^{+2}, Co^{+2}, or Mn^{+2} (data not shown) is because their destabilization effects on the DNAs surpassed their stabilizing forces. The T_m values of the DNA complexes with Ca^{+2}, and Mg^{+2} differ due to different modes of their binding with DNA caused by the marginally different electro positivity of the metals. Electrophoresis and FTIR studies revealed some crucial differences between Ca-DNA and Mg-DNA complexes: (i) a stronger affinity of Ca-phosphate binding (direct interaction) compared to Mg-phosphate binding (indirect through water) , (ii) stronger Mg-base binding (direct binding) as compared to Ca-base binding (weaker, indirect through water), (iii) chelate formation with N7 of guanine and closest phosphate group seen in case of Ca-DNA, and not for Mg-DNA (Ahmad *et al.*, 2003). Many of these findings were also supported by crystal structure data (Chiu and Dickerson, 2000; Minasov *et al.*, 1999). In fact the spectral profile of the Ca^{+2} chelate formation with N7 of guanine and closest phosphate, is quite similar to Cr^{+3}-DNA interactions (Ahmad *et al.*, 2003; Arakawa *et al.*, 2000, 2001). Ca^{+2} also has a strong helix stabilizing effect, which is absent with transition metal ions, and often wins over Mg^{+2} for affinity to DNA. These unique binding characteristics enable the Ca-DNA duplexes to give better resolution than Mg^{+2} ions and other metal ions studied here.

The mismatch stability series starting with the most stable mismatch is G-T > G-G = A-G > G-A = T-G > A-A > T-T > A-C > T-C > C-C > C-A > C-T (Ke and Wartell, 1993). While several reports exist that differ slightly in their stability series (Aboul-ela *et al.*, 1985;

Gaffney and Jones, 1989) the differences are fairly minor and can be attributed to the difference in starting material chosen for investigation. In our work, the mismatches that exist in various DNA hybrids are, CP-VT (A-C, T-G); CP-MT (G-T, T-G); CP-OT (T-T, C-A). According to the mismatch stability series, the order of stability of the duplexes should hence be CP-MT > CP-VT > CP-OT. This could also be confirmed from our results. For all metallized DNA experiments, T_{m2} values for CP-OT, were always lower than CP-VT/MT, due to the presence of a highly unstable C-A mismatch in CP-OT. For most experiments however, the T_{m2} values of CP-VT and CP-MT were almost comparable, (except in the case of Mg^{+2}, where T_{m2} for CP-MT > CP-VT). Although CP-VT and CP-MT differed in their first mismatch, the second mismatch was identical in both duplexes. Besides, destabilization arising out of mismatches often depends on other factors like, nearest neighbor base pairs (Ke and Wartell, 1993). This combined with the location of the mismatches in CP-VT and CP-MT, probably prevents their resolution.

The pKa value for the phosphodiester backbone ranges from 1 to 3 and it is thus highly negatively charged at physiological pH (Brown *et al.,* 2013). The interaction of metal ion with the phosphodiester backbone is more favourable at higher pH values, when the backbone is more negative. Additionally the interaction with nucleobases is also preferred at higher pH values (≥ 8) (Wood *et al.,* 2002). We demonstrate that pH 7 is less suitable for the required resolution between the duplexes (Figure 7.5 B). On increasing the pH to 8, a higher resolution could be achieved. This follows directly from the above stated principles. However, as we increased the pH value further, the resolution was slightly decreased. This

could be attributed to the alkaline denaturation of DNA at higher pH values, which is perhaps aided by the prolonged treatment of DNA duplexes at higher pH (20 h) and also due to the presence of base mismatches in the DNA hybrids.

Unlabeled probes are often used in HRM analysis to obtain better resolution from otherwise uninformative melt curves (Erali *et al.,* 2008). However, the HRM assays also have certain limitations such as, their inability to reveal all the sequence variants in a target (Tong and Giffard, 2012) with usual problems arising in the case of homozygous variants (Wittwer, 2009). Hence, HRM has been coupled with special PCR based technique, qRT-PCR-HRM, for species differentiation of malaria where however, multiple steps of mRNA isolation and reverse transcription of a conserved region of the 18S rRNA of *Plasmodium* are involved (Chua *et al.,* 2015). The HRM method we report here does not involve cumbersome steps of molecular protocols. The mere effect of the metal ions could enhance the desired signal resolution in the HRM for differentiation of the target alleles. The highly sensitive detection (0.25 pmoles.μl^{-1} of target DNA) capability offered by the method has greatly emphasized its application potential for non-invasive detection of malaria in clinical samples. Notably, for non-invasive detection, parasite DNA samples primarily collected from extraneous body fluids like saliva, urine etc. are estimated in qPCR and this method of malaria detection has been shown to have a positive correlation with microscopy based detection of malaria parasite (Nwakanma *et al.,* 2009; Sutherland and Hallett, 2009).

7.5 Conclusion

Uniquely selected 26 mer long native DNA target stretches from the gene of each of the four major *Plasmodium* species that translate to a conserved sequence of the malarial biomarker pLDH and absent in the hLDH homologues were employed in HRM analysis using a common capture probe. The capture probe was fully complementary to the *P. falciparum* target and had two base mismatches each, with the target DNAs of *P. vivax, P. malariae*, and *P. ovale*. Distinct resolution of fluorescence signal in otherwise identical HRM profiles for each of the four DNA duplexes was achieved by using Ca^{+2} or Mg^{+2} as resolution probe. The other selected metals from the transition metal group could not furnish the signal resolution to differentiate the target DNA duplexes. Ca-DNA duplexes gave better resolution than Mg-DNA duplexes. Remarkable resolution achieved with these metals could easily distinguish four out of five duplexes as compared to un-metallized DNA. The structural studies on DNA-metal interactions confirmed that Ca^{+2} and Mg^{+2} metal ions interact differently among the duplexes with different nucleotide mismatches leading to enhanced fluorescence signal resolution among the targets in the HRM profile. This novel approach with metal mediated resolution of HRM fluorescence signals has great promise for species specific distinction of *Plasmodium* species, in non-invasively obtained patient samples.

Figures

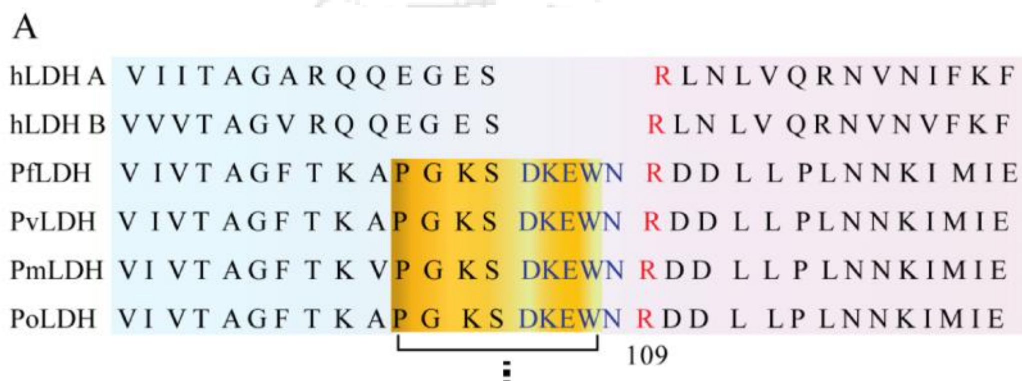

B

Notation	Sequence (5'-3')	Significance	GenBank Ref
FT	CCAGGAAAGAGTGACAAAGAATGGAA	*P. falciparum* target	AF251291
VT	CCAGGAAAGAGCGACAAGGAATGGAA	*P. vivax* target	EU262983
MT	CCAGGAAAGAGTGATAAGGAATGGAA	*P. malariae* target	AY486059
OT	CCTGGAAAAAGTGACAAAGAATGGAA	*P. ovale* target	AY486058
NC	AGCTTCTCGAGCTACAGGTCTTTTAG	Non-complementary	-
CP	TTCCATTCTTTGTCACTCTTTCCTGG	Capture probe	-

Figure 7.1: (A) Multiple sequence alignment of the conserved region of *Plasmodium falciparum* LDH (PfLDH), *Plasmodium vivax* LDH (PvLDH), *Plasmodium malariae* LDH (PmLDH) and *Plasmodium ovale* LDH (PoLDH) and the equivalent region in hLDH A, and hLDH B. (B) Probes used in the study, with their notations. The target probes were derived from the conserved region of LDH proteins of *Plasmodium*. Mismatched bases in VT, MT, and OT have been underlined.

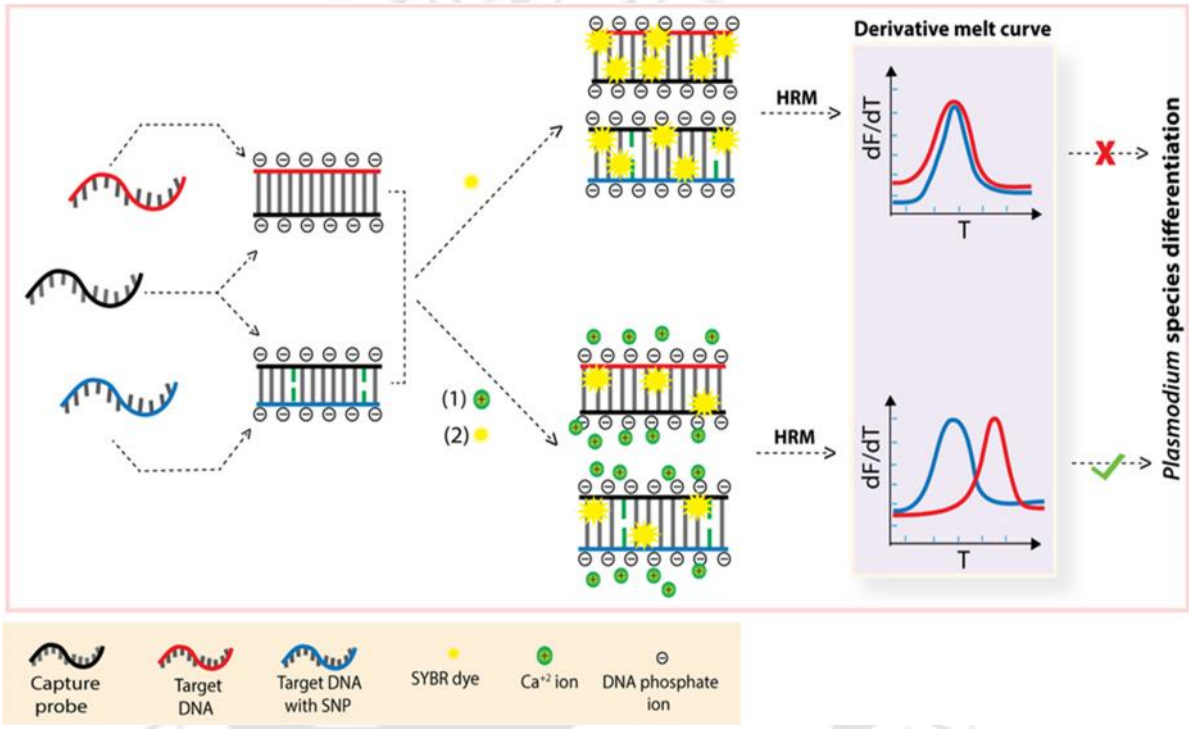

Figure 7.2: Scheme for the strategy used to enhance HRM signal resolution between *Plasmodium* species.

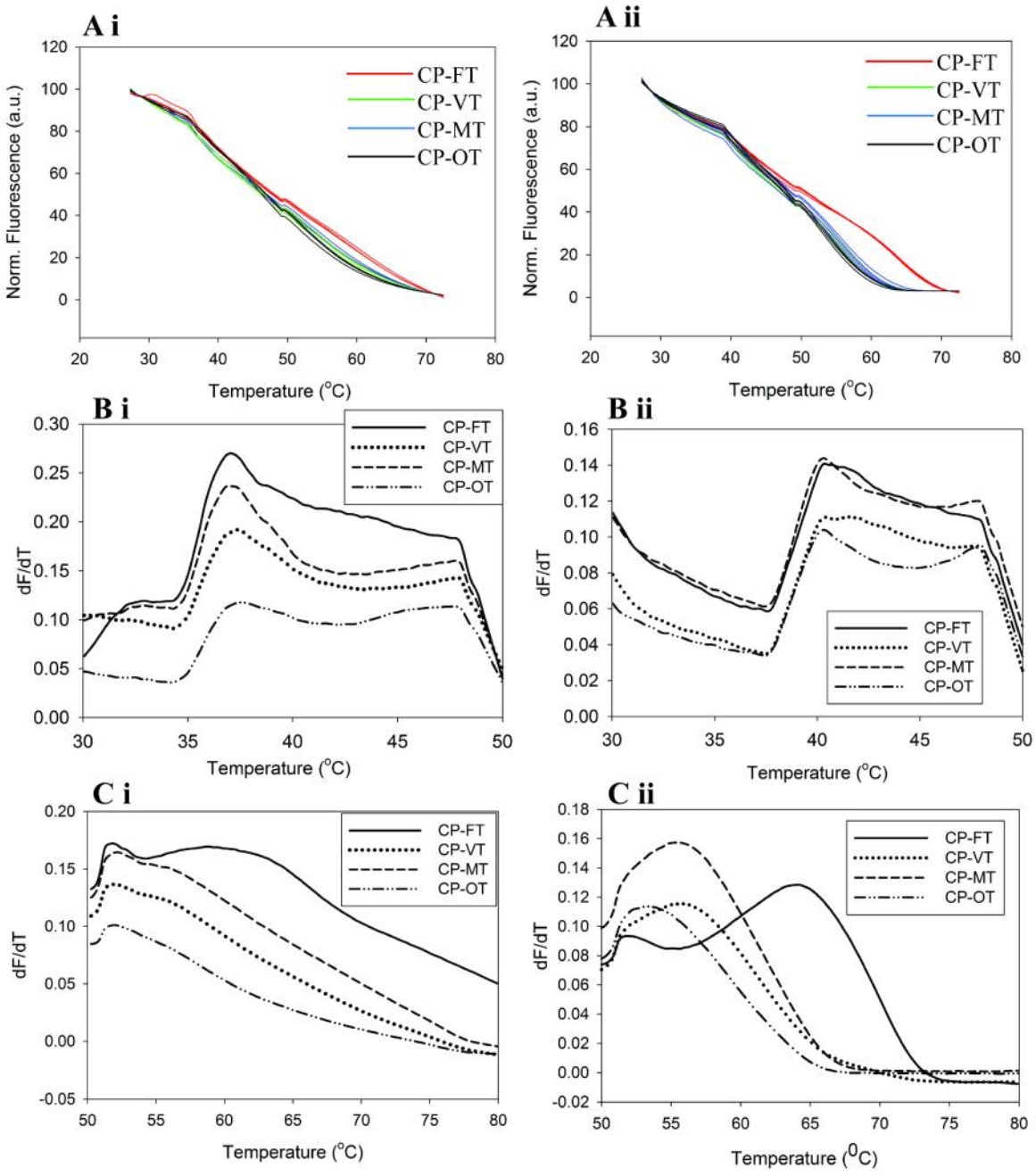

Continued...

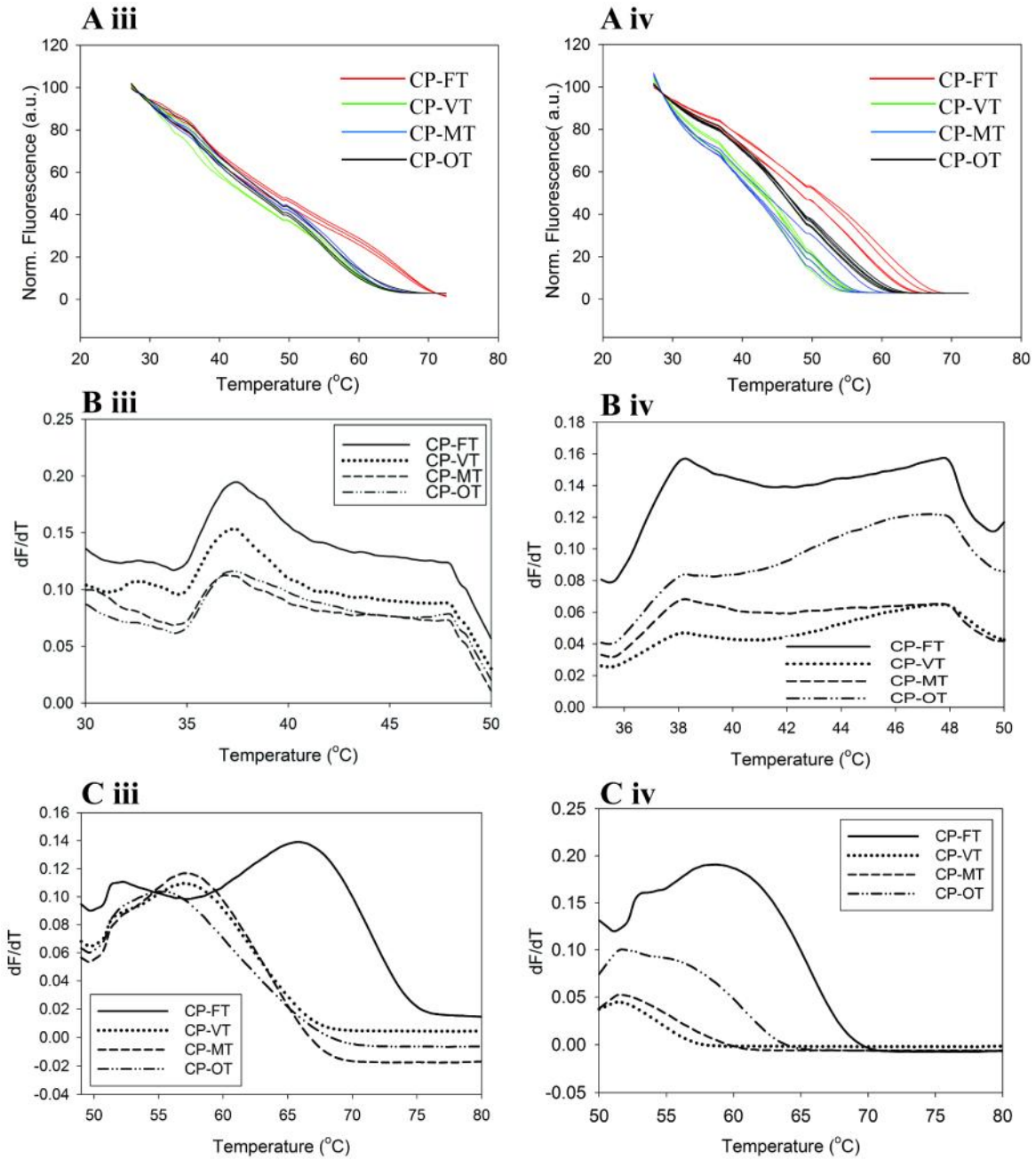

Figure 7.3: (Ai-Aiv) Normalized melt curves for dsDNA complexes, CP-FT/VT/MT/OT; Derivative curves for dsDNA complexes, CP-FT/VT/MT/OT, in the range (Bi-Biv) 30 °C-50 °C and (Ci-Civ) 50 °C-80 °C, for (Ai-Ci) un-metallized, (Aii-Cii) Ca-metallized, (Aiii-Ciii) Mg-metallized, (Aiv-Civ) Ni-metallized complexes. In all (B), and (C), an average of at least three or more curves has been shown for each species for clarity.

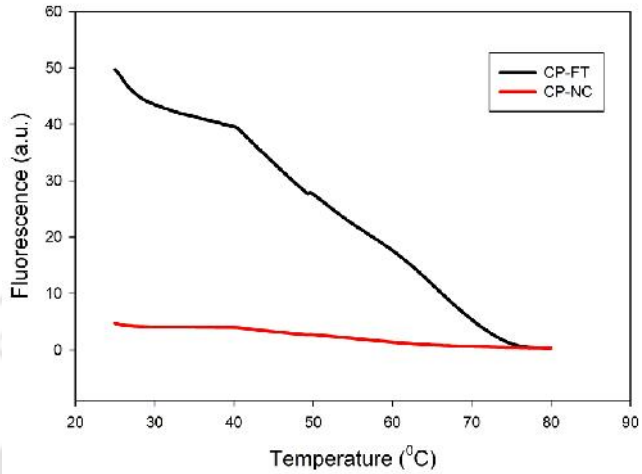

Figure 7.4: Melting curve of CP-NC, in comparison to CP-FT. At least four or more control (CP-NC) were included in each HRM run as a negative control. CP-FT consistently resulted in no absolute fluorescence and hence no melting curve as shown here.

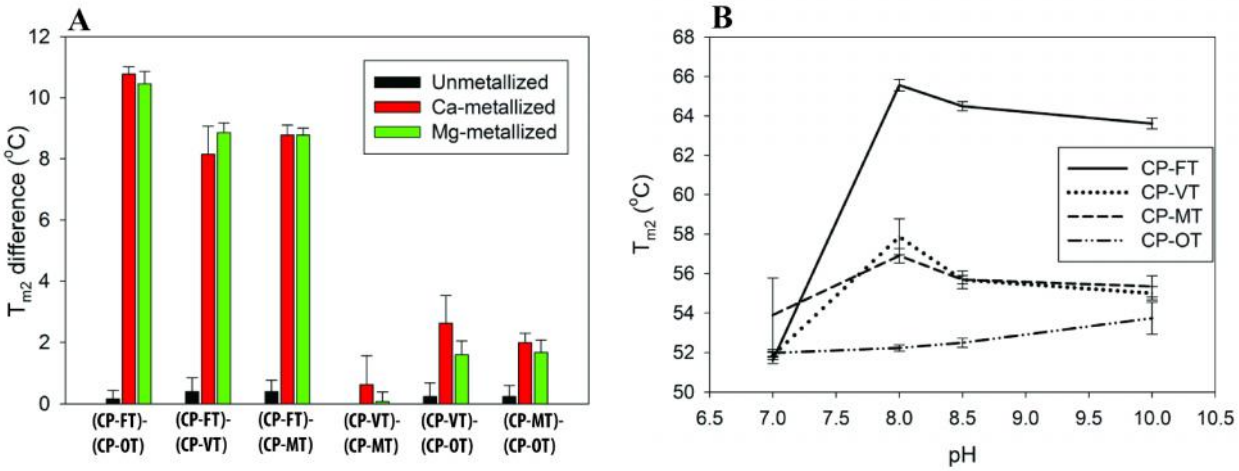

Figure 7.5: (A) Difference in T_{m2} between various DNA duplexes, for un-metallized, Ca-metallized, and Mg-metallized DNA. (B) Effect of pH on T_{m2} of various DNA duplexes, for Ca-metallized DNA.

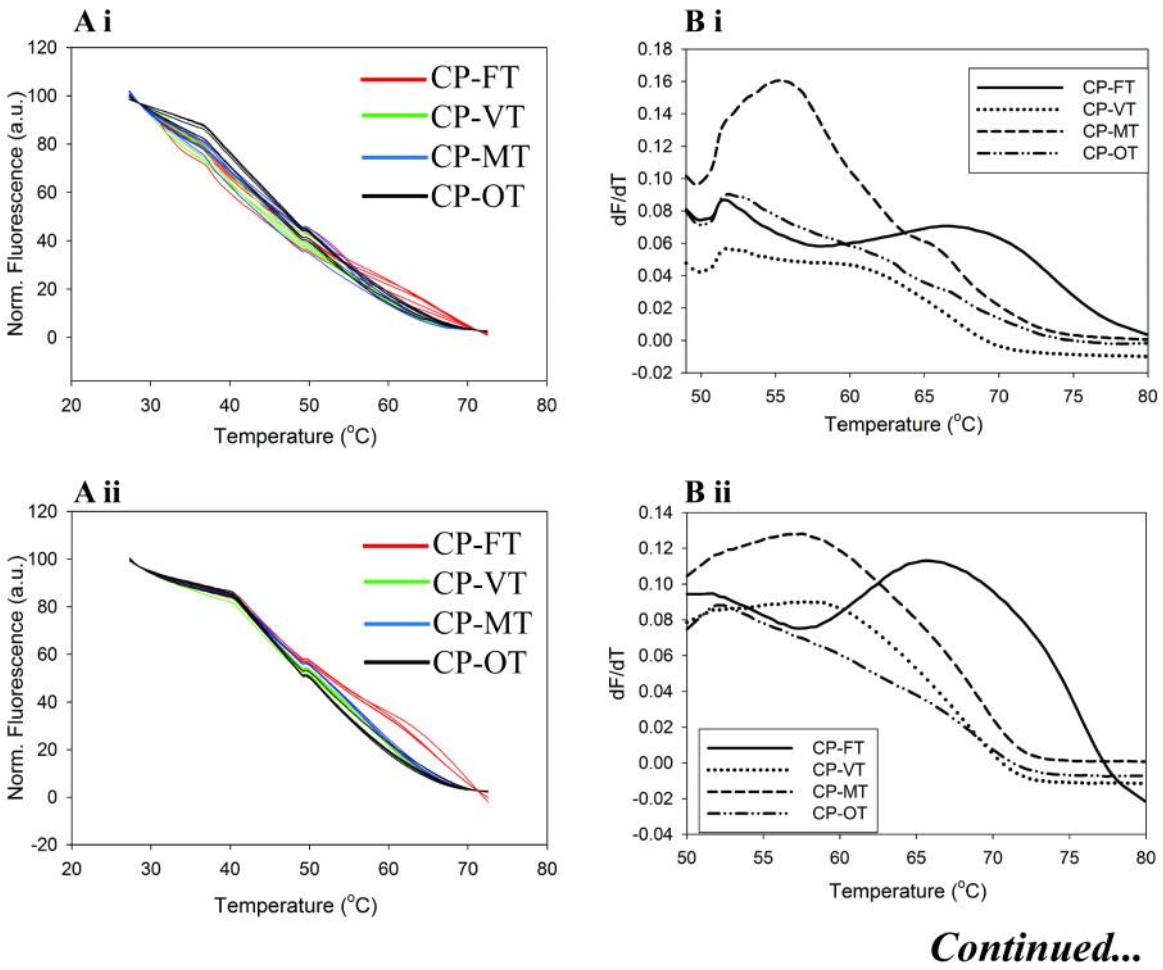

Continued...

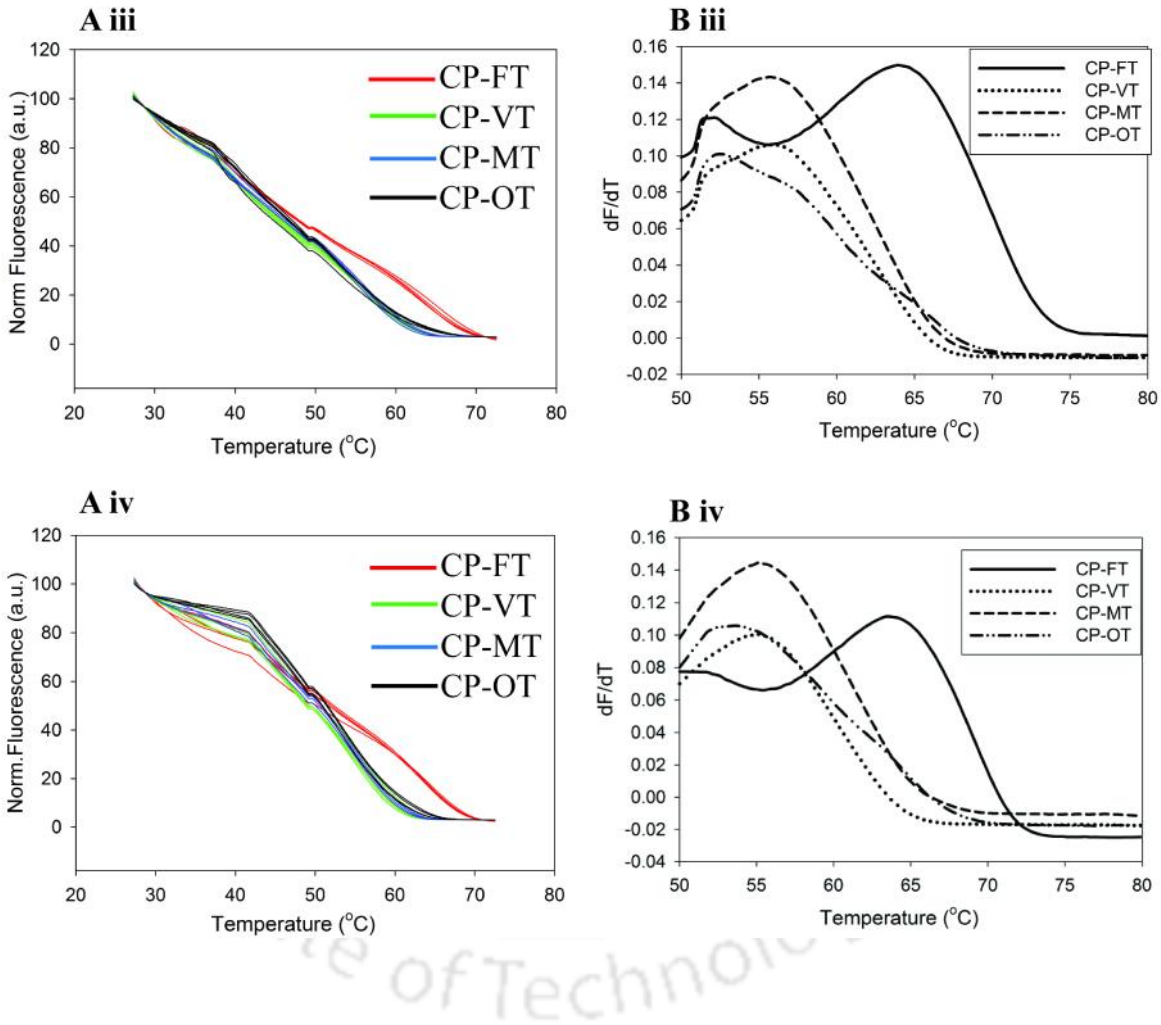

Figure 7.6: (Ai-Aiv) Normalized fluorescence curves. (Bi-Biv) Derivative melt curves for Ca-metallized DNA duplexes CP-FT, CP-VT, CP-MT, CP-OT, and CP-NC at (i) pH 7, (ii) pH 8, (iii) pH 8.5, and (iv) pH 10.

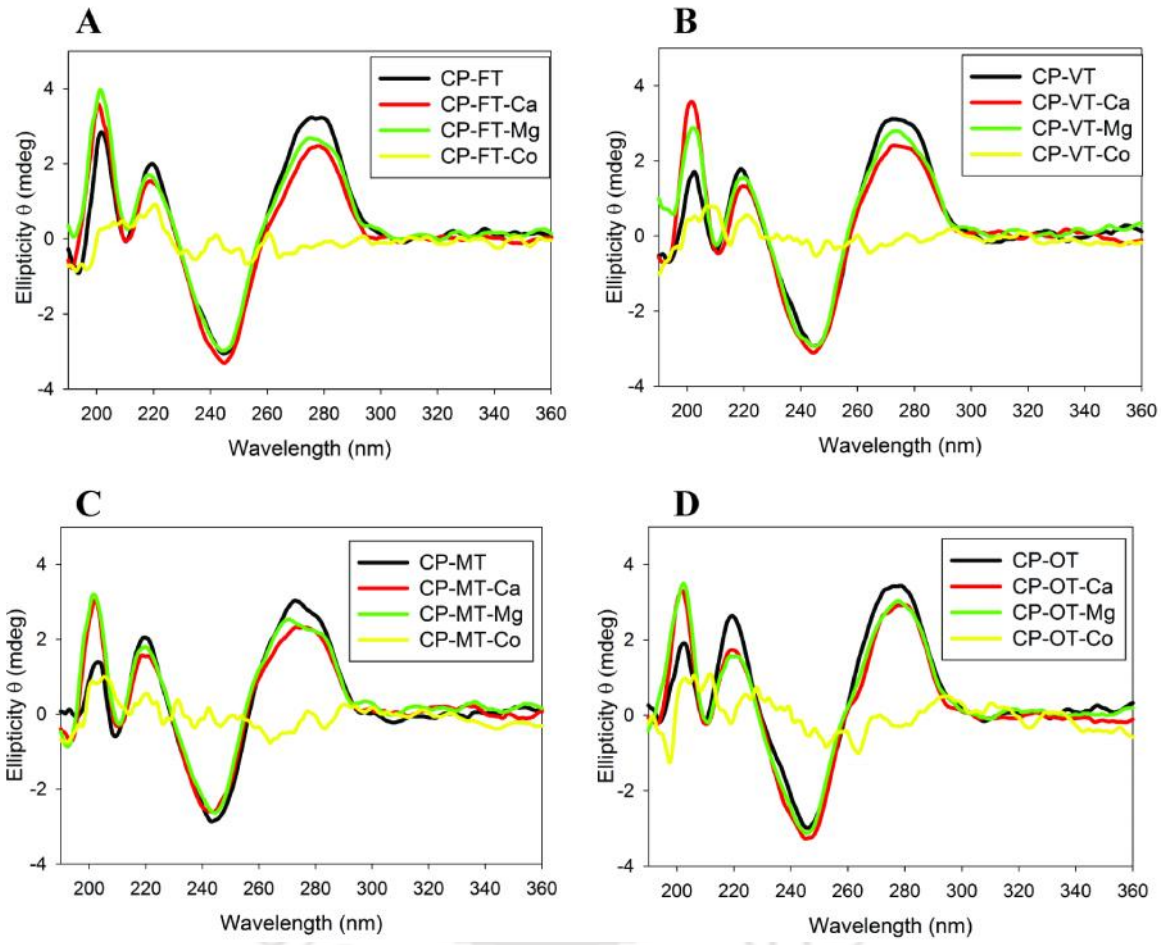

Figure 7.7: CD spectra of un-metallized (black), Ca-metallized (red), Mg-metallized (green), Co-metallized (yellow) DNA duplexes, where (A) CP-FT, (B) CP-VT, (C) CP-MT, (D) CP-OT.

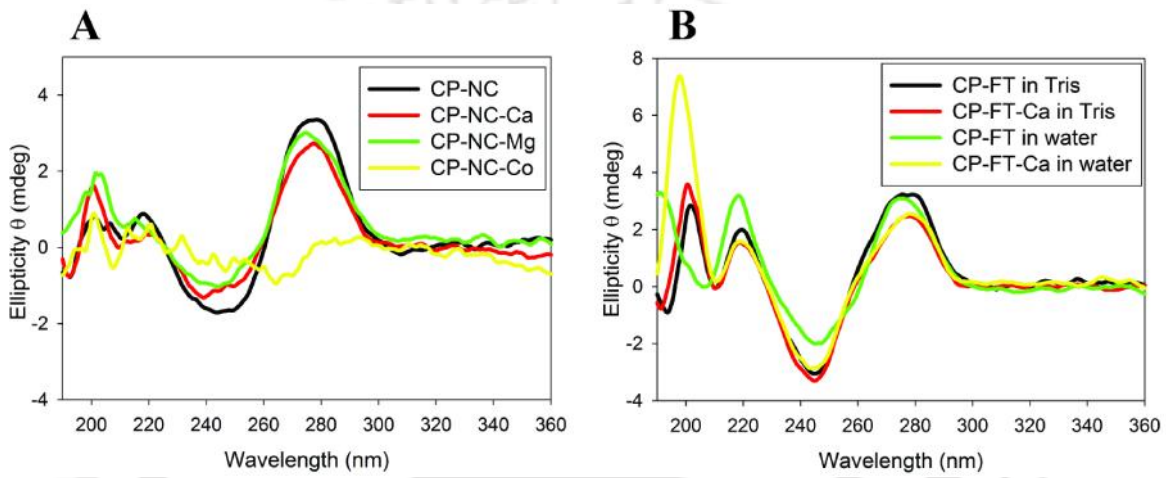

Figure 7.8: (A) CD spectra of un-metalized (black), Ca-metallized (red), Mg-metallized (green), Co-metallized (yellow) DNA duplex CP-NC. CD bands exhibit the characteristic peaks for B-form of DNA, however low amplitude of peaks as compared to that shown in figure 7.7, are a result of poor base stacking in case of CP-NC; (B) CD spectra of CP-FT and Ca-metallized CP-FT, in both water and Tris buffer. Minor changes in peak position and amplitude is attributed to the change in pH conditions. A similar profile of peak shift was observed for both mediums i.e. water and Tris buffer, negating the effect of buffer and further strengthening the claim that Ca ions improve HRM resolution.

Conclusion and Future Directions of Research

The major goal defined for the present work was to develop DNA based detection systems against the potent malarial biomarker PfLDH. The reason for our inclination towards this nucleic acid based recognition system has already been elaborated elsewhere. To achieve this goal, the functionally active biomarker protein PfLDH along with the relevant control proteins from the human host namely, hLDH A, and hLDH B were prepared with adequate purity from the native gene or corresponding clones following the protocols of molecular biology. The structural and functional integrities of the expressed proteins were ascertained by analyzing their secondary structure, sedimentation coefficient and enzyme kinetic profiles. Four independent proof-of-concepts using DNA based recognition system were considered namely, (A) Development of aptamer based colorimetric detection for PfLDH, (B) Development of aptasensor for electrochemical detection of PfLDH, (C) DNA templated silver nanoclusters for fluorescence based detection of PfLDH and (D) High resolution melting of metallized DNA duplexes for species differentiation of *Plasmodium* parasite.

We initially focused on aptamer as biorecognition molecule and successfully developed a specific ssDNA aptamer (termed as P38) against the target PfLDH following the SELEX technique. The aptamer was extensively characterized for its sequence, secondary structure, PfLDH binding constant etc. and confirmed its novelty on all the characteristics. The aptamer as per the proof of concept (A) was utilized and validated its efficiency to detect PfLDH in a colorimetric assay using salt or cationic surfactant mediated

aggregation of AuNPs. In brief, the aptamer binds to PfLDH in a malaria positive sample leaving behind the colloidal AuNPs, which are then instantaneously aggregated by the salt or cationic surfactants present in the solution transforming the solution to a blue color. The change in color was linearly correlated with the concentration of PfLDH producing a dynamic range for quantitative detection of the biomarker in samples. The format we adopted for the colorimetric assay though based on a previous report, two novel contributions made by us have enriched the method to a new level. The first one is the use of rationally designed new aptamer that we developed by introducing counter SELEX for all the control proteins thus authenticating the specificity of the aptamer for the target, and the second one is the substitution of the salt or other previously used cationic surfactants by benzalkonium chloride (BCK) as novel AuNPs aggregating agent. BCK gave better sensitivity and greater dynamic range than the previously reported salt or cationic surfactants as aggregating agents. The sensitivity reported by us is in the clinically relevant range and thus the method has the potential to be developed as an assay of practical essence for detection of malaria in clinical laboratories.

The aptamer P38 so developed was also explored in an electrochemical transducer platform as per the proof of concept (B) with an aim to develop highly sensitive sensor for detection of submicroscopic infections. For this, low cost graphene oxide (GO) was prepared from powdered pencil graphite and immobilized physically over glassy carbon electrode (GCE) along with the aptamer to finally construct the aptasensor. The DNA-aptasensor exhibited unprecedented high sensitivity towards PfLDH in a dual detection platform using impedimetry as well as voltammetry techniques. With the help of a redox probe the presence

of PfLDH in human serum sample was impedimetrically detected down to a femtomolar level. The specificity of the biorecognition system on the electrode was confirmed voltammetrically by measuring the NADH formed as a result of the enzymatic activity of PfLDH captured by the GO- immobilized P38 aptamer. Interference studies with the relevant control proteins demonstrated the specificity of the fabricated aptasensor towards PfLDH. Besides, the developed aptasensor was successfully tested in real samples received from two *P. vivax* infected patients. We project this highly sensitive electrochemical aptasensor formulation as a viable concept for developing a PoC diagnostic device to detect low parasitemia samples in yes/no format.

In our third approach (C), DNA-templated fluorescent silver nanocluster (AgNC) based reporting system was developed for indirect detection of PfLDH enzyme. The cofactor, NAD^+ strongly quenched the fluorescence of DNA-templated AgNCs and the phenomenon was exploited to detect NAD^+/NADH based PfLDH catalyzed reaction in a turn-off approach. The detection limit obtained here can satisfy the NAD^+ detection requirements for clinical samples. The practical applicability of the method was also validated in real samples. The applicability of the method was also extrapolated to a widely used industrial enzyme, alcohol dehydrogenase through which we suggest its application potential to monitor different NAD^+/NADH based dehydrogenase systems. An in-depth investigation performed by us on different ssDNAs for their AgNC scaffolding efficiency revealed that the seeding of AgNC is strongly dependent on structure and sequence of the DNA. This was confirmed from the results generated from comprehensive stability studies of the AgNCs in the presence of DNA denaturants, and different pH and temperature

conditions. This investigation has confirmed that in addition to the requirement of C-rich regions in the sequence, the presence of suitable hairpin structure is essential in the DNA to host the seeding of stable fluorescent AgNC. The study also advances our understanding on the tentative ring size and the hairpin stem length of the DNA necessary for the formation and stabilization of AgNC and hence, these criteria may be considered as a general guideline in selecting ssDNA candidates for developing fluorescent AgNC.

In our final work as per (D), an effort has been made to develop a method for species specific differentiation of *Plasmodium* parasites. The conventional biomarker, PfLDH is not suitable to be used directly for the differentiation due to lack of distinct structural and functional features among the orthologous LDH proteins from different *Plasmodium* species. However, the amino acid stretch DKEWN, which is conserved across the four *Plasmodium* species but absent in the corresponding human counterpart, exhibits minor differences in the nucleotide sequences corresponding to this region in the orthologous genes across the four major malaria species. Here, we selected 26-mer long native ssDNA stretches from the gene of each of the four major *Plasmodium* species as targets, and employed them in HRM analysis using a common capture probe. The capture probe was fully complementary to the *P. falciparum* target and had two base mismatches each, with the target DNAs of *P. vivax*, *P. malariae*, and *P. ovale*. Distinct resolution of fluorescence signal in otherwise identical HRM profiles for each of the four DNA duplexes could be achieved by using Ca^{+2} or Mg^{+2} as resolution probe. The other selected divalent metals from the transition metal group however, failed to foster the HRM signal resolution. Ca-DNA duplexes gave better resolution than Mg-DNA duplexes. Remarkable HRM resolution

achieved with these alkaline earth metals could easily distinguish four out of the five duplexes. The structural studies on DNA-metal interactions confirmed that Ca^{+2} and Mg^{+2} metal ions interact differently among the duplexes with different nucleotide mismatches leading to enhanced fluorescence signal resolution among the targets in the HRM profile. This novel approach with metal mediated resolution of HRM fluorescence signals has great potential for species specific distinction of *Plasmodium* parasites.

Finally, we attempted to evaluate our works by comparing few critical performance factors with prominent DNA based PfLDH detection systems reported so far as shown in table C.1. The HRM based detection adopted by us, though was not prepared to target the PfLDH biomarker has been included in the table to compare the response, and preparation time needed for the assay. The HRM based assay could detect as low 0.25 $pmole.\mu l^{-1}$ of target DNA. The LODs achieved through the (A) colorimetric assay using AuNP-P38 and (B) electrochemical aptasensor using P38-GO-GCE are comparable to those of several prominent sensors/assays and are in clinically relevant range. The response time required for the three methods (A-C) are in the lowest edge in a scale of the previously reported methods. Among the four methods developed by us, the HRM assay required highest response time because of involving prolonged programming based operation of the system. In terms of stability, the electrochemical platform was found to be quite stable, while the stability information was unavailable for many reported works for comparison. So far, none of the reported PfLDH detection methods were successful for species differentiation. In our work, differentiation among *Plasmodium* species using orthologous *pldh* segments as targets was accomplished for the first time with the help of HRM technique. Notably, targeting genomic

DNA for species differentiation has potential for non-invasive detection of malaria in samples obtained from saliva or urine of patients.

Table C.1: Comparison of the performance parameters for the developed analytical/biosensing methods developed here (green) with some prominent reports on DNA based PfLDH detection methods (yellow).

Method	**Sensitivity (LOD)**	**Response Time (min)***	**Preparation Time (h)***	**Stability ($T_{1/2}$)[a]**	**Species differe-ntiation**
(A) Colorimetric assay using AuNP-P38	281 ± 11 pM	2	1.3	7 days	No
(B) Electrochemical aptasensor using P38-GO-GCE	0.5 fM[b]	2	30	1.3 months	No
(C) Fluorescence based assay using ssDNA-AgNCs	1.32 ± 0.03 nM	2	2	10 h	No
(D) HRM assay using Ca-DNA duplexes	0.25 pmoles.µl^{-1} [c]	30	22	N.A.[f]	Yes
AuNP– aptamer based colorimetric assay (Jeon *et al*., 2013)	10.3 pM	2	0.67	N.A.[f]	No
DNA origami assembly (Godonoga *et al*, 2016)	500 nM	60	1.25	N.A.[f]	No

Aptamer based PoC device (Dirkzwager *et al*., 2016)	37 pM	50	17	2 months[d]	No
Colorimetric NTB assay (Dirkzwager *et al*., 2015)	36 pM[5]	40	1 for 96-well based assay, 3 for bead based assay	11 days[d]	No
AuNP– aptamer based colorimetric assay (Lee *et al*, 2014)	2.94 pM	5	0.67	N.A.[f]	No
Electrochemical aptasensor (Lee *et al*., 2012b)	1 pM	2	16	N.A.[f]	No
Fluorescence sensor on MoS_2 sheets (Geldert *et al*., 2016)	550 pM	10	N.A.	N.A.[f]	No
AuNP– aptamer based colorimetric assay (Cheung *et al*., 2013)	419 pM[e]	2	48.5	N.A.[f]	No

* Approximate values. [a] $T_{1/2}$ refers to the time at which ~ 50 % of the initial response decreased. [b]As low as this value of PfLDH could be detected. [c]As low as this value of a conserved region in the *pldh* gene was detectable. [d]No significant decrease in stability observed within this period. [e]Unit changed for better comparison. [f]Not available/reported.

Scope for future work

The works presented in this thesis offer many new detection strategies for malaria diagnosis. However, to materialize these concepts for viable diagnostic products of commercial importance several gaps need to be bridged in these works among which we feel the following points are critical to be addressed first. (a) The exact mechanism of interaction between the aptamer and the PfLDH protein that sets the foundation for this evolved DNA based biorecognition element to grant specificity needs to be elucidated. Analysis through advance techniques like, X-ray crystallography and NMR spectroscopy may provide the information to decipher the mode of interaction between these two complementary entities. This binding information will eventually help to design rationally a chemical approach for stable immobilization of the aptamer over GO/electrode, which in turn will award an operationally stable electrochemical aptasensor. (b) The stabilities of AuNP, and AgNC employed for the corresponding colorimetric and fluorescence based detection of malaria need to be improved to surpass the existing stabilities of the optical probes cited in the table C1. (c) We envision that our aptamer-AuNP based PfLDH detection approach will be a big step forward if the concept could be implemented in a lab-on-chip platform with optical mode of detection. To achieve this, the concept needs to be translated to a suitable solid sensor platform using low cost biocompatible material such as, paper and PDMS complying the ASSURED (Affordable, Sensitive, Specific, User-friendly, Rapid, Equipment free, Deliverable) mandate of WHO for expediency in the low income countries. (d) Finally, the method for HRM based species specific differentiation of *Plasmodium* parasite using

metallized DNA needs to be evaluated with different real samples to perform the clinical validation following standard protocols.

Bibliography

Abdolhosseinzadeh S., Asgharzadeh H., Kim S. H., Fast and fully-scalable synthesis of reduced graphene oxide, Sci. Rep. 5:10160, (2015).

Abeku T., Kristan M., Jones C., Beard J., Mueller D., et al. Determinants of the accuracy of rapid diagnostic tests in malaria case management: evidence from low and moderate transmission settings in the East African highlands. Malar. J. 7, 202, (2008).

Aboul-ela F., Koh D., Tinoco I. Jr., Base-base mismatches. Thermodynamics of double helix formation for dCA3XA3G + dCT3YT3G (X, Y = A,C,G,T). Nucleic Acids Res. 13, 4811, (1985).

Adhikari B., Banerjee A., Facile synthesis of water soluble fluorescent silver nanoclusters and HgII sensing, Chem. Mater. 22, 4364–4371, (2010).

Ahmad R., Arakawa H., Tajmir-Riahi H. A., A comparative study of DNA complexation with Mg(II) and Ca(II) in aqueous solution: major and minor grooves bindings. Biophys. J. 84, 2460–2466, (2003).

Aich P., Labiuk L. S., Tari W. L., Delbaere T. J. L., Roesler J. W., et al. M-DNA: A complex between divalent metal ions and DNA which behaves as a molecular wire. J. Mol. Biol. 294, 477-485, (1999).

Alnasser Y., Ferradas C., Clark T., Calderon M., Gurbillon A., Colorimetric Detection of Plasmodium vivax in Urine Using MSP10 Oligonucleotides and Gold Nanoparticles, PLoS Negl. Trop. Dis. | DOI:10.1371/journal.pntd.0005029, (2016).

Anastassopoulou J., Metal–DNA interactions, J. Mol. Struct. 651–653, 19–26, (2003).

Andree H. A., Nemerson Y., Tissue factor: regulation of activity by flow and phospholipid surfaces. Blood Coagul. Fibrinolysis. 6, 189–197, (1995).

Arakawa H., Ahmad R., Naoui M., Tajmir-Riahi H. A., A comparative study of calf thymus DNA binding to Cr(III) and Cr(VI) ions. Evidence for the guanine N-7-chromium-phosphate chelate formation. J Biol Chem. 275(14):10150-3, (2000).

Arakawa H., Watanabe N., Tajmir-Riahi H. A., Calf-Thymus DNA interaction with Cr(III)-gallate and Cr(III)-ethyl gallate studied by FTIR spectroscopy and capillary electrophoresis. Bull. Chem. Soc. Jpn. 74:1075-1082, (2001).

Armah H. B., Wilson N. O., Sarfo B. Y., Powell M. D., Bond V. C., et al. Cerebrospinal fluid and serum biomarkers of cerebral malaria mortality in Ghanaian children. Malar. J. 6, 147, (2007).

Avila P. E., Kirchgatter K., Brunialti K. C. S., Oliveita A. M., Siciliano R. F., et al. Evaluation of a rapid dipstick test, Malar-CheckTM, for the diagnosis of Plasmodium

falciparum malaria in Brazil. Revista do Instituto de Medicina Tropical de São Paulo 44, 293–296, (2002).

Baker J., McCarthy J., Gatton M., Kyle D. E., Belizario V., et al. Genetic diversity of Plasmodium falciparum histidine rich protein 2 (PfHRP2) and its effect on the performance of PfHRP2 based rapid diagnostic tests. J. Infect. Dis. 192, 870 –877, (2005).

Baldwin R. L., Structure and mechanism in protein science. A guide to enzyme catalysis and protein folding, Protein Science 9, 207–207, (2000).

Barbas III F. C., Burton R. D., Scott K. J., Silverman J. G., Quantitation of DNA and RNA, General Procedures, Appendix 3, Phage Display, Cold Spring Harbor Laboratory Press, Cold Spring Harbor, NY, USA, (2001).

Bendezu J., Rosas A., Grande T., Rodriguez H., Llanos-Cuentas A., et al. Field evaluation of a rapid diagnostic test (ParascreenTM) for malaria diagnosis in the Peruvian Amazon. Malar. J. 9, 154, (2010).

Bereczky S., Martensson A., Gil J. P., Farnert A., Short report: Rapid DNA extraction form archive blood spots on filter paper for genotyping of Plasmodium falciparum. Am. J. Trop. Med. Hyg. 72(3), 249–251, (2005).

Bernal-Mizrachi L., Jy W., Jimenez J. J., Pastor J., Mauro L. M., et al. High levels of circulating endothelial microparticles in patients with acute coronary syndromes. Am. Heart J. 145, 962–970, (2003).

Bin X., Kraatz B-H., Interaction of metal ions and DNA films on gold surfaces: an electrochemical impedance study. Analyst 134, 1309–1313, (2009).

Bjorkman A., Martensson, A., Risks and Benefits of Targeted Malaria Treatment Based on Rapid Diagnostic Test Results. Clin. Infect. Dis. 51(5):512–514, (2010).

Bousema T., Okell L., Felger I., Drakeley C., Asymptomatic malaria infections: detectability, transmissibility and public health relevance, Nat. Rev. Microbiol. doi:10.1038/nrmicro3364, (2014).

Bozdech Z., Llinás M., Pulliam B. L., Wong E. D., Zhu J., et al. The transcriptome of the intraerythrocytic developmental cycle of Plasmodium falciparum. PLoS Biol. 1, e5, (2003).

Bradford M. M., Rapid and sensitive method for the quantization of microgram quantities of protein utilizing the principle of protein-dye binding. Anal. Biochem. 72, 248–254 (1976).

Brown H. W., Iverson L. B., Anslyn E., Foote S. C., Organic Chemistry, Cengage Learning, p168, (2013).

Brown W. M., Yowell C. A., Hoard A., Vander Jagt T. A., Hunsaker L. A., et al. Comparative structural analysis and kinetic properties of lactate dehydrogenases from the four species of human malarial parasites. Biochemistry 43, 6219–6229, (2004).

Cameron A., Read J., Tranter R., et al. Identification and activity of a series of azole-based compounds with lactate dehydrogenase-directed antimalarial activity. J. Biol. Chem, 279: 31 429–31 439, (2004).

Candiano G., Bruschi M., Musante L., Santucci L., Ghiggeri G. M., et al. Blue silver: a very sensitive colloidal Coomassie G-250 staining for proteome analysis. Electrophoresis 25,1327-33 (2004).

Casals-Pascual C., Idro R., Gicheru N., Gwer S., Kitsao B., et al. High levels of erythropoietin are associated with protection against neurological sequelae in African children with cerebral malaria. Proc. Natl. Acad. Sci. USA 105, 2634 – 2639, (2008).

Centres for disease control and prevention (CDC) (http://www.cdc.gov/malaria/about/biology/parasites.html)

Chaikuad A., Fairweather V., Conners R., Joseph-Horne T., Turgut-Balik D., et al. Structure of lactate dehydrogenase from Plasmodium vivax: Complexes with NADH and APADH. Biochemistry 44, 16221–16228, (2005).

Chakma B., Jain P., Singh N. K., Goswami P., Development of an indicator displacement based detection of malaria targeting HRP-II as biomarker for application in point-of-care settings. Anal Chem. 18;88 (20):10316-10321, (2016).

Chanda P., Hamainza B., Mulenga S., Chalwe V., Msiska C., et al. Early results of integrated malaria control and implications for the management of fever in under-five children at a peripheral health facility: A case study of Chongwe rural health centre in Zambia. Malar. J. 8, 49, (2009).

Chang Y-M., Chen C. K-M., Hou M-H., Conformational changes in DNA upon ligand binding monitored by circular dichroism. Int. J. Mol. Sci. 13, 3394-3413, (2012).

Chansuda W., Rapid diagnostic techniques for malaria control. Trends Parasitol. 17, 307–309, (2001).

Chen D., Feng H., Li J., Graphene Oxide: Preparation, Functionalization, and Electrochemical Applications, Chem. Rev. 112, 6027−6053, (2012).

Chen F., Flaherty B. R., Cohen C. E., Peterson D. S., Zhao Y., Direct detection of malaria infected red blood cells by surface enhanced Raman spectroscopy, Nanomedicine 12, 1445–1451, (2016a).

Chen K., Chou L. Y. T., Song F., Chan W. C. W., Fabrication of metal nano shell quantum-dot barcodes for bio molecular detection, Nano Today 8, 228—234, (2013).

Chen K., Yuen C., Aniweh Y., Preiser P., Liu Q., Towards ultrasensitive malaria diagnosis using surface enhanced Raman spectroscopy, Sci. Rep. 6:20177, (2016b).

Chen M. M., Shi L., Sullivan Jr., D. J., Haemoproteus and Schistosoma synthesize heme polymers similar to Plasmodium hemozoin and β-hematin. Mol. Biochem. Parasitol. 113, 1–8, (2001).

Cheung Y. W., Kwok J., Law A. W., Watt R. M., Kotaka M., et al. Structural basis for discriminatory recognition of Plasmodium lactate dehydrogenase by a DNA aptamer Proc. Natl. Acad. Sci. USA 110(40), 15967-72, (2013).

Chiodini P. L., Bowers K., Jorgensen P., Barnwell J. W., Grady K. K., et al. The heat stability of Plasmodium lactate dehydrogenase-based and histidine-rich protein 2-based malaria rapid diagnostic tests. Trans. R. Soc. Trop. Med. Hyg. 101, 331–337, (2007).

Chiu T. K., Dickerson R. E., 1A crystal structures of B-DNA reveal sequence-specific binding and groove-specific bending of DNA by magnesium and calcium. J. Mol. Biol. 301(4):915-45, (2000).

Cho E. J., Lee J. W., Ellington A. D., Applications of aptamers as sensors. Annu. Rev. Anal. Chem. 2, 241–264, (2009).

Choi S., Beeler A. B., Pradhan A., Watkins E. B., Rimoldi J. M., et al. Generation of oxamic acid libraries antimalarials and inhibitors of Plasmodium falciparum lactate dehydrogenase. J. Comb. Chem. 9, 292–300, (2007).

Chua K. H., Lim S. C., Ng C. C., Lee P. C., Lim Y. A., et al. Development of High Resolution Melting Analysis for the Diagnosis of Human Malaria, Sci. Rep. 5:15671, (2015).

Chung C. T., Niemela S. L., Miller R. H., One-step preparation of competent Escherichia coli: Transformation and storage of bacterial cells in the same solution. Proc. Natl. Acad. Sci. USA 86, 2172-2175 (1989).

Combes V., Taylor T. E., Juhan-Vague I., Mège J-L., Mwenechanya J., et al. Circulating endothelial microparticles in malawian children with severe falciparum malaria complicated with coma. JAMA. 291, 2542–2544, (2004).

Conners R., Schambach F., Read J., Cameron A., Sessions, R. B., et al. Mapping the binding site for gossypol-like inhibitors of Plasmodium falciparum lactate dehydrogenase. Mol. Biochem. Parasitol. 142, 137–148, (2005).

Conroy A., Lafferty E., Lovegrove F., Krudsood S., Tangpukdee N., et al. Whole blood angiopoietin-1 and -2 levels discriminate cerebral and severe (non-cerebral) malaria from uncomplicated malaria. Malar. J. 8,295, (2009).

Cote J. L., Kim F., Huang J., Langmuir-Blodgett Assembly of Graphite Oxide Single Layers, J. Am. Chem. Soc.131, 1043–1049, (2009).

Crews N., Wittwer C. T., Montgomery J., Pryor R., Gale B., Spatial DNA melting analysis for genotyping and variant scanning. Anal. Chem. 81(6):2053-8, (2009).

Cross J., Singer J. E., Cationic surfactants (Vol. 53). Boca Raton: CRC Press, (1994).

Dal-Bianco M., Köster K., Kombila U., Kun J. F. J., Grobusch M., et al. High prevalence of asymptomatic Plasmodium falciparum infection in Gabonese adults. Am. J. Trop. Med. Hyg. 77(5), pp. 939–942, (2007).

Dando C., Schroeder E. R., Hunsaker L. A., Deck L. M., Royer R. E., et al. The kinetic properties and sensitivities to inhibitors of lactate dehydrogenases (LDH1 and LDH2) from Toxoplasma gondii: comparisons with pLDH from Plasmodium falciparum. Mol. Biochem. Parasitol. 118, 23–32, (2001).

de Oliveira A. M., Skarbinski J., Ouma P. O., Kariuki S., Barnwell J. W., Performance of malaria rapid diagnostic tests as part of routine malaria case management in Kenya. Am. J. Trop. Med. Hyg. 80, 470 –474, (2009).

de Souza Castilho M., Laube T., Yamanaka H., Alegret S., Pividori M. I., Magneto immunoassays for Plasmodium falciparum histidine rich protein 2 related to malaria based on magnetic nanoparticles. Anal. Chem. 83, 5570–5577, (2011).

Deck L. M., Royer R. E., Chamblee B. B., Hernandez V. M., Malone R. R., et al. Selective inhibitors of human lactate dehydrogenases and lactate dehydrogenase from the malarial parasite Plasmodium falciparum. J. Med. Chem. 41, 3879–3887, (1998).

Delahunt C., Horning P. M., Wilson K. B., Proctor L. J., Hegg C. M., et al. Limitations of haemozoin-based diagnosis of Plasmodium falciparum using dark-field microscopy, Malar. J., 13:147, (2014).

Desakorn V., Dondorp A. M., Silamut K., Pongtavornpinyo W., Sahassananda D., et al. Stage-dependent production and release of histidine-rich protein 2 by Plasmodium falciparum. Trans. R. Soc. Trop. Med. Hyg. 99, 517–524, (2005).

Dirkzwager M. R., Kinghorn A. B., Richards J. S., Tanner J. A., APTEC: aptamer-tethered enzyme capture as a novel rapid diagnostic test for malaria. Chem. Commun. 51(22), 4697-700, (2015).

Dirkzwager M. R., Liang S., Tanner J. A., Development of Aptamer-Based Point-of-Care Diagnostic Devices for Malaria Using Three-Dimensional Printing Rapid Prototyping, ACS Sens. 1, 420−426, (2016).

Döbeli H., Trzeciak A., Gillessen D., Matile H., Srivastava I. K., et al. Expression, purification, biochemical characterization and inhibition of recombinant Plasmodium falciparum aldolase. Mol. Biochem. Parasitol. 41(2):259-68, (1990).

Dragan A. I. , Pavlovic R. , McGivney J. B. , Casas-Finet J. R. , Bishop E. S. , et al. SYBR Green I: Fluorescence properties and interation with DNA. J. Fluoresc. (4):1189-99, (2012).

Duguid J., Bloomfield V. A., Benevides J., Thomas G. J. Jr., Raman spectroscopy of DNA-metal complexes. I. Interactions and conformational effects of the divalent cations: Mg, Ca, Sr, Ba, Mn, Co, Ni, Cu, Pd, and Cd. Biophys. J. 65(5):1916-28, (1993).

Duhovny D., Nussinov R., Wolfson H. J., Efficient Unbound Docking of Rigid Molecules. In Gusfield et al., Ed. Proceedings of the 2'nd Workshop on Algorithms in Bioinformatics (WABI) Rome, Italy, Lecture Notes in Computer Science 2452, pp. 185-200, Springer Verlag, (2002).

Dunn C. R., Banfield M. J., Barker J. J., Higham C. W., Moreton K. M., The structure of lactate dehydrogenase from Plasmodium falciparum reveals a new target for anti-malarial design. Nat. Struct. Mol. Biol. 3, 912–915, (1996).

Eichhorn G. L., Shin Y. A., Interaction of metal ions with polynucleotides and related compounds. XII. The relative effect of various metal ions on DNA helicity. J Am Chem Soc. 90(26):7323-8, (1968).

Eisen D. P., Saul A., Disappearance of pan-malarial antigen reactivity using the ICT Malaria P.f/ P.vTM kit parallels decline of patent parasitaemia as shown by microscopy. Trans. R. Soc. Trop. Med. Hyg. 94, 169–170, (2000).

Ellington A. D., Szostak J. W., In vitro selection of RNA molecules that bind specific ligands. Nature 346, 818-822 (1990).

Erali M., Voelkerding K. V., Wittwer C. T., High resolution melting applications for clinical laboratory medicine, Exp Mol Pathol. 85(1):50-8, (2008).

Fan J., Matsumoto Y., Wilson M. D., Nucleotide sequence and DNA secondary structure, as well as replication protein A, modulate the single-stranded abasic endonuclease activity of APE1, J. Biol. Chem. 281(7), pp. 3889–3898, (2006).

Feldman A. B., Progress toward rapid malaria screening based on mass spectrometry. 2006, Lab Tech. Link: http://www.cli-online.com/fileadmin/artimg/progress-toward-rapid-malaria-screening-based-on-mass-spectrometry.pdf

Ferrari A. C., Robertson J., Interpretation of Raman spectra of disordered and amorphous carbon, Phy. Rev. B 61(20),14095-14107, (2000).

Fleischer B., Editorial: 100 years ago: Giemsa's solution for staining of plasmodia. Trop. Med. Int. Health. 9, 755–756, (2004).

Fogg C., Twesigye R., Batwala V., Piola P., Nabasumba C., et al. Assessment of three new parasite lactate dehydrogenase (pan-pLDH) tests for diagnosis of uncomplicated malaria. Trans. R. Soc. Trop. Med. Hyg. 102, 25–31, (2008).

Fokina A. A., Stetsenko D. A., François J. C., DNA enzymes as potential therapeutics: towards clinical application of 10-23 DNAzymes, Expert Opin. Biol. Ther. 15(5):689-711, (2015).

Forney J. R., Magill A. J., Wongsrichanalai C., Sirichaisinthop J., Bautista C. T., et al. Malaria rapid diagnostic devices: performance characteristics of the ParaSight F device determined in a multisite field study. J. Clin. Microbiol. 39, 2884–2890, (2001).

Frank O., Mohr M., Maultzsch J., Thomsen C., Riaz I., et al. Raman 2D-Band Splitting in Graphene: Theory and Experiment, ACS Nano 5(3), 2231–2239, (2011).

Frank R., Hargreaves R., Clinical biomarkers in drug discovery and development. Nat. Rev. Drug Discov. 2, 566–580, (2003).

Frasch S. C., Henson P. M., Nagaosa K., Fessler M. B., Borregaard N., et al. Phospholipid flip-flop and phospholipid scramblase 1 (PLSCR1) co-localize to uropod rafts in formylated Met-Leu-Phe-stimulated neutrophils. J. Biol. Chem. 279, 17625–17633, (2004).

Frazer K. A., Murray S. S., Schork N. J., Topo E. J., Human genetic variation and its contribution to complex traits. Nat. Rev. Genet. (4):241-51, (2009).

Freyssinet J. M., Cellular microparticles: what are they bad or good for? J. Thromb. Haemost. 1, 1655–1662, (2003).

Fry M., Webb E., Pudney M., Effect of mitochondrial inhibitors on adenosine-triphosphate levels in Plasmodium falciparum. Comp. Biochem. Physiol. B 96, 775–782, (1990).

Gaffney L. B., Jones A. R., Thermodynamic comparison of the base pairs formed by the carcinogenic lesion O6-methylguanine with reference both to Watson-Crick pairs and to mismatched pairs. Biochemistry 28, 5881-5889, (1989).

Gamboa D., Ho M-F., Bendezu J., Torres K., Chiodini P. L., et al. A large proportion of P. falciparum isolates in the amazon region of Peru lack pfhrp2 and pfhrp3: implications for malaria rapid diagnostic tests. PLoS ONE 5, e8091, (2010).

Garrett L. N., Sekine R., Dixon A. W. M., Tilley L., Bamberye R. K., et al. Bio-sensing with butterfly wings: naturally occurring nano-structures for SERS-based malaria parasite detection, Phys. Chem. Chem. Phys. 17, 21164, (2015).

Geldert K. A., Zhang X., Zhang H., Lim C. T., Highly Sensitive and Selective Aptamer-Based Fluorescence Detection of a Malarial Biomarker Using Single-Layer MoS2 Nanosheets, ACS Sens. 1, 1315−1321, (2016).

Gikunoo E., Abera A., Woldesenbet E., A Novel Carbon Nanofibers Grown on Glass Microballoons Immunosensor: A Tool for Early Diagnosis of Malaria, Sensors 14, 14686-14699, (2014).

Godonoga M., Lin Y-T., Oshima A., Sumitomo K., Tang M., et al. A DNA aptamer recognising a malaria protein biomarker can function as part of a DNA origami assembly, Sci. Rep. 6:21266, (2016).

Gomez M. S., Piper R. C., Hunsaker L. A., Royer R. E., Deck L. M., et al. Substrate and cofactor specificity and selective inhibition of lactate dehydrogenase from the malarial parasite P. falciparum. Mol. Biochem. Parasitol. 90, 235–246, (1997).

Goncalves L., Subtil A., de Oliveira M. R., Rosario V., Lee P. W., et al. Bayesian latent class models in malaria diagnosis. PLoS ONE 7, e40633, (2012).

Green M. R., Sambrook J., Molecular Cloning: a laboratory manual-4th ed. Cold Spring Harbour Laboratory Press, Cold Spring Harbour, New York, USA (2012).

Guirgis B. S. S., Cunha C. S., Gomes I., Cavadas M., Silva I., et al. Gold nanoparticle-based fluorescence immunoassay for malaria antigen detection, Anal. Bioanal. Chem. 402:1019–1027, (2012).

Gulka C. P., Swartz J. D., Trantum J. R., Davis K. M., Peak C. M., et al. Coffee Rings as Low-Resource Diagnostics: Detection of the Malaria Biomarker Plasmodium falciparum Histidine-Rich Protein-II Using a Surface-Coupled Ring of Ni(II)NTA Gold-Plated Polystyrene Particles, ACS Appl. Mater. Interfaces 6, 6257−6263, (2014).

Gulka C. P., Swartz J. D., Wright D. W., Ni(II)NTA AuNPs as a low resource malarial diagnostic platform for the rapid colorimetric detection of Plasmodium falciparum Histidine-Rich Protein-2, Talanta 135, 94–101, (2015).

Guo S., Dong S., Biomolecule-nanoparticle hybrids for electrochemical biosensors. Trends Anal. Chem. 28:96-109, (2009).

Guo Z., Gatterman M. S., Hood L., Hansen J. A., Petersdorf E. W., et al. Oligonucleotide Arrays for High-Throughput SNPs Detection in the MHC Class I Genes: HLA-B as a Model System, Genome. Res. 12(3): 447–457, (2002).

Gwinn G. E., O'Neill P., Guerrero J. A., Bouwmeester D., Fygenson K. D., Sequence-Dependent Fluorescence of DNA-Hosted Silver Nanoclusters , Adv. Mater. 20, 279–283, (2008).

Haest, C.W., Interactions between membrane skeleton proteins and the intrinsic domain of the erythrocyte membrane. Biochim. Biophys. Acta. 694, 331–352, (1982).

Han B., Wang E., Oligonucleotide-stabilized fluorescent silver nanoclusters for sensitive detection of biothiols in biological fluids, Biosens. Bioelectron, 26, 2585–2589, (2011).

Handa S. P., Serum lactic acid dehydrogenase isozyme determination in myocardial infarction. Postgrad. med. J. 43, 141-145, (1967).

Hassan M. A. H., Abdelsayed V., Khder S. R. A., Khaled M., AbouZeid M. K., et al. Microwave synthesis of graphene sheets supporting metal nanocrystals in aqueous and organic media, J. Mater. Chem. 19, 3832–3837, (2009).

He L., Luo Y., Zhi W., Wu Y., Zhou P., A colorimetric aptamer biosensor based on gold nanoparticles for the ultrasensitive and specific detection of tetracycline in milk. Aust. J. Chem. 66(4), 485–490, (2013).

Heffler M., Walters D. R., Kugel F. J., Using electrophoretic mobility shift assays to measure equilibrium dissociation constants: GAL4-p53 binding DNA as a model system. Biochem. Mol. Biol. Educ. 40(6), 383–387, (2012).

Hendriksen I. C. E., Mwanga-Amumpaire J., von Seidlein L., Mtove G., White L. J., et al. Diagnosing severe falciparum malaria in parasitaemic African children: A prospective evaluation of plasma PfHRP2 measurement. PLoS Med. 9, e1001297, (2012).

Hernández-Ainsa S., Keyser U. F., DNA origami nanopores: developments, challenges and perspectives, Nanoscale 6, 14121-14132, (2014).

Hewitt C. O., Eszes C. M., Sessions R. B., Moreton K. M., Dafforn T. R., et al. A general method for relieving substrate inhibition in lactate dehydrogenases. Protein Eng. 12, 491–496, (1999).

Hopkins H., González J. I., Polley D. S., Angutoko P., Ategeka J., et al. Highly Sensitive Detection of Malaria Parasitemia in a Malaria-Endemic Setting: Performance of a New Loop-Mediated Isothermal Amplification Kit in a Remote Clinic in Uganda, J. Infect Dis. 208(4), 645–652, (2013).

Howard R. J., Uni S., Aikawa M., Aley S. B., Leech J. H., Secretion of a malarial histidine-rich protein (Pf HRP II) from Plasmodium falciparum infected erythrocytes. J. Cell Biol. 103, 1269–1277, (1986).

Hulka B., Epidemiologic Studies Using Biological Markers - Issues for Epidemiologists. Cancer Epidemiol. Biomarkers Prev. 1, 13–19, (1991).

Hurdayal R., Achilonu I., Choveaux D., Coetzer T. H. T., Goldring D. J. P., Anti-peptide antibodies differentiate between plasmodial lactate dehydrogenases. Peptides 31, 525–532, (2010).

Iqbal J., Sher A., Rab, A., Plasmodium falciparum histidine rich protein 2-based immunocapture diagnostic assay for malaria: cross-reactivity with rheumatoid factors. J. Clin. Microbiol. 38 (3): 1184–1186, (2000).

Iqbal J., Siddique A., Jameel M., Hira P. R., Persistent histidine rich protein 2, parasite lactate dehydrogenase and pan malarial antigen reactivity after clearance of Plasmodium falciparum monoinfection. J. Clin. Microbiol. 42, 4237–4241, (2004).

Jacoby R. C., Owings J. T., Holmes J., Battistella F. D., Gosselin R. C., et al. Platelet activation and function after trauma. J. Trauma 51, 639–647, (2001).

Jain P., Chakma B., Patra S., Goswami P., Potential Biomarkers and Their Applications for Rapid and Reliable Detection of Malaria, BioMed Research International, Volume 2014, Article ID 852645, http://dx.doi.org/10.1155/2014/852645, (2014).

Jakobsen P. H., Morris-jones S., Ronn A., Hviid L., Theander T. G., et al. Increased plasma concentrations of sICAM-1, sVCAM-1 and sELAM-1 in patients with Plasmodium falciparum or P. vivax malaria and association with disease severity. Immunology 83,665-669, (1994).

Japrung D., Henricus M., Li Q., Maglia G., Bayley H., Urea Facilitates the Translocation of Single-Stranded DNA and RNA through the a-HemolysinNanopore, Biophys. J. 98, 1856–1863, (2010).

Jelinek T., Amsler L., Grobusch M., Nothdurft H., Self-use of rapid tests for malaria diagnosis by tourists. The Lancet 354, 1609, (1999).

Jensen M. D., Conley M., Helstowski L. D., Culture of Plasmodium falciparum: The role of pH, glucose, and lactate. J. Parasitol. 69, 1060–1067, (1983).

Jeon W., Lee S., Manjunatha D. H., Ban C., A colorimetric aptasensor for the diagnosis of malaria based on cationic polymers and gold nanoparticles. Anal. Biochem. 439, 11–16, (2013).

Jiang Z., Li G., Zhang M., Electrochemical sensor based on electro-polymerization of β-cyclodextrin and reduced-graphene oxide on glassy carbon electrode for determination of gatifloxacin, Sens. Actuators B 228, 59–65, (2016).

John C. C., Panoskaltsis-Mortari A., Opoka R. O., Park G. S., Orchard P. J., et al. Cerebrospinal fluid cytokine levels and cognitive impairment in cerebral malaria. Am. J. Trop. Med. Hyg. 78, 198 – 205, (2008).

Jorgensen P., Chanthap L., Rebueno A., Tsuyuoka R., Bell D., Malaria rapid diagnostic tests in tropical climates: the need for a cool chain. Am. J. Trop. Med. Hyg. 74, 750–754, (2006).

Kakoti A., Goswami P., Multifaceted analyses of the interactions between human heart type fatty acid binding protein and its specific aptamers, Biochim. Biophys. Acta. 1861(1), 3289–3299, (2016).

Kang J., Liu Y., Xie M. X., Li S., Jiang M., et al. Interactions of human serum albumin with chlorogenic acid and ferulic acid, Biochim. Biophys. Acta. 1674, pp. 205–214, (2004).

Kavanagh K. L., Elling R. A., Wilson D. K., Structure of Toxoplasma gondii LDH1 active-site differences from human lactate dehydrogenases and the structural basis for efficient APAD+ use. Biochemistry 43, 879–889, (2004).

Ke S-H, Wartell M. R., Influence of nearest neighbor sequence on the stability of base pair mismatches in long DNA: determination by temperature-gradient gel electrophoresis. Nucleic Acids Res. 21(22), 5137-5143, (1993).

Keyser U.F., Enhancing nanopore sensing with DNA nanotechnology, Nat. Nanotechnol. 11, 106–108, (2016).

Kilejian A., Histidine-Rich Protein as a Model Malaria Vaccine. Science 201, 922–924, (1978).

Kim D. H., Yeo S. H., Park J. M., Choi J. Y., Lee T. H., et al. Genetic markers for diagnosis and pathogenesis of Alzheimer's disease. Gene 545(2):185-93, (2014).

Kim Y. S., Kim J. H., Kim I. A., Lee S. J., Jurng J., et al. A novel colorimetric aptasensor using gold nanoparticle for a highly sensitive and specific detection of oxytetracycline. Biosen. Bioelectron. 26, 1644–1649. (2010).

Klein E. Y., Antimalarial drug resistance: a review of the biology and strategies to delay emergence and spread, Int. J. Antimicrob. Agents 41, 311–317, (2013).

Klein R., Lin E., Zhang B., Luster A., Tollett J., et al. Neuronal CXCL10 directs CD8_ T-cell recruitment and control of west nile virus encephalitis. J. Virol. 79, 11457–11466, (2005).

Knez K., Spasic D., Janssen F. P. K., Lammertyn J., Emerging technologies for hybridization based single nucleotide polymorphism detection. Analyst 139, 353, (2014).

Krishnamoorthy K., Veerapandian M., Yun K., Kim S. J., The chemical and structural analysis of graphene oxide with different degrees of oxidation, Carbon 53, 38–49, (2013).

Kuzuya A., Watanabe R., Yamanaka Y., Tamaki T., Kaino M., et al. Nanomechanical DNA Origami pH Sensors, Sensors 14(10), 19329-19335, (2014).

Kyabayinze D., Tibenderana J., Odong G., Rwakimari J., Counihan H., Operational accuracy and comparative persistent antigenicity of HRP2 rapid diagnostic tests for Plasmodium falciparum malaria in a hyperendemic region of Uganda. Malar. J. 7, 221, (2008).

Kypr J., Kejnovska I., Renciuk D., Vorlıckova M., Circular dichroism and conformational polymorphism of DNA. Nucleic Acids Res. 37(6), 1713–1725, (2009).

Laemmli U. K. Cleavage of structural proteins during the assembly of the head of bacteriophage T4. Nature 227, 680–685, (1970).

Laferi H., Kandel K., Pichler H., False positive dipstick test for malaria. N. Engl. J. Med. 337, 1635–1636, (1997).

Lau Y.L., Fong M. Y., Mahmud R., Chang P. Y., Palaeya V., et al. Specific, sensitive and rapid detection of human Plasmodium knowlesi infection by loop mediated isothermal amplification in blood samples. Malar. J. 10,197, (2011).

Laue T. M., Shah B. D., Ridgeway T. M., Pelletier S. L., Analytical ultracentrifugation in biochemistry and polymer science (pp. 90–125). Cambridge: Royal Society of Chemistry, (1992).

Lee C-A., Tsai Y-C., Preparation of multiwalled carbon nanotube-chitosan-alcohol dehydrogenase nanobiocomposite for amperometric detection of ethanol, Sens. Actuators B, 138(2), Pages 518–523, (2009).

Lee J. S.; Lytton-Jean A. K. R., Hurst S. J., Mirkin C. A., Silver nanoparticle-oligonucleotide conjugates based on DNA with triple cyclic disulfide moieties. Nano Lett. 7, 2112-2115, (2007).

Lee M. A., Tan C. H., Aw L. T., Tang C. S., Singh M., et al. Real-time fluorescence-based PCR for detection of malaria parasites, J Clin Microbiol. 40(11):4343-5, (2002).

Lee N., Baker J., Andrews K.T., Gatton M. L., Bell D., et al. Effect of sequence variation in Plasmodium falciparum histidine rich protein 2 on Binding of specific monoclonal antibodies: implications for rapid diagnostic tests for malaria. J. Clin. Microbiol. 44, 2773–2778, (2006a).

Lee N., Baker J., Bell D., McCarthy J., Cheng Q., Assessing the genetic diversity of the aldolase genes of Plasmodium falciparum and Plasmodium vivax and its potential effect on performance of aldolase detecting rapid diagnostic tests. J. Clin. Microbiol. 44, 4547–4549, (2006b).

Lee P. W., Ji D. D., Liu C. T., Rampao H. S., Rosario V., et al. Application of loop-mediated isothermal amplification for malaria diagnosis during a follow up study in Sao Tome. Malar. J. 11, 408, (2012a).

Lee S., Manjunatha H. D., Jeon W., Ban, C., Cationic Surfactant-Based Colorimetric Detection of Plasmodium Lactate Dehydrogenase, a Biomarker for Malaria, Using the Specific DNA Aptamer. PLoS ONE v 9, Issue 7, e100847, (2014).

Lee S., Song K. M., Jeon W., Jo H., Shim Y. B., et al. A highly sensitive aptasensor towards Plasmodium lactate dehydrogenase for the diagnosis of malaria. Biosens. Bioelectron. 35, 291–296, (2012b).

Leech J., Barnwell J., Aikawa M., Miller L., Howard R., Plasmodium falciparum malaria association of knobs on the surface of infected erythrocytes with a histidine-rich protein and the erythrocyte skeleton. J. Cell Biol. 98, 1256–1264, (1984).

Lesniak W., Bielinska A. U., Sun K., Janczak K. W., Shi X. Y., et al. Silver/Dendrimer Nanocomposites as Biomarkers: Fabrication, Characterization, in Vitro Toxicity, and Intracellular Detection, Nano Lett. 5, 2123–2130, (2005).

Li H., Rothberg L. Colorimetric detection of DNA sequences based on electrostatic interactions with unmodified gold nanoparticles. Proc. Natl. Acad. Sci. USA 101, 14036–14039, (2004).

Li W., Liu L., Fu Y., Sun Y., Zhang J., et al. Effects of polymorphic DNA on the fluorescent properties of silver nanoclusters, Photochem. Photobiol. Sci. 12, 1864, (2013).

Li Y., Ning Y. S., Li L., Peng D. D., Dong W. Q., et al. Preparation of a monoclonal antibodies against Plasmodium falciparum glutamate dehydrogenase and establishment of colloidal gold-immunochromatographic assay. Di Yi Jun Yi Da Xue Xue Bao. 25(4):435-8, (2005).

Liang L., Tajmir-Riahi H. A., Subirade M., Interaction of β-Lactoglobulin with Resveratrol and its Biological Implications, Biomacromolecules 9, pp. 50–56, (2008).

Lin L., Liu Y., Zhao X., Li J., Sensitive and rapid screening of T4 polynucleotide kinase activity and inhibition based on coupled exonuclease reaction and graphene oxide platform, Anal. Chem. 83, 8396-8402, (2011).

Liu B., Sun Z., Zhang X., Liu J., Mechanisms of DNA Sensing on Graphene Oxide, Anal. Chem. 85, 7987−7993, (2013a).

Liu J., Li Q., Zou Y., Qian Q., Jin Y., et al. The Dependence of Graphene Raman D‑band on Carrier Density, Nano lett. 13, 6170−6175, (2013b).

Liu J., Zhong Y., Lu P., Hong Y., Lam J. W. Y., et al. A superamplification effect in the detection of explosives by a fluorescent hyperbranched poly(silylenephenylene) with aggregation-enhanced emission characteristics, Polym. Chem. 1, 426–429, (2010).

Liu S., Zeng H. T., Hofmann M., Burcombe E., Wei J., et al. Antibacterial Activity of Graphite, Graphite Oxide, Graphene Oxide, and Reduced Graphene Oxide: Membrane and Oxidative Stress, ACS Nano 5(9), 6971–6980, (2011).

Liu X., Abbott L. N., Characterization of the nanostructure of complexes formed by single- or double-stranded oligonucleotides with a cationic surfactant. J. Phys. Chem. B 114, 15554–15564, (2010).

Loh P. K., Bao Q., Eda G., Chhowalla M., Graphene oxide as a chemically tunable platform for optical applications, Nat. Chem. 2, 1015–1024, (2010).

Lovegrove F. E., Tangpukdee N., Opoka R. O., Lafferty E. I., Rajwans N., et al. Serum angiopoietin-1 and -2 levels discriminate cerebral malaria from uncomplicated malaria and predict clinical outcome in African children. PLoS ONE 4, e4912, (2009).

Lucchi N., Jain V., Wilson N., Singh N., Udhaykumar V., et al. Potential serological biomarkers of cerebral malaria. Dis. Markers. 31: 327–335, (2011).

Lukianova-Hleb Y. E., Campbell M. K., Constantinou E. P., Braam J., Olson S. J., et al. Hemozoin-generated vapor nanobubbles for transdermal reagent- and needle-free detection of malaria, Proc. Natl. Acad. Sci. USA 900–905, 111:3, (2014).

Lynn A., Chandra S., Malhotra P., Chauhan V. S., Heme binding and polymerization by Plasmodium falciparum histidine rich protein II: influence of pH on activity and conformation. FEBS Lett. 459, 267–271, (1999).

Makler M. T., Palmer C. J., Ager A. L., A review of practical techniques for the diagnosis of malaria. Ann. Trop. Med. Parasitol. 92, 419–433, (1998).

Malleret B., Claser C., Ong A. S. M., Suwanarusk R., Sriprawat K., et al. A rapid and robust tri-color flow cytometry assay for monitoring malaria parasite development. Sci. Rep. 1,118, (2011).

Maltha J., Gamboa D., Bendezu J., Sanchez L., Cnops L., et al. Rapid diagnostic tests for malaria diagnosis in the Peruvian Amazon: Impact of pfhrp2 gene deletions and cross reactions. PLoS ONE 7, e43094, (2012).

Maltha J., Gillet P., Bottieau E., Cnops L., van Esbroeck M., et al. Evaluation of a rapid diagnostic test (CareStartTM Malaria HRP-2/pLDH (Pf/pan) Combo Test) for the diagnosis of malaria in a reference setting. Malar. J. 9, 171, (2010).

Mariette N., Barnadas C., Bouchier C., Tichit M., Menard D., Country-wide assessment of the genetic polymorphism in Plasmodium falciparum and Plasmodium vivax antigens detected with rapid diagnostic tests for malaria. Malar. J. 7, 219, (2008).

Markwalter F. C., Davis M. K., Wright W. D, Immunomagnetic capture and colorimetric detection of malarial biomarker Plasmodium falciparum lactate dehydrogenase, Anal. Bio-chem., 493, 30e34, (2016a).

Markwalter F. C., Ricks K. M., Bitting A. L., Mudenda L., Wright W. D., Simultaneous capture and sequential detection of two malarial biomarkers on magnetic microparticle, Talanta 161, 443–449, (2016b).

Martin S. K., Rajasekariah G. H., Awinda G., Waitumbi J., Kifude C., Unified parasite lactate dehydrogenase and histidine-rich protein ELISA for quantification of Plasmodium falciparum. Am. J. Trop. Med. Hyg. 80, 516–522, (2009).

Matsudaira P., Sequence from picomole quantities of proteins electroblotted onto polyvinylidene difluoride membranes. J. Biol. Chem. 262(21), 10035–10038, (1987).

Maurer J. J., Rapid detection and limitations of molecular techniques. Annu. Rev. Food Sci. Technol. 2:259–279, (2011).

Mawili-Mboumba D. P., Akotet M. K. B., Ngoungou E. B., Kombila M., Evaluation of rapid diagnostic tests for malaria case management in Gabon. Diagn. Micr. Infec. Dis. 66, 162–168, (2010).

Mayxay M., Pukrittayakamee S., Chotivanich K., Looareesuwan S., White N. J., Persistence of Plasmodium falciparum HRP-2 in successfully treated acute falciparum malaria. Trans. R. Soc. Trop. Med. Hyg. 95, 179–182, (2001).

McKeague M., DeRosa C. M., Challenges and Opportunities for Small Molecule Aptamer Development. J. Nucleic Acids. 2012:748913, (2012).

McMorrow M. L., Masanja M. I., Kahigwa E., Abdulla S. M. K., Kachur S. P., Quality assurance of rapid diagnostic tests for malaria in routine patient care in rural Tanzania. Am. J. Trop. Med. Hyg. 82, 151–155, (2010).

Mens F. P., Matelon J. R., Nour Y. M. B., Newman M. D., Schallig H., Laboratory evaluation on the sensitivity and specificity of a novel and rapid detection method for malaria diagnosis based on magneto-optical technology (MOT), Malar. J., 9:207, (2010).

Menting J. G., Tilley L., Deady L. W., Ng K., Simpson R. J., et al. The antimalarial drug, chloroquine, interacts with lactate dehydrogenase from Plasmodium falciparum. Mol. Biochem. Parasitol. 88, 215–224, (1997).

Miller L. H., Ackerman H. C., Su X. Z., Wellems T. E., Malaria biology and disease pathogenesis: insights for new treatments, Nat Med. 19(2):156-67, (2013).

Min J., Xia X. M., Dong Z., Yuan L., Yu L. X., et al. Spectroscopic studies on the interaction of cinnamic acid and its hydroxyl derivatives with human serum albumin, Mol. Struct. 692, pp. 71–80, (2004).

Min K., Cho M., Han S. Y., Shim Y. B., Ku J., et al. A simple and direct electrochemical detection of interferon-γ using its RNA and DNA aptamers. Biosens. Bioelectron. 23, 1819–1824, (2008).

Minasov G., Tereshko V., Egli M., Atomic-resolution crystal structures of B-DNA reveal specific influences of divalent metal ions on conformation and packing. J. Mol. Biol. 291, 83-99, (1999).

Moody A., Rapid diagnostic tests for malaria parasites. Clin. Microbiol. Rev. 15, 66–78, (2002).

Moon Y. S., Kusunose T., Sekino T., CTAB-assisted synthesis of size- and shape-controlled gold nanoparticles in SDS aqueous solution. Mater. Lett. 63, 2038–2040, (2009).

Morassin B., Fabre R., Berry A., Magnaval J. F., One year's experience with the polymerase chain reaction as a routine method for the diagnosis of imported malaria. Am. J. Trop. Med. Hyg. 66, 503–508, (2002).

Murray C. K., Bennett J. W., Rapid diagnosis of malaria. Interdiscip. Perspect. Infect. Dis. 2009: 415953. doi:10.1155/2009/415953, (2008).

Newman D. M., Heptinstall J., Matelon R. J., Savage L., Wears M. L., et al. A magneto-optic route toward the in vivo diagnosis of malaria: Preliminary results and preclinical trial data. Biophys. J. 95, 994–1000, (2008).

Newman D. M., Matelon R. J., Wears M. L., Savage L. B., The in vivo diagnosis of malaria: Feasibility study into a magneto-optic fingertip probe. IEEE J. Sel. Top. Quantum Electron. 16, 573–580, (2010).

Ngo H. T., Gandra N., Fales A. M., Taylor S. M., Vo-Dinh T., Sensitive DNA detection and SNP discrimination using ultrabright SERS nanorattles and magnetic beads for malaria diagnostics, Biosens. Bioelectron. 81, 8–14, (2016).

Nicastri E., Bevilacqua N., Schepisi M. S., Paglia M. G., Meschi S., et al. Accuracy of malaria diagnosis by microscopy, rapid diagnostic test, and PCR methods and evidence of antimalarial overprescription in non-severe febrile patients in two Tanzanian hospitals. Am. J. Trop. Med. Hyg. 80, 712–717, (2009).

Noedl H., Yingyuen K., Laoboonchai A., Fukuda M., Sirichaisinthop J., et al. Sensitivity and specificity of an antigen detection ELISA for malaria diagnosis. Am. J. Trop. Med. Hyg. 75, 1205–1208, (2006).

Noland G. S., Briones N., Sullivan Jr D. J., The shape and size of hemozoin crystals distinguishes diverse Plasmodium species. Mol. Biochem. Parasitol. 130, 91–99, (2003).

Nwakanma D., Gomez-Escobar N., Walther M., Crozier S., Dubovsky F., et al. Quantitative Detection of Plasmodium falciparum DNA in Saliva, Blood, and Urine, J. Infect. Dis. 199(11):1567-74, (2009).

O'Neill R. P., Young K., Schiffels D., Fygenson K. D., Few-Atom Fluorescent Silver Clusters Assemble at Programmed Sites on DNA Nanotubes, Nano Lett. 12, 5464−5469, (2012).

Oddoux O., Debourgogne A., Kantele A., Kocken C. H., Jokiranta T. S., et al. Identification of the five human Plasmodium species including P. knowlesi by real-time polymerase chain reaction, Eur J Clin Microbiol Infect Dis. 30(4):597-601, (2011).

Ohnoa R., Ohnukia H., Wanga H., Yokoyamaa T., Endob H., et al. Electrochemical impedance spectroscopy biosensor with interdigitated electrode for detection of human immunoglobulin A. Biosens. Bioelectron. 40, 422-426, (2013).

Okell L. C., Ghani A. C., Lyons E., Drakeley C. J., Submicroscopic infection in Plasmodium falciparum-endemic populations: a systematic review and meta-analysis. J Infect Dis. 200(10), 1509-17, (2009).

Oliveira B. C. S., Oliveira-Brett A. M., In situ evaluation of chromium–DNA damage using a DNA-electrochemical biosensor. Anal. Bioanal. Chem. 398:1633–1641, (2010).

Oliveira M. F., Silva J. R., Dansa-Petretski M., de Souza, W., Lins U., et al. Haem detoxification by an insect. Nature 400, 517–518, (1999).

Olszewski, K.L., Llinás, M., Central carbon metabolism of Plasmodium parasites. Mol. Biochem. Parasitol. 175, 95–103, (2011).

Ono T., Yoshida K., Saotome Y., Sakabe R., Okamoto I., et al. Synthesis of covalently linked parallel and antiparallel DNA duplexes containing the metal-mediated base pairs T–Hg(II)–T and C–Ag(I)–C. Chem. Commun. 47, 1542-1544, (2011).

Pagola S., Stephens P. W., Bohle D. S., Kosar A. D., Madsen, S. K., The structure of malaria pigment β-haematin. Nature 404, 307–310, (2000).

Palmer C. J., Lindo J. F., Klaskala W. I., Quesada J. A., Kaminsky R., et al. Evaluation of the OptiMAL test for rapid diagnosis of Plasmodium vivax and Plasmodium falciparum malaria. J. Clin. Microbiol. 36, 203–206, (1998).

Parra M. E., Evans C. B., Taylor D. W., Identification of Plasmodium falciparum histidine-rich protein 2 in the plasma of humans with malaria. J. Clin. Microbiol. 29, 1629–1634, (1991).

Paul K. B., Kumar S., Tripathy S., Vanjari S. R. K., Singh V., et al. A highly sensitive self-assembled monolayer modified copper doped zinc oxide nanofiber interface for detection of Plasmodium falciparum histidine-rich protein-2: targeted towards rapid, early diagnosis of malaria, Biosens. Bioelectron. 80, 39–46, (2016).

Peng H. P, Hu Y., Liu P., Deng Y. N., Wang P., et al. Label-free electrochemical DNA biosensor for rapid detection of mutidrug resistance gene based on Au nanoparticles/toluidine blue–graphene oxide nanocomposites, Sens. Actuators B, 207, 269–276, (2015).

Peng W. K., Kong T. F., Ng C. S., Chen L., Huang Y., et al., Micromagnetic resonance relaxometry for rapid label-free malaria diagnosis, Nat. Med. 20, 1069–1073, (2014).

Peng Y., Wu J., Wang J., Li W., Yu S., Study and evaluation of Wondfo rapid diagnostic kit based on nano-gold immunochromatography assay for diagnosis of Plasmodium falciparum. Parasitol. Res. 110, 1421–1425, (2012).

Pesce A., Fondy P. T., Stolzenbach F., Castillo F., Kaplan O. N., The comparative enzymology of lactic dehydrogenases. J. Biol. Chem. 242(9), 2151–2167, (1967).

Petty J. T., Story S. P., Juarez S., Votto S. S., Herbst A. G., et al. Optical sensing by transforming chromophoric silver clusters in DNA nanoreactors, Anal. Chem. 84, 356–364, (2012).

Petty J. T.; Zheng J., Hud N. V., Dickson R. M., DNA-templated Ag nanocluster formation., J. Am. Chem. Soc. 126 (16), 5207-5212, (2004).

Pfaller M. A., Krogstad D. J., Parquette A. R., Nguyen-Dinh P., Plasmodium falciparum: Stage-specific lactate production in synchronized cultures. Ex. Parasitol. 54, 391–396, (1982).

Piper R., Lebras J., Wentworth L., Hunt-Cooke A., Houzé S., et al. Immunocapture diagnostic assays for malaria using Plasmodium lactate dehydrogenase (pLDH). Am. J. Trop. Med. Hyg. 60, 109–118, (1999).

Pirnstill W. C., Coté L. G., Malaria Diagnosis Using a Mobile Phone Polarized Microscope, Sci. Rep. 5:13368, (2015).

Pisciotta J. M., Ponder E. L., Fried B., Sullivan D., Hemozoin formation in Echinostoma trivolvis rediae. Int. J. Parasitol. 35, 1037–1042, (2005).

Popenda M., Szachniuk M., Antczak M., Purzycka K. J., Lukasiak P., *et al*. Automated 3D structure composition for large RNAs. Nucleic Acids Res. 40, e112, (2012).

Rakotonirina H., Barnadas C., Raherijafy R., Andrianantenaina H., Ratsimbasoa A., et al. Accuracy and reliability of malaria diagnostic techniques for guiding febrile outpatient treatment in malaria endemic countries. Am. J. Trop. Med. Hyg. 78, 217–221, (2008).

Ramutton T., Hendriksen I., Mwanga-Amumpaire J., Mtove G., Olaosebikan R., et al. Sequence variation does not confound the measurement of plasma PfHRP2 concentration in African children presenting with severe malaria. Malar. J., 11,276, (2012).

Read J. A., Wilkinson K. W., Tranter R., Sessions R. B., Brady R. L., Chloroquine binds in the cofactor binding site of Plasmodium falciparum lactate dehydrogenase. J. Biol. Chem. 274, 10213 –10218, (1999).

Rebelo M., Sousa C., Shapiro M. H., Mota M. M., Grobusch P. M., et al. A Novel Flow Cytometric Hemozoin Detection Assay for Real-Time Sensitivity Testing of Plasmodium falciparum, PLoS ONE 8: 4, e61606, (2013).

Richards C. I., Choi S., Hsiang J. C., Antoku Y., Vosch T., et al. Oligonucleotide-stabilized Ag nanocluster fluorophores, J. Am. Chem. Soc. 130, 5038–5039, (2008).

Richardson D. C., Ciach M., Zhong K. J. Y., Crandall I., Kain K. C., Evaluation of the Makromed dipstick assay versus PCR for diagnosis of Plasmodium falciparum malaria in returned travelers. J. Clin. Microbiol. 40, 4528–4530, (2002).

Robertson D. L., Joyce G. F., Selection in vitro of an RNA enzyme that specifically cleaves single stranded DNA. Nature 344, 467-468 (1990).

Rock E. P., Marsh K., Saul A. J., Wellems T. E., Taylor D. W., et al. Comparative analysis of the Plasmodium falciparum histidine-rich proteins HRP-I, HRP-II and HRP-III in malaria parasites of diverse origin. Parasitology 95 (Pt 2), 209–227, (1987).

Rodríguez-Acosta A., Domínguez N. G., Aguilar I., Girón. M. E., Characterization of Plasmodium falciparum glutamate dehydrogenase-soluble antigen. Braz. J. Med. Biol. Res. 31, 1149-1155, (1998).

Roth E., Plasmodium falciparum carbohydrate metabolism - a connection between host-cell and parasite. Blood Cells. 16, 453–460, (1990).

Rothemund P. W. K., Folding DNA to create nanoscale shapes and patterns, Nature 440, 297-302, (2006).

Royer R., Deck L., Campos N., Hunsaker L., Jagt V., Biologically active derivatives of gossypol: syntheis and antimalarial activities of peri-acylated gossylic nitriles. J. Med. Chem. 29, 1799-1801, (1986).

Sabato D. G., Kaplan O. N., The denaturation of lactic dehydrogenases: I. The effect of sodium dodecyl sulfate. J. Biol. Chem. 239, 438–443, (1964).

Salentin S., Schreiber S., Haupt V. J., Adasme M. F., Schroeder M., PLIP: fully automated protein–ligand interaction profiler. Nucleic Acids Res. 43, W443-447 (2015).

Schmidt M. T., Schaechter M., Topics and ecological and environmental microbiology. Academic press. p584, (2011).

Schneider E. L., Marletta M. A., Heme binding to the histidine-rich protein II from Plasmodium falciparum. Biochemistry 44(3):979-86, (2005).

Schneidman-Duhovny D., Inbar Y., Nussinov R., Wolfson H. J., PatchDock and SymmDock: servers for rigid and symmetric docking. Nucleic Acids Res. 33: W363-367, (2005).

Schuck P., Size distribution analysis of macromolecules by sedimentation velocity ultracentrifugation and Lamm equation modeling. Biophys. J. 78, 1606–1619, (2000).

Sengupta B., Springer K., Buckman G. J., Story P. S., Abe H. O., et al. DNA Templates for Fluorescent Silver Clusters and I-Motif Folding, J. Phys. Chem. C. 113, 19518–19524, (2009).

Sessions R. B., Dewar V., Clarke A. R., Holbrook J., A model of Plasmodium falciparum lactate dehydrogenase and its implications for the design of improved antimalarials and the enhanced detection of parasitaemia. Protein. Eng. 10,301-6, (1997).

Shamsi H. M., Kraatz B-H., Interactions of metal ions with DNA and some applications. J. Inorg. Organomet. Polym. 23:,4-23, (2013).

Sharma J., Yeh H. C., Yoo H., Werner J. H., Martinez J. S., Silver nanocluster aptamers: in situ generation of intrinsically fluorescent recognition ligands for protein detection, Chem. Commun. 47, 2294–2296, (2011b).

Sharma M. K., Rao V. K., Agarwal G. S., Rai G. P., Gopalan N., et al. Highly sensitive amperometric immunosensor for detection of Plasmodium falciparum histidine rich protein 2 in serum of humans with malaria: comparison with a commercial kit. J. Clin. Microbiol. 46, 3759–3765, (2008).

Sharma M. K., Rao V. K., Merwyn S., Agarwal G. S., Upadhyay S., et al. A novel piezoelectric immunosensor for the detection of malarial Plasmodium falciparum histidine rich protein-2 antigen. Talanta 85, 1812–1817, (2011a).

Shoemark D. K., Cliff M. J., Sessions R. B., Clarke A. R., Enzymatic properties of the lactate dehydrogenase enzyme from Plasmodium falciparum. FEBS J. 274, 2738–2748, (2007).

Sikarwar B., Sharma P. K., Srivastava A., Agarwal G. S., Boopathi M., et al. Surface plasmon resonance characterization of monoclonal and polyclonal antibodies of malaria for biosensor applications, Biosens. Bioelectron. 60, 201–209, (2014).

Singh N., Saxena A., Awadhia S. B., Shrivastava R., Singh M. P., Evaluation of a rapid diagnostic test for assessing the burden of malaria at delivery in India. Am. J. Trop. Med. Hyg. 73, 855–858, (2005).

Slater A. F., Swiggard W. J., Orton B. R., Flitter W. D., Goldberg D. E., et al. An iron-carboxylate bond links the heme units of malaria pigment. Proc. Natl. Acad. Sci. USA. 88, 325–329, (1991).

Smith K. D., Korgel A. B., The importance of the CTAB surfactant on the colloidal seed-mediated synthesis of gold nanorods. Langmuir 24(3), 644–649, (2008).

Solomonov I., Osipova M., Feldman Y., Baehtz C., Kjaer K., et al. Crystal nucleation, growth, and morphology of the synthetic malaria pigment β-hematin and the effect thereon by quinoline additives: The malaria pigment as a target of various antimalarial drugs. J. Am. Chem. Soc. 129, 2615–2627, (2007).

Song H-O., Lee B., Bhusal R. P., Park B., Yu K., et al. Development of a Novel Fluorophore for Real-Time Biomonitoring System, PLoS ONE 7(11), e48459, (2012).

Srivastava I. K., Schmidt M., Certa U., Döbeli H., Perrin, L. H., Specificity and inhibitory activity of antibodies to Plasmodium falciparum aldolase. J. Immunol. 144:1497–503, (1990).

Stoeva S. I., Lee J. S., Smith J. E., Rosen S. T., Mirkin C. A., Multiplexed detection of protein cancer markers with biobarcoded nanoparticle probes. J. Am. Chem. Soc. 128, 8378-8379, (2006).

Sui Y., Potula R., Dhillon N., Pinson D., Li S., et al. Neuronal apoptosis is mediated by CXCL10 overexpression in simian human immunodeficiency virus encephalitis. Am. J. Pathol. 164, 1557–1566, (2004).

Sullivan D. J., Gluzman I. Y., Goldberg D. E., Plasmodium hemozoin formation mediated by histidine-rich proteins. Science 271, 219–222, (1996).

Sutherland C.J., Hallett R., Detecting malaria parasites outside the blood, J Infect Dis. 199(11):1561-3, (2009).

Swartz J. D., Gulka C. P., Haselton F. R., Wright D. W., Development of a Histidine-Targeted Spectrophotometric Sensor Using Ni(II)NTA-Functionalized Au and Ag Nanoparticles, Langmuir 27, 15330–15339, (2011).

Tanford C., Physical chemistry of macromolecules. New York: Wiley, (1961).

Tang L., Wang Y., Li Y., Feng H., Lu J., et al. Preparation, Structure, and Electrochemical Properties of Reduced Graphene Sheet Films, Adv. Funct. Mater. 19, 2782–2789, (2009).

Tangpukdee N., Duangdee C., Wilairatana P., Krudsood S., Malaria Diagnosis: A Brief Review. Korean J. Parasitol. 47, No. 2: 93-102, (2009).

Tiwari I., Singha M., Pandeya M. C., Sumana G., Electrochemical genosensor based on graphene oxide modified iron oxide–chitosan hybrid nanocomposite for pathogen detection Sens. Actuators B 206, 276–283, (2015).

Tjitra E., Suprianto S., Dyer M., Currie B. J., Anstey N. M., Field evaluation of the ICT malaria P.f/P.v immunochromatographic test for detection of Plasmodium falciparum and Plasmodium vivax in patients with a presumptive clinical diagnosis of malaria in Eastern Indonesia. J. Clin. Microbiol. 37, 2412–2417, (1999).

Tjitra E., Suprianto S., McBroom J., Currie B. J., Anstey N. M., Persistent ICT malaria P.f/P.v panmalarial and HRP2 antigen reactivity after treatment of Plasmodium falciparum malaria is associated with gametocytemia and results in false positive diagnoses of Plasmodium vivax in convalescence. J. Clin. Microbiol. 39, 1025–1031, (2001).

Tong S. Y. C., Giffard P. M., Microbiological applications of high-resolution melting analysis. J. Clin. Microbiol. 50(11): 3418–3421, (2012).

Tuerk C., Gold L., Systematic evolution of ligands by exponential enrichment: RNA ligands to bacteriophage T4 DNA polymerase. Science 4968, 505-510 (1990).

Turkevich J., Stevenson P. C., Hillier J. A., Study of the nucleation and growth processes in the synthesis of colloidal gold. Discuss. Faraday Soc. 11, 55–75, (1951).

Tyagi S., Kramer F. R., Molecular Beacons in Diagnostics, F1000 Med. Rep. 4: 10, (2012).

Uguen C., Rabodonirina M., De Pina J. J., Vigier J. P., Martet G., et al. ParaSight-F rapid manual diagnostic test of Plasmodium falciparum infection. Bull. World Health Organ. 73, 643–649, (1995).

Valle M. R., Quakyi I. A., Amuesi J., Quaye J. T., Nkrumah F. K., et al. Detection of antigens and antibodies in the urine of humans with Plasmodium falciparum malaria. J. Clin. Microbiol. 29, 1236–1242, (1991).

Veigas B., Pedrosa P., Carlos F. F., Mancio‐Silva L., Grosso A. R., et al. One nanoprobe, two pathogens: gold nanoprobes multiplexing for point‐of‐care, J. Nanobiotechnol. 13:48, (2015).

Vesell S. E., Formation of human lactate dehydrogenase isozyme patterns in vitro. Proc. Natl. Acad. Sci. USA 54, 111–117, (1965).

Wagner J. T., Ludeman H., Farber P. M., Lottspeich F., Krauth–Siegel R. L., Glutamate dehydrogense, the marker protein of Plasmodium falciparum : cloning, expression and characterization of malarial enzyme. Eur. J. Biochem. 258, 813-819, (1998).

Wang L., Liu X., Hu X., Song S., Fan C., Unmodified gold nanoparticles as a colorimetric probe for potassium DNA aptamers. Chem. Commun. 3780–3782, (2006).

Wang X., Lim J. H., Son A., Characterization of denaturation and renaturation of DNA for DNA hybridization, Environ. Health. Toxicol. 29: e2014007, (2014b).

Wang Y., Tang L., Li Z., Lin Y., Li J., In situ simultaneous monitoring of ATP and GTP using a graphene oxide nanosheet based sensing platform in living cells, Nat. Protoc. 9, 1944-1955, (2014a).

Wei W., Lu R., Tang S., Liu X., Highly cross-linked fluorescent poly (cyclotriphosphazene-co-curcumin) microspheres for the selective detection of picric acid in solution phase, J. Mat. Chem. A 3, 4604, (2015).

Wellems T. E., Howard R. J., Homologous genes encode two distinct histidine-rich proteins in a cloned isolate of Plasmodium falciparum. Proc. Natl. Acad. Sci. USA 83, 6065–6069, (1986).

Wenisch C., Spitzauer S., Florris-Linau K., Rumpold H., Vannaphan S., et al. Complement Activation in Severe Plasmodium falciparum malaria. Clin. Immunol. Immunopathol. 85, 166–171, (1997).

Winter V. J., Cameron A., Tranter R., Sessions R. B., Brady R. L., Crystal structure of Plasmodium berghei lactate dehydrogenase indicates the unique structural differences of these enzymes are shared across the Plasmodium genus. Mol. Biochem. Parasitol. 131, 1–10, (2003).

Wittwer C. T., High-resolution DNA melting analysis: advancements and limitations. Hum. Mutat. 30(6), 857–859, (2009).

Wohlgamuth C. H., McWilliams M. A., Slinke J. D., DNA as a Molecular Wire: Distance and Sequence Dependence, Anal. Chem. 85, 8634−8640, (2013).

Wongsrichanalai C., Barcus, M. J., Muth S., Sutamihardja A., Wernsdorfer W.H., A review of malaria diagnostic tools: microscopy and rapid diagnostic test (RDT). Am. J. Trop. Med. Hyg. 77, 119 –127, (2007).

Wood O. D., Dinsmore J. M., Bare A. G, Lee S. J., M-DNA is stabilised in G•C tracts or by incorporation of 5-fluorouracil. Nucleic Acids Res. 30(10): 2244–2250, (2002).

World Malaria Report, 2015, http://www.who.int/malaria/publications/world-malaria-report-2015/en/

Wu M., Kempaiah R., Huang J. P-J., Maheshwari V., Liu J., Adsorption and Desorption of DNA on Graphene Oxide Studied by Fluorescently Labeled Oligonucleotides, Langmuir 27, 2731–2738, (2011).

Wu Y., Liu L., Zhan S., Wang F., Zhou P., Ultrasensitive aptamer biosensor for arsenic (III) detection in aqueous solution based on surfactant-induced aggregation of gold nanoparticles. Analyst 137(18), 4171–4178, (2012a).

Wu Y., Zhan S., Wang F., He L., Zhi W., et al. Cationic polymers and aptamers mediated aggregation of gold nanoparticles for the colorimetric detection of arsenic (III) in aqueous solution. Analyst 48(37), 4459–4461, (2012b).

Xia F., Zuo X., Yang R., Xiao Y., Kang D., et al. Colorimetric detection of DNA, small molecules, proteins, and ions using unmodified gold nanoparticles and conjugated polyelectrolytes. Proc. Natl. Acad. Sci. USA 107, 10837–10841, (2010).

Xiao Y., Patolsky F., Katz E., Hainfeld J. F., Willner I., "Plugging into enzymes": Nanowiring of redox enzymes by a gold nanoparticle. Science 21, 1877-1881, (2003).

Yang S., Parmley S. F., A bradyzoite stage-specifically expressed gene of Toxoplasma gondii encodes a polypeptide homologous to lactate dehydrogenase. Mol. Biochem. Parasitol. 73, 291–294, (1995).

Yang S., Parmley S. F., Toxoplasma gondii expresses two distinct lactate dehydrogenase homologous genes during its life cycle in intermediate hosts. Gene 184, 1–12, (1997).

Yang X., Gan L., Han L., Wang E., Wang J., High-Yield Synthesis of Silver Nanoclusters Protected by DNA Monomers and DFT Prediction of their Photoluminescence Properties, Angew. Chem. Int. Ed. 52, 2022 –2026, (2013).

Yeh C-H., Sharma J., Han J. J., Martinez S. J., Werner H. J., A DNA−Silver Nanocluster Probe That Fluoresces upon Hybridization, Nano Lett. 10 (8), pp 3106–3110, (2010).

Yeh C-H., Sharma J., Shih M-I., Vu M. D., Martinez S. J., et al. Fluorescence Light-Up Ag Nanocluster Probe that Discriminates Single-Nucleotide Variants by Emission Color, J. Am. Chem. Soc. 134(28): 11550–11558, (2012).

Yeo S-J., Huong D. T., Han J-H., Kim J- Y., Lee W-J., et al. Performance of coumarin-derived dendrimer-based fluorescence-linked immunosorbent assay (FLISA) to detect malaria antigen, Malar. J. 13:266, (2014).

Yuan Z., Chen C-Y., Li W-H., Chang T-H., Fluorescent silver nanoclusters stabilized by DNA scaffolds, Chem. Commun. 50, 9800, (2014).

Yuen C., Liu Q., Magnetic field enriched surface enhanced resonance Raman spectroscopy for early malaria diagnosis, J. Biomed. Opt. 17(1), 017005, (2012).

Zhang B., Chan Y., Lu B., Diamond M., Klein R., CXCR3 mediates region-specific antiviral T cell trafficking within the central nervous system during west nile virus encephalitis, J. Immunol. 180:2641-2649, (2008).

Zhang Z., Fu X., Li K., Liu R., Peng D., et al. One-step fabrication of electrochemical biosensor based on DNA-modified three-dimensional reduced graphene oxide and chitosan nanocomposite for highly sensitive detection of Hg(II), Sens. Actuators B 225, 453–462, (2016).

Zhao W., Brook M. A., Li Y., Design of gold nanoparticle-based colorimetric biosensing assays , Chem. biochem. 13;9(15):2363-71, (2008).

Zipper H., Brunner H., Bernhagen J., Vitzthum F., Investigations on DNA intercalation and surface binding by SYBR Green I, its structure determination and methodological implications. Nucleic Acids Res. 12;32 (12):e103, (2004).

Zuker M., Mfold web server for nucleic acid folding and hybridization prediction. Nucleic Acids Res. 31(13), 3406–3415, (2003).

List of Publications

Publications in refereed journals

Priyamvada Jain, Babina Chakma, Naveen K. Singh, Sanjukta Patra, Pranam Goswami, Metal-DNA interactions improve signal in high resolution melting of DNA for species differentiation of *Plasmodium* parasite. (Communicated)

Priyamvada Jain, Babina Chakma, Sanjukta Patra, Pranab Goswami, Hairpin stabilized fluorescent silver nanoclusters for quantitative detection of NAD^+ and monitoring NAD^+/NADH based enzymatic reactions. Analytica Chimica Acta, 956, 2017, 48–56

Priyamvada Jain, Smita Das, Babina Chakma , Pranab Goswami, Aptamer-graphene oxide for highly sensitive dual electrochemical detection of *Plasmodium* lactate dehydrogenase. Analytical Biochemistry, 514, 2016, 32-37

Priyamvada Jain, Babina Chakma, Naveen K. Singh, Sanjukta Patra, Pranab Goswami, Aromatic Surfactant as Aggregating Agent for Aptamer-Gold Nanoparticle-Based Detection of *Plasmodium* Lactate Dehydrogenase. Molecular Biotechnology, 58(7), 2016, 497-508

Babina Chakma, **Priyamvada Jain**, Naveen K. Singh, and Pranab Goswami, Development of an Indicator Displacement Based Detection of Malaria Targeting HRP-II as Biomarker for Application in Point-of-Care Settings. Analytical Chemistry, 88 (20), 2016, 10316–10321

Priyamvada Jain, Babina Chakma, Sanjukta Patra, Pranab Goswami, Potential Biomarkers and Their Applications for Rapid and Reliable Detection of Malaria. BioMed Research International, volume 2014, 2014, article ID 852645, http://dx.doi.org/10.1155/2014/852645

Patents filed

Pranab Goswami, Naveen Kumar Singh, **Priyamvada Jain**, Babina Chakma (2016). Title of the invention: Dna aptamers specifically binding to *Plasmodium falciparum* glutamate dehydrogenase (PFGDHa). Application no.201631025722

Abstracts published in conferences

Priyamvada Jain, Babina Chakma, Sanjukta Patra, Pranab Goswami, Template structure dependent bright red silver nanoclusters for NAD^+ detection in enzyme catalyzed reactions, IUMRS-International Conference of Young Researchers on Advanced Materials (IUMRS-ICYRAM 2016) organized by Materials Research Society of India (MRSI) and Indian Institute of Science Bangalore, held at Indian Institute of Science Bangalore, India, during December 11-15. Conference proceeding page No. 128

Babina Chakma, **Priyamvada Jain**, Pranab Goswami, Development of indicator displacement based detection of malaria targeting HRP II as biomarker for point- of- care and analytical settings, IUMRS-International Conference of Young Researchers on Advanced Materials (IUMRS-ICYRAM 2016) organized by Materials Research Society of India (MRSI) and Indian Institute of Science Bangalore, held at Indian Institute of Science Bangalore, India, during December 11-15. Conference proceeding page No. 128

Smita Das, **Priyamvada Jain**, Babina Chakma, Pranab Goswami, Paper based electrochemical sensor for species specific detection of malaria. 4th International Conference on Advanced Nanomaterials and Nanotechnology (ICANN-2015), Dec 08-11, 2015, held at Indian Institute of Technology Guwahati, Abstract ID: J1034

Priyamvada Jain, Sanjukta Patra, Pranab Goswami, Development of aptamers against *Plasmodium* lactate dehydrogenase for accurate diagnosis of malaria. Asian Congress on Biotechnology-2013 organized by The Asian Federation of Biotechnology, 15-19 December, 2013 in New Delhi, Abstract No. 350

Appendix

Table A1: List of bacterial strains

Strain	Description
Escherichia coli DH5α (Novagen)	F'ϕ80dlacZΔM15 Δ (lacZYA-argF) U169 endA1 recA1 hsdR17 (rk^-mk^+) deoR thi-1 phoA supE44 λ^- gyrA96 relA1
Escherichia coli BL21 (DE3) (Novagen)	F^- ompT hsdSB (rB- mB-) gal dcm (DE3). Derivation of B834. (Parental strain: B834; Resistance: none)

Table A2: Culture medium for bacteria

Medium	Composition
Luria Bertani broth (LB) (1 L)	Casein enzymic hydrolysate 10 g, Yeast extract 5 g, NaCl 10 g, pH 7.5 $\pm$ 0.2
Luria Bertani agar (LB) (1 L)	Casein enzymic hydrolysate 10 g, Yeast extract 5 g, NaCl 10 g, Agar 15 g, pH 7.5 $\pm$ 0.2

Table A3: Buffers and solutions

Solutions for plasmid isolation	
Solution I	50 mM glucose, 25 mM Tris-Cl buffer, 10 mM EDTA, pH 8.0
Solution II	0.2 N NaOH, 1 % SDS
Solution III	5 M potassium acetate, pH adjusted to 4.8 with acetic acid
Buffer for agarose gel electrophoresis	
TAE buffer (50X) 1L	242 g Tris base, 57.1 ml glacial acetic acid, 100 ml 0.5 M EDTA (pH 8), adjust final volume to 1L with water
Solution for competent cell preparation	
Transformation and storage solution (TSS)	10 % (w/v) polyethylene glycol, 5 % (v/v) dimethyl sulfoxide and 50 mM $MgCl_2$ in LB broth, pH 6.5
Buffers for protein purification	
Lysis/Equilibration buffer	20 mM sodium phosphate buffer, 300 mM NaCl, pH 8
Washing buffer	20 mM sodium phosphate buffer, 300 mM NaCl, supplemented with varying concentration of imidazole (30 mM, 50 mM, or 60 mM), pH 8

Elution buffer	20 mM sodium phosphate buffer, 300 mM NaCl, 350 mM imidazole, pH 8

Buffers/solutions for SDS-PAGE

30 % acrylamide-bisacrylamide gel solution (100 ml)	29.2 g acrylamide, 0.8 g bisacrylamide
Tris-HCl, pH 6.8, 0.5 M (100 ml)	6.06 g Tris base, pH adjusted to 6.8 with 2 N HCl
Tris-HCl, pH 8.8, 1.5 M (100 ml)	18.18 g of Tris base, pH adjusted to 8.8 with 2 N HCl
Gel running buffer (10X)	30.0 g of Tris base, 144.0 g of glycine, and 10.0 g of SDS in 1000 ml of water.
SDS gel loading buffer (2X)	100 mM Tris/HCl (pH 6.8), 4 % (w/v) SDS, 0.2% (w/v) bromophenol blue dye, 20 % (v/v) glycerol, 200 mM DTT or β-mercaptoethanol
Staining solution (blue silver staining) (100 ml)	10 ml ortho phosphoric acid, 10 g w/v ammonium sulfate, 0.12 g w/v CBB G250, 20 ml methanol and 70 ml water

Buffers/solutions for western blotting	
Phosphate buffer saline (PBS)	11.5 g di-sodium hydrogen orthophosphate, 2.96 g sodium dihydrogen orthophosphate, 5.84 g sodium chloride, pH 7.4
Phosphate buffer saline with Tween 20 (PBST)	PBS containing 0.1 % Tween 20
Transfer buffer	25 mM Tris base, 39 mM glycine, 20 % (v/v) Methanol
Ponceau solution (Sigma)	0.1 % PonceauS in 5 % acetic acid
Blocking buffer	5 % BSA in PBST

Solutions for SELEX	
Binding buffer	50 mM sodium phosphate buffer, pH 7.4, 50 mM NaCl, 5 mM KCl, 2.5 mM $MgCl_2$
Coupling buffer	20 mM Tris HCl, pH 7.5, 0.5 M NaCl, 1 mM EDTA
TBE buffer (5X)	54 g of Tris base, 27.5 g of boric acid, 20 mL of 0.5 M EDTA (pH 8.0)
10 % acrylamide-bisacrylamide gel solution (75:1), 15 ml	5 ml of 30 % acrylamide-bisacrylamide solution (75:1), 3 ml TBE buffer (5X), 105 µl 10 % APS, 10 µl TEMED, 6.8 ml water

Table A4: List of antibodies

Antibody	Source	Working condition	Working dilution	Usage
Anti-poly-histidine antibody	Mouse/monoclonal	RT/2 h	1:2000	As primary antibody
Anti-mouse IgG (Fab specific)-peroxidase antibody	Goat/monoclonal	RT/1 h	1:5000	As secondary antibody

Table A5: List of primers

Primers for cloning

Name	Sequence (5′-3′)
PfLDH	Forward BamHI-**ATGGCACCAAAAGCAAAAATCG**
	Reverse XhoI-**TTAAGCTAATGCCTTCATTCTC**
hLDH B	Forward EcoRI-**ATGGCAACTCTTAAGGAAAAACT**
	Reverse XhoI-**CTACAGGTCTTTTAGGTCCTTCT**

Primers for SELEX

Name	Sequence (5′-3′)
F1	**CACCTAATACGACTCACTATAGCGGA**
R1	**GCAAGCTTGTTCGAGCCAG**
R1-biotin	biotin-**GCAAGCTTGTTCGAGCCAG**

Table A6: List of antibiotics

Name	Stock concentration $mg.ml^{-1}$	Solvent	Working concentration $\mu g.ml^{-1}$
Ampicillin	100	water	100
Kanamycin	100	water	50